Published by Saint Petersburg
Mining University

SINCE 1907

E-ISSN 2541-9404
ISSN 2411-3336

# JOURNAL OF MINING INSTITUTE

ZAPISKI GORNOGO INSTITUTA

## SCIENTIFIC JOURNAL

Volume 261
№ 3 • 2023

INDEXING IN
SCOPUS (Q1)
WEB OF SCIENCE (ESCI)

WWW.PMI.SPMI.RU

Journal of Mining Institute

Saint Petersburg Mining University

The International Competence Center for Mining Engineering Education under the auspices of UNESCO

The scientific periodical “Journal of Mining Institute” is published since 1907 by Saint Petersburg Mining University – the first higher technical educational institution in Russia, founded in 1773 by the decree of Catherine II as the embodiment of the ideas of Peter I and M.V. Lomonosov on the training of engineers for the development of mining business.

The International Competence Center for Mining Engineering Education under the auspices of UNESCO operates on the basis of Saint Petersburg Mining University and contributes to active interaction of the Journal with the international scientific community.

The purpose of the Journal is to create an information space in which Russian and foreign scientists can present results of their theoretical and empirical research on the problems of the mining sector.

Published articles cover the issues of geology, geotechnical engineering and engineering geology, mining and petroleum engineering, mineral processing, energy, geoecology and life safety, economics of raw materials industries.

The Journal is indexed by Scopus (Q1), Web of Science Core Collection (ESCI), DOAJ Seal, RSCI, GeoRef, Google Scholar, RSCI. It is included in the White list of the Ministry of Education and Science of the Russian Federation.

The Journal is published six times a year. The average first decision time is one month.

Articles are published free of charge. Translation is provided by the author.

---

Photo on the cover is an exhibit of the Mining Museum – wolframite, a cluster of board-shaped black crystals with shading, including prismatic transparent scepter-shaped quartz crystals (Karaobinskoye deposit, Karaganda Region, Kazakhstan). The Mining Museum received it in 1981. Wolframite is a tungsten ore, used in the production of steel, for obtaining heat-resistant materials, for making high-speed tools, special bore bits for drilling holes. It is used in ferrous metallurgy, electrical engineering, chemical and other industries.

The Mining Museum is the world’s third largest natural-science exposition, it contains more than 230 thousand exhibits, including precious metals and stones, unique collections of minerals, ores, rocks, paleontological remains, meteorites, a collection of models and prototypes of mining equipment, pieces of stone-cutting and jewelry art.

# JOURNAL OF MINING INSTITUTE

ZAPISKI GORNOGO INSTITUTA

PEER-REVIEWED SCIENTIFIC JOURNAL

Published since 1907

ISSN 2411-3336
e-ISSN 2541-9404

Volume 261

ST. PETERSBURG • 2023

**Journal founder: Saint Petersburg Mining University**



## Sections

• Geology • Geotechnical Engineering and Engineering Geology • Economic Geology • Energy

Registration Certificate PI No. FS77-70453 dated 20.07.2017

PH License No. 06517 dated 09.01.02

Editorial staff: Head of the Editorial Center V.L.Lebedev; Editors: E.S.Dribinskaya, M.G.Khachirova, V.E.Filippova, L.V.Nabieva, M.V.Skvortsova
Computer Design: N.N.Sedykh, V.I.Kashirina


Passed for printing 19.07.2023. Format 60 × 84/8. Academic Publishing Division 40.
Circulation: 300 copies. Order 554. Printed by RIC of Saint Petersburg Mining University. Free sale price.

**Mailing address of the Journal Founder and the Editorial Board**
21st Linia V.O., No. 2, St. Petersburg, Russia, 199106
Phone: +7 (812) 328-8416; Fax +7 (812) 327-7359;
E-mail: pmi@spmi.ru Journal website: pmi.spmi.ru

# CONTENTS

**Journal of Mining Institute.** 2023. Vol. 261


*Editorial*

# *ENERGY EFFICIENCY IN THE MINERAL RESOURCES AND RAW MATERIALS COMPLEX*

Energy efficiency and energy saving at all times and especially at the present stage of development of industry and economy have played an extremely important role. Regardless of which countries and according to what criteria they build energy development plans, energy efficiency and energy saving are always a priority. This fully applies to the mineral resources complex, in which energy consumption as a whole makes up a large share of total consumption. The resources mined in the mineral resources complex are themselves a source of energy. The energy sector is evolving in many ways. Many scientific works, the results of which are reflected in publications, confirm the relevance of research in the energy efficiency field. But the approach to individual decisions in the mineral resource industry is specific and it is worth of separate consideration. Recently, much attention has been paid to "green energy" and renewable energy sources. However, energy efficiency in the field of traditional generation and consumption remains an urgent problem and its solution is in constant development. One of the main directions for improving energy efficiency is the development of autonomous systems for the electrical and thermal power engineering. All these problems are reflected in a special volume of the Journal of the Mining Institute, the articles are divided into four sections: energy efficiency of the electric drive in the mineral resources complex (MRC); energy efficiency of industrial plants and enterprises in MRC; power quality and renewable sources in MRC; autonomous power supply systems in MRC. The presented articles contain valuable material from the scientific and practical points of view and can form the basis for further research in the energy efficiency field.

A number of articles are devoted to the solution of issues on the electric drive energy efficiency. In the article by *Oksana Yu. Ganzulenko*, *Ani P. Petkova* the results of the use of a linear rack-and-pinion drive as part of a sucker rod pump drive are presented, which makes it possible to reduce energy consumption in oil production up to 10 % in the form of a significant increase in efficiency. Article by *Mikhail S. Ershov*, *Aleksandr N. Komkov*, *Evgeniy A. Feoktistov* is devoted to the creation of an original mathematical model of the system asynchronous electric drive – drill string – bit – rock. The value of the research lies in the creation of a correct model that allows you to calculate the energy efficiency of various drilling modes with the existing composition of the electrical complex. Article by *Dmitriy I. Shishlyannikov*, *Valeriy Yu. Zverev*, *Anna G. Zvonareva et. al.* is devoted to the necessity of improvement the sucker-rod pumps drive operating in marginal and complicated well conditions in oil production. Solutions to improve the energy efficiency of hydraulic drives of sucker-rod pumps are proposed. One of the most important factors in the efficient operation of the mineral processing plant is the reliable haul trucks operation. The article by *Alexander N. Nazarychev*, *Grigory V. Dyachenok*, *Yuriy A. Sychev* defines the main mechanical external influences that determine the degree of possible defects in the electric drive of a haul truck. The authors propose practical recommendations for increasing the reliability of the operation of electric drive individual unit, which is associated with energy efficiency in the system of costs for extraction and transportation of minerals. The article by *Maxim G. Rakhutin et al*. studies the influence of the working fluid temperature influence on the losses of a mining hydraulic excavator on the example of using the Komatsu PC750-7 excavator. Based on the power loss criteria application, it is proposed to reasonably choose the working fluid type and operating modes of the hydraulic system.

The topic of energy efficiency of plants and enterprises is presented in several articles. Article by *Vladimir Ju. Bazhin et. al.* is devoted to the results of theoretical and experimental studies in the field of raw aluminosilicate smelting process. Research is aimed at creating an algorithm for controlling the technological process. Article by *Roman V. Klyuev et. al*. considers the electricity consumption forecasting at any stage of power supply. The article presents a new approach in the field of load forecasting, in particular, in MRC enterprises, the use of ensemble learning methods, in particular a recurrent neural network model, is proposed. In the article by *Aleksandr V. Nikolaev*, *Stefan Vöth*, *Aleksey V. Kychkin* a cybernetic model of electricity demand management on the example of the main fan installation is presented.

The model is implemented on the Internet of Things platform and allows you to determine in advance the electricity costs caused by the operation of the main fan installation. The article by *Ekaterina A. Yushkova*, *Vladimir A. Lebedev* presents an original solution to the energy efficiency problem of a vacuum plant for the fuel oil distillation using pinch analysis. The rticle determines the optimal flow heat capacity of the installation that ensures an increase in its efficiency.

In the section of the electricity quality improvement and development of using the renewable sources and storage devices, an article by *Valery M. Zavyalov et al.* presents an original solution to the issue of charging the mining electric locomotive battery installations and is of practical interest. Article by *Aleksandr N. Skamyin et al.* is devoted to the unsolved problem of determining the supply network not by calculation, but experimentally, the material of the article is a big step towards achieving this goal. In the article by *Fedor S. Nepsha et al*. an original approach to solving the problem of using renewable energy sources in the mining industry is proposed.

Particular attention should be paid to the section devoted to autonomous power supply systems, the implementation of which raises unsolved problems. Article by *Sergey S. Chervonchenko*, *Vladimir Ya. Frolov* is dedicated to solving the urgent problem of ensuring the reliability of power supply of remote consumers. In emergency conditions, it is proposed to use rechargeable batteries. In the article by *Vadim A. Shpenst et al.* an algorithm for the operation of an autonomous electrical complex with adaptive regulation is proposed, taking into account the mode of electricity consumption and emergency situations.

*Responsible scientific editors of the volume*: *Doctor of Engineering Sciences Yaroslav E. Shklyarskiy*, *Candidate of Engineering Sciences Aleksandr N. Skamyin*, *Doctor of Engineering Sciences Miguel Jiménez Carrizosa*

ISSN 2411-3336; e-ISSN 2541-9404

JOURNAL OF MINING INSTITUTE

Zapiski Gornogo instituta

Journal homepage: pmi.spmi.ru

Research article

# Energy efficiency of the linear rack drive for sucker rod pumping units

**Oksana Yu. GANZULENKO**✉, **Ani P. PETKOVA**
*Saint Petersburg Mining University, Saint Petersburg, Russia*

***How to cite this article*:** Ganzulenko O.Yu., Petkova A.P. Energy efficiency of the linear rack drive for sucker rod pumping units. Journal of Mining Institute. 2023. Vol. 261, p. 325-338. EDN HIGAOE

***Abstract.*** At present, in order to increase oil production and reduce economic costs in the development of marginal fields, the development of a cluster method using compact mobile drives of sucker rod pumping units (SRPU) is relevant. The aim of the work is to analyze the ways to improve the energy efficiency of the SRPU by reducing the loss of mechanical and electrical energy, to select the most energy-efficient compact drive for the development of marginal fields in the cluster method, to carry out the kinematic and strength calculations of the drive of the selected size, to develop an adaptive control system for a group of drives in the cluster development of drillings. According to the results of the performed calculations, the linear rack-and-gear drive has the highest efficiency of the drive mechanism. The kinematic and strength calculations of a linear rack-and-gear drive with a stroke length of 1120 mm and a load of up to 8 tons are presented. It was shown that the usage of a direct torque control system and a kinetic energy storage system for the SRPU drive elements and a rod string is an effective means of reducing energy costs in oil production from marginal fields. The use of the developed system for storing and redistributing the potential energy of the rods between the SRPUs that lift oil made it possible to eliminate fluctuations in the power consumption, reduce the power peak value by three times, the peak value of the current consumed from the electric network by two times, and reduce losses in the input converter and cables by three times.

***Keywords*:** energy efficiency; marginal fields; balanced pumping unit; chain vertical drive; hydraulic drive; linear rack-and-gear drive; performance coefficient

***Received: 15.03.2023*** ***Accepted: 20.06.2023*** ***Online: 19.07.2023*** ***Published: 19.07.2023***

**Introduction.** The oil and gas industry has remained one of the top priorities in the economic and industrial sector of Russia for a long time [1-3]. To maintain a stable growth in the production of hydrocarbon resources, it is necessary both to develop new fields, and to improve the existing technologies and create the new ones for extracting oil as well. However, it is more difficult to maintain such growth every year, old fields are being depleted and require more and more complex and expensive equipment to support the production process, but the discovery of new fields with easily recoverable reserves is declining [4-6]. Therefore, fields with hard-to-recover reserves (TRIZ) attract much attention. According to current data, the share of hard-to-recover reserves in the total oil reserve in May 2022 exceeded 66 % [7], which indicates their high importance in the country's energy balance. TRIZ can be divided into the following groups: high-viscosity oils [8-10]; low-permeability and low-porosity reservoirs [4, 11, 12]; depleted fields [5, 13, 14]; long-distance fields [3, 15, 16]; low-productive layers [17-19]. The latter are very popular in Russia due to the presence of large oil reserves and a more convenient geographical location [20].

To increase oil production and reduce economic costs, field development is carried out in clusters [21-23]. This cluster development is not a solution to the problem due to the use of sucker rod pumping units (SRPU), in which balanced and unbalanced pumping units (S-K) are used as drives, which are of little use in the development of marginal fields [24]. Let us consider and analyze methods for improving the energy efficiency of the development of marginal fields.

Mechanical drives SRPU currently used in oil production in our days are divided into balanced and unbalanced. In balancing drives (S-K), the reciprocating movement of the suspension point of the rods is carried out by a swinging lever – a balancer connected by a crank and rod mechanism (KShM) to the transmission shaft [25]. In unbalanced drives, the reciprocating movement of the suspension point of the rods is carried out by mechanisms using flexible elements (chains or ropes) [26]. Hydraulic and linear gearless drives SRPU are also known, drives based on linear motors, linear drives based on gear-rack and lead screw-nut systems [27, 28]. It is obvious that the performance coefficient of the mechanism depends on the level of losses in the structural elements of the drive and its kinematic scheme [26, 29, 30].

The sucker rod pumping unit receives mechanical energy from the line of rods, which performs reciprocating motion by means of the pumping unit drive. It converts the electrical energy supplied to the drive motor into mechanical energy. Thus, the energy efficiency of the SRPU directly depends on the amount of electrical and mechanical energy losses in various elements of the drive construction. The main ones include losses in the SRPU drive mechanism and electrical losses in the drive motor and start-up and control equipment.

The electrical energy consumed by the drive is highly dependent on power fluctuations in the drive motor cycle. So, during the S-K operation, significant fluctuations in the power consumption occur, which can change up to seven times in one cycle of the pump. For squirrel-cage induction motors used as a drive motor, power surges lead not only to significant voltage drops in the power system, but also to thermal and mechanical overloads of the motor.

The use of reversible rack and pinion linear and chain drives leads to additional losses in the motor and in the run-up control equipment during its start-up. To reduce these losses in the drive motor control system, it is necessary to use frequency converters and energy-efficient control algorithms. In addition to frequency control of the motor, when several pump drives work together during cluster well development, it is possible to use the kinetic energy of the rod moving down when oil is lifted [27]. Thus, the energy efficiency of the SRPU drive is determined by the losses of mechanical and electrical energy during operation.

The aim of the research is to analyze ways to improve the energy efficiency of sucker rod pumping units by reducing losses of mechanical and electrical energy, to select the most energy-efficient compact drive for the development of marginal fields in a cluster method, to carry out the kinematic and strength calculations of a drive with the selected size, and to develop an adaptive control system for a group of drives in cluster well development.

**Methods and materials.** The research methodology includes the following steps:

• selection of a compact drive for marginal fields with the highest performance coefficient of the drive mechanism;

• kinematic calculations of the drive for the selected standard size, allowing to determine the parameters of the gear train and the maximum allowable loads and restrictions on the speed of the rack movement (number of double strokes) for the selected motor-reducer;

• strength calculations for the bending of the pinion shaft teeth, allowing to choose the material and method of heat treatment of the pinion shaft and rack and surface hardening of the teeth, withstanding a load on the rod up to 80 kN;

• determination manufacturing sequence of the parts and the drive assembly, allowing to manufacture the developed drive with a load on the rod up to 80 kN;

• development of an adaptive control system (ACS) for a group of drives on a well pad with a down stem energy recovery system that reduces the energy consumption of the actuators by controlling the number of double strokes and rod stroke.

Estimation of mechanical energy losses in drives of various designs is performed by calculating their performance coefficient.

*Calculation of the SRPU drive mechanism performance coefficient.* A comparison of SRPU drives was made: based on a beam-balanced pumping unit, a vertical chain drive designed by RNTC VNIIneft [25], a linear drive based on a rack-toothed wheel system developed in the present research, a drive based on a screw-nut system, and a hydraulic drive.

We use a known data for a comparative analysis of the mechanical part of the drives performance coefficient. To calculate the performance coefficient of the drive mechanism, we will consider the mechanical power of the drive motor as the input power, and the mechanical power transmitted to the polished rod as the output. The drive performance coefficient is equal to the product of its components performance coefficients.

The kinematic scheme of the beam-balanced pumping unit is shown in Fig.1, *a* [30]. It consists of: balancer head (1); a balancer located on a pair of plain bearings (2); connecting rod-crank (3); connecting rod-crank support (4); V-belt drive (5, 6); three-stage gearbox (7), consisting of three pairs of cylindrical gears on rolling bearings (8, 10, 11); crank mechanism (9), consisting of pairs of sliding connecting rod-balancer.

The performance coefficient of the beam-balanced pumping unit is estimated by the formula

$$\eta_{SK} = \eta_{MC}\eta_{Vbd}\left(\eta_{RB}\eta_{SGD}\right)^{k}\eta_{CM}\eta_{PB},$$

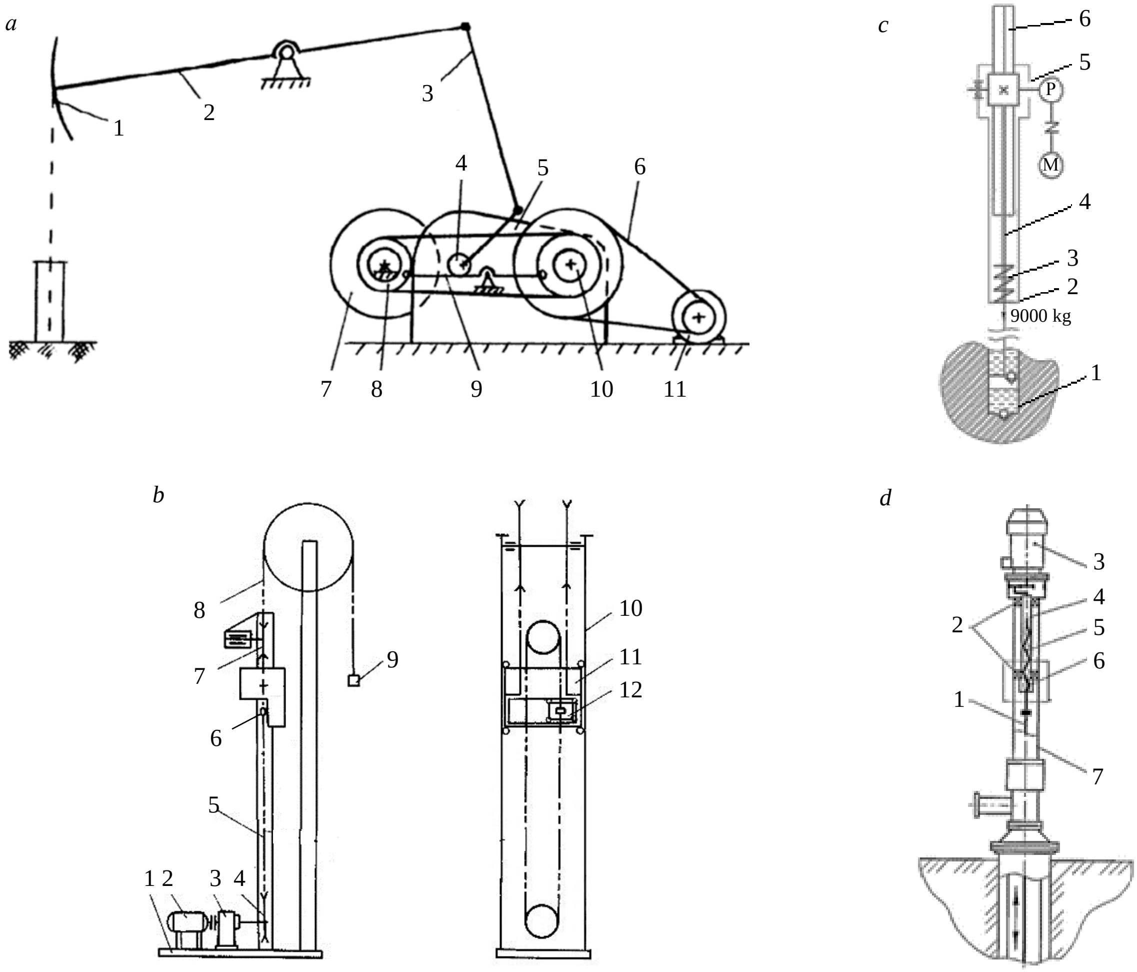


Fig.1. Kinematic scheme of a beam-balanced pumping unit (*a*), a drive with a movable carriage (*b*), a developed the linear rack-and-gear (*c*), a drive with a lead screw without reversing the drive motor (*d*)

where $\eta_{MC}$ – performance coefficient of the mechanical coupling, $\eta_{MC}$ = 0.98; $\eta_{Vbd}$ – performance coefficient of the V-belt drive, $\eta_{Vbd}$ = 0.96; $\eta_{RB}$ – performance coefficient of the rolling bearing, $\eta_{RB}$ = 0.992; $\eta_{SGD}$ – performance coefficient of the spur gear drive, $\eta_{SGD}$ = 0.97; *k* – number of gear stages, *k* = 3; $\eta_{CM}$ – performance coefficient of the crank mechanism, $\eta_{CM}$ = 0.98; $\eta_{PB}$ – performance coefficient of the plain bearings, $\eta_{PB}$ = 0.985*. After substituting the given average values, we obtain:

$$\eta_{sk} = 0.98 \cdot 0.96 \cdot (0.97 \cdot 0.992)^3 \cdot 0.98 \cdot 0.99 = 0.81,$$

that is in good agreement with the data value 0.80-0.85*.

The kinematic scheme of the SRPU chain drive design [25] is shown in Fig.1, *b*: 1 – frame; 2 – electric motor; 3 – reducer; 4 – drive pulley; 5 – continuous flexible link (chain); 6 – attachment point; 7 – guide element; 8 – open flexible link (chain or cables); 9 – a column of rods; 10 – rack; 11 – counterweight; 12 – carriage. The drive includes a mechanical coupling, a single-stage gearbox, a chain drive, a friction pair, a guide element – a carriage, and two rolling bearings that support the drive pulley.

The formula for calculating the performance coefficient of a chain drive has the form [25]:

$$\eta_{CD} = \eta_{MC} (\eta_{RB} \eta_{SGD})^K \eta_{OSD} \eta_{PB} \eta_{RB},$$

where $\eta_{MC}$ – performance coefficient of the mechanical coupling, $\eta_{MC}$ = 0.98; $\eta_{RB}$ – performance coefficient of the rolling bearing, $\eta_{RB}$ = 0.992; $\eta_{SGD}$ – performance coefficient of the spur gear drive, $\eta_{SGD}$ = 0.97; $\eta_{OSD}$ – performance coefficient of the open chain drive, $\eta_{OSD}$ = 0.92; $\eta_{PB}$ – performance coefficient of the plain bearings, $\eta_{PB}$ = 0.985.

After substituting the values, we get:

$$\eta_{CD} = 0.98 \cdot (0.97 \cdot 0.992)^1 \cdot 0.92 \cdot 0.985 \cdot 0.992 = 0.848.$$

The kinematic scheme of the developed linear rack-and-gear is shown in Fig.1, *c* in [31]. The drive contains a KAZ-97 bevel gearbox manufactured by SEW EURODRIVE, a rack and pinion system supported by a rolling bearing, a gearbox bearing (1 – base-support; 2 – damper; 3 – housing; 4 – rack; 5 – mechanism with gearbox and electric motor; 6 – cover-guide).

The formula for calculating the performance coefficient of the linear rack-and-gear is [30]:

$$\eta_{LRG} = \eta_{BG} \eta_{RB} \eta_{SGD},$$

где $\eta_{BG}$ – the performance coefficient the bevel gear, $\eta_{BG}$ = 0.965; $\eta_{RB}$ – performance coefficient of the rolling bearing, $\eta_{RB}$ = 0.992; $\eta_{SGD}$ – performance coefficient of the spur gear drive, $\eta_{SGD}$ = = 0.97 [25].

After substituting the values, we get:

$$\eta_{LRG} = 0.965 \cdot 0.97 \cdot 0.992 = 0.93.$$

The design of the drive based on the lead screw-nut system without reversing the drive motor is shown in Fig.1, *d* [27]: 1 – rod; 2 – bearing; 3 – motor-reducer; 4 – driven shaft; 5 – lead screw; 6 – nut; 7 – support.

The formula for calculating the transmission performance coefficient of the lead screw – nut system has the form [32]:

$$\eta_{SNS} = \eta_{PR} \eta_{RB} \eta_{RS},$$

where $\eta_{PR}$ – performance coefficient of the planetary gearbox, $\eta_{PR}$ = 0.96; $\eta_{RB}$ – performance coefficient of the rolling bearing, $\eta_{RB}$ = 0.992; $\eta_{RS}$ – roller screw, $\eta_{RS}$ = 0.89 [33].

After substituting the values, we get:

* Machine elements. URL: http://www.detalmach.ru/lect22.htm?ysclid=ley83k1mnn254975055 (accessed 22.05.2023).

$$\eta_{SNS} = 0.96 \cdot 0.89 \cdot 0.992 = 0.85.$$

The performance coefficient of the SRPU hydraulic drive depends on the applied hydraulic circuit and the level of leakage. Due to the complexity of the methods used, for a comparative assessment, we use the known values $\eta_{HP}$ = 0.91-0.75, depending on the level of leaks [34].

Based on the calculations, we choose a linear rack drive that has the highest efficiency among analogues.

Further, for the selected standard size of a linear rack-and-gear drive with a stroke length of 1120 mm and a load of up to 80 kN, a kinematic calculation was performed to determine the parameters of the gear train and the maximum allowable loads and restrictions on the rack movement speed (number of double strokes) for the selected gear motor.

*Kinematic drive calculation*. For calculations, the maximum stroke length of the rack ($L_0$ = = 1120 mm), the maximum speed of the rack and the loads acting on the rod ($F$ = 60 and 80 kN) are used. Kinematic calculation allows you to determine the linear speed of the rack, the number of double strokes per minute, select the diameter of the drive gear, the gear ratio of the gear-rack transmission, and select the gear motor.

The circumferential speed of rotation of the gear is equal to the linear speed of the rack [33]:

$$V_w = V_0 = \frac{\pi D n}{1000}, \tag{1}$$

where $D$ – gear wheel diameter, mm; $n$ – wheel gear frequency, $\text{min}^{-1}$.

We choose the tooth module of the gear wheel $m$ = 8 mm. In order to reduce torque, the number of teeth is taken as low as possible $Z$ = 14.

The gear wheel diameter is calculated by the formula [33]

$$D = mZ = 8 \cdot 14 = 112. \tag{2}$$

The gear wheel rotation frequency is determined from the formula (1):

$$n = \frac{V_0 \cdot 1000}{\pi D}. \tag{3}$$

According to the experimental data available for SRPU, the speed of movement of the rod is from 0.25 to 0.5 m/s or from 15 to 30 m/min.

The linear speed of the rod (rack) is determined by the formula [33]

$$V_0 = \frac{2 L_0 n_{ds}}{1000}, \tag{4}$$

where $L_0$ – rack stroke length; $n_{ds}$ – number of double strokes per minute,

$$n_{ds} = \frac{V_0 \cdot 1000}{2 L_0}. \tag{5}$$

For the speed of the rack in the range of 0.25-0.5 m/s, we determine the number of double strokes per minute (Table 1).

*Table 1*

**Calculated parameters of the drive with rack stroke length $L_0$ = 1120 mm**

| $V_0$ | | $n$, $\text{min}^{-1}$ | $n_{ds}$, min | $F$, кN | $P_1$, kW |
|---|---|---|---|---|---|
| m/s | m/min | | | | |
| 0.25 | 15 | 42.7 | 6.7 | 60 | 15 |
| | | | | 80 | 20 |
| 0.3 | 18 | 51.2 | 8 | 60 | 18 |
| | | | | 80 | 24 |
| 0.5 | 30 | 85.4 | 13.4 | 60 | 30 |
| | | | | 80 | 40 |

We determine the power of the drive motor by the formula [33]

$$P_1 = \frac{V_0 F}{1000}, \tag{6}$$

where $F$ – acting on the rod force, N; $V_0$ – rod stroke speed (rack), m/s.

For rack stroke speeds in the range of 0.25-0.5 m/s and rod load $F$ = 60-80 kN, the required drive motor power is presented in Table 1. The motor power values at $V_0$ = 0.3 m/s and load F = 60 and 80 kN are 18 and 24 kW, respectively.

We determine the torque of the gear motor by the formula [33]

$$M = \frac{DF}{2}. \tag{7}$$

At the load of 60 kN, we determine the torque $M$ = 3360 N/m.

The wheel gear rotation frequency $n$ equals to the speed of the output shaft $n_2$, it is calculated by the formula [33]

$$n_2 = \frac{n_1}{i}, \tag{8}$$

where $n_1$ – motor rotation speed; $i$ – reduction gear ratio.

Then for $V_0$ = 0.3 m/s and $F$ = 60-80 kN at the electric motor rotation speed $n_1$ = 1480 min$^{-1}$, the reduction gear ratio $i$ = 28.9, which should be taken into account when choosing a geared motor.

For this drive size $L_0$ = 1120 mm and $F$ = 60-80 kN, a SEWEURODRIVE KAZ-97 gear motor with $n_1$ = 1480 min$^{-1}$, $P_1$ = 22 kW, $i$ = 18.96, $n_2$ = 78 min$^{-1}$ was selected. For this gearbox, the permissible radial load is 19.4 kN. Service factor (service factor) $S_f$ = 1.35. Rated output torque $M_{n2}$ = 3210 N/m. Maximum output torque $M_{n2\max}$ = 4300 N/m. Dimensional characteristics of the reducer – hollow shaft with $d$ = 70 mm with a key.

Thus, the use of a motor with a power of 22 kW is possible with restrictions on the speed of the rack in the range of 0.25-0.3 m/min and a maximum allowable load of 73.3 kN. A speed of 0.5 m/s at a given load of 60-80 kN is possible when using a geared motor with a power of 30 kW or more. At a speed of 0.3 m/s and a load of 80 kN, the minimum power is 24 kW, the torque is 4480 N/m. The specified parameters of the motor-gearbox do not allow working with such load.

Then, the calculations are performed for the bending strength of the gear shaft teeth, based on the results of which the material and method of heat treatment and surface hardening of the teeth are selected.

*Calculation of drive elements for strength*. Calculation of gear wheel teeth for bending strength is carried out according to the formula

$$\sigma_F = \frac{P k_F y_F}{b_w m}, \tag{9}$$

where $P$ – circumferential force, N; $k_F$ – load distribution ratio; $y_F$ – tooth shape factor, depending on the number of teeth, with $Z$ = 14 $y_F \approx 3.9$; $b_w$ – ring gear width, $b_w$ = 139.5 mm; $m$ – gear wheel tooth module, $m$ = 8 mm.

The load distribution ratio is calculated by the formula [33]

$$k_F = k_{F\beta} k_{Fv}, \tag{10}$$

where $k_{F\beta}$ – ratio of uneven load distribution along the length of the tooth, with an almost symmetrical arrangement of supports and a ratio of width $b_w$ to diameter $D$ ($\psi_{bd}$ = 140/112 = 1.2) $k_{F\beta}$ = 1.14 (Table 2); $k_{Fv}$ – dynamic load factor, with 7th degree of accuracy and peripheral speed up to 3 m/s $k_{Fv}$ = 1.15 (Table 3); $k_F$ = 1.14 ·1.15 = 1.31.

*Table 2*

**The value of load uneven distribution ratio $k_{F\beta}$**

| $\psi_{bd} = \frac{b_w}{D}$ | The location of the wheels relative to the supports | | | |
|---|---|---|---|---|
| | Symmetrical | Asymmetrical | | Cantilevered |
| | | More hard shaft | Less hard shaft | |
| 0.2 | 1.00 | 1.00 | 1.05 | 1.15 |
| 0.4 | 1.00 | 1.04 | 1,10 | 1.22 |
| 0.6 | 1.03 | 1.08 | 1.16 | 1.32 |
| 0.8 | 1.06 | 1.13 | 1.22 | 1.45 |
| 1.0 | 1.10 | 1.18 | 1.29 | – |
| 1.2 | 1.14 | 1.23 | 1.36 | – |

*Table 3*

**The value of dynamic load factor $k_{Fv}$ for spur wheels**

| Degree of accuracy | Surface teeth hardness, HB | Peripheral speed *v*, m/s | | |
|---|---|---|---|---|
| | | Up to 3 | 3-8 | 8-12 |
| 6 | < 350 | 1.00 | 1.20 | 1.30 |
| | > 350 | 1.00 | 1.20 | 1.30 |
| 7 | < 350 | 1.15 | 1.35 | 1.45 |
| | > 350 | 1.15 | 1.25 | 1.36 |
| 8 | < 350 | 1.25 | 1.45 | – |
| | > 350 | 1.20 | 1.35 | – |
| 9 | < 350 | 1.35 | – | – |
| | > 350 | 1.30 | – | – |

With the base number of cycles, the permissible values of the bending strength are determined by the formula [33]

$$[\sigma]_F = \frac{\sigma_{F^o limb}}{[n]_{F'}[n]_{F''}}, \qquad (11)$$

where $\sigma_F{}^0{}_{limb}$ – stresses determined by the heat treatment mode, MPa; factor $[n]_F' = 1.75$ for steels after normalization, hardening with subsequent drawing and surface hardening, 1.8 – after bulk hardening and 1.55 – after carburizing and quenching; factor $[n]_F'' = 1$ for stamped, 1.15 for forged and 1.3 for cast parts.

$\sigma_F{}^0{}_{limb}$ values depends on technological parameters of the heat treatment: 1.8 HB – normalized wheels; 500-550 MPa – bulk hardening, HRCэ = 45-55; 700 MPa – surface hardening, HRCэ = 48-58; 900 MPa – carburizing and quenching, HRCэ = 57-60.

For a stamped wheel made of hardened with subsequent drawing steel of grade 40Cr with surface hardening $\sigma_F{}^0{}_{limb}$ = 700 MPa, for a stamped wheel made of 20Cr steel grade after carburizing $\sigma_F{}^0{}_{limb}$ = 900 MPa. Safety factor $[n]_F$ = 1.75 for steel after surface hardening and $[n]_F$ = 1.55 for carburized steel.

We calculate the allowable stress by the formula (11):

for steel grade 40Cr after surface hardening $[\sigma]_F$ = 700/1.75 = 400 MPa,

for steel grade 20Cr after carburizing and quenching $[\sigma]_F$ = 900/1.55 = 580 MPa.

The stress in the teeth are calculated according to the formula (9):

under $P = F = 60$ kN, $\sigma_F = \frac{60000 \cdot 1.31 \cdot 3.9}{139.5 \cdot 8} = 275$ MPa; $\sigma_F \le [\sigma]_F$;

under $P = F = 80$ kN, $\sigma_F = \frac{80000 \cdot 1.31 \cdot 3.9}{139.5 \cdot 8} = 367$ MPa; $\sigma_F \le [\sigma]_F$.

Thus, the selected module of hardened and tempered 40Cr steel with surface hardening withstands a load of up to 80 kN.

*The parts manufacturing process of the linear rack-and-gear drive with a stroke length of 1120 mm.* The necessary information for the components manufacture of the SRPU linear rack-and-gear drive elements is presented in Table 4.

*Table 4*

**Manufacturing technology and materials for linear rack-and-gear drive parts**

| Part name | Manufacturing type | Workpiece/Material |
|---|---|---|
| Rack – gear shaft (assembly) | | |
| Gear shaft | Milling processing | Steel 40CrNi |
| Rack | Milling processing | Steel 40Cr |
| Small lock | Milling processing | Plate 20/Steel 3 |
| Lock | Milling processing | Steel 45 |
| Hob | Turning processing | Steel 45 |
| Spacer | Turning processing | Steel 20 |
| Liner | Laser cutting | Sheet 2/Steel 10 |
| Housing (assembly) | | |
| Bottom wall | Milling processing | AlMg3 |
| Upper guiding rail | Milling processing | Steel 45 |
| Side guiding rail | Milling processing | Steel 45 |
| Guiding rack | Locksmith processing | CuZnPb 59-1 |
| Guiding bar | Locksmith processing | CuZnPb 59-1 |
| Left wall | Milling processing | AlMg3 |
| Right wall | Milling processing | AlMg3 |
| Upper wall | Milling processing | AlMg3 |
| Ring | Locksmith processing | Steel 45 |
| Substitute (welding) | | |
| Front wall | Laser cutting | Plate 20/Steel10 |
| Console | Locksmith processing | Plate 40/Steel 10 |
| Console | Locksmith processing | Pipe 80×50×3/Steel 10 |
| Bearings roller | Turning processing | Rolled bar 35/Steel 45 |
| Corner | Locksmith processing | Sheet 6/Steel 10 |
| Wall | Laser cutting and bending | Sheet 6/Steel 10 |
| Lug | Locksmith processing | Plate 20/Steel 3 |
| Column shaft (welding) | | |
| Wall | Laser and milling processing | Plate 25/Steel 10 |
| External compression spring | Finished product | |
| Internal compression spring | Finished product | |
| Pipe | Welding | Pipe 219×5 |
| Plate (disk) | Laser cutting | Plate 25/Steel 3 |
| Rod | Turning processing | Pipe 41×3.5 |
| Valve | Turning processing | Rolled bar 45/Steel 3 |
| Half cover left | Turning processing | CuZnPb 59-1 |
| Half cover right | Turning processing | CuZnPb 59-1 |
| Cup (welding) | | |
| Cup disk | Turning processing | Plate 25/Steel 3 |
| Cup pipe | Turning processing | Pipe 54×3 |
| Casing body (welding) | | |
| Wall | Laser cutting and bending | Sheet 2/ Steel 3 |
| Handle | Locksmith processing | Rolled bar 14/Steel 20 |
| Back wall | Laser cutting | Sheet 2/ Steel 3 |
| Flange (welding) | | |
| Bar | Laser cutting | Sheet 4/ Steel 10 |
| Bar | Laser cutting | Sheet 4/ Steel 10 |
| Bar | Laser cutting | Sheet 4/ Steel 10 |

*Drive assembly process* (Fig.2). The lower wall of the housing was installed on the gear motor (Fig.2, *a*). A bearing was pressed on the gear shaft (Fig.2, *b*), then it was installed into the gearbox, the side wall was screwed (Fig.2, *c*). Then, the guiding bar with the liner was installed in the housing (Fig. 2, *d*).

*Journal of Mining Institute*. 2023. Vol. 261. P. 325-338


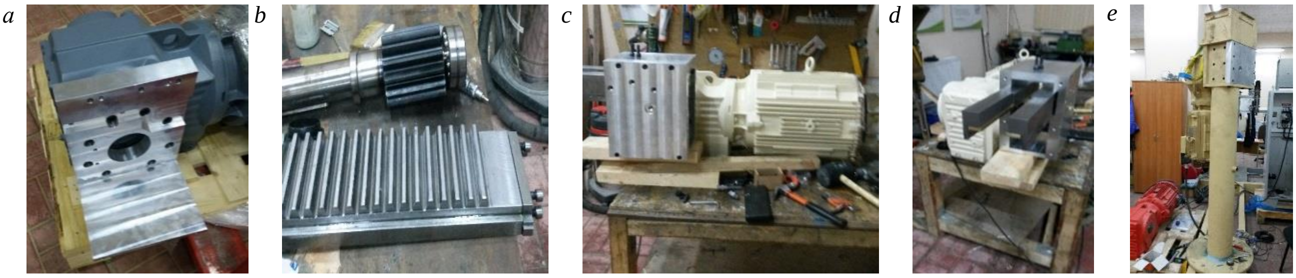


Fig.2. Stages of assembling a linear rack-and-gear drive (SRPU)

After that, the assembly of the column shaft was carried out (Fig.2, *e*). Springs and a cup were installed in it. Then the gearbox with the engine assembly was installed on the mounting platform, after that the holes in the column flange and the gearbox housing were combined, the substitute was installed on the gearbox housing, after that a gear rack was installed, which was turned over with the teeth down and moved along the guides until it stops, turning the shaft. The casing is installed on the substitute in a vertical position and is used in the complete set of the drive for testing on the well when protecting the mechanism from moisture and dust. When carrying out the research tests, the casing body was not installed to control visually the movements of the rack.

For the assembled drive, an adaptive control system for a group of drives on a well pad was developed with a system for recuperating the energy of the downward moving rod, which makes it possible to reduce the energy consumption of the drives by regulating the number of double strokes and the stroke of the rod.

Optimization of the oil production algorithms in terms of energy efficiency and consumption is based on mathematical modeling methods in the Simulink Power System Blockset simulation system. To create a model of the system, mathematical models of hydraulic and mechanical (system pump – rod string and SRPU drive), electrical (frequency converter, energy storage, and electric motor), electronic (regulator) components of a rod string were used [35]. The technique for developing a mathematical model of a column is presented in [36].

The adaptive ACS (automatic control system) of the drives group developed in this work generates commands for the frequency converter. The frequency converter generates a voltage of the required frequency and amplitude to the asynchronous motor power. The asynchronous electric motor connected to the gearbox through a clutch transmits torque to the rack-and-pinion mechanism, the rack is connected to the polished rod and imparts reciprocating motion to it. The kinetic energy of the downward moving rods is stored in a capacitor bank. The ACS distributes the accumulated energy between the drives when the formation fluid is lifted, provides optimal control in accordance with the well flow rate, controls the pump with optimal filling, provides programmatic hydraulic impact prevention, which improves the service life and reliability of the drive. The drives are connected to each other and to the capacitor bank by means of a DC link.

The developed adaptive scheme of the ACS, which controls the group of drives with energy recovery, and its implementation for two SRPU drives are shown in Fig.3, *a*. The experimental sample of the ACS has two channels for connecting two SRPU drives and is one common control and power box, which houses frequency converters (FC), a process controller and a DC link capacitor (Fig.3, *b*). This system also has power and information channels. The pump drives are considered as a part of the group as control objects with their own control systems, and their information channels are connected to a high-level control system through an information converter. In view of the fact that to improve the energy efficiency of oil production, the kinetic energy of the downward moving rod, accumulated in the capacitor bank, is used, the power channels of the SRPU drives are connected

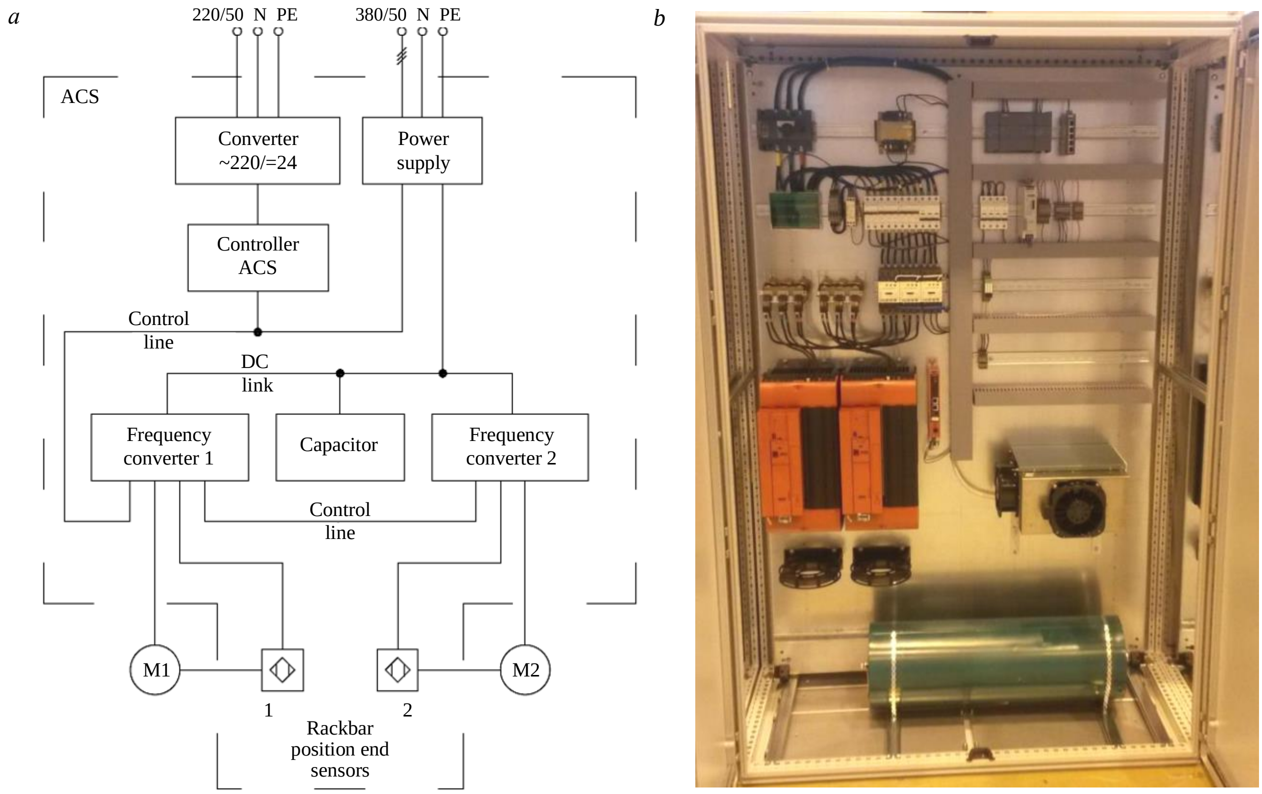


Fig.3. Functional electrical circuit of the ACS experimental sample (*a*); power supply and control box for the group of two SRPU drives (*b*)

to each other and the energy storage device through a DC link, and one of the ACS tasks is to distribute the accumulated energy between two drives.

**Discussion of the results.** The calculation analysis of the drives performance coefficient showed that the developed linear rack-and-gear drive has the highest efficiency among analogues. The compactness of the drive and the ability to install it directly at the wellhead can reduce operating costs and commissioning time, which also contributes to an increase in the economic efficiency of oil production.

For the drive size and for rod loads of 60-80 kN, a SEWEURODRIVE KAZ-97 was chosen the gear motor with $n_1$ = 1480 min$^{-1}$, $P_1$ = 22 kW, $i$ = 19, $n_2$ = 78 min$^{-1}$, $S_f$ = 1.35, $M_{n2}$ = 3210 N/m. The use of a 22 kW motor-reducer limits the rack stroke speed within 0.25-0.3 m/min and the allowable load is 73.3 kN. With designed loads of 60-80 kN, the rack stroke speed of 0.5 m/s is acceptable for motors with power of more than 30 kW. At speed of 0.3 m/s and a load of 80 kN, the minimum power is 24 kW, and at speed of 0.5 m/s and a load of 60 kN it is 30 kW.

For the selected motor-reducer with a power of 22 kW, with the rack stroke length unchanged, restrictions on the speed of movement of the rod or loads on the rod are possible by reducing the speed of the gear and the number of double strokes, as well as the speed of the rack. This can be achieved by reducing the frequency of the current supplied to the motor, which is achieved by using a frequency converter in the drive control system. The use of the frequency converter also allows frequency converter when stopping and changing the direction of movement and reducing inertial loads when reversing the direction of movement.

At speed of 0.3 m/s, load of 80 kN, and speed of 0.5 m/s, a load of 60 kN it is required to use a gearbox with larger dimensions than SEWEURODRIVE KAZ-97. A suitable option for these conditions is the Bonfiglioli A803 24.5 P200 BN200L4 geared motor with characteristics $P_1$ = 30 kW, $n_1$ = 1470 min$^{-1}$, $n_2$ = 60 min$^{-1}$, $M_{n2}$ = 4377 N·m, $S_f$ = 1.5, radial load on the output shaft $R_{n2}$ = = 4330 N.

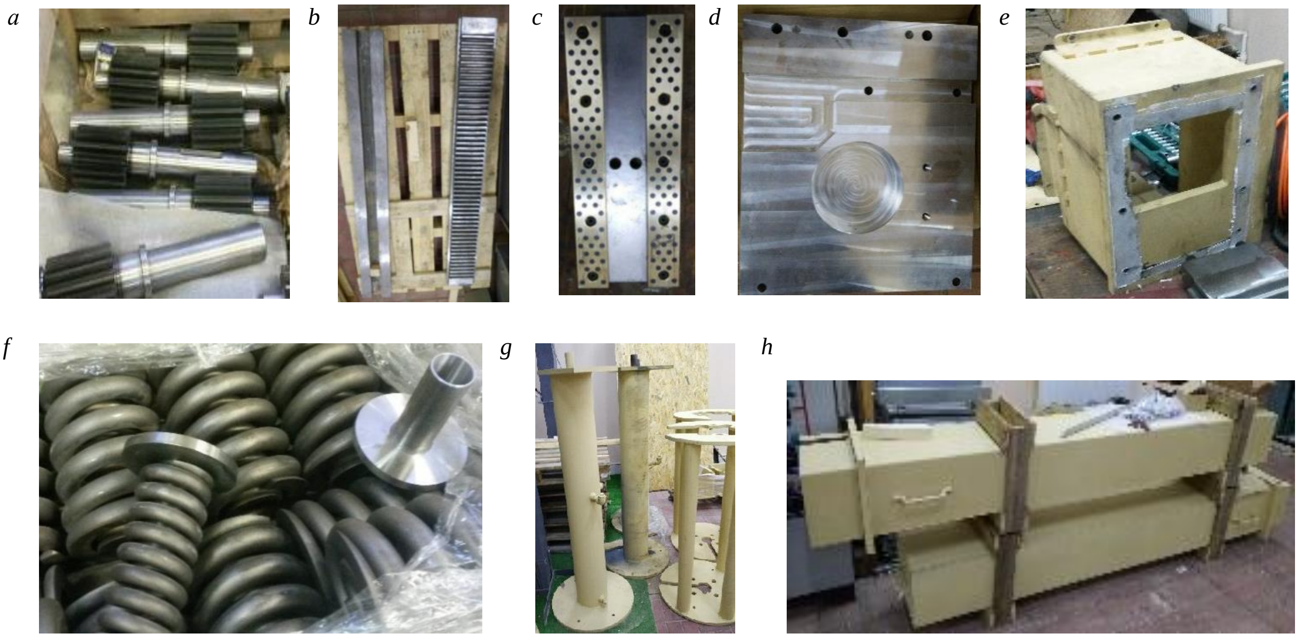


Fig.4. Assembly units of the linear rack-and-gear drive SRPU

Based on the results of the calculation for the bending strength of the teeth, a gear shaft made of tempered steel 40CrNi with surface hardening of the teeth was selected, which can withstand load up to 80 kN. Also, taking into account the calculations, materials and manufacturing technologies for the remaining components and parts of the drive were selected, and technological parameters of heat treatment were selected. Photos of some parts are shown in Fig.4: gear shaft (steel 40CrNi, tempered + the teeth surface hardened with high frequency currents (HFC) (Fig.4, *a*), gear rack (steel 40Cr, tempered, Fig.4, *b*), housing parts with liners made of brass CuZnPb 59-1 and walls made of aluminum alloy AlMg3 (Fig.4, *c*, *d*). The column shaft, casing body, substitute, and cup are welded constructions made of carbon steels.

Also, mechanical (turning and milling) processing and heat treatment (normalization) of parts (small lock, lock, hob and spacer in accordance with Table 4) for assembling a rack with the gear shaft and laser cutting of liner parts (Fig.4, *c*) was done. Fine machining of casing body parts (Fig.4, *d*) was carried out in accordance with Table 4. For the manufacture of the substitute (Table 4) the finishing machining, laser cutting, and welding of parts were performed (Fig.4, *e*).

Manufactured and heat-treated springs are shown in Fig.4, *f*. For the manufacture of the column shaft and the cup the laser cutting, turning and milling, and then welding of the parts were performed (Table 4). The column assembly with the cup and springs installed inside is shown in Fig.4, *g*. For the casing body manufacture the laser cutting, bending, and welding of parts were performed (Table 4), finished casings are shown in Fig.4, *h*.

Figure 5 shows the assembly of linear rack-and-gear drive with a stroke length of 1200 mm and a rod load of up to 80 kN, mounted on a test bench for testing at idle. The asynchronous electric motor transmitting torque to the rack-and-gear mechanism is connected through an elastic coupling to a gearbox that transmits reciprocating motion to the pump rod. The rack-and-pinion linkage consists of a toothed rack mounted on column and gear shaft that moves in the vertical direction to provide reciprocating motion of the pump rods. The toothed rim of the gear shaft during the electric motor rotation, being engaged with the toothed rack, moves it vertically upwards on the forward stroke, and vertically downwards during the reverse rotation of the motor on the reverse stroke.

The toothed rack stand at the upper end is rigidly connected to the rod column shaft by means of a cleet, which ensures the transmission of force from the drive to the rod string. In the U-shaped toothed rack stand, along the axis of the pump stroke, there is a longitudinal open channel for moving the rod inside the stand.

 

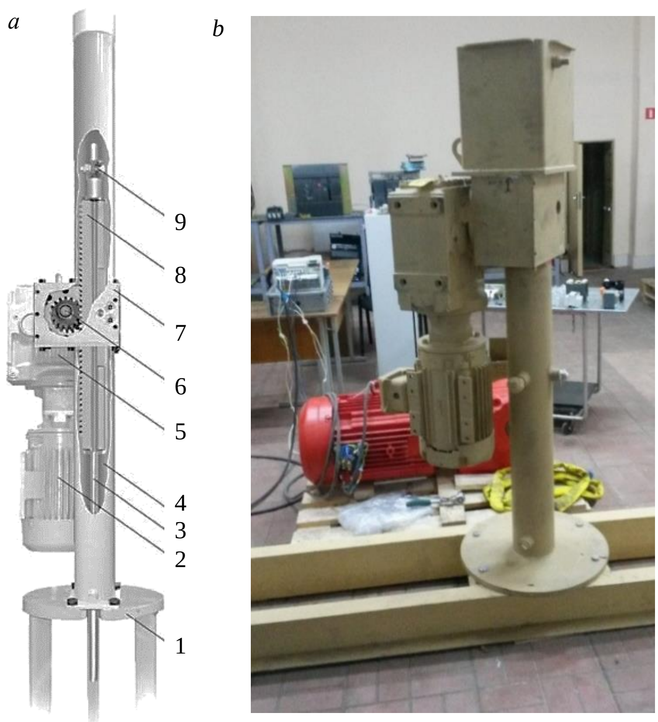


Fig.5. Design (*a*) and manufactured rack-and-gear drive assembly (*b*)

1 – basement; 2 – asynchronous electric motor; 3 – polished rod; 4 – oil bath; 5 – reducer; 6 – gear and axle; 7 – mechanism case; 8 – gear rack; 9 – rod holder

Under the bottom edge of the drive stand there is a lubrication oil pan that sinks the bottom of the stand to provide lubrication during each stroke. The lubrication pan is an annular cavity formed by two pipes hermetically connected at the bottom, filled with grease, which is pumped into the upper part of the cavity. The inner tubular wall of the pan is located around the wellhead and fits freely inside the hole of the rack to provide movement, and the outer wall of the tubular pan is located around the rack. The drive also contains a spring located inside the cavity in the pan under the lower edge of the stand for braking the rack when the pump moves down and accelerating the rack during the forward stroke of the pump up.

When the stand moves up the microprocessor control system of the linear rack-and-gear drive ensures the operation of the electric motor in the driving mode, and when it is moving down – in the braking mode (generator mode). The pump drives operating in the well cluster are connected by a DC link, to which a high-capacity capacitor bank is connected to accumulate and store the energy generated in the generator mode during the downward stroke of the rod. The accumulated energy is consumed by the electric motor in the forward stroke of the rod up during operation in the driving (loaded) mode. The microprocessor control system, which selects the pumping intensity for each pump, regulates the consumption of stored energy for lifting oil, which makes it possible to use electricity more economically.

To implement energy-efficient control of a group of drives on a cluster of closely spaced wells with energy recovery, an adaptive automatic control system is proposed that includes an input converter, a controlled current source that provides processes for charging and discharging a high-capacity capacitor (rod energy storage) and issuing commands to start and stop the drives included in the group, work in driving and generator modes. The proposed adaptive ACS makes it possible to implement algorithms for energy-efficient control of groups of SRPU drives, which reduce fluctuations in power consumption and current by choosing the plunger speed, the number of SRPU swings, and the duration of the pause between them in accordance with the flow rate of wells.

The most effective electrical way to increase performance coefficient is to use the developed system for storing and redistributing the potential energy of rods between SRPUs that lift oil. This made it possible to eliminate fluctuations in power consumption, reduce its peak value by three times, the peak value of the current consumed from the network by two times, and reduce losses in the input converter and cables by three times.

The use of an energy recovery system allows us to decrease capital costs by reducing the cross-section of network cables, using an input transformer or a lower power diesel generator set in case of autonomous power supply to a group of drives.

Thus, usage of a direct torque control system and a kinetic energy storage system for SRPU drive elements and a rod column are an effective tool for reducing energy costs in oil production from marginal fields.

**Conclusion.** The analysis of ways for improving the energy efficiency of sucker rod pumps by mechanical means has been carried out. It is shown that the most effective mechanical way to increase the performance coefficient is to use a linear rack-and-gear drive of the developed design, which makes it possible to increase the set up performance coefficient by 10 % compared to analogues. It is necessary to take into account the fluctuations in power consumption existing in the cycle of operation of the electric motor of the drive, leading to a decrease in the performance coefficient of the electric motor. Kinematic and strength calculations of a linear rack-and-gear drive with a stroke length of 1120 mm and a load of up to 80 kN are performed, the processes of its manufacture, heat treatment of parts and assembly are described. The drive was assembled and tested at idle.

The developed group energy-efficient mobile drives of the SRPU and adaptive automatic control systems are designed to equip the "clusters" of wells in oil fields with modern domestic energy-saving equipment for oil production to replace obsolete and worn-out equipment, as well as for import substitution of the equipment.

With sufficiently large production volumes overall energy efficiency and a reduction in capital and operating costs can bring significant economic benefits, and the payback period for group ACS can be no more than a year due to the possibility of equipping group ACS with any type of SRPU drives. The energy efficiency of oil production will increase, the cost of well construction will decrease, the environmental load on oil production zones will decrease, the overall level of production automation and the technological culture of oil production as a whole will increase.

## REFERENCES

1. Korolev N., Kozyaruk A., Morenov V. Efficiency Increase of Energy Systems in Oil and Gas Industry by Evaluation of Electric Drive Lifecycle. *Energies*. 2021. Vol. 14. Iss. 19. N 6074. DOI: 10.3390/en14196074

2. Zakaev D., Nikolaichuk L., Filatova I. Problems of Oil Refining Industry Development in Russia. *International Journal of Engineering Research and Technology*. 2020. Vol. 13. N 2, p. 267-270. DOI: 10.37624/IJERT/13.2.2020.267-270

3. Samylovskaya E., Makhovikov A., Lutonin A. et al. Digital Technologies in Arctic Oil and Gas Resources Extraction: Global Trends and Russian Experience. *Resources*. 2022. Vol. 11. Iss. 3. N 29. DOI: 10.3390/resources11030029

4. Tananykhin D., Palyanitsina A., Rahman A. Analysis of Production Logging and Well Testing Data to Improve the Development System for Reservoirs with Complex Geological Structure. *Procedia Environmental Science, Engineering and Management*. 2020. Vol. 7. N 4, p. 629-648.

5. Korolev M., Rogachev M., Tananykhin D. Regulation of filtration characteristics of highly watered terrigenous formations using complex chemical compositions based on surfactants. *Journal of Applied Engineering Science*. 2020. Vol. 18. Iss. 1, p. 147-156. DOI: 10.5937/jaes18-24542

6. Mardashov D., Duryagin V., Islamov S. Technology for Improving the Efficiency of Fractured Reservoir Development Using Gel-Forming Compositions. *Energies*. 2021. Vol. 14. Iss. 24. N 8254. DOI: 10.3390/en14248254

7. Prischepa O., Nefedov Y., Nikiforova V., Xu Ruiming. Raw material base of Russia's unconventional oil and gas reserves (hydrocarbons shale strata). *Frontiers in Earth Science*. 2022. Vol. 10. N 958315. DOI: 10.3389/feart.2022.958315

8. Jie Yu, Hongping Quan, Shihao Chang, Zhiyu Huang. Research on a fluorine-containing asphaltene dispersant and its application in improving the fluidity of heavy oil. *Journal of Molecular Liquids*. 2023. Vol. 375. N 121318. DOI: 10.1016/j.molliq.2023.121318

9. Lei He, Yong Dai, Jingjie Hou et al. MXene based immobilized microorganism for chemical oxygen demand reduction of oilfield wastewater and heavy oil viscosity reduction to enhance recovery. *Journal of Environmental Chemical Engineering*. 2023. Vol. 11. Iss. 2. N 109376. DOI: 10.1016/j.jece.2023.109376

10. Anqi He, Junjian Li, Mengchen Jiang et al. Study of cyclic waterflooding for improving oil recovery in Lukeqin heavy oil reservoir. *Geoenergy Science and Engineering*. 2023. Vol. 223. N 211467. DOI: 10.1016/j.geoen.2023.211467

11. Wan-Li Kang, Bo-Bo Zhou., Issakhov M., Gabdullin M. Advances in enhanced oil recovery technologies for low permeability reservoirs. *Petroleum Science*. 2022. Vol. 19. Iss. 4, p. 1622-1640. DOI: 10.1016/j.petsci.2022.06.010

12. Chunxue Cui, Zhijun Zhou, Ziang He. Enhance oil recovery in low permeability reservoirs: Optimization and evaluation of ultra-high molecular weight HPAM/phenolic weak gel system. *Journal of Petroleum Science and Engineering*. 2020. Vol. 195. N 107908. DOI: 10.1016/j.petrol.2020.107908

13. Pothula G.K., Vij R.K., Bera A. An overview of chemical enhanced oil recovery and its status in India. *Petroleum Science*. 2023. DOI: 10.1016/j.petsci.2023.01.001

14. Bera A., Vij R. K., Shah S. Impact of newly implemented enhanced oil and gas recovery screening policy on current oil production and future energy supply in India. *Journal of Petroleum Science and Engineering*. 2021. Vol. 207. N 109196. DOI: 10.1016/j.petrol.2021.109196

15. Zhijuan Zhao, Yan Li, Yougang Tang, Xinjie Ji. Conceptual design and numerical analysis of a novel platform for marginal oilfields development. *Ocean Engineering*. 2019. Vol. 187. N 106145. DOI: 10.1016/j.oceaneng.2019.106145

16. Dmitrieva D., Romasheva N. Sustainable Development of Oil and Gas Potential of the Arctic and Its Shelf Zone: The Role of Innovations. *Journal of Marine Science and Engineering*. 2020. Vol. 8. Iss. 12. N 1003. DOI: 10.3390/jmse8121003

17. Peng Fei, Luo Dongkun, Yin Chengfang et al. Tight Oil Accumulation Characteristics and Resource Potential Evaluation of the Xiagou Formation in Qingxi Depression, Jiuquan Basin. *Energy Procedia*. 2019. Vol. 158, p. 5940-5945. DOI: 10.1016/j.egypro.2019.01.528

18. Jingwei Cui, Rukai Zhu, Sen Li et al. Development patterns of source rocks in the depression lake basin and its influence on oil accumulation: Case study of the Chang 7 member of the Triassic Yanchang Formation, Ordos Basin, China. *Journal of Natural Gas Geoscience*. 2019. Vol. 4. Iss. 4, p. 191-204. DOI: 10.1016/j.jnggs.2019.08.002

19. Leusheva E., Brovkina N., Morenov V. Investigation of Non-Linear Rheological Characteristics of Barite-Free Drilling Fluids. *Fluids*. 2021. Vol. 6. Iss. 9. N 327. DOI: 10.3390/fluids6090327

20. Mukhametshin V.Sh., Andreev A.V., Akhmetov R.T. Increase of resourse base usage efficiency in hard removable oil fields. *Petroleum Engineering.* 2015. Vol. 13. N 4, p. 122-125 (in Russian).

21. Wen-Jun Huang, De-Li Gao. Analysis of drilling difficulty of extended-reach wells based on drilling limit theory. *Petroleum Science*. 2022. Vol. 19. Iss. 3, p. 1099-1109. DOI: 10.1016/j.petsci.2021.12.030

22. Abramov A. Agile methodology of well pad development. *Journal of Petroleum Exploration and Production Technology*. 2020. Vol. 10. Iss. 8, p. 3483-3496. DOI: 10.1007/s13202-020-00993-3

23. Abramov A. Optimization of well pad design and drilling – well clustering. *Petroleum Exploration and Development*. 2019. Vol. 46. Iss. 3, p. 614-620. DOI: 10.1016/S1876-3804(19)60041-8

24. Urazakov K.R., Molchanova V.A., Tugunov P.M. Method for calculating dynamic loads and energy consumption of a sucker rod installation with an automatic balancing system. *Journal of Mining Institute*. 2020. Vol. 246, p. 640-649. DOI: 10.31897/PMI.2020.6.6

25. Valovskij V.M., Akhunov R.M., Manko M.I., Fedoseenko N.V. Patent N 2150607 RF. Oil-well sucker-rod pump drive. Publ. 10.06.2000. Bul. N 16.

26. Dmitriev D.V., Fadeev V.G., Sadykov A.F., Ermakov R.A., Kashapov R.R., Novikov N.V. Patent N 2482332 RF. Beamless pumping unit. Publ. 20.05.2013. Bul. N 14.

27. Beck T.L., Anderson R.G., Peterson R.G., MacDonald M.A. Patent N 8152492 U.S. Linear Rod Pump Apparatus and Method. Publ. 10.04.2012.

28. A.Kurkov. Patent N 20200224651 U.S. Linear rack drive for submersible rod pump for oil production. Publ. 16.07.2020.

29. Sivenkov A.V., Chirkova O.S., Konchus D., Mikhailov A.V. Development of Flux for Protection of the Surface of Liquid-Metallic Low-Melting-Point Fusible Melt. *Key Engineering Materials*. 2020. Vol. 854, p. 126-132. DOI: 10.4028/www.scientific.net/KEM.854.126

30. Mukhametshin H.N. Application for an invention № 94039340 RF. Beam-balanced pumping unit. Publ. 20.08.1996.

31. Petkov P.P., Petkova A.P., Brunman V.E., Volkov A.N., Kochneva O.V., Balabanov K.V. Patent N 167305 RF. Linear drive of the sucker rod pumping unit. Publ. 27.12.2016. Bul. N 36.

32. Mehdiyev K.K. Evaluation of the Efficiency of Operation of Barbed Depth Pumps on Marine Deposits in the Conditions of Intensive Sand and Water Management. *Socar Proceedings.* 2019. N 4, p. 53-60. DOI: 10.5510/OGP20190400411

33. Artykaeva E.M. Energy-saving electrical equipment of oil-producing installations with a plunger submersible pump: Avtoref. dis. kand. tekhn. nauk. Cheboksary: Chuvashskii gosudarstvennyi universitet im. I.N.Ulyanova, 2012, p. 21 (in Russian).

34. Ivanovskii V.N. Energy of oil production: main directions of energy consumption optimization. *Inzhenernaya praktika*. 2011. N 6, p. 18-26.

35. Lysenko V.D., Graifer V.I. Development of marginal oil fields. Moscow: Nedra-Biznestsentr, 2001, p. 562 (in Russian).

36. Brunman V.E., Vataev A.S., Volkov A.N. et al. Optimizing Pump-Drive Operation to Improve the Energy-Efficiency of Oil Extraction. *Russian Engineering Research*. 2017. Vol. 37. N 6, p. 479-484. DOI: 10.3103/S1068798X17060089

***Authors:*** **Oksana Yu. Ganzulenko,** *Candidate of Engineering Sciences, Associate Professor, Ganzulenko_OY@pers.spmi.ru, https://orcid.org/0000-0001-7415-2996* (*Saint Petersburg Mining University, Saint Petersburg, Russia*), **Ani P. Petkova,** *Doctor of Engineering Sciences, Professor, https://orcid.org/0000-0001-6728-4579* (*Saint Petersburg Mining University, Saint Petersburg, Russia*).

*The authors declare no conflict of interests.*

ISSN 2411-3336; e-ISSN 2541-9404

JOURNAL OF MINING INSTITUTE

Zapiski Gornogo instituta

Journal homepage: pmi.spmi.ru

Research article

# A complex model of a drilling rig rotor with adjustable electric drive

**Mikhail S. ERSHOV**✉, **Aleksandr N. KOMKOV**, **Evgeniy A. FEOKTISTOV**
*National University of Oil and Gas "Gubkin University", Moscow, Russia*

***How to cite this article*:** Ershov M.S., Komkov A.N., Feoktistov E.A. A complex model of a drilling rig rotor with adjustable electric drive. Journal of Mining Institute. 2023. Vol. 261, p. 339-348. EDN YEEWZJ. DOI: 10.31897/PMI.2023.20

***Abstract*.** A modified mathematical model of an asynchronous electric drive of the rotor – a drill string – a bit – a rock is considered and implemented, which develops and generalizes the results of previously performed studies. The model includes the following subsystems: a model of an asynchronous drive with vector control; a model of formation of the resistance moment at the bottom of the bit, taking into account the peculiarities of the interaction between the bit and the rock; a model of a multi-mass mechanical part that takes into account the deformation of the drill string; subsystem for the drilling rig energy-technological parameters formation. The integrated model makes it possible to calculate and evaluate the selected drilling modes, taking into account their electro-mechanical, energy and technological efficiency and the dynamics of drilling processes. The performed computer simulation of drilling modes confirmed the possibility of a stick-slip effect accompanied by high-frequency vibrations during bit stops, which may change the direction of rotation of the bit, its accelerated wear and unscrewing of the drilling tool. Long bit stops lead to a significant decrease in the average bit rotation speed, which can explain the decrease in the ROP and increase in energy consumption when drilling in the zone of unstable bit rotation. The model can be used as a base for further improvement of rotary drilling control systems.

***Keywords*:** asynchronous adjustable electric drive; drilling rig rotor; drilling modes; stick-slip effect; energy efficiency

***Received: 13.10.2022*** ***Accepted: 13.12.2022*** ***Online: 10.03.2023*** ***Published: 19.07.2023***

**Introduction.** The drilling rig rotor with electric drive is distinguished by a complex mechanical part (Fig.1). The rotation of the motor rotor through the transmission device is transmitted to the rotor of the drilling rig and through the drill pipes column (DPC) – to the bit. By drilling rig rotor moment, applied to the top of the string, and the bit moment of resistance, applied to the bottom of the string, drill pipes are deformed and twisted at a certain angle, the value of which depends on the length, diameter and elastic properties of the string and can reach tens of revolutions. During the drilling process, the twist angle can remain practically unchanged, while the bit rotates uniformly. When the angle of twist changes during the drilling process, an uneven, unstable rotation of the bit occurs (stick-slip effect) with long stops, immersions in the rock and bit breaks, as well as the appearance of torsional and longitudinal self-oscillations of the drilling tool [1]. This mode occurs when working with PDC bits of the cutting-attrition type especially often (more than 50 % of the drilling time). Unstable bit rotation modes can prevail during well drilling [2, 3], reducing the energy efficiency of drilling and accelerating the drilling tools wear [4, 5]. This work is dedicated to creation a complex model of a drilling rig with an asynchronous electric drive of the rotor – a drill string – a bit – rock, simulating the main processes of electric rotary drilling, with a set of characteristics for analyzing the electro-mechanical, energy and technological efficiency of drilling modes. The results of the work develop the earlier studies results [6-8].

EDN YEEWZJ
DOI: 10.31897/PMI.2023.20

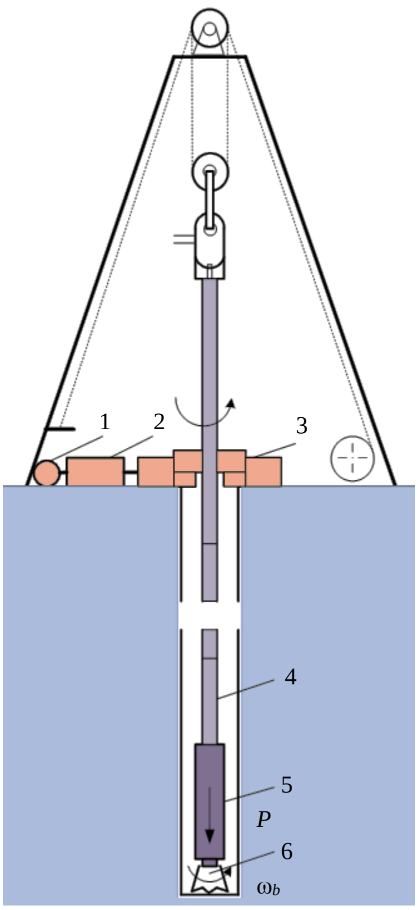


Fig.1. Drilling rig scheme

1 – rotor drive; 2 – transmission devices; 3 – drilling rig rotor; 4 – drill pipe string; 5 – column bottom layout; 6 – drilling bit

**Methodology.** Modeling of the asynchronous the drilling rig electric drive was carried out in the Matlab Simulink environment. The block diagram of the base model is shown in Fig.2. The model includes the following main subsystems: IM-Subsystem – a model of an asynchronous motor with a vector control system based on PI flux linkage, speed and current controllers; Meh-Subsystem – a model of the mechanical part of the electric drive, including a motor rotor, a drilling rig rotor, transmission mechanisms and a drill string; dual-mass model of the rotor drive mechanical part is shown in Fig.3; $T_{b0}$-Subsystem, $T_{b1}$-Subsystem, $T_b$-Subsystem – subsystems of the drag moment model on the bit; ETP-Subsystem – a subsystem for the formation of energy-technological drilling parameters.

The main nominal parameters of the AFD series rotor drive asynchronous motor are as follows: power 1000 kW; voltage 660 V; current 1075 A; torque 9620 N·m; speed 993 rpm.

"Motor modeling was carried out in coordinates ($x$, $y$), the rotation speed of which is equal to the rotation speed of the stator field ($\omega_\kappa = \omega_1$), with the base voltage vector ($uS_x = U_1$; $uS_y = 0$)" [7]. The mathematical model of the engine is represented by the following system of equations in operator form*:

$$\begin{aligned}
U_1 &= r(1+T_S's)i_{Sx} - \omega_1 L_S' i_{Sy} - (k_R/T_R)\psi_{Rx} - k_R p\omega_m \psi_{Ry};\\
0 &= r(1+T_S's)i_{Sy} + \omega_1 L_S' i_{Sx} - (k_R/T_R)\psi_{Ry} + k_R p\omega_m \psi_{Rx};\\
0 &= -k_R R_R i_{Sx} + (1/T_R + s)\psi_{Rx} - (\omega_1 - p\omega_m)\psi_{Ry};\\
0 &= -k_R R_R i_{Sy} + (1/T_R + s)\psi_{Ry} + (\omega_1 - p\omega_m)\psi_{Rx};\\
T_m &= 1.5p(\psi_{Rx} i_{Sy} - \psi_{Ry} i_{Sx}),
\end{aligned} \qquad (1)$$

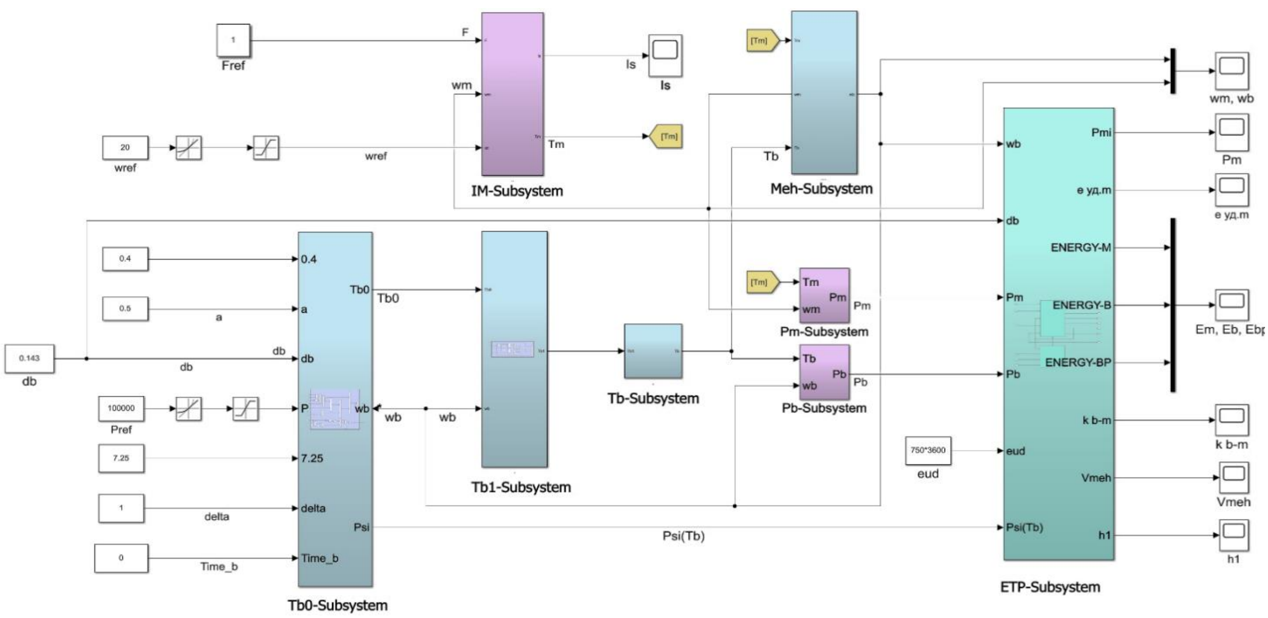


Fig.2. Structural diagram of the drilling rig rotor with asynchronous drive

* German-Galkin S.G. Matlab & Simulink. Design of machatronic systems on PC. St. Petersburg: Korona-Vek, 2020, p. 368.

EDN YEEWZJ
DOI: 10.31897/PMI.2023.20




where $\omega_1$ = 104.7 $s^{-1}$ is the synchronous speed; $p$ = 3 is the pole pairs number; $\omega_m$ – motor shaft speed; $\psi_{Rx}$, $\psi_{Ry}$ – rotor flux linkage along the axes $x$, $y$; $\psi_{Sx}$, $\psi_{Sy}$ – stator flux linkage along the axes $x$, $y$; $i_{Rx}$, $i_{Ry}$ – rotor currents along the axes $x$, $y$; $i_{Sx}$, $i_{Sy}$ – stator currents along the axes $x$, $y$; $T_m$ – motor moment; $s$ – operator; $R_R$, $R_S$ – rotor and stator active resistances; $L_m$, $L_R$, $L_S$ – rotor and stator mutual and self-inductance; $T_R = L_R/R_R$ – rotor time constant; $T'_S = L'_S / r$ – stator time constant; $r = R_S + + k_r^2 R_R$; $k_r = L_m/L_R$; $L'_S = L_S - - L_m^2/L_R$.

The parameters included in the equations of system (1) are as follows: $R_R$ = 0.00267 Ω; $r$ = 0.939 Ω; $k_r$ = = 0.939; $L'_S$ = 0.00034 H; $T'_S$ = 0.068 s; $T_R$ = 1.064 s.

Determination of motor parameters – active resistances, inductances and time constants, as well as parameters of PI controllers – was carried out according to the following methods [8-10]. In the parallel form of writing the transfer function expression, the parameters of the flux linkage PI controller were $P_\psi$ = 410, $I_\psi$ = 14. The PI controllers parameters of speed and current, tuned to the technical optimum were: $P_\omega$ = 166, $I_\omega$ = 16.5 (for speed controller) and $P_I$ = 3, $I_I$ = 10 (for current controller).

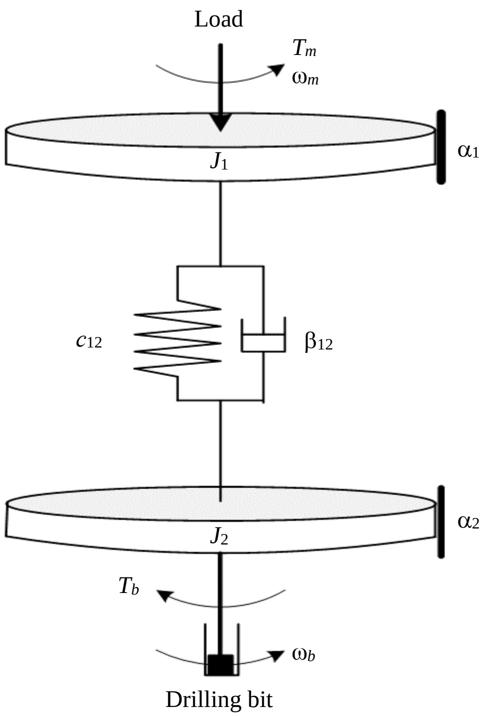


Fig.3. Dual-mass model of rotor drive mechanical part

The mechanical part of the electric drive is implemented in the form of multi-mass (from two to four masses) equivalent systems in the Meh-Subsystem block. The initial data for modeling correspond to a drilling rig of the BU-5000/320 type. The length of the drill pipe string is assumed to be 3000 m, the pipe diameter $d_t$ = 0.127 (wall thickness 0.09 m), the layout of the bottom of the DPC is made of UBT pipes 203×80 (90 m), the bit diameter $d_t$ = 0.295 m (PDC bit 295.3FD257M-A27). The mathematical model of a dual-mass mechanical system in operator form is represented by the following system of equations:

$$s\omega_m J_1 = T_m - \left(\frac{c_{12}}{s} + \beta_{12}\right)(\omega_m - \omega_b) - T_{r1};$$

$$s\omega_b J_2 = \left(\frac{c_{12}}{s} + \beta_{12}\right)(\omega_m - \omega_b) - T_b,$$

where $\omega_b(t)$ – bit rotation speed, rad/s; $T_{r1}$ – moment of resistance of the first mass, N·m; $T_b$ – moment of resistance applied to the second mass (torque on the bit), N·m; $T_{r1}$ – first mass resistance moment, determined by the product of the external viscous friction α coefficient on engine speed $\omega_m$.

Estimated moments of inertia of the two-mass system elements: $J_1$ = 66.5, $J_2$ = 12.5 kg·m$^2$; stiffness factor $c_{12}$ = 22.8 N·m/rad; viscous friction coefficient $\beta_{12}$ = 0.06 N·m·s/rad; external viscous friction coefficient α = 0.5 N·m·s/rad.

The formulation of operator equations for a three- and four-mass system also does not cause difficulties. Estimated three-mass system elements moments of inertia are: $J_1$ = 55, $J_2$ = 17, $J_3$ = 7 kg·m$^2$; stiffness coefficients $c_{12}$ = 25, $c_{23}$ = 263 N·m/rad; viscous friction coefficients: $\beta_{12}$ = = $\beta_{23}$ = 0.03 N·m·s/rad. Estimated four-mass system elements moments of inertia are: $J_1$ = 55, $J_2$ = 8.5, $J_3$ = 8.5 kg·m$^2$; stiffness coefficients $c_{12}$ = 50, $c_{23}$ = 50, $c_{34}$ = 263 N·m/rad; viscous friction coefficients $\beta_{12}$ = $\beta_{23}$ = $\beta_{34}$ = 0.02 N·m·s/rad. All parameters of the mechanical system are given to the motor rotation speed.

EDN YEEWZJ
DOI: 10.31897/PMI.2023.20

The determination of the moment $T_b$ is implemented in three blocks: $T_{b0}$-Subsystem; $T_{b1}$-Subsystem and $T_b$-Subsystem. Modeling of the bit resistance moment is carried out in the $T_{b0}$-Subsystem block according to the following expression [1]:

$$T_{b0}(t) = 0.4ad_b^2P\left(1+\frac{7.25}{\omega_b(t)+\delta_0}\right)\psi(t_b), \quad (2)$$

where $a$ – empirical coefficient; $P$ – axial load on the bit, N; $\omega_b(t)$ – bit rotation speed, rad/s; $\delta_0 = 1$ – correction, rad/s; $\psi(t_b)$ – a function that takes into account the change in torque during drilling as the bit wears out over time $t_b$, h.

The parameters were determined taking into account the resistance of rocks to destruction during well drilling [11, 12].

According to the source [1], $\psi(t_b)$ function can be represented by the following relationship:

$$\psi(t_b) = 1 + 0.002t_b + 0.000051t_b^2.$$

The maximum axial load on the bit during modeling can reach $P = 200$ kN; the value of the empirical coefficient for soft rocks $a = 1$, for hard rock $a = 0.5$; maximum bit rotation speed $\omega_b = 21$ rad/s (200 rpm).

The transition from the static moment of resistance $T_{b0}(t)$ to the moment $T_b(t)$, which takes into account frictional changes in the moment when passing through zero, is carried out in the $T_{b1}$-Subsystem block (according to the Stribeck model [13, 14]):

$$T_{b1}(t) = \rho T_{b0}(t), \quad (3)$$

where $\rho = 1\text{sign}\omega_b$; $|\omega_b| > 0.001$; $\rho = 1.1\text{sign}\omega_b$; $|\omega_b| \le 0.001$.

In subsystem $T_b$-Subsystem the presence in the drill string of not only torsional, but also longitudinal vibrations, which change the axial load on the bit during drilling, is taken into account; modeling of such oscillations was carried out according to the harmonic law [15]. The formula for determining the resulting drag moment on the bit is [8]

$$T_b = T_{b1}(1 + h\sin vt) + \xi(t),$$

where $h$ – coefficient that takes a value from 0 to 1; $v$ – angular frequency of longitudinal oscillations corresponding to values from 0.5 to 3 Hz; $\xi(t)$ – white noise function to take into account longitudinal random oscillations with an amplitude value of 3 kN·m.

Calculation of the instantaneous (at time t) power $P_m(t)$ on the motor shaft and power on the bit $P_b(t)$ is carried out based on the values of the moments $T_m(t)$, $T_b(t)$ and velocities $\omega_m(t)$, $\omega_b(t)$ in $P_m$-Subsystem and $P_b$-Subsystem blocks:

$$P_m(t) = T_m(t)\omega_m(t); \quad P_b(t) = T_u(t)\omega_u(t).$$

In the ETP-Subsystem block, the energy and technological parameters of the drilling rig are calculated. The total energy consumption of the electric drive and the energy on the bit during drilling time $T$ are determined by the following expressions:

$$E_m(T) = \int_0^T P_m(t)dt; \quad E_b(T) = \int_0^T P_b(t)dt.$$

The ratio of energy costs on the bit and on the engine determines the energy efficiency factor of the drive

$$k_{b-m}(T) = \frac{E_b(T)}{E_m(T)}.$$

Energy and technological characteristics are linked through indicators of the specific energy intensity of various rocks – Mechanical specific energy (MSE) [16, 17]. According to energy logging data, which may be included in modern geological and technological studies, the values of specific energy consumption for the rock destruction (Table 1), depending on the energy intensity class of the rock, can vary from several units to several thousand kW·h/m$^3$ [18]. Specific $e_{sp}$ (MSE) and general $E_b(t)$ energy intensity on the bit allow you to determine the mechanical speed of drilling Rate of penetration (ROP)

$$v_{meh} = \frac{E_b(T)}{e_{sp} T F_b} = \frac{\bar{P}_b}{e_{sp} F_b},$$

where $F_b$ – bit area, m$^2$; $\bar{P}_b$ – average power on the bit (integral estimate over time $T$), kW.

*Table 1*

**Drilling power consumption indicators** [18]

| Rock class | Energy intensity | Specific energy consumption $e_{sp}$, kW·h/m$^3$ |
|---|---|---|
| I | Minimal | Up to 15.6 |
| II | | 15.6-31.2 |
| III | | 31.2-62.5 |
| IV | Low | 62.5-125 |
| V | | 125-250 |
| VI | Avarage | 250-500 |
| VII | | 500-1000 |
| VIII | High | 1000-2000 |
| IX | | 2000-4000 |
| X | Maximal | Over 4000 |

The value of the mechanical drilling speed allows you to determine another characteristic indicator of rotary drilling – a deepening per one revolution of the bit

$$h_1 = k \frac{v_{meh}}{\omega_b(T)},$$

where $k = \pi/1800$ – dimension factor.

In drilling, the reciprocal of $h_1$ is also used, called the Rate of penetration index (RPI).

Along with the specific energy consumption on the bit, necessary for the destruction of the rock, it is proposed to introduce an indicator of the total specific cost of the rotor electric drive

$$e_{sp.m} = \frac{E_m(T)}{v_{meh} T F_b} = \frac{\bar{P}_m}{v_{meh} F_b},$$

where $\bar{P}_m$ – average value of the electric drive power (integral estimate for the time $T$), kW.

The energy of the electric drive includes the energy on the bit, as well as the energy spent on idle rotation of the DPC, and energy losses due to friction, including the friction of the string against the borehole walls. Therefore, the total specific energy consumption for drilling significantly exceeds the specific energy consumption for rock destruction $e_{sp.m} \gg e_{sp}$. In this case, the parameter $e_{sp.m}$ easier to determine in practice during drilling.

Thus, a modified complex model is proposed: an asynchronous electric drive of the rotor – a drill string – a bit – a rock. The model is a nonlinear feedback system, which makes it possible for self-oscillations to appear in the system [19, 20]. The main input parameters of the model are WOB $P_{ref}$ (Weight on bit – WOB) and rotation speed $n_{ref}$, rpm (Revolution per minute – RPM) [21-24], and output – electromechanical parameters of the drive (speeds, torques, currents, powers), as well as energy and technological characteristics of the drilling rig [18, 25-28]. Parameter (WOB×RPM) combination determines the drilling modes, and the output parameters allow you to evaluate the selected

EDN YEEWZJ
DOI: 10.31897/PMI.2023.20

drilling modes from the standpoint of their electromechanical, energy and technological efficiency and taking into account the dynamics of drilling processes [29-31].

**Results disscution.** Some simulation results for the indicated drilling rig, initial data and drilling modes are presented in Table 2.

*Table 2*

**Results of simulation of electric driven rotary drilling modes**

| Mode number | Parameters | | | | | | |
|---|---|---|---|---|---|---|---|
| | WOB×RPM, kN·rpm | $P_m$, kW | $P_b$, kW | $K_{b-m}$ | $v_{meh}$, m/h | $h_1$, mm/rev | $e_{sp.m}$, kW·h/m$^3$ |
| 1 | 20×20 | 30.2 | 2.3 | 0.078 | 0.07 | 0.10 | 6237 |
| 2 | 40×30 | 59.8 | 5.5 | 0.096 | 0.17 | 0.14 | 5073 |
| 3 | 80×50 | 143.1 | 15.3 | 0.108 | 0.45 | 0.21 | 4491 |
| 4 | 120×70 | 255.1 | 29.8 | 0.117 | 1.25 | 0.27 | 4116 |
| 5 | 160×90 | 374.4 | 45.8 | 0.123 | 1.33 | 0.30 | 3933 |
| 6 | 200×110 | 523.2 | 65.3 | 0.125 | 1.90 | 0.34 | 3857 |
| 7 | 20×70 | 103.3 | 12.7 | 0.123 | 0.38 | 0.08 | 3919 |
| 8 | 60×90 | 198.1 | 26.3 | 0.133 | 0.77 | 0.14 | 3625 |
| 9 | 100×110 | 313.6 | 42.9 | 0.137 | 1.26 | 0.18 | 3525 |
| 10 | 120×130 | 450.4 | 62.4 | 0.139 | 1.83 | 0.23 | 3474 |
| 11 | 180×150 | 603.0 | 84.8 | 0.141 | 2.49 | 0.27 | 3426 |
| 12 | 20×120 | 202.4 | 21.6 | 0.107 | 0.63 | 0.08 | 4521 |
| 13 | 40×130 | 265.3 | 30.4 | 0.115 | 0.89 | 0.10 | 4199 |
| 14 | 80×150 | 396.0 | 50.1 | 0.127 | 1.47 | 0.15 | 3805 |
| 15 | 120×170 | 547.0 | 72.6 | 0.133 | 2.13 | 0.19 | 3621 |
| 16 | 120×30 | 82.0 | 5.1 | 0.062 | 0.14 | 0.21 | 7816 |

One of the main tasks in drilling operations is the analysis of drilling modes in the coordinates (WOB×RPM) [32-35]. The first six modes refer to modes of unstable bit rotation and, as shown in Fig.4, in the coordinates (WOB×RPM) separating the zone of bit uniform rotation from the zone of non-uniform rotation with long stops. In the considered modes, a low level of mechanical drilling speed is noted, which is explained by the large diameter of the bit and the rather high energy intensity of class VII rock (accepted 750 kW·h/m$^3$). For a bit with a diameter of 0.128 m, when drilling rocks of II-III energy intensity classes, the mechanical drilling speed reaches several tens of meters per hour. The given values of the bit depth are quite large, in the literature, you can find lower values of the depth limit, but the calculation is carried out per the rotation of the engine rotor, rather than the bit, the ratio of which is determined by the gear ratio.

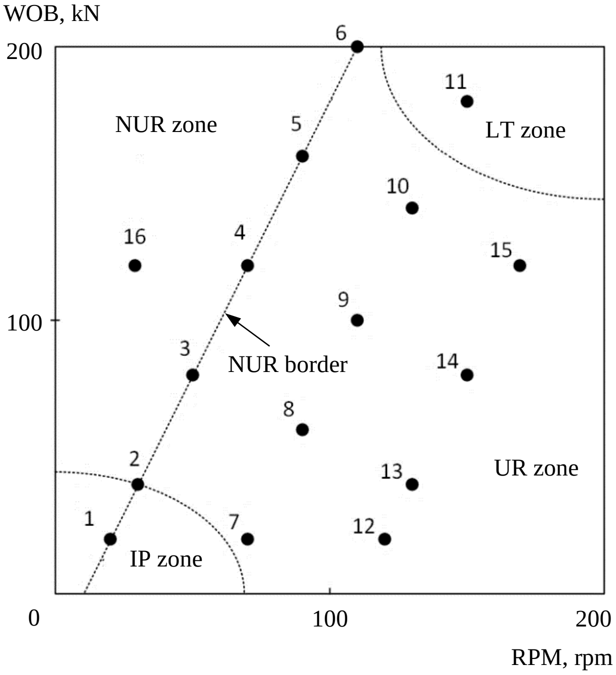


Fig.4. Rotary drilling modes

NUR – non-uniform rotation of the bit; UR – uniform rotation of the bit; IP – insufficient parameters; LT – lateral torsion

Based on the analysis of the modes (1-15), it can be concluded that according to the energy-technological characteristics it is difficult to single out the modes of non-uniform rotation (NUR) of the bit if they are close to the zone of uniform rotation (UR). So, according to all characteristics, modes 4 (on the border of zones) and 9 (inside the UR zone) are close. The further the NUR mode is from the UR zone, for example, mode 16, the easier it is to establish

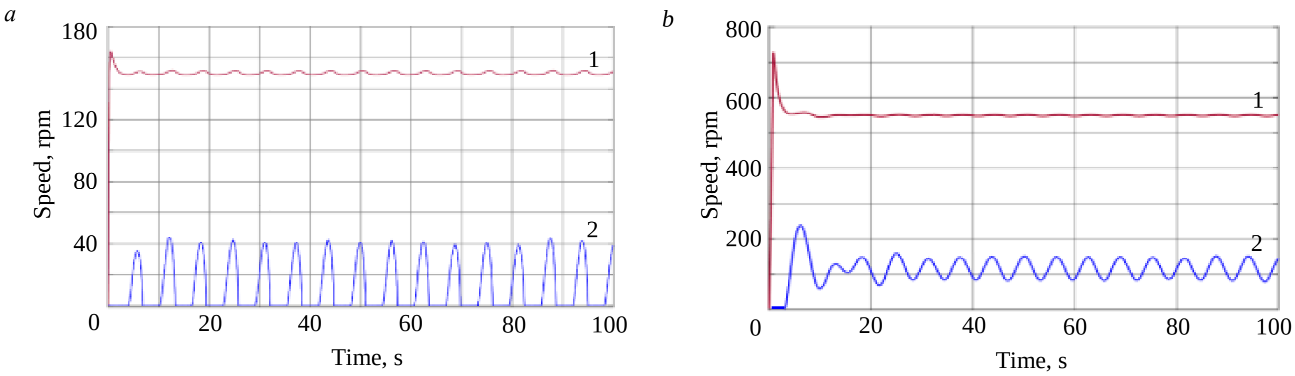


Fig.5. Rotor (1) and bit (2) speed curves in mode 16 of non-uniform bit rotation with long stops (*a*) and in mode 9 of uniform rotation (*b*)

the fact of unstable bit rotation using the given characteristics. For modes inside the NUR zone is typical a clear decrease in ROP and an increase in energy costs. The bit and the drilling rig rotor speed curves for mode 16 are shown in Fig.5, *a*. For comparison, Figure 5, *b* shows bit and rotor speed graphs for the mode of bit uniform rotation at point 9, in which bit speed fluctuations are much smaller and there are no bit stops. It should be noted that in both cases, the drive motor was started without load, with the clutch between the motor and the drilling rig rotor disconnected, and with a smooth increase in the set speed. Long bit stops lead to a significant decrease in the average bit speed, which can explain the decrease in the ROP and increase in energy consumption when drilling in the NUR zone. In the process of drilling, wear of the bit occurs, which, according to equation (2), affects the moment of resistance of the bit, while the boundary of the zone of uneven rotation of the bit moves to the right, increasing the NUR zone area of the bit. On the other hand, the size of the zone of uneven rotation is also affected by the diameter of the bit, when it decreases, the boundary of the zone of uneven rotation of the bit shifts to the left, reducing the NUR zone area of the bit.

Along with the zones of uniform and non-uniform rotation of the bit, Figure 4 shows a zone of insufficient drilling parameters (insufficient parameters) [20], where drilling is inefficient due to low ROP. The UR zone can also be divided, in its upper part (mode 11) the mechanical drilling speed is maximum, but in this case, accelerated wear of the bit occurs and a mode of impacts of the string against the borehole wall occurs – lateral vibrations (backward whirl) [21].

In the unstable non-uniform rotation modes of the bit, as can be seen from Fig.5, *a*, there are stops of the bit lasting several seconds. In modes 1-6, at the border of non-universal rotation, the stops are minimal and increase as the operating point moves deeper into the NUR zone, reaching ten seconds. When the figure is scaled up, it can be seen that at the stopping intervals, the process of changing the speed decays [9]. As shown in Fig.6, *a*, the speed "freezes" from small positive and negative initial values, tending to zero. There are high-frequency oscillations (up to 3000 Hz) – torsional vibration, which reduces the resource of the bit. The conversion of high-frequency velocity oscillations into accelerations made it possible to obtain a vibration curve in the units of measurement adopted in drilling – shocks. The calculated graph of the bit vibration, presented in Fig.6, *b*, confirms in practice the possibility of dangerous vibrations, reaching several tens of shocks [25, 34].

It has been established that in the fading intervals, the bit is affected by positive and negative moments exceeding 80 kN·m, which correspond to the forces acting on the cutters (teeth) of the bit up to 15-20 kN, which is consistent with the critical force at which chipping of a reinforcing plate of the tooth can occur [26, 27]. In addition, the achieved value of the moment acting on the bit exceeds the recommended unscrewing force of the threaded connection of the bit. For a threaded connection up to 185.7 mm, it is 21.7 kN·m, which is much less than the moment values achieved on the bit. This confirms the possibility of accelerated wear and loss (unscrewing) of the bit and the inexpediency of

EDN YEEWZJ
DOI: 10.31897/PMI.2023.20

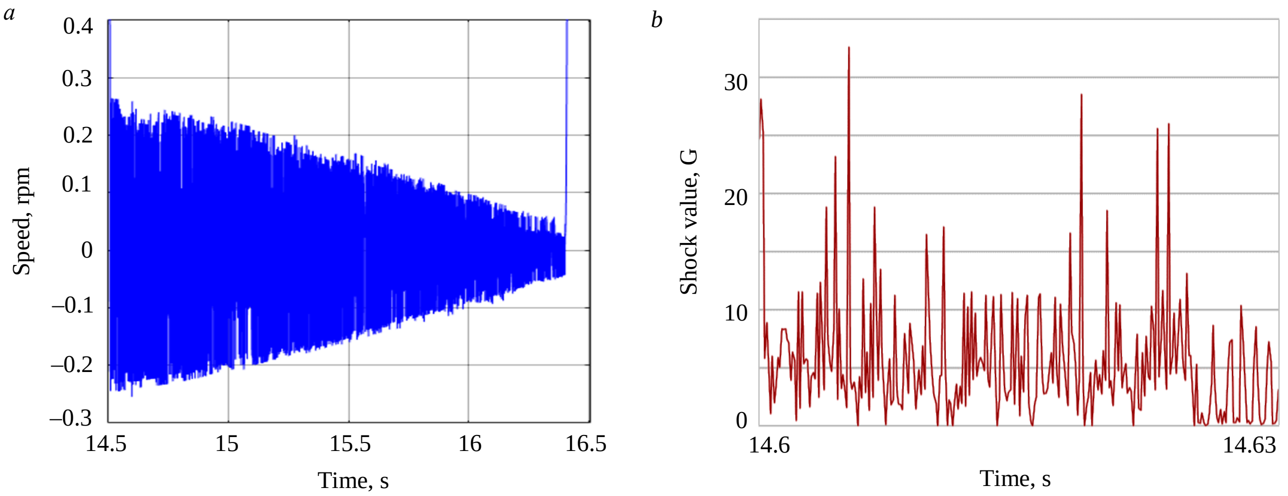


Fig.6. High-frequency oscillations (*a*) and vibration (*b*) of the bit when stopped and in stick-slip mode

the bit operation in stick-slip modes [27, 32]. Particularly rapid wear of the bit at high-frequency torsional vibrations is due to a change in the direction of bit rotation, in which the reaction force of the rock is directed not towards the bit teeth, but tangentially to them, causing chipping of the reinforcing plates of teeth and pulling out the teeth from the bit body sockets [33, 34]. Taking into account the design of PDC bits, it is more reasonable to model the frictional changes in the moment on the bit $T_b(t)$ when the speed passes through zero using a model that differs from model (3) by an upward shift along the *y*-axis. A possible variant of such a model is presented in the work [35]. The calculations have shown that such a shift leads to an increase in the risk of a stick-slip effect.

**Conclusion.** A modification of the complex model of asynchronous electric drive of the rotor – drill string – bit – rock is proposed, which makes it possible to calculate and evaluate the selected drilling modes, taking into account their electromechanical, energy and technological efficiency [36-38] and dynamics of drilling processes [29, 30, 39]. Simulation results are consistent with rotary drilling practice [40-42]. The performed computer simulation of drilling modes confirmed the possibility of the stick-slip effect occurrence, accompanied by high-frequency vibrations during bit stops, during which it is possible to change the direction of rotation of the bit, its accelerated wear and unscrewing of the drilling tool. The model can be used as a base for further improvement of the control of the rotary [43-45] and other [46-49] drilling methods.

## REFERENCES

1. Yunin E.K. Self-oscillations in deep drilling. Moscow: Librokom, 2013, p. 264 (in Russian).

2. Guangjian Dong, Ping Chen. A Review of the Evaluation, Control, and Application Technologies for Drill String Vibrations and Shocks in Oil and Gas Well. *Shock and Vibration*. 2016. N 7418635, p. 34. DOI: 10.1155/2016/7418635

3. Saldivar Márquez M.B., Boussaada I., Mounier H., Niculescu S.-I. Analysis and Control of Oilwell Drilling Vibrations. A Time-Delay Systems Approach. Springer International Publishing Switzerland, 2015, p. 282. DOI: 10.1007/978-3-319-15747-4

4. Yang Liu, Wei Lin, Chávez J.P., De Sa R. Torsional stick-slip vibrations and multistability in drill-strings. *Applied Mathematical Modelling*. 2019. Vol. 76, p. 545-557. DOI: 10.1016/j.apm.2019.06.012

5. Liping Tang, Xiaohua Zhu, Xudong Qian, Changshuai Shi. Effects of weight on bit on torsional stick-slip vibration of oil well drill string. *Journal of Mechanical Science and Technology*. 2017. Vol. 31. N 10, p. 4589-4597. DOI: 10.1007/s12206-017-0905-7

6. Ershov M.S., Balitsky V.P., Melik-Shakhnazarova I.A. Rotary table DC drive operation under conditions of unstable rotation of drill bit. *Mining Informational and Analytical Bulletin*. 2020. N 11, p. 166-179 (in Russian). DOI: 10.25018/0236-1493-2020-11-0-166-179

7. Ershov M.S., Komkov A.N., Feoktistov E.A. Operation of DC and AC drives of rotary table in unstable rotation mode of drill bit. *Mining Informational and Analytical Bulletin*. 2021. N 6, p. 153-167 (in Russian). DOI: 10.25018/0236_1493_2021_6_0_153

8. Ershov M.S., Feoktistov E.A. Impact of unstable drilling on energy efficiency of drill rotor drive. *Mining Informational and Analytical Bulletin*. 2022. N 1, p. 148-161 (in Russian). DOI: 10.25018/0236_1493_2022_1_0_148

9. Dardan Klimenta, Antti Hannukainen, Antero Arkkio. Estimating the parameters of induction motors in different operating regimes from a set of data containing the rotor cage temperature. *Electrical Engineering*. 2018. N 100, p. 139-150. DOI: 10.1007/s00202-016-0497-8

10. Vaziri V., Oladunjoye I.O., Kapitaniak M. et al. Parametric analysis of a sliding-mode controller to suppress drill-string stick-slip vibration. *Meccanica*. 2020. N 55, p. 2475-2492. DOI: 10.1007/s11012-020-01264-5

11. Dvoynikov M.V. Research on Technical and Technological Parameters of Inclined Drilling. *Journal of Mining Institute*. 2017. Vol. 223, p. 86-92. DOI: 10.18454/PMI.2017.1.86

12. Dolgiy I.E., Nikolaev N.I. Resistance of rocks to crushing during well drilling. *Journal of Mining Institute*. 2016. Vol. 221, p. 655-660. DOI: 10.18454/PMI.2016.5.655

13. Saldivar B., Mondié S., Ávila Vilchis J.C. The control of drilling vibrations: A coupled PDE-ODE modeling approach. *International Journal of Applied Mathematics and Computer Science*. 2016. Vol. 26. N 2, p. 335-349. DOI: 10.1515/amcs-2016-0024

14. Pogorelov D.Yu., Lysikov N.N. Bit-rock interaction forces in computer-aided simulation of drillstring dynamics. *Oil and Gas Business*. 2019. N 3, p. 211-236 (in Russian).

15. Koronatov V.A. Fundamentals of the mathematically rigorous theory of deep drilling. *Systems. Methods. Technologies*. 2020. N 2 (46), p. 23-29 (in Russian). DOI: 10.18324/2077-5415-2020-2-23-29

16. Kunshin A., Dvoynikov M., Timashev E., Starikov V. Development of Monitoring and Forecasting Technology Energy Efficiency of Well Drilling Using Mechanical Specific Energy. *Energies*. 2022. Vol. 15 (19). DOI: 10.3390/en15197408

17. Kadochnikov V.G., Dvoynikov M.V. Development of Technology for Hydromechanical Breakdown of Mud Plugs and Improvement of Well Cleaning by Controlled Buckling of the Drill String. *Applied Sciences*. 2022. Vol. 12 (13). DOI: 10.3390/app12136460

18. Lukyanov E.E., Kudasheva S.V. Guidelines for the interpretation of mud logging data. Novosibirsk: Istoricheskoe nasledie Sibiri, 2016, p. 512 (in Russian).

19. Vromen T.G.M., Dai C.H., Van de Wouw N. et al. Mitigation of torsional vibrations in drilling systems: a robust control approach. *IEEE Transactions on Control Systems Technology*. 2019. Vol. 27. Iss. 1. N 8094252, p. 249-265. DOI: 10.1109/TCST.2017.2762645

20. Tengesdal N.K., Hovda S., Holden C. A Discussion on the Decoupling Assumption of Axial and Torsional Dynamics in Bit-rock Models. *Journal of Petroleum Science and Engineering*. 2021. Vol. 202. N 108070. DOI: 10.1016/j.petrol.2020.108070

21. Amorim Jr. D.S., Santos O.L.A., Azevedo R.C. New industry standards to increase the reliability of drilling operations. *Holos*. 2019. Vol. 6, p. 1-14. DOI: 10.15628/Holos.2019.9009

22. Neskoromnykh V.V., Popova M.S., Golovchenko A.E. et al. Method of drilling process control and experimental studies of resistance forces during bits drilling with PDC cutters. *Journal of Mining Institute*. 2020. Vol. 245, p. 539-546. DOI:10.31897/PMI.2020.5.5

23. Neskoromnykh V.V., Chikhotkin A.V. Analysis of rock destruction mechanics by PDC cutters with regard to dynamic cutting–shearing processes and resistance. *Mining Informational and Analytical Bulletin*. 2020. N 4, p. 127-136 (in Russian). DOI: 10.25018/0236-1493-2020-4-0-127-136

24. Neskoromnykh V.V., Popova M.S., Zotov Z.G., Liu Baochang. Algorithm of diamond drilling system control. *Bulletin of the Tomsk Polytechnic University. Geo Assets Engineering*. 2022. Vol. 333. N 2, p. 81-89 (in Russian). DOI: 10.18799/24131830/2022/2/3562

25. Abdul Rani A.M., Khairiyah I., Ab Adzis A.H. et al. Investigation on the effect of changing rotary speed and weight bit on PCD cutter wear. *Journal of Petroleum Exploration and Production Technology*. 2020. Vol. 10, p. 1063-1068. DOI: 10.1007/s13202-019-00795-2

26. Tretyak A.A., Litkevich Yu.F., Borisov K.A. Influence of torsional and longitudinal vibrations on drilling speed and formation of breakdowns of cutting elements of PDC reinforced drill bits. *Bulletin of the Tomsk Polytechnic University. Geo Assets Engineering*. 2019. Vol. 330. N 12, p. 135-141 (in Russian). DOI: 10.18799/24131830/2019/12/2410

27. Borisov K.A., Tretyak A.A., Sidorova E.V. Impact of vibrations on strength properties of drill bits reinforced by PDC. *Prospect and protection of mineral resources*. 2019. N 12, p. 33-37 (in Russian).

28. Tretyak A.Ya., Sidorova E.V., Litkevich Yu.F. et al. Drilling bit PDC plates lifetime control. *Bulletin of the Tomsk Polytechnic University. Geo Assets Engineering*. 2021. Vol. 332. N 8, p. 28-35 (in Russian). DOI: 10.18799/24131830/2021/8/3302

29. Litvinenko V.S., Dvoynikov M.V. Methodology for determining the parameters of drilling mode for directional straight sections of well using screw downhole motors. *Journal of Mining Institute*. 2020. Vol. 241, p. 105-112. DOI: 10.31897/PMI.2020.1.105

30. Neskoromnykh V.V., Popova M.S. Development of a drilling process control technique based on a comprehensive analysis of the criteria. *Journal of Mining Institute*. 2019. Vol. 240, p. 701-710. DOI: 10.31897/PMI.2019.6.701

31. Kozyaruk A.E. Development experience and development prospect of electromechanical technological complexes of movement and positioning of technic shelf development equipment. *Journal of Mining Institute*. 2016. Vol. 221, p. 701-705. DOI: 10.18454/PMI.2016.5.701

32. *Zhiqiang Huang, Yachao Ma, Qin Li, Dou Xie*. Geometry and force modeling, and mechanical properties study of polycrystalline diamond compact bit under wearing condition based on numerical analysis. *Advances in Mechanical Engineering*. 2017. Vol. 9 (6), p. 1-15. DOI: 10.1177/1687814017702080

33. Guohui Zhang, Xiwen Zhang, Rong Chen et al. Pediction method of rock stratum anti-diamond characteristics of carbonate rocks used in Qinghai YingXi block. 2018 3rd International Conference on Advances in Energy and Environment Research (ICAEER 2018), September 2018, Guilin, China. E3S Web of Conferences. 2018. Vol. 53 (12). N 03002, p. 1-5. DOI: 10.1051/e3sconf/20185303002

34. Zalyaev M.F. The exploration of vibration while drilling wells on termokarstovoe gas deposit. *Oil and Gas Business*. 2015. N 4. Vol. 13, p. 36-40 (in Russian).

35. Leonov G.A., Kiseleva M.A. Stability of electromechanical models of drilling systems under discontinuous loads. *Doklady Physics*. 2012. Vol. 57. N 5, p. 206-209 (in Russian).

36. Dvoynikov M.V., Nutskova M.V., Blinov P.A. Developments Made in the Field of Drilling Fluids by Saint Petersburg Mining University. *International Journal of Engineering, Transactions A: Basics*. 2020. Vol. 33. Iss. 4, p. 702-711. DOI: 10.5829/IJE.2020.33.04A.22

37. Litvinenko V.S., Dvoynikov M.V. Monitoring and control of the drilling string and bottomhole motor work dynamics. *Topical Issues of Rational use of Natural Resources*. 2019. Vol. 2, p. 804-809. DOI: 10.1201/9781003014638-42

38. Guanggjian Dong, Ping Chen. A Review of the Evaluation, Control, and Application Technologies for Drill String Vibrations and Shoks in Oil and Gas Well. *Shock and Vibration*. 2016. N 7418635, p. 34. DOI: 10.1155/2016/7418635

39. Ritto T.G., Ghandchi-Tehrani M. Active control of stick-slip torsional vibrations in drill-strings. *Journal of Vibration and Control*. 2018. Vol. 25. Iss.1, p. 1-9. DOI: 10.1177/1077546318774240

EDN YEEWZJ
DOI: 10.31897/PMI.2023.20

40. Pérez-Aracil J., Camacho-Gómez C., Pereira E. et al. Eliminating Stick-Slip Vibrations in Drill-Strings with a Dual-Loop Control Strategy Optimised by the CRO-SL Algorithm. *Mathematics.* 2021. Vol. 9. N 1526. DOI: 10.3390/math9131526

41. Pavković D., Šprljan P., Cipek M., Krznar M. Cross-axis control system design for borehole drilling based on damping optimum criterion and utilization of proportional-integral controllers. *Optimization and Engineering*. 2021. Vol. 22, p. 51-81. DOI: 10.1007/s11081-020-09566-z

42. Wei Lin, Paez Chavez J., Yang Liu et al. Stick-slip suppression and speed tuning for a drill-string system via proportional-derivative control. *Applied Mathematical Modelling*. 2020. Vol. 82, p. 487-502. DOI: 10.1016/j.apm.2020.01.055

43. Vaziri V., Kapitaniak M., Wiercigroch M. Suppression of drill-string stick–slip vibration by sliding mode control: Numerical and experimental studies. *European Journal of Applied Mathematics*. 2018. Vol. 29. Iss. 5, p. 805-825. DOI: 10.1017/S0956792518000232

44. Litvinenko V.S., Dvoinikov M.V. Justification of the Technological Parameters Choice for Well Drilling by Rotary Steerable Systems. *Journal of Mining Institute*. 2019. Vol. 235, p. 24-29. DOI: 10.31897/PMI.2019.1.24

45. MacLean J.D.J., Vaziri V., Aphalec S.S., Wiercigrochd M. Feedback control method to suppress stick-slip in drill-strings featuring delay and actuation constraints. *The European Physical Journal Special Topics*. 2021. Vol. 230, p. 3627-3642. DOI: 10.1140/epjs/s11734-021-00228-4

46. Simonyants S.L, Al Taee M. Stimulation of the Drilling Process with the Top Driven Screw Downhole Motor. *Journal of Mining Institute.* 2019. Vol. 238, p. 438-442. DOI: 10.31897/PMI.2019.4.438

47. Dvoynikov M.V., Sidorkin D.I., Kunshin A.A., Kovalev D.A. Development of hydraulic turbodrills for deep well drilling. *Applied Sciences* (*Switzerland*). 2021. Vol. 11. Iss. 16. DOI: 10.3390/app11167517

48. Dvoynikov M., Kunshin A., Blinov P., Morozov V. Development of Mathematical Model for Controlling Drilling Parameters with Screw Downhole Motor. *International Journal of Engineering, Transactions A: Basics*. 2020. Vol. 33. Iss.7, p. 1423-1430. DOI: 10.5829/IJE.2020.33.07A.30

49. Podoliak A.V., Blinov P.A. The technology of directional drilling in ice via drills on carrying cable. *International Journal of Applied Engineering Research*. 2016. Vol. 11 (9), p. 6411-6417.

***Authors*: Mikhail S. Ershov,** *Doctor of Engineering Sciences, Professor, https://orcid.org/0000-0002-7772-0095* (*National University of Oil and Gas* "*Gubkin University*", *Moscow, Russia*), **Aleksandr N. Komkov,** *Candidate of Engineering Sciences, Head of Department, https://orcid.org/0000-0002-1010-6971* (*National University of Oil and Gas* "*Gubkin University*", *Moscow, Russia*), **Evgeniy A. Feoktistov,** *Student, https://orcid.org/0000-0002-9490-3854* (*National University of Oil and Gas* "*Gubkin University*", *Moscow, Russia*).

*The authors declare no conflict of interests.*

ISSN 2411-3336; e-ISSN 2541-9404

JOURNAL OF MINING INSTITUTE

Zapiski Gornogo instituta

Journal homepage: pmi.spmi.ru

Research article

# Evaluation of the energy efficiency of functioning and increase in the operating time of hydraulic drives of sucker-rod pump units in difficult operating conditions

**Dmitriy I. SHISHLYANNIKOV**[1], **Valeriy Yu. ZVEREV**[1], **Anna G. ZVONAREVA**[2]✉, **Sergey A. FROLOV**[1], **Anna A. IVANCHENKO**[1]

[1] *Perm National Research Polytechnic University, Perm, Russia*

[2] *Saint Petersburg Mining University, Saint Petersburg, Russia*

***How to cite this article*:** Shishlyannikov D.I., Zverev V.Yu., Zvonareva A.G., Frolov S.A., Ivanchenko A.A. Evaluation of the energy efficiency of functioning and increase in the operating time of hydraulic drives of sucker-rod pump units in difficult operating conditions. Journal of Mining Institute. 2023. Vol. 261, p. 349-362. EDN XLRCWN

***Abstract*.** The necessity of improving the drives of the sucker-rod hydraulic pump units (SRHP), operated in conditions of marginal and complicated wells, is substantiated. For complicated oil production conditions, it is promising to use the SRHP drive, which makes it possible to select and set rational operating modes for downhole equipment. The results of comparative tests of conventional mechanical and hydraulic actuators SRHP with pneumatic and electrodynamic balancing types are presented. A generalized indicator for evaluating the effectiveness of the advanced SRHP drives functioning, the energy efficiency coefficient, is proposed. It has been experimentally proven that the use of the SRHP drive with pneumatic balancing is characterized by low energy efficiency of the well fluid production process. The use of the tested SRHP hydraulic drive made it possible to successfully eliminate asphalt, resin, and paraffin deposits and minimize the well downtime. The results of the tests of the traditional SRHP mechanical drive and the hydraulic drive with electrodynamic balancing showed a satisfactory energy efficiency of the latter. The advantage of the SRHP drive with electrodynamic balancing is the simplicity of the design of the hydraulic part. The process of energy regeneration during the drive control system operation causes an increase in the reactive power component in the oil field network and the appearance of harmonic interference that adversely affects the consumers operation. Technical solutions aimed at improving the operation energy efficiency and increasing the operating time of SRHP drives in the conditions of marginal and complicated wells are proposed. The methodological bases for assessing the economic efficiency of the introduction of the advanced SRHP drives are given.

***Keywords*:** sucker-rod hydraulic pump; hydraulic drive; energy efficiency; balancing; comparative tests; difficult operating conditions

***Acknowledgment.*** The research was supported by the Ministry of Science and Higher Education of the Russian Federation (Project N FSNM-2023-0005).

***Received: 14.03.2023*** ***Accepted: 20.06.2023*** ***Online: 19.07.2023*** ***Published: 19.07.2023***

**Introduction.** A significant number of production wells in the oil fields of Russia and neighboring countries are at the final (third and fourth) operation stages. Such wells are characterized by low flow rates ($Q$ = 1-15 m$^3$/day) and the presence of factors that complicate the operation of submersible equipment [1-3]. A low-yield and complicated oil wells operation is carried out mainly with the use of sucker-rod hydraulic pump units (SRHP), equipped with a mechanical drive – balancing pumping units (SK) [4]. In the delivery ranges of sucker rod pumps of $Q$ = 30-45 m$^3$/day, SRHP is characterized by a fairly high energy efficiency, the efficiency of a serviceable installation is η = 0.36-0.54.

The presence of complicating factors and low well flow rates cause a sharp decrease in the efficiency of the SRHP (η = 0.02-0.05 with a power factor of the SK drive motors not exceeding cosφ = 0.3) [5]. As a result, the performance indicators of the SRHP are significantly reduced, while the cost of oil production, on the contrary, is unreasonably increased [6]. The value of specific energy consumption for the well fluid lifting using conventional SRHP for low-rate and complicated wells is 5-10 times higher than similar values for medium- and high-rate wells [7, 8].

The use of SRHP non-balance drives, which make it possible to ensure long-stroke operating modes of downhole pumps and increase the installation energy efficiency during the marginal well operation, is limited by the flexible links (chains, V-belts, steel ropes, etc.) low reliability. This fact causes the frequent replacement of the short-lived elements of the flexible links, equipment downtimes and, as a consequence, oil companies significant material losses.

In the works of domestic and foreign researchers, it is indicated that one of the ways to improve the SRHP operation efficiency and reliability during the marginal and complicated wells operation is the use of a hydraulic drive (HD) [9, 10]. SRHP drive is characterized by mobility, low material consumption, ease of adjustment and wide ranges of change in operational parameters. These advantages make it possible to select and set the SRHP HD operation modes, which are rational in terms of the unit energy consumption for lifting the formation fluid, as well as to increase the efficiency of implementing the technical and technological measures to eliminate the negative consequences of complicating factors [11, 12].

The tasks of evaluating the energy efficiency of the serially produced SRHP HD and developing technical solutions aimed at improving the reliability of their operation in difficult operating conditions are both relevant and of scientific and practical interest.

**Methods.** The development and trial operation of SRHP HD started in the USA in the 40s of the XX century. Specialists of Vickers, Pelton, Axelson companies created and tested original designs of SRHP HD, which had worse performance characteristics compared to balancing SK, which led to their low distribution. At the same time, compactness, mobility, and wide possibilities for automating the operation of these drives determined the prospects for research aimed at their further improvement. Domestic specialists developed SRHP HD, the design schemes of which are similar to those used abroad, and proposed the original solutions, for example, the installation of an acceleration graphic point (AGP) designed by professor G.V.Molchanov [11]. The general classification of SRHP HD according to design features is given in Table 1.

*Table 1*

**SRHP HD design features classification** [11]

| Kinematic connection of the power body and the balancing device | Balancing method | | | | | |
|---|---|---|---|---|---|---|
| | Static | | | Dynamic | | Unbalanced |
| | Pheumatic | Loading | Mutual | Inertial | Electro-dynamic | |
| Hydraulic | Pneumatic accumulator drive | Drive with individual load. installations with tubing as a balancing weight | Mutual balancing of two or more installations | Using a flywheel with an individual drive | – | Unbalanced drives |
| Mechanical rigid | – | Balanced rigid connection | – | Using a flywheel mounted on the motor shaft | Machine operation in generator mode | Partially balanced drives |
| Mechanical flexible | – | Balancing load on rope suspension | – | – | – | – |

Modern mass-produced samples of SRHP HD are equipped with systems for monitoring operation parameters and self-diagnostics: by monitoring the pressure values in the discharge pipelines, dynamometering is carried out, i.e. assessment of the load, technical condition and efficiency of the downhole pumping equipment. The position control of the rod string suspension point position, the polished rod stroke and oscillation frequency is carried out by means of sensors (magnetic type markers).

The factors that have the greatest impact on the SRHP HD operation efficiency and the amount of their operating time in the oil field conditions include: the adopted balancing method; the performed balancing quality; energy transfer method from the balancing device to the power body; power structure [5].

The choice of the SRHP HD balancing device is carried out taking into account its energy intensity, operational stability (reduced durability), pre-charging technology at the initial start-up, as well as maintaining and regulating the installation operation mode (Table 2) [11].

*Table 2*

**SRHP HD balancing device main parameters**

| Parameter | Balancing device | | |
|---|---|---|---|
| | Pneumatic | Weighing | Inertial |
| Specific energy intensity, kJ/kg | 25-30 | 1-6 | 100-200 |
| Efficiency, % | 97 | 98 | 95 |
| Energy storage time, h | Not limited | Not limited | 0.05-0.1 |
| Number of charge-discharge cycles | $10^7$ | Not limited | Not limited |
| Reduced durability (per 1 m of SRSP stroke), h | $1.7 \cdot 10^4$ | Not limited | Not limited |

The task of balancing the SRHP HD in practice can be solved in several ways, which differ in the accepted balancing criteria [13]: balancing by maximum loads, by the average work value or the standard deviation from the average work value of. These criteria have been developed for balancing SK, which are characterized by machine load mode that is different from the load of the SRHP HD machine. For a balanced SK, the torque change law on the motor shaft is close to a sinusoid, while for a balanced hydraulic drive it is characterized by a graph close to a straight line [1].

The SRHP drive is considered to be perfectly balanced if the instantaneous power at any moment of time is constant and equal to the average power developed by the motor in one drive cycle [14]. Since it is difficult to ensure the electric motor instantaneous power constancy during the SRHP HD operation cycle, the equilibrium condition is determined based on the minimum power dispersion for the full cycle of SRHP HD operation [11]. It follows that it is rational to determine balancing quality assessment and the SRHP HD functioning energy efficiency in the oil field conditions by continuously measuring the electric motor power during the drive operation and subsequent analysis of the obtained measurement from the wattmeters [15, 16].

In the oil fields of Russia and the countries of the near abroad, the SRHP HD with pneumatic and electrodynamic balancing are most widely used. They consist of a pumping station and a power hydraulic cylinder that provides reciprocating movement of the sucker rod suspension point (SRSP), are equipped with remote control systems, remote monitoring and built-in self-diagnostics systems, which allows you to quickly change the operating parameters of the SRHP HD and downhole equipment [11].

Together with the specialists of OOO “LUKOIL-Perm”, the studies to assess the load and energy efficiency of the operation of the SRHP HD with pneumatic and electrodynamic balancing were carried out. The research program included the performance of comparative tests of SRHP drives – mechanical balancing drives SK-8 and serially produced SRHP HD: with pneumatic balancing NPK-10-8-6 (Fig.1, *a*); with electrodynamic balancing SRHP HD 80-3.5 “Geyser” (Fig.1, *b*).

Journal of Mining Institute. 2023. Vol. 261. P. 349-362 EDN XLRCWN


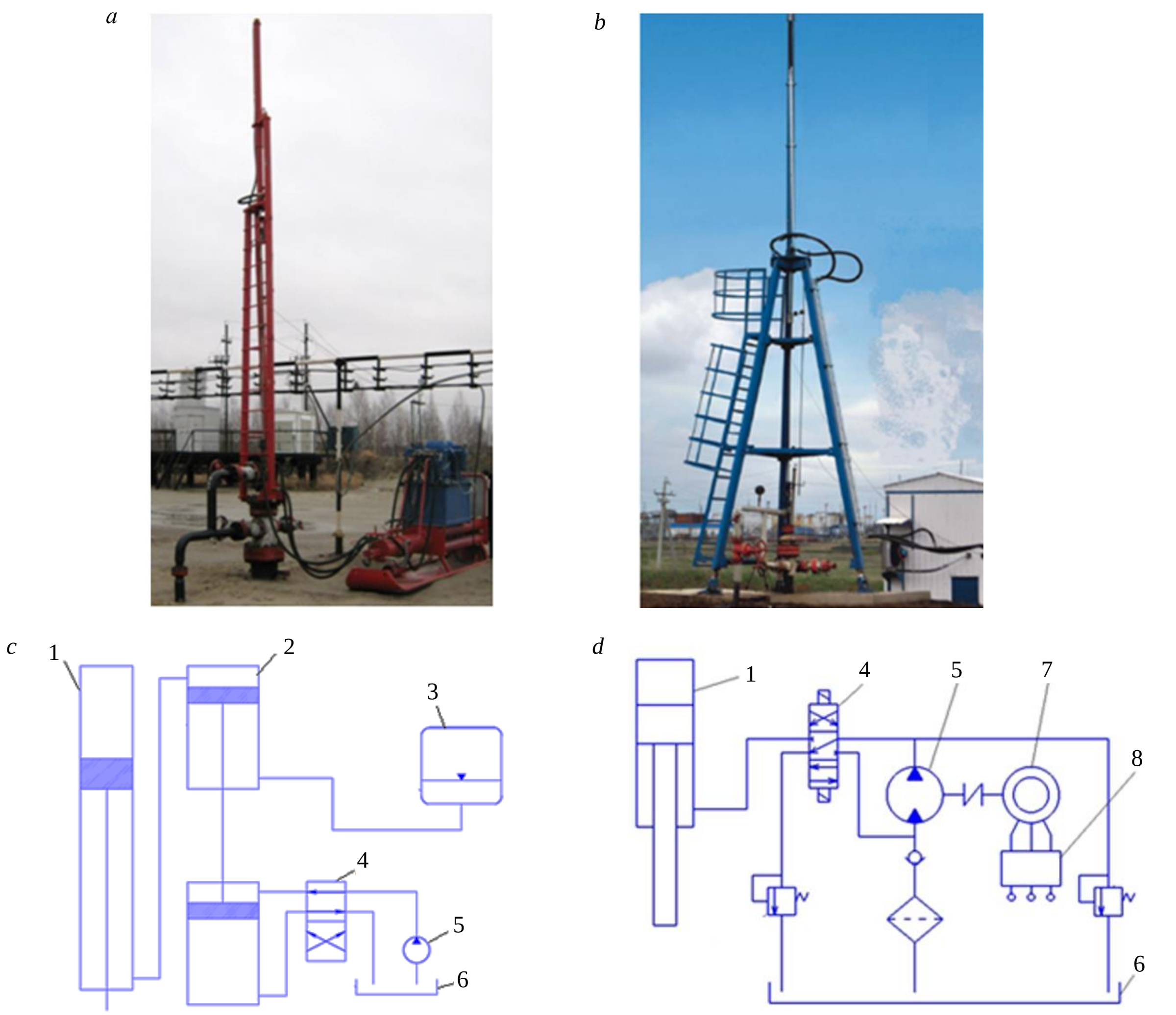


Fig.1. SRHP drives general view (*a*, *b*) and schematic hydraulic diagrams (*c*, *d*): *a*, *c* – NPK-10-8-6; *b*, *d* – SRHP HD 80-3.5 “Geyser”

1 – power hydraulic cylinder; 2 – intermediate hydraulic cylinder; 3 – pneumatic accumulator; 4 – hydraulic distributor; 5 – hydraulic pump; 6 – tank; 7 – electric motor; 8 – block of intelligent control system

Evaluation of the change nature and the load magnitude of the SRHP HD, the surveyed pumping units energy performance determination were carried out using the AKD-SK software and recording complex manufactured by OOO “NPP “ROS” (Perm). The complex is designed to monitor the energy parameters of SRHP HD motors, is commercially available, certified as a measuring instrument (N 19988-10 in the State Register of Measuring Instruments). Power measurement ranges 4-30 kW, channel sampling frequency up to 1 kHz, the main reduced measurement error is not more than 5 %. The “AKD-SK” complex is installed permanently in the SRHP HD control station, continuously registers the wattmeters of the SRHP HD motors, which allows you to control the amount of energy consumption, determine the SRHP HD balance degree, analyze the nature of changes in the loads of the drives during the monitoring process [17].

The software-registration complex “AKD-SK” (Fig.2, *a*) has a modular design. The complex consists of a switching unit, a controller, a power sensor and a magnetic marker. The connection diagram of the software-registration complex in the control station SRHP is shown in Fig.2, *b*. Magnetic marker allows you to fix the lower (upper) position of the SRSP.

The SRHP HD electric motors parameters are determined in accordance with the formulas:

• effective value of current

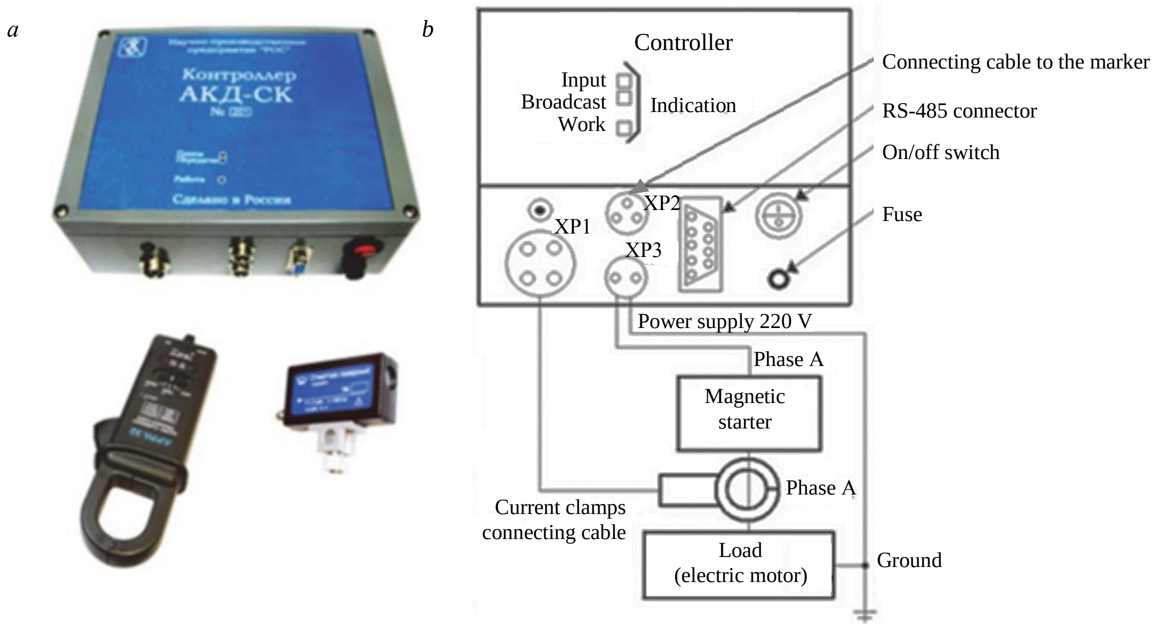


Fig.2. Software-registration complex “AKD-SK”: *a* – general view; *b* – block diagram

$$I_{\text{ef}} = \sqrt{\frac{1}{n}\sum_{m=1}^{n} i_m^2} \; ,$$

where $n$ – number of measurement points for a fixed time interval $\Delta T$; $i_m$ – instantaneous value of the current at the $m$-th moment of time, A;

• effective voltage value

$$U_{\text{ef}} = \sqrt{\frac{1}{n}\sum_{m=1}^{n} u_m^2} \; ,$$

$u_m$ – instantaneous value of the phase-to-phase voltage at the $m$-th moment of time, V.

Active $N_{\text{a}}$ (kW) and full power $S_w$ (kVA) of the SRHP HD electric motor are calculated in accordance with the formulas:

$$N_{\text{a}} = \frac{3}{n}\sum_{m=1}^{n} u_m i_m \; ;$$

$$S_w = 3 I_{\text{ef}} U_{\text{ef}} \; .$$

The power factor is given by

$$\cos\varphi = N_{\text{a}} / S_w \; .$$

Operational control data is stored in the instrument's non-volatile memory. At the request of the oil field engineering and technical specialists, they are transferred to the operator network. Using specialized software, the analysis and visualization of information obtained during monitoring is carried out.

As an example, Fig.3 shows a wattmeter diagram obtained during the operation of the motor of the balancing SK-8 [18]. The marker (green

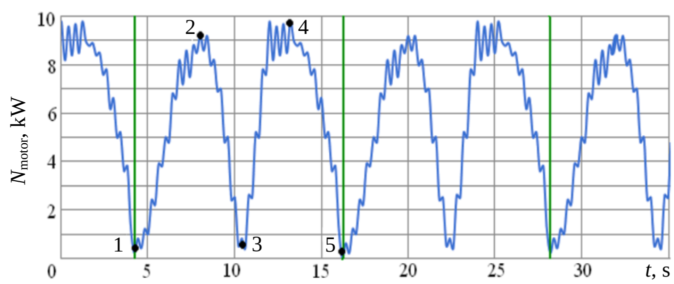


Fig.3. Wattmeter diagram of the balancing motor SK-8: lower (1, 5), horizontal (2, 4) and upper (3) crank position

color) indicates the upper position of the SRSP, which corresponds to the lower position of the crank. Each movement cycle of the SK balancer head (one swing) is characterized by two power maxima, the difference between the values of which (for balanced SK) should not exceed 10 % [11].

The well flow rates, where the studies were carried out, was determined according to the data of verified measuring instruments equipped with verified measuring instruments. The research was carried out in two stages. First, the measurements were carried out on a well equipped with a SRHP with a SK-8 type mechanical drive. Then the SK was replaced by the HD and the same scope of tests was performed, which made it possible to correctly obtain a comparative assessment of the energy efficiency of the operation of the SRHP drives [19].

The average daily specific energy consumption for the well fluid production during the operation of the SRHP was calculated by the formula

$$H_{w.i} = \Sigma W_{\text{day}i} / Q_{\text{ph}.i},$$

where $\Sigma W_{\text{day}i}$ – total energy costs for the operation of the SRHP for the $i$-th operation day, kWh; $Q_{\text{ph}.i}$ – productivity of the SRHP for the $i$-th operation day, m$^3$/day.

The average value of the specific energy consumption for the well fluid production during the operation of the SRHP for the $t$ period was calculated by the formula

$$H_w = \sum_{i=1}^{t} H_{w.i} / t.$$

Comparative evaluation of the advanced SRHP hydraulic drives performance efficiency was carried out by determining the value of the drive energy efficiency coefficient in accordance with the formula

$$k_{\text{e.ef}} = H_{w.\text{b}} / H_{w.\text{test}},$$

where $H_{w.\text{b}}$ – specific energy consumption average value for the production of well fluid during the operation of SRHP equipped with a balancing SK (base value of specific energy consumption), kWh/m$^3$; $H_{w.\text{test}}$ – the specific energy consumption average value for the production of well fluid during the operation of the tested SRHP HD, kWh/m$^3$.

A promising SRHP HD with pneumatic balancing was tested on Oblivskoye field well 109b. The program of comparative tests provided for the specific energy consumption determination for the reservoir fluid production during the operation of SRHP equipped with a SK-8 type mechanical drive and a NPK-10-8-6 hydraulic drive. Parameters of the tested SRHP are following: pump suspension depth $L$ = 1534.9 m; stroke length $S_0$ = 2.5 m; double strokes number $n$ = 5.5 min$^{-1}$. The specific energy consumption for lifting the well fluid when SRHP was equipped with a hydraulic drive NPK-10-8-6 was $H_{\text{w.test}}$ = 25.6 kWh/m$^3$, which is almost twice as high as on the balancing mechanical SK-8 ($H_{\text{w.b}}$ = 12.8 kWh/m$^3$), with the use of which the investigated well was operated earlier (Table 3). The value of the energy efficiency coefficient was $k_{\text{e.ef}}$ = 0.45.

*Table 3*

**SRHP HD test results**

| Drive type | Hydraulic drive NPK-10-8-6 | | | SRHP HD 80-3.5 “Geyser” | |
|---|---|---|---|---|---|
| | SK-8 | NPK-10-8-6 | NPK-10-8-6 | SK-8 | SRHP HD 80-3.5 “Geyser” |
| Used motors | 22 kW; 970 rpm | 15 kW; 1480 rpm | 15 kW; 1480 rpm | 22 kW; 970 rpm | 37 kW; 1480 rpm |
| Operating parameters | $S_0$ = 2.5 m; $n$ = 5.5 min$^{-1}$ | $S_0$ = 2.5 m; $n$ = 5.5 min$^{-1}$ | $S_0$ = 5.0 m; $n$ = 1.8 min$^{-1}$ | $S_0$ = 2.5 m; $n$ = 5.5 min$^{-1}$ | $S_0$ = 2.5 m; $n$ = 5.5 min$^{-1}$ |
| Measurement time, days | 9 | 7 | 42 | 6 | 5 |
| Average daily energy consumption, kWh/day | 123.8 | 294.0 | 228.6 | 117.0 | 128.9 |
| Average daily liquid flow rate, m$^3$/day | 9.7 | 11.5 | 9.7 | 10.4 | 10.1 |
| Specific energy consumption, kWh/m$^3$ | 12.8 | 25.6 | 23.6 | 11.25 | 12.76 |
| Energy efficiency ratio | – | 0.45 | 0.54 | – | 0.88 |

The analysis of the wattmeter data obtained during the examination of a hydraulic drive with pneumatic balancing showed that in the given conditions, the maximum power value when lifting the SRSP is $N_{motor}$ = 12.1 kW, and when the rod is lowered $N_{motor}$ = 4.8 kW (Fig.4, *a*).

As the SRSP moves upwards, the loading of the drive motor increases, since the energy stored by the pneumatic accumulator is consumed (see Fig.1, *c*, pos.3). The insufficient volume of the latter causes the presence of pronounced peaks in the signal of the electric motor active power of the tested SRHP HD. The presence of asphalt-resin-paraffin deposits in the well has a significant effect on the load formation process: the pump rod string and the pump plunger move unevenly, periodically "hanging", which causes the appearance of local peaks and power dips on the wattmeter diagram of the tested SRHP HD electric motor (Fig.4, *a*).

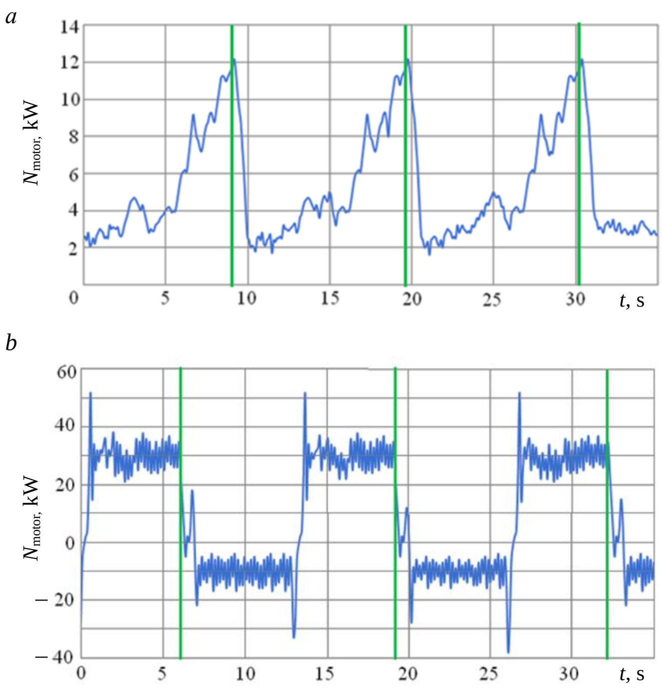


Fig.4. Drive motor power change:
*a* – hydraulic drive pumping station NPK-10-8-6 with pneumatic balancing; *b* – pumping station station SRHP HD 80-3.5 "Geyser" with electrodynamic balancing [24]; SRSP top position is shown in green

To reduce the specific energy consumption for oil production, a rod pump was replaced in the well. The stroke length of the SRHP rod was increased to $S_0$ = 5.0 m, the number of double strokes was reduced to $n$ = 1.8 min$^{-1}$. A slight decrease in the specific energy consumption for the production of well fluid was noted (up to $H_{w.test}$ = 23.6 kWh/m$^3$). The energy efficiency coefficient increased to $k_{e.ef}$ = 0.54. High specific energy consumption and uneven loads during the operation of the SRHP HD NPK-10-8-6 are due to the imperfection of the chosen balancing method: the energy stored by the pneumatic accumulator during the reverse stroke of the SRSP is objectively not enough to significantly reduce the drive power during the working stroke.

Wide ranges of the HD operation mode parameters regulation allow them to be successfully used in complicated operating conditions of the SRHP. For example, in the trial operation course of a promising hydraulic drive NPK-10-8-6, a shutdown of the drive was recorded due to the sucker rod string hanging due to the formation of asphalt, resin, and paraffin deposits (ARPD) in the pumping and compressor pipeline [20-22]. Starting the drive in the well resuscitation mode (swing frequency and stroke length automatically change depending on the load in the SRSP) with a set number of oscillations $n$ = 1 min$^{-1}$ and a rod stroke $S_0$ = 0.5 m, together with the hot oil supply to the annulus, made it possible rinse the ARPD. After 2 h of drive operation in the specified mode, the stroke of the rod increased to the set value $S_0$ = 2.5 m, after 3 h the load in the SRSP returned to normal, the operation of the SRHP was returned to the nominal mode without current workover of the well [15].

Comparative tests of SRHP equipped with a mechanical drive with SK-8 balancing pumping unit and a hydraulic drive with electrodynamic balancing SRHP HD 80-3.5 "Geyser" were carried out at Sosnovskoye oil field well 404. A distinctive feature of the scheme of this hydraulic drive is the presence of an intelligent electronic control system (IECS) unit for the oil station drive motor (see Fig.1, *d*, pos. 7, 8), which includes a frequency converter and an inverter [23].

During the tests, the well was operated with the following SRHP parameters: pump suspension depth $L$ = 1560.1 m; stroke length $S_0$ = 2.5 m; the number of double strokes $n$ = 5 min$^{-1}$ (Table 3). The specific energy consumption for lifting the well fluid during the operation of the SRHP equipped with the hydraulic drive SRHP HD 80-3.5 “Geyser” was $H_{w.test}$ = 12.76 kWh/m$^3$, which is slightly higher than the values of specific energy consumption obtained from measurements on mechanical SK-8 drive ($H_{w.b}$ = 11.25 kWh/m$^3$), with which this well was previously operated. On the wattmeter diagram of the motor of the pumping station SRHP HD 80-3.5 “Geyser” (Fig.4, *b*), it is possible to distinguish sections of the working and reverse stroke of the power hydraulic cylinder rod [24].

During the working stroke, the HP pumping station motor with electrodynamic balancing works with a rated load, the power factor is cosφ = 0.85. When the power hydraulic cylinder rod is lowered, the motor SRHP HD 80-3.5 “Geyser” recuperates 25-29 % of energy into the oil field network, which corresponds to the results of similar studies [7].

The energy recuperated into the oil field network of the IECS of the SRHP HD 80-3.5 “Geyser” pumping station is characterized by the presence of higher harmonics in the current and voltage signals, which is due to the frequency converter operation. Voltage waveform distortion negatively affects the work of electricity consumers: the efficiency of the generation processes, transmission, and use of energy in the oil field network is reduced; electrical equipment insulation aging occurs; the losses in the windings of electrical machines increase [15, 25, 26].

**Results discussion.** Both tested SRHP HD showed lower energy efficiency compared to traditional mechanical drives SK-8. A common disadvantage of SRHP HD with pneumatic balancing is the use of two working agents – gas and liquid, which necessitates the use of two separate leakage compensation systems. In most SRHP HD models with pneumatic balancing, the frequency of double strokes of the power hydraulic cylinder rod is regulated by increasing the pause between strokes due to the lower reliability of variable pumps compared to the pumps with a constant supply. This significantly reduces the energy efficiency of the considered hydraulic drives. Nevertheless, a number of manufacturers continue to produce and sell SRHP drives with pneumatic balancing on the market, since satisfactory adjusting characteristics and lower metal consumption compared to mechanical SK allow the described SRHP HD to be successfully used in complicated operating conditions of downhole equipment.

The advantage of SRHP HD with dynamic and electrodynamic balancing is the hydraulic part design simplicity. The open type of hydraulic transmission does not provide for the use of additional equipment to compensate for leaks. The regulation of operating parameters is carried out by using a frequency drive, which allows using volumetric constant flow motor-pumps in the design.

Significant shortcomings of the considered drives should be noted. The process of energy recovery during the operation of the IECS causes an increase of the reactive power in the oil field network and the harmonic interference (parasitic EMF) appearance, which negatively affects the work of consumers [7, 27, 28]. Power balance correction in the field network is provided by installing expensive compensating devices, which increases the operating costs for the maintenance of well equipment [29].

Elimination of this disadvantage is possible when using electricity consumers switching circuit as part of the SRHP HD with electrodynamic balancing, which ensures the accumulation and use of recuperated electricity for the operation of auxiliary consumers and peripheral devices SRHP (Fig.5).

The essence of the technical solution developed by the authors is as follows. The reverse relays of the power hydraulic cylinder and the electric power accumulator are installed in the consumer circuit of the SRHP HD under consideration. When lifting the power hydraulic cylinder rod and SRSP, the voltage from the power grid is supplied to the frequency converter (FC) and then to the electric motor M1 of the hydraulic drive pumping station. By means of the frequency converter, the speed of the M1 motor rotor and the supply of the hydraulic drive pump are controlled, which makes it possible to change the stroke rate of the SRSP (*n*). The relay K of the hydraulic cylinder (HC) reverse run is de-energized, and its closed contact K.2 supplies a control signal to close the automatic battery power switch directly from the network.

EDN XLRCWN

**Journal of Mining Institute.** 2023. Vol. 261. P. 349-362
© Dmitriy I. Shishlyannikov, Valeriy Yu. Zverev, Anna G. Zvonareva, Sergey A. Frolov, Anna A. Ivanchenko, 2023

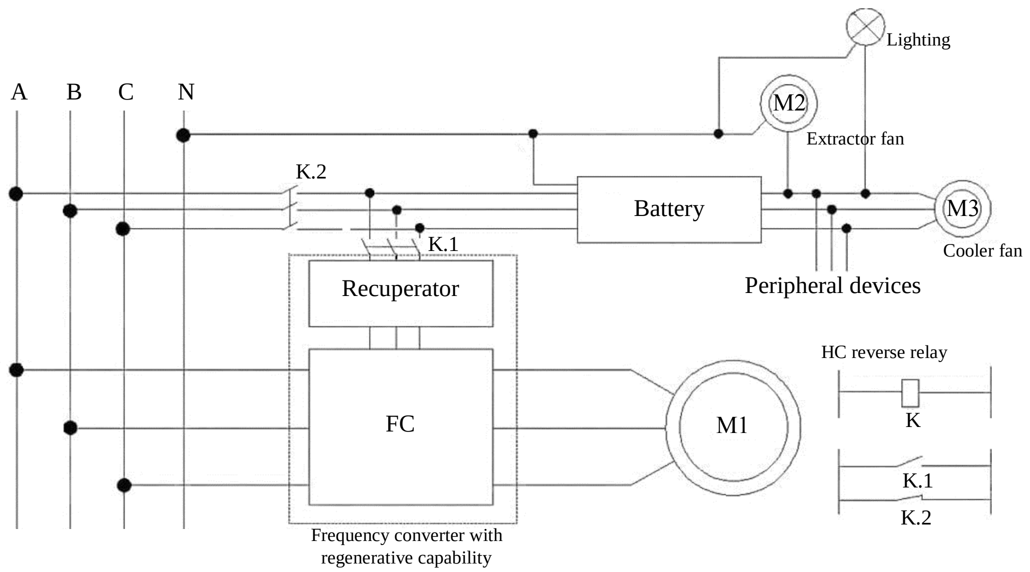


Fig.5. Switching scheme of electric power consumers as a part of SRHP hydraulic drives with electrodynamic balancing

When lowering the SRSP, the working fluid from the power hydraulic cylinder rod end is supplied to the pump, which operates as a hydraulic motor, spinning the M1 motor rotor. Motor M1 operates in generator mode. The generated electricity through the heat exchanger and the closed-circuit breaker, controlled by contact K.1 of the hydraulic cylinder reverse stroke relay K, is fed to the battery and then, as necessary, is consumed during the operation of the auxiliary consumers of the hydraulic drive. The motor M2 of the exhaust fan in the drive block box or the motor M3 of the working fluid cooler fan (radiator), and lighting devices can act as such. Various connection schemes and the use of electrical equipment allow you to supply receivers of different types and voltages.

Electricity from the battery can be spent on the operation of SRHP peripherals: rod rotators, local heating devices, dosing units for reagents, etc. The described technical solution ensures the efficient use of the generated and stored energy during the operation of the SRHP HD with electrodynamic balancing.

From the point of view of the analysis of the kinematic parameters of the movement of the SRSP and the loads on the electric motor, the examined hydraulic drive “Geyser” should be considered as unbalanced. These drives require high power motors. Significant dynamic loads cause an accelerated consumption of the drives resource with electrodynamic balancing, which determines the increase in operating costs for their maintenance in working condition.

A common disadvantage of SRHP HD with the dynamic balancing is a change in the direction of counter torque from an external load on the motor-pumps shafts and drive electric motors. Since these parts, as a rule, have small cross-sectional dimensions and are mated with the rest of the drive units by means of spline connections, they are characterized by frequent failures associated with metal fatigue and the destruction of splines. Over 41 % of the failures of the SRHP HD hydraulic part with dynamic balancing occur due to the failure of the axial piston pumps of the hydraulic power transmission. This negative phenomenon is typical for drives with electrodynamic balancing and for SRHP HD with the inertial type of balancing.

An analysis of the theoretical and experimental studies results shows that the use of electrodynamic and pneumatic methods of balancing the SRHP HD negatively affects the energy efficiency and reliability of the operation of the pumping unit as a whole. The load balancing devices are characterized by maximum efficiency and durability (see Table 2).

In SRHP HD with load balancing, a load is used as an energy accumulator of the balancing device. The advantage of such drives is the design simplicity and reliability. At the same time, these HDs are characterized by increased metal consumption, comparable to SRHP hydraulic drives with pneumatic balancing, and worse mounting ability.

The authors proposed and patented the scheme of the SRHP HD with a load balancing (Fig.6). The drive consists of a power hydraulic cylinder 1 and a balancing load-hydraulic accumulator 2 (it is a vertically mounted hydraulic cylinder with weights fixed on the rod), the rod cavities of which are connected by a pipeline 3 as communicating vessels. The pipeline 3 through the check valve 4 is connected to the high-pressure cavity 5 of the intermediate double-sided cylinder 6. The pump 7 supplies the working fluid from the oil tank 8 to the piston cavities of the power hydraulic cylinder 1 and the hydraulic load accumulator 2 through the hydraulic distributor 9. The working fluid is cleaned by the filter 10. Pump protection 7 overload protection is implemented by a safety valve 11.

The working fluid pumping into the cavity of low pressure 12 and high pressure 5 of the intermediate double-sided cylinder 6 is carried out by the pump 7 through the hydraulic distributor 13. The working fluid is drained from the rod cavities of the power hydraulic cylinder 1 and the load-hydraulic accumulator 2 through a two-position hydraulic distributor 14 through an adjustable throttle 15. Working pressure in the hydraulic system is controlled by manometers (pressure sensors) 16-18. The number of swings and stroke of the power hydraulic cylinder 1 are determined by the readings of sensors 19, the signals from which are transmitted to the intelligent control unit (ICU) 20. In the drain line of SRHP HD, the fluid flow is switched by the distributor 21 to the controlled throttle 22 for damping loads on the final sections of the SRSP movement.

After filling the hydraulic system with a working fluid and installing the described SRHP HD above the wellhead, its work is carried out as follows. The power hydraulic cylinder rod 1 is connected to the pump rod string and the downhole pump plunger. The lifting of the power cylinder rod 1 is carried out by pumping the working fluid by the pump 7 from the tank 8 into the piston cavity of the hydraulic load accumulator 2 when the hydraulic distributor 9 is switched to position II. At the same time, in the SRSP, a load $G_p$ occurs on the rod of the power hydraulic cylinder 1, balanced by the weight of the loads $G_a$, fixed on the rod of the hydraulic load accumulator 2. The weight of the balancer with the same design parameters of the power hydraulic cylinder and the balancing hydraulic cylinder of the hydraulic load accumulator is calculated by the formula

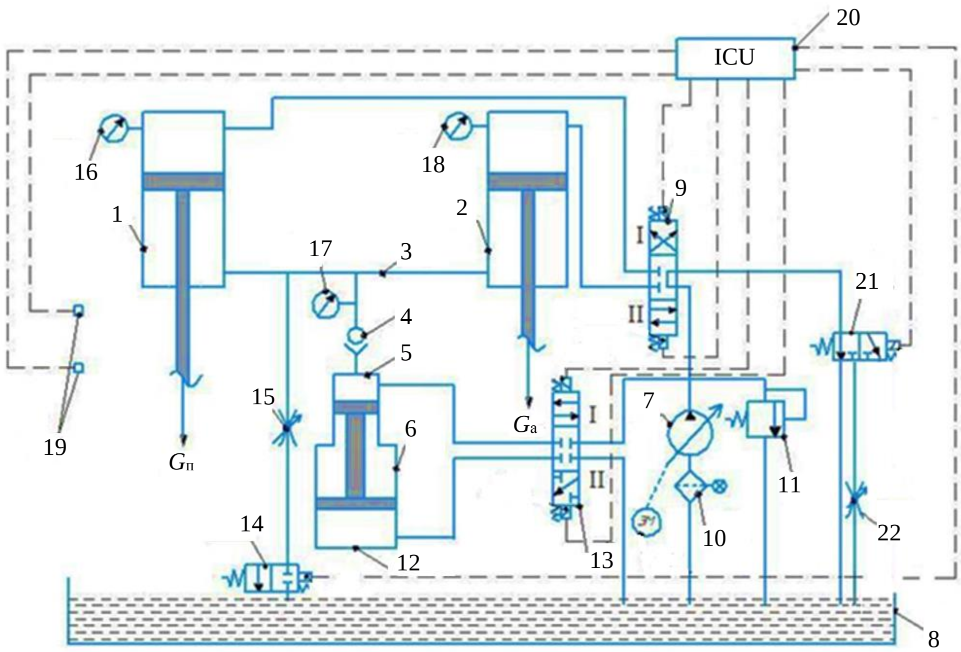


Fig.6. Hydraulic scheme of advanced SRHP drive with load balancing

$$G_a = G_{rod} + 0.5G_{liq},$$

where $G_{rod}$ – sucker rod string weight in liquid, kN; $G_{liq}$ – liquid column weight, kN [11].

The working fluid from the piston cavity of the power hydraulic cylinder 1 through the distributor 9 is fed into the drain line by means of a two-position distributor 21, which, at the SRHP movement final stage, switches the fluid flow to the throttle 22, braking the power hydraulic cylinder 1 piston.

The signal from the ICU 20 to the magnetic coil of the hydraulic distributor 9 ensures that the latter is switched to position I. The working fluid from the tank 8 is supplied by an adjustable pump 7 to the piston cavity of the power hydraulic cylinder 1, the reverse stroke of the SRHP and the plunger of the borehole pump is carried out. In this case, the working fluid from the rod cavity of the power hydraulic cylinder 1 is displaced into the rod cavity of the balancing hydraulic cylinder of the load-hydraulic accumulator 2. The loads weighting $G_a$, fixed on the rod of the load-hydraulic accumulator 2, rise, and energy is accumulated to balance the SRHP HD. From the hydraulic load accumulator cylinder 2 piston cavity, the liquid is drained through the hydraulic distributors 9 and 21 into the oil tank 8.

If it is necessary to reduce the power hydraulic cylinder 1 stroke, a working fluid partial discharge from the pipeline 3 is realized through the adjustable throttle 15 and the two-position hydraulic valve 14 into the oil tank 8. The working fluid injection into the rod cavities of the power cylinder 1 and balancing hydraulic cylinder 2 to increase the stroke length of the SRSP is carried out through the pipeline 3 by the intermediate double-sided hydraulic cylinder 6. The process is implemented as follows. ICU 20 sends a signal to the control coil of the hydraulic distributor 13 and switches it to position I. The working fluid is pumped by the pump 7 into the high-pressure cavity 5 of the intermediate double-sided hydraulic cylinder 6, while the liquid is forced out of the low-pressure cavity 12 into the oil tank 8.

After cavity 5 is filled, the hydraulic valve 13 switches to position II at the ICU 20 signal, the low-pressure cavity 12 of the intermediate double-sided hydraulic cylinder 6 is filled with working fluid from the oil tank 8, from the high-pressure cavity 5, the working fluid is displaced through the check valve 4 into the pipeline 3. Operation of the intermediate hydraulic cylinder 6 and the hydraulic distributor 13 is carried out until the rod cavities of the power 1 and balancing 2 hydraulic cylinders are filled with a given volume of working fluid, which ensures the required amount of movement of the SRSP, its actual value is determined by the readings of sensors 19. Change in the amount of return-but-translational movements of the rod of the power hydraulic cylinder 1 per unit time is carried out by regulating the supply of the positive displacement pump 7.

The application of the described scheme and operation algorithm ensures the balancing of the SRHP HD and its energy efficient operation in the oil field [30]. The proposed HD scheme simplicity and the dynamic loads minimization on the drive elements will increase the time between failures of the entire SRHP, which will positively affect the profitability of the oil production process [31-33]. A distinctive feature of the SRHP HD circuit is the absence of a make-up pump: leakage compensation and the supply of working fluid to the rod cavities of the power hydraulic cylinder and the balancing load hydraulic accumulator are carried out by means of an intermediate double-sided hydraulic cylinder, which simplifies the drive design.

The assessment of the economic efficiency of the load-balancing HD implementation can be carried out by comparing the net present value *NPV* in the operation of oil wells with SRHP, equipped with traditional SK mechanical drives and the proposed HD [34, 35]. Factors influencing the assessment of economic efficiency are presented in Table 4.

The peculiarity of the projects comparison is that the drives service life is different: the average service life of the SRHP HD is 1.5-2 times less than that of the SK mechanical drive. To compare projects at different times, you can apply the method of chain repetition: determine the smallest multiple of the terms of projects and compare the sums of their net present value [36].

*Table 4*

**Assessment of economic efficiency when replacing the SRHP mechanical drive with a hydraulic one**

| Factors leading to an increase in net present value | Factors leading to a decrease in net present value |
|---|---|
| Reduction of unit costs for electricity | Increase in the number of repairs and maintenance of the drive |
| Reduced drive installation costs (there is no need for massive foundations, as for mechanical SKs) | Increase in the cost of purchasing spare parts during repair and restoration work (hydraulic and electrical parts of drives) |
| Reducing the number of ongoing well repairs | Reducing the service life by 1.5-2 times compared to mechanical SK |

It is assumed that the sales proceeds will be the same for the compared projects, since the performance of the SRHP does not differ. The change in net present value $\Delta NPV_\Sigma$ is to reduce operating costs, change the income tax, the difference in capital investments, and the amount of depreciation. Thus, the change in the net present value when replacing the traditional SRHP mechanical drive with a promising hydraulic drive is generally determined by the expression

$$\Delta NPV_\Sigma = \sum_{t=0}^{P} \frac{\Delta O_t - \Delta T_t \pm \Delta C_t \pm \Delta A_t}{(1+r)^t},$$

where $P$ – project implementation period, years; $\Delta O_t$ – change in operating costs for period $t$, rub.; $\Delta T_t$ – change of the income tax for the period $t$, rub.; $\Delta C_t$ – difference in capital investments for period $t$, rub.; $\Delta A_t$ – difference in depreciation for the period $t$, rub.; $r$ – discount rate adopted for project evaluation, unit share.

The reduction in operating costs will be achieved by reducing the unit cost of electricity and the cost of ongoing well workovers [37]. It should be taken into account that the use of HD with load balancing entails an increase in the number of repairs, maintenance of the drive and the purchase of spare parts during repair and restoration work (hydraulic and electrical parts of drives) [38]. The formula for calculating the reduction in operating costs from the implementation of the SRHP HD scheme with load balancing can be represented as

$$\Delta O_t = \Delta O_{\text{el.en}} + \Delta O_{\text{wo}} - \Delta O_{\text{mt}} + \Delta A,$$

where $\Delta O_{\text{el.en}}$ – operating costs reduction for electricity for the production of well fluid, rub.; $\Delta O_{\text{wo}}$ – reduction of operating costs for current workovers, rub.; $\Delta O_{\text{mt}}$ – additional operating costs associated with an increase in the number of repairs and maintenance of drives, rub.; $\Delta A$ – difference in depreciation, rub.

To calculate the savings in energy costs for the production of well fluids, data are needed on the average daily electricity consumption during the operation of the SRHP HD with load balancing and the average daily flow rate of the well fluid. In further studies, it is planned to create an industrial design of SRHP HD and conduct the test of the proposed drive, during which the necessary data will be obtained.

**Conclusion.** SRHP HD design and operation features show the prospects for their further improvement and widespread implementation in the oil fields of Russia and the CIS countries in the complicated and marginal oil wells operation. The described approaches, methodology and equipment for conducting experimental studies make it possible to perform a comparative assessment of the effectiveness of the functioning of mechanical and hydraulic drives of SRHPs in terms of the energy efficiency coefficient.

Introduction of SRHP HD with the electrodynamic balancing of power accumulators into the switching circuits allows accumulating and using recuperated electric power for operation of the auxiliary consumers and peripheral devices of SRHP. Minimization of reactive power and parasitic EMF in oilfield networks is provided. A promising scheme of the SRHP HD with load balancing is proposed, which provides the possibility of effective balancing of the drive and reducing the dynamic loading of its power elements.

*The authors are grateful to N.N.Sofina, Director of OOO "NPP "ROS" (Perm), for assistance in planning and conducting experimental studies, and to the staff of OOO "LUKOIL-Perm" for advice and assistance in conducting research.*

## REFERENCES

1. *Ivanovskii V.N.* Increasing interest in sucker rod pumping units – what is the reason? *Territoriya NEFTEGAZ*. 2013. N 8, p. 46-47 (in Russian).

2. Myrzakhmetov B.A., Nurkas Zh.B., Sultabaev A.E. Protection of downhole pumping equipment in case of high sand production. *Gornyi zhurnal*. 2022. N 7, p. 82-86 (in Russian). DOI: 10.17580/gzh.2022.07.14

3. Bealessio B.A., Blánquez Alonso N.A., Mendes N.J. et al. A review of enhanced oil recovery (EOR) methods applied in Kazakhstan. *Petroleum*. 2021. Vol. 7. Iss. 1, p. 1-9. DOI: 10.1016/j.petlm.2020.03.003

4. Lavrenko S., Klushnik I., Iarmolenko V. Test results for hydraulic drives of sucker-rod pumping units. *ARPN Journal of Engineering and Applied Sciences*. 2019. Vol. 14. N 16, p. 2881-2885.

5. Grigorev S.L., Demidov O.V. Rod pump hydraulic drive – a new oil production technology. *Territoriya NEFTEGAZ*. 2010. N 10, p. 59 (in Russian).

6. Xinmin Song, Debin Qu, Cunyou Zou. Low cost development strategy for oilfields in China under low oil prices. *Petroleum Exploration and Development*. 2021. Vol. 48. Iss. 4, p. 1007-1018. DOI: 10.1016/S1876-3804(21)60085-X

7. Drozdov A.N., Blokhin S.A., Pak D.X. et al. Analysis of the efficiency of the hydralic drive "Geron" application as an alternative to the usage of standart pumpjack. Trudy nauchno-prakticheskoi konferentsii s mezhdunarodnym uchastiem "Inzhenernye sistemy – 2019", 3-5 April 2019, Moscow, Russian Federation. Moscow: Peoples' Friendship University of Russia. 2019, p. 360-366 (in Russian).

8. Fei Yao, Yu-xue Sun, Dekui Xu et al. Research Status and Development Trend of Clean Operation Technology in Domestic Onshore Oilfield. Proceedings of the International Field Exploration and Development Conference 2020. Singapore: Springer, 2021, p. 2331-2342. DOI: 10.1007/978-981-16-0761-5_220

9. Youhong Sun, Yuanling Shi, Qingyan Wang, Zongwei Yao. Study on speed characteristics of hydraulic top drive under fluctuating load. *Journal of Petroleum Science and Engineering*. 2018. Vol. 167, p. 277-286. DOI: 10.1016/j.petrol.2018.04.003

10. Abebe A., Tadesse Y., Beyene A. Conversion of Thermally Amplified Hydraulic Shock for Power Generation: Modeling and Experimental Analyses. *Journal of Energy Resources Technology*. 2023. Vol. 145. Iss. 2. N 022103. DOI: 10.1115/1.4054826

11. Molchanov A.G. Scientific basis for the design and operation of hydraulically driven sucker-rod pumping units for oil production: Avtoref. dis. ... d-ra tekhn. nauk. M.: Gosudarstvennaya akademiya nefti i gaza im. I.M.Gubkina, 1998, p. 34 (in Russian).

12. Sidorkin D.I., Kupavykh K.S. Justification on choosing screw pumping units as energy efficient artificial lift technology. *Energetika. Proceedings of CIS Higher Education Institutions and Power Engineering Associations.* 2021. Vol. 64. N 2, p. 143-151. DOI: 10.21122/1029-7448-2021-64-2-143-151

13. Urazakov K.R., Molchanova V.A., Tugunov P.M. Method for calculating dynamic loads and energy consumption of a sucker rod installation with an automatic balancing system. *Journal of Mining Institute*. 2020. Vol. 246, p. 640-649. DOI: 10.31897/PMI.2020.6.6

14. Nickell I., Treiberg T. Autonomous Control of Well Downtime to Optimize Production and Cycling in Sucker Rod Pump Artificially Lifted Wells. SPE Artificial Lift Conference and Exhibition – Americas, 23-25 August 2022, Galveston, USA. OnePetro, 2022. N SPE-209743-MS. DOI: 10.2118/209743-MS

15. Ustinov A.N., Tyaktev M.V., Shishlyannikov D.I. et al. Increasing the efficiency of hydraulic drives of sucker-hole pumping units for oil production. *Mining Equipment and Electromechanics.* 2017. N 7 (134), p. 26-31 (in Russian).

16. Eisner P., Langbauer C., Fruhwirth R.K. Comparison of a novel finite element method for sucker rod pump downhole dynamometer card determination based on real world dynamometer cards. *Upstream Oil and Gas Technology*. 2022. Vol. 9. N 100078. DOI: 10.1016/j.upstre.2022.100078

17. Kunshin A., Dvoynikov M., Timashev E., Starikov V. Development of Monitoring and Forecasting Technology Energy Efficiency of Well Drilling Using Mechanical Specific Energy. *Energies*. 2022. Vol. 15. Iss. 19. N 7408. DOI: 10.3390/en15197408

18. Moreno G.A., Garriz A.E. Sucker rod string dynamics in deviated wells. *Journal of Petroleum Science and Engineering*. 2020. Vol. 184. N 106534. DOI: 10.1016/j.petrol.2019.106534

19. Teplyakova A.V., Azimov A.M., Alieva L., Zhukov I.A. Improvement of manufacturability and endurance of percussion drill assemblies: Review and analysis of engineering solutions. *Mining Informational and Analytical Bulletin*. 2022. N 9, p. 120-132 (in Russian). DOI: 10.25018/0236_1493_2022_9_0_120

20. Shuqiang Wang, Shimin Dong, Xuelin Yu. Transverse vibration simulation of sucker rod string under normally distributed load caused by viscoelastic fluid in a curved wellbore. *Journal of Sound and Vibration*. 2022. Vol. 536. N 117181. DOI: 10.1016/j.jsv.2022.117181

21. Dong Shimin, Wang Hongbo. Simulation model of lateral vibration of sucker rod string in directional wells and point arrangement optimization of centralizer. *Acta Petrolei Sinica*. 2020. Vol. 41. Iss. 12, p. 1686-1696. DOI: 10.7623/syxb202012021

22. Wang Hong-bo, Dong Shi-min. A model for the transverse vibration simulation of sucker rod strings with axial reciprocating motion in curved wellbores. *Engineering Mechanics*. 2020. Vol. 37. N 10, p. 228-237. DOI: 10.6052/j.issn.1000-4750.2019.12.0731

23. Omirbekova Z., Aktaukenov D., Amangeldiyev A., Abdallah A. Developing Predictive Oil Well Diagnostics Based on Intelligent Algorithms. IEEE International Conference on Smart Information Systems and Technologies, 28-30 April 2021, Nur-Sultan, Kazakhstan. IEEE, 2021, p. 1-7. DOI: 10.1109/SIST50301.2021.9465959

24. Shishlyannikov D.I., Tyaktev M.M., Ivanchenko A.A. et al. Assessment of hydraulic drives loading of sucker rod downhole pumping units. *Construction of oil and gas wells on land and sea.* 2019. N 4, p. 34-39 (in Russian). DOI: 10.30713/0130-3872-2019-4-34-39

25. Ruichao Zhang, Yuqiong Yin, Liangfei Xiao, Dechun Chen. A real-time diagnosis method of reservoir-wellbore-surface conditions in sucker-rod pump wells based on multidata combination analysis. *Journal of Petroleum Science and Engineering*. 2021. Vol. 198. N 108254. DOI: 10.1016/j.petrol.2020.108254

26. Takács G. A critical analysis of power conditions in sucker-rod pumping systems. *Journal of Petroleum Science and Engineering*. 2022. Vol. 210. N 110061. DOI: 10.1016/j.petrol.2021.110061

27. Savinkin V.V., Sandu A.V., Ratushnaya T.Yu. et al. Study of redistribution of the oil complex power drive effectiveness for marginal wells when installing construction of recuperative action electro hydro cylinder. *Bulletin of the Tomsk Polytechnic University. Geo Assets Engineering*. 2021. Vol. 332. N 2, p. 229-244 (in Russian). DOI: 10.18799/24131830/2021/2/3058

28. Skamyin A., Shklyarskiy Ya., Dobush I. et al. An assessment of the share contributions of distortion sources for various load parameters. *International Journal of Power Electronics and Drive Systems*. 2022. Vol. 13. N 2, p. 950-959. DOI: 10.11591/ijpeds.v13.i2.pp950-959

29. Shklyarskiy Ya., Skamyin A., Vladimirov I., Gazizov F. Distortion Load Identification Based on the Application of Compensating Devices. *Energies*. 2020. Vol. 13. Iss. 6. N 1430. DOI: 10.3390/en13061430

30. Litvinenko V.S., Sergeev I.B. Innovations as a Factor in the Development of the Natural Resources Sector. *Studies on Russian Economic Development*. 2019. Vol. 30. N 6, p. 637-645. DOI: 10.1134/S107570071906011X

31. D.I.Shishlyannikov, A.A.Ivanchenko, S.A.Frolov, V.Yu.Zverev, A.V.Nikolaev. Patent N 2779011 RF. Rod pump hydraulic drive. Publ. 30.08.2022. Bul. N 25.

32. Isaev A.A., Aliev M.M.O., Drozdov A.N. et al. Improving the Efficiency of Curved Wells' Operation by Means of Progressive Cavity Pumps. *Energies*. 2022. Vol. 15. Iss. 12. N 4259. DOI: 10.3390/en15124259

33. Cherepovitsyn A., Rutenko E. Strategic Planning of Oil and Gas Companies: The Decarbonization Transition. *Energies*. 2022. Vol. 15. Iss. 17. N 6163. DOI: 10.3390/en15176163

34. Ponomarenko T., Marin E., Galevskiy S. Economic Evaluation of Oil and Gas Projects: Justification of Engineering Solutions in the Implementation of Field Development Projects. *Energies*. 2022. Vol. 15. Iss. 9. N 3103. DOI: 10.3390/en15093103

35. Tarabarinova T.A., Golovina E.I. Capitalization of mineral resources as an innovation ecological strategy. *Geology and Mineral Resources of Siberia*. 2021. N 4 (48), p. 86-96 (in Russian). DOI: 10.20403/2078-0575-2021-4-86-96

36. Yashin S.N., Trifonov Yu.V., Koshelev E.V. Comparison of Replacement Chain and Equivalent Annual Annuity Approaches to Evaluate Technological Innovation of the Company. *Financial Analytics: Science and Experience*. 2018. Vol. 11. Iss. 1, p. 32-42 (in Russian). DOI: 10.24891/fa.11.1.32

37. Ruidong Zhao, Jinya Li, Zhen Tao et al. Research and Application of Rod/Tubing Wearing Prediction and Anti-Wear Method in Sucker Rod Pumping Wells. SPE Middle East Oil and Gas Show and Conference, 18-21 March 2019, Manama, Bahrain. OnePetro, 2019. N SPE-194955-MS. DOI: 10.2118/194955-MS

38. Aliyev E.A., Gabibov I.A., Ismailova R.A., Huseynov R.O. Application of new repair technology in the restoration of plungers of borehole rod pumps. *SOCAR Proceedings*. 2022. N SI2, p. 1-4 (in Russian). DOI: 10.5510/OGP2022SI200730

***Authors*: Dmitriy I. Shishlyannikov,** *Doctor of Engineering Science*, *Professor*, *https://orcid.org/0000-0002-7395-6869* (*Perm National Research Polytechnic University*, *Perm*, *Russia*), **Valeriy Yu. Zverev,** *Candidate of Engineering Science*, *Associated Professor*, *https://orcid.org/0009-0002-2483-132X* (*Perm National Research Polytechnic University*, *Perm*, *Russia*), **Anna G. Zvonareva,** *Candidate of Economics*, *Assistant Lecturer*, *Zvonareva_AG@pers.spmi.ru*, *https://orcid.org/0000-0002-4468-5342* (*Saint Petersburg Mining University*, *Saint Petersburg*, *Russia*), **Sergey A. Frolov,** *Assistant Lecturer*, *https://orcid.org/0009-0008-7720-5991* (*Perm National Research Polytechnic University*, *Perm*, *Russia*), **Anna A. Ivanchenko,** *Assistant Lecturer*, *https://orcid.org/0009-0005-9667-2606* (*Perm National Research Polytechnic University*, *Perm*, *Russia*).

*The authors declare no conflict of interests.*

ISSN 2411-3336; e-ISSN 2541-9404

JOURNAL OF MINING INSTITUTE

Zapiski Gornogo instituta

Journal homepage: pmi.spmi.ru

*Research article*

# A reliability study of the traction drive system in haul trucks based on failure analysis of their functional parts

**Alexander N. NAZARYCHEV, Grigory V. DYACHENOK ✉, Yuriy A. SYCHEV**
*Saint Petersburg Mining University, Saint Petersburg, Russia*

***How to cite this article*:** Nazarychev A.N., Dyachenok G.V., Sychev Yu.A. A reliability study of the traction drive system in haul trucks based on failure analysis of their functional parts. Journal of Mining Institute. 2023. Vol. 261, p. 363-373. EDN HCLPJB

***Abstract.*** The efficiency of a mining and processing plant depends on the level of complex mechanization of the production process. In mineral extraction, haulage is a major cost category, with haul trucks being the key component of the mining transportation system. To improve production performance, mining operations can increase their haulage turnover and reduce transportation costs, which necessitates making haul trucks more reliable. This can be done by improving their mean time to first failure (MTFF) indicators. This article analyzes the reliability status of the traction drive system inhaul trucks operating in the mineral resources sector. It provides a quantitative assessment of traction drive system failures resulting from part defects and discusses the associated repair costs. By examining failure data from 2018 to 2022 and the results of vibration tests performed on a diesel generator, the study reveals that the most expensive failures are associated with defects in the synchronous generator, which are primarily caused by elevated external vibrations. Based on basic vibration tests and vibration spectra tests at different operating modes, recommendations have been formulated concerning the generator's robustness to external mechanical forces and the ways to increase the generator's protection grade to prevent dust intrusion. The study also identifies the frequency range that poses the greatest risk of damage to the windings.

***Keywords*:** traction motor; mining trucks; reliability; equipment health; defects; failures; synchronous generator

***Received: 14.03.2023*** ***Accepted: 20.06.2023*** ***Online: 19.07.2023*** ***Published: 19.07.2023***

**Introduction.** Currently, haul trucks are extensively utilized in open-pit mining to transport broken ore and rocks [1-3]. In the mining sector, transportation often accounts for 70 % of the total production costs [4, 5], with a major share attributed to traction drive system (TDS) repairs [6]. Haul truck downtime is caused by both scheduled maintenance and repair and emergency repairs resulting from TDS failures [7-9].

The traction drive system consists of a synchronous generator (SG), a control cabinet (CC), and an asynchronous traction motor (ATM) installed on each rear wheel of a haul truck.

To improve the reliability, safety, and efficiency of operating open-pit haul trucks while ensuring optimal maintenance costs, it is necessary to conduct studies to assess and ensure TDS reliability [10-12]. Considering that haul trucks operate in diverse climatic conditions across more than 80 countries worldwide*, often under extreme conditions [13-15], there are stringent requirements as to the ability of the TDS to withstand environmental factors.

To date, various studies have been conducted to enhance the reliability of electric motors and their components. These studies include:

* BELAZ consumers. URL: https://belaz.by/about/consumers/ (accessed 20.12.2022).

• Remote vehicle health monitoring (the engine, the electric drive, and the hydraulic system) to prevent accidents and carry out maintenance and repairs based on the actual condition of the dump truck, rather than using the traditional preventive maintenance approach [16].

• Predicting wear of theelectric motor bearings. Studies in this area [17, 18] explore methods for predicting the remaining lifespan of electric motor bearings using mathematical models.

• Fault finding in asynchronous motors through a multilevel combination of information [19, 20]. The referenced studies present models, one of which gives a conditional probability for different engine performance states based on data obtained from laboratory tests, while the other one identifies the operating modes of an electric motor based on subharmonic parameters.

• Assessing the probability of failure in an asynchronous motor within an electric drive through testing vibration and electrical parameters [21-23].

• Monitoring the state of synchronous generators using electrical signals. This work [24] contributes practical results in fault detection for operating synchronous generators connected to power systems.

• Assessing the life cycle of electric drives to improve power system efficiency. The referenced study [25] proposes a technique for evaluating the health status of electric drives based on normalized amplitudes of frequency components.

• Evaluating the reliability of the traction motor by the calculation method and the fault tree analysis [26-28].

Despite the diverse range of the studies mentioned, there is a notable lack of research specifically dedicated to the reliability of traction motors in mining trucks. While some studies [29, 30], address the reliability of mining trucks, they primarily focus on failures in components such as the internal combustion engine, undercarriage, or wheel motor gearbox, etc. The issue of traction drive system reliability is only considered superficially in such works.

This is an applied study. Based on analyzing operational data, we determined the causes of TDS failures and identified the parts that demand the utmost attention. The major advantage of the study lies in conducting field tests on a synchronous generator after repairs instead of usinga software package withidealized conditions. Checking its health status after operation in a quarry allows to understand the impact of operating conditions and external mechanical vibration loads on the electric drive's reliability. We emphasize that it is important to bridge the gap between scientific research and industrial applications.

**Methods.** We conducted reliability tests of haul trucks, analyzing 326 cases of TDS part failures over a 5-year period from 2018 to 2022. To ensure that the sample was representative, haul trucks operating in various regions and climatic conditions were included in the study, encompassing Vietnam, Iran, Uzbekistan, Kazakhstan, Kuzbass, Novosibirsk region, and the Republic of Khakassia. Figure 1 shows the number of TDS part failures during the period under study. Figure 2 presents the cost ratio for restoring the individual TDS parts.

The charts show that the number of TDS failures due to SG failures is much lower compared to CC failures, while SG restoration costs account for three-fourths of the total sum. The reason for this is that it is impossible to perform SG repairs on site, which necessitates additional costs for transporting the damaged part to the manufacturer or a specialized repair company. Moreover, it is usually costly components such as the winding, rotor, and bearing assembly that require repairs. Consequently, these factors result in prolonged downtime for mining trucks.

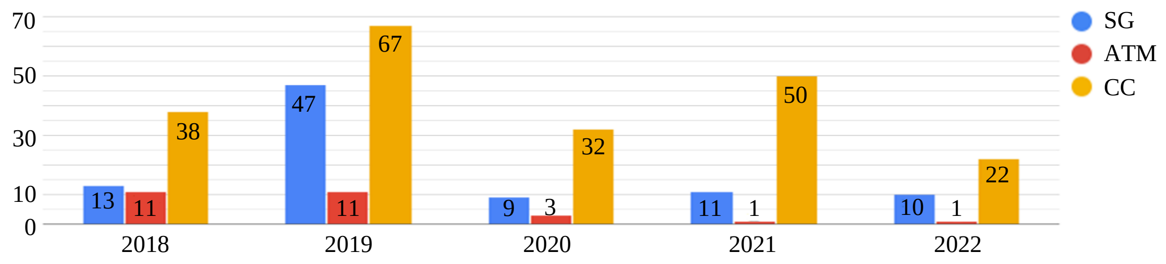


Fig.1. TDS part failures in haul trucks from 2018 to 2022

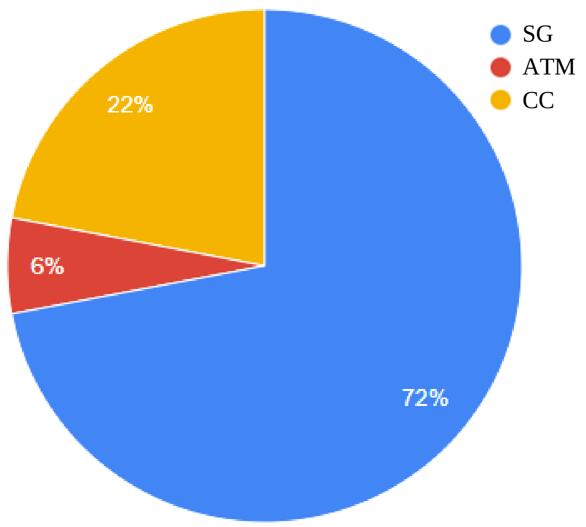


Fig.2. TDS repair costs breakdown from 2018 to 2022

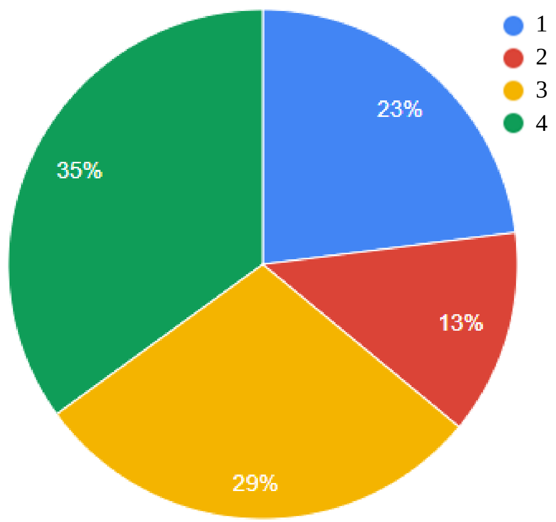


Fig.3. SG failure causes
1 – bearing assembly; 2 – other; 3 – manufacturing defect; 4 – stator winding lead burn-off

Taking into consideration the frequency of SG malfunctions and the largest share of SG costs in TDS restoration, the article will now focus on analyzing TDS failures resulting from SG failures.

Figure 3 illustrates the distribution of SG failuresby individual part failures, which is based on a dataset of 90 failures in haul trucks. SG failures happen due to the challenging and adverse operating conditions and modes experienced by haultrucks, which differ from those of stationary electric drives. These conditions include fluctuating climatic conditions, high levels of dust and humidity, frequent starts and stops, and high thermal and vibration loads [31-33].

Considering the demanding conditions ranging from temperate climates to northern latitudes in which haul trucks operate [34-36], the SG mustwithstand the impact of particular environmental factors and needs to meet several requirements:

- ambient temperature ranging from –50 to +50 °C;
- permissible upper value of the relative humidity of 100 % at a temperature of 25 °C;
- operation at an altitude up to 1,200 m above sea level;
- the IP21 rating of the generator in accordance with the GOST 14254-96 titled "Degrees of protection provided by enclosures (IP code)";
- operating conditions corresponding to the M28 design category according to GOST 17516.1-90 titled "Electrical articles. General requirement for environment mechanical stability";

• differential pressure at the inlet duct and filters not exceeding 1 kPa at an air flow rate of 1 $m^3/s$;

• maximum bearing temperature not exceeding 125 °C;

• vibration velocities not exceeding 10 mm/s at idle and 15 mm/s under load;

• the electric drive must ensure the reliable operation of a haul truck at various mines with dust concentrations of up to 10 $mg/m^3$.

Let us consider all types of SG faults in more detail from the most to least common as shown in Fig.3. The "other" category includes the following failure causes: coil deformations caused by transportation; winding displacement in the direction of rotation; short circuit at the stator winding lead.

The study revealed that during operation, a conductive path formed between the generator leadsdue to dust and moisture accumulationon the surfaces of the terminal blocks. As a result, an interphase short circuit occurred, leading to an SG failure. Considering the SG's operating conditions, it is recommended to improve the insulation of the stator winding lead in order to increase insulation.

Nearly one-third of SG failures occurred due to bearing assembly issues, including the following: bearing roller failure (defective bearing); bearing separator failure (manufacturing defect); lack of or an insufficient amount of lubrication.

Often, one cause of failure triggers another. For instance, insufficient lubrication in the bearing assembly leads to a separator failure. Moreover, it results in overheating within the bearing assembly as the heat generated during operation cannot be uniformly dissipated [37, 38]. To minimize such failures, it is necessary to improve incoming quality control procedures and perform ongoing health checks during operation.

One of the reasons for SG failures is the low quality of components caused by the negligence of electrical machine assemblers.

Now we will discuss several individual SG issues that led to haul truck failures and downtime:

• Rotor excitation coil burn-off at the junction with the lead. Such a failure is caused by the lack or low quality of solderingat the junction between the generator pole and the lead to the slip rings at the connection with the terminal strip.

• Damage to the SG's stator winding caused by a broken piece of the pole core. The probable reason for the failure of this component, which operates under impact loads, is the low strength and plastic characteristics, imperfections in the cast structure, and the absence of heat treatment that should have enhanced the mechanical properties and material structure.

• Fracture of the stator winding lead due to insufficient bolt tightening.

• Damage to the SG's winding as a result of a short circuit to frame. The reason for the damage is the failure to comply with the requirements of the design documentation for the isolation of the outlet busbars or process flow errors.

One of the major types of faults is the stator winding lead burn-off. This category of faults includes the stator winding lead burn-off from the conducting ring of the stator winding and coil-to-coil connection faults in the winding [39]. The most probable cause is high vibration levels [40-42] exceeding permissible ones. The prolonged exposure to vibrations is a recognized risk factor for various diseases among truck drivers [43-45]. Furthermore, it should be considered that during the operation of a haul truck, clayey sediment could accumulate on the SG's housing cavity. This accumulation causes a deterioration in heat dissipation from the windings [46-48], as well as an imbalance and increased vibration.

To investigate potential causes for faults in windings, we conducted vibration tests that were aimed at determining general vibration levels and their spectra in various operating modes of a diesel generator set (DGS). In our tests, we used a reconditioned generator operating at an open-pit mine in the Kemerovo region. The following operating modes were tested: idling at speeds of 900 rpm and 1,900 rpm; with loads applied to the braking resistor at 800 rpm and 1,800 rpm.

During the tests, it was observed that the maximum vibration level occurs at rpm values ranging from 1,800 to 1,900. Therefore, for further analysis, we will focus solely on these rotational frequencies.

Figure 4 shows the 14 vibration measurement locations used in our tests:

• points 1, 2, and 3: the vertical, horizontal, and axial vibrations of the bearing assembly of the generator from the slip ringside;

• points 4, 5, and 6: the vertical, horizontal, and axial vibrations of the generator frame from the diesel engine side;

• points 7, 8, and 9: the vertical, horizontal, and axial vibrations of the generator's left support from the diesel engine side;

• points 10 and 11: the vertical and axial vibrations of the diesel engine cylinder block from the generator side;

• points 12 and 13: the vertical and horizontal vibrations of the diesel engine cylinder block from the radiator side;

• point 14: the horizontal vibration of the DGS frame under the diesel engine.

**Discussion of the results.** Table 1 presents the results of measuring the root mean square (RMS) values of the DGS's vibration velocity within the frequency range of 10 to 5,000 Hz. The data shows that both at idle and under load, the vibration of the generator frame remains below the limit of 10 and 15 mm/s, respectively. The exception is some non-standardized points near the generator's bearing shield. It is worth noting that the overall vibration levels in the engine area at individual pointsare considerably higher than in the generator area. The results are presented as relative units compared to the permissible values for the generator's vibration velocity, with values exceeding the permissible limits highlighted in bold.

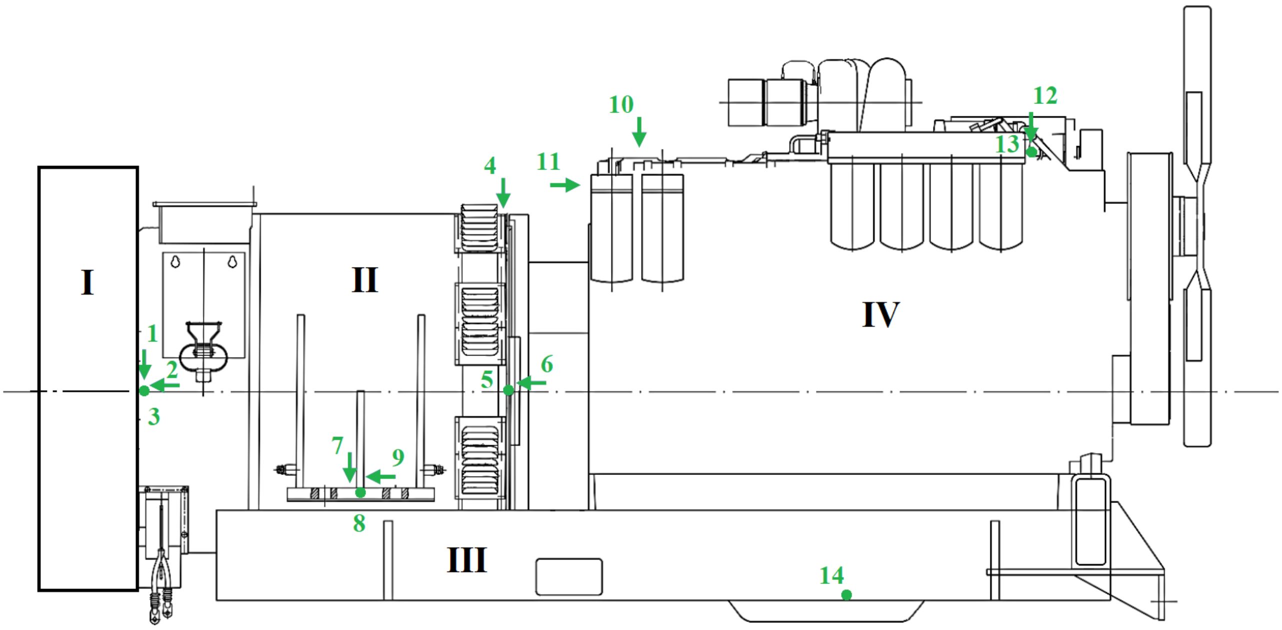


Fig.4. Measurement locations for vibration tests conducted on a diesel generator set
I – fan casing; II – synchronous generator; III – diesel generator set frame; IV – diesel engine

*Table 1*

**Relative RMS values of the generator's vibration velocity, r.u.**

| Measurement locations | Idling at *n* = 900 rpm | Idling at *n* =1,900 rpm | Load on the braking resistor at *n* = 800 rpm, *I* = 250 A | Load on the braking resistor at *n* =1,800 rpm, *I* = 330A |
|---|---|---|---|---|
| 1 | 0.46 | **1.05** | 0.31 | 0.89 |
| 2 | 0.58 | **1.62** | 0.44 | 1.08 |
| 3 | 0.31 | **1.57** | 0.27 | **1.30** |
| 4 | 0.36 | 0.55 | 0.31 | 0.48 |
| 5 | 0.22 | 0.63 | 0.13 | 0.42 |
| 6 | 0.27 | 0.80 | 0.23 | 0.57 |
| 7 | 0.41 | 0.56 | 0.28 | 0.69 |
| 8 | 0.26 | 0.95 | 0.21 | 0.68 |
| 9 | 0.27 | 0.67 | 0.20 | 0.49 |
| 10 | 0.39 | 1.08 | 0.29 | 0.55 |
| 11 | 0.22 | 1.34 | 0.16 | 0.38 |
| 12 | 0.45 | **3.71** | 0.34 | **1.44** |
| 13 | 0.27 | 0.53 | 0.15 | 0.43 |
| 14 | 0.47 | 1.07 | 0.30 | **1.77** |

During the tests, the DGS's vibration acceleration values were measured for two frequency ranges: up to 55 Hz and up to 200 Hz, as specified in the GOST 17516.1-90 titled "Electrical articles. General requirement for environment mechanical stability" for the M28 design category. The results are presented in Table 2, with indicators exceeding the operating limit highlighted in bold. Based on the results, it can be concluded that the external impact on the generator within the frequency range of 0 to 55 Hz complies with the M28 design category requirements, as stated in GOST 17516.1-90. However, the primary contribution to the overall level of generator vibration comes from harmonics with frequencies ranging from 60 to 300 and 400 Hz, which exhibit significantly higher magnitudes compared to vibrations within the 0-55 Hz range. These harmonics pose the greatest risk to the generator's winding as its resonant frequencies lie within this range. Therefore, the M28 requirements are not applicable to this particular generator. Instead, the M37 design category requirements regarding units installed on piston engines should be used (frequencies ranging from 0.5 to 500 Hz; vibration acceleration up to 100 m/s$^2$).

*Table 2*

**Maximum generator vibration accelerations relativeto the boundary value, frequency ranges 0-55/0-200 Hz, r.u.**

| Measurement locations | Idling at *n* = 900 rpm | Idling at *n* =1,900 rpm | Load on the braking resistor at *n* = 800 rpm, *I* = 250 A | Load on the braking resistor at *n* =1,800 rpm, *I* =330A |
|---|---|---|---|---|
| 1 | 0.043/0.135 | 0.106/0.444 | 0.024/0.199 | 0.101/0.457 |
| 2 | 0.092/0.171 | 0.158/0.605 | 0.037/0.265 | 0.158/0.485 |
| 3 | 0.011/0.123 | 0.047/**1.630** | 0.014/0.146 | 0.038/**1.930** |
| 4 | 0.033/0.111 | 0.068/0.167 | 0.017/0.218 | 0.060/0.321 |
| 5 | 0.019/0.058 | 0.085/0.187 | 0.024/0.033 | 0.093/0.166 |
| 6 | 0.028/0.087 | 0.065/0.359 | 0.014/0.147 | 0.084/0.340 |
| 7 | 0.028/0.164 | 0.045/0.516 | 0.025/0.139 | 0.075/0.808 |
| 8 | 0.035/0.084 | 0.095/0.456 | 0.027/0.119 | 0.139/0.404 |
| 9 | 0.025/0.088 | 0.061/0.264 | 0.016/0.124 | 0.076/0.297 |
| 10 | 0.020/0.096 | 0.098/0.156 | 0.009/0.169 | 0.107/0.201 |
| 11 | 0.013/0.036 | 0.210/0.184 | 0.019/0.047 | 0.073/0.218 |
| 12 | 0.012/0.053 | 0.614/0.659 | 0.019/0.148 | 0.212/0.440 |
| 13 | 0.034/0.075 | 0.033/0.259 | 0.017/0.077 | 0.065/0.240 |
| 14 | 0.024/0.328 | 0.084/0.729 | 0.026/0.235 | 0.133/**3.150** |

Figure 5 presents the vibration spectrum of the diesel engine cylinder block for the most active zone (frequency ranges of 1.5 to 2.5 and 3 to 3.5 kHz). The extent to which these high-frequency components affect the generator remains unknown.

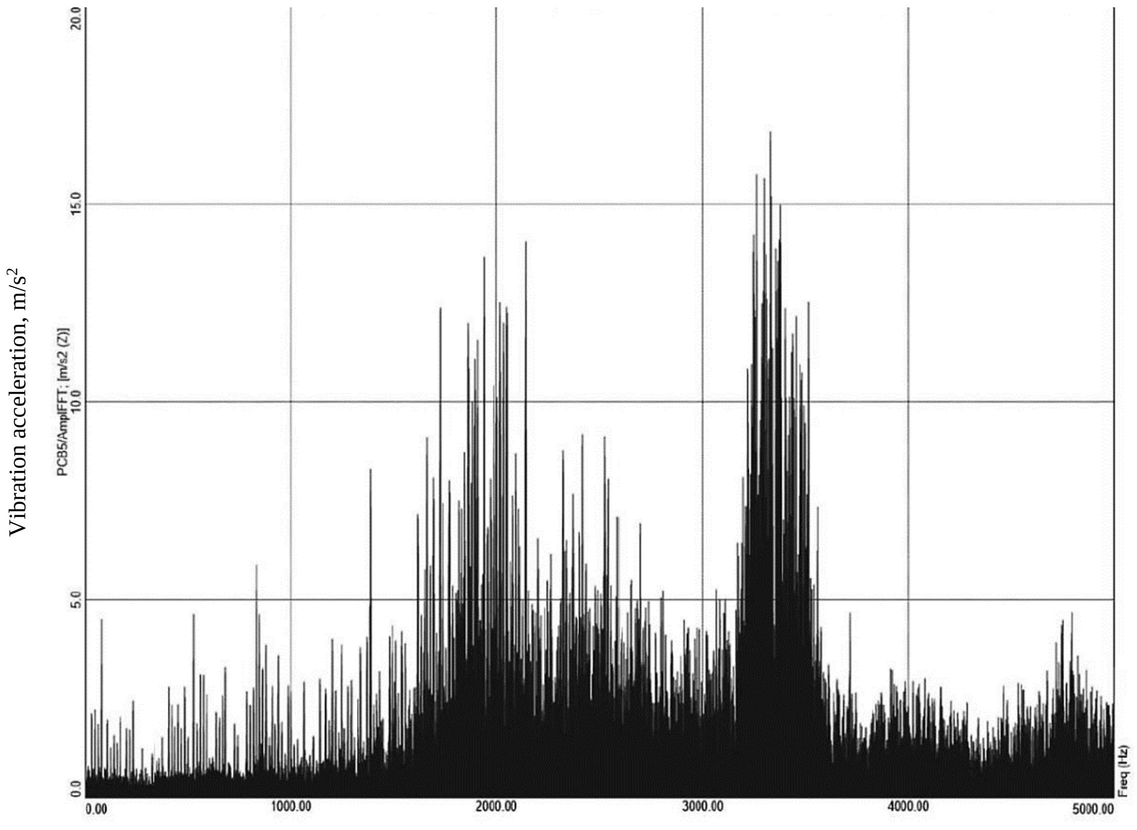


Fig.5. Vibration acceleration spectrum of the diesel engine cylinder block from the radiator side in the vertical direction (point 12)

Table 3 provides the vibration acceleration values for two measurement locations: the generator's left support from the diesel engine side (point 8) and the DGS frame under the diesel engine (point 14). These values are based on the harmonics of the rotation frequency at 1,846 rpm, 330 A for the braking resistor being loaded. Table 3 demonstrates that the diesel engine is a distinct source of vibration at harmonics 3.5 and 5. Figure 6 illustrates the vibration acceleration spectrum for the aforementioned measurement locations. Importantly, the spectrum type remains consistent regardless of the generator's load, indicating that the vibration is of a mechanical nature.

*Table 3*

**Vibration accelerations of the generator support and the DGS frame under the diesel engine in the horizontal direction**

| Frequency, Hz | Harmonic number | Vibration acceleration, r.u. | |
|---|---|---|---|
| | | Generator support | Diesel engine frame |
| 31.01 | 1 | 0.13 | 0.09 |
| 61.59 | 2 | 0.22 | 0.05 |
| 77.09 | 2.5 | 0.44 | 0.06 |
| 108.44 | **3.5** | **0.15** | **0.47** |
| 152.16 | **5** | **0.08** | **3.13** |
| 1093.57 | **36.5** | **0.07** | **0.7** |
| 1131.31 | **37** | **0.15** | **1.1** |
| 1167.99 | **38** | **0.05** | **0.96** |

The high values observed in the axial vibration of the generator's bearing assembly (point 3) are associated with the harmonics within the frequency range from 150 Hz to 200 Hz, as indicated in Table 4. This occurrence can be attributed to the resonant characteristics of the part. When testing a similar generator at a plant site, it was found that the natural frequency of the generator's bearing shield was 180 Hz, as depicted in Fig.7.

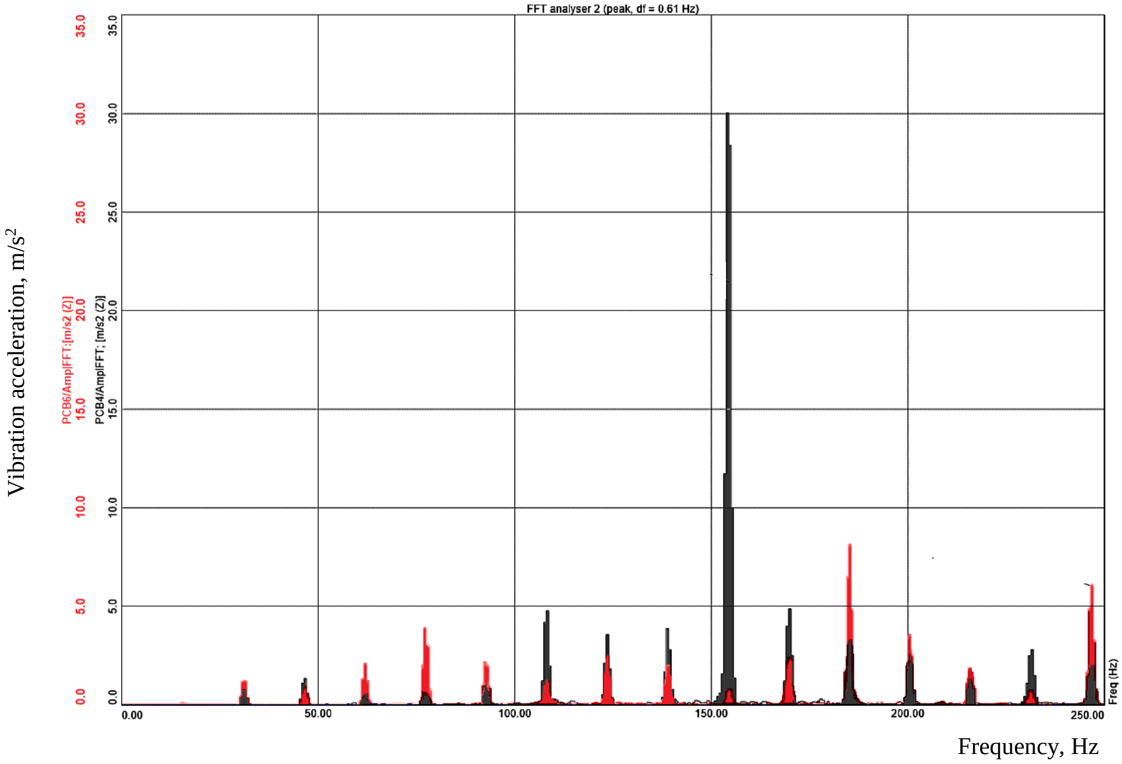


Fig.6. Vibration acceleration spectrum of the generator's support (point 8 – red) and the DGS frame under the diesel engine (point 14 – black) in the horizontal direction at 1,846 rpm

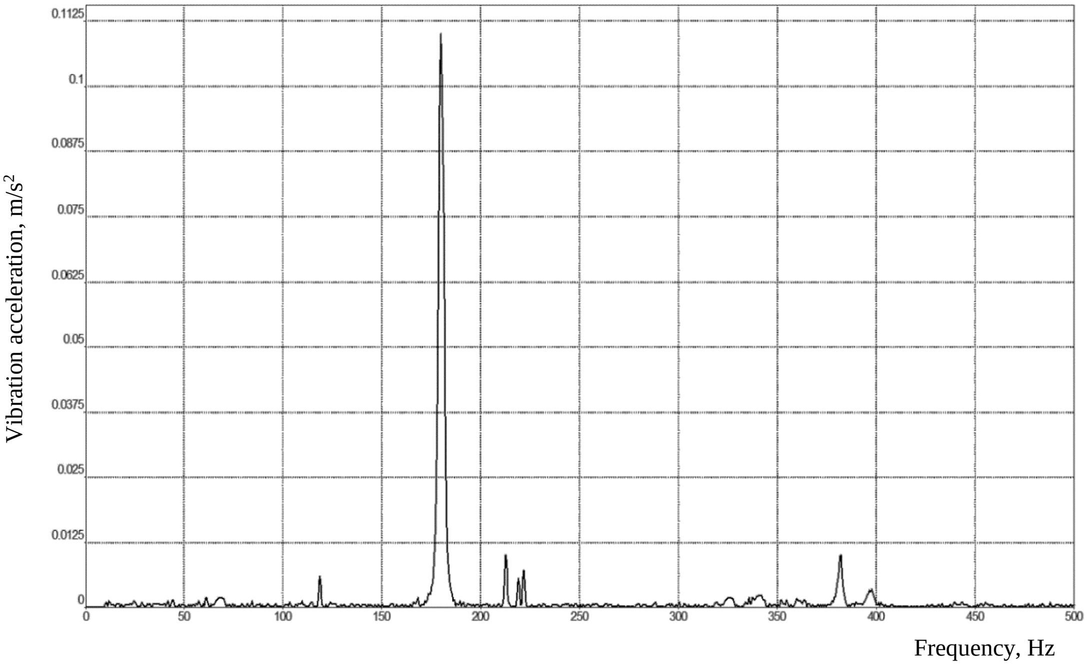


Fig.7. Vibration acceleration spectrum of the generator's end shield in the axial direction

*Table 4*

**Vibration acceleration of the bearing assembly in the axial direction by frequency harmonics at 1,914 rpm, 325 A**

| Frequency, Hz | 31.7 | 63.6 | 95.2 | 127.1 | 143.3 | 159.2 | 175.3 | 190.9 | 205.2 |
|---|---|---|---|---|---|---|---|---|---|
| Harmonic number | 1 | 2 | 3 | 4 | 4.5 | 5 | 5.5 | 6 | 6.5 |
| Vibration acceleration, r.u. | 0.01 | 0.07 | 0.21 | 0.31 | 0.35 | 0.47 | **1.26** | **1.92** | **1.62** |

**Conclusion.** Based on the results of vibration tests, this article examined traction drive system (TDS) failures in haultrucks, analyzed the causes of synchronous generator (SG) failures, and conducted bench tests of a diesel generators set (DGS) to identify the causes of stator winding failures. The following conclusions can be drawn:

• Our analysis of SG failures revealed that the stator winding (35 %) and the bearing assembly (29 %) are the functional units with the highest failure degrees. Failures in the stator winding encompass issues such as stator winding lead burn-off and coil-to-coil connection faults in the winding.

• The primary cause of stator winding failures is the excessive external vibration impact on the generator, surpassing the levels given in relevant technicalspecifications.

• The general level ofthe vibration velocity of the generator frame at speeds ranging from 1,800 to 1,900 rpm does not exceed the permissible values outlined in the regulatory documents.

• The external mechanical impact on the generator does not align with the M28 design category requirements as defined in GOST 17516.1-90 titled "Electrical articles. General requirement for environment mechanical stability". It has been determined that the M37 design category requirements should be used (frequencies ranging from 0.5 Hz to 500 Hz with vibration acceleration of up to 100 m/s$^2$).

• The test results indicate that generator vibration is practically unaffected by its load and is primarily attributed to mechanical causes.

• The most hazardous vibrations to the generator windings lie within the frequency range of 60 Hz to 200 Hz. The engine has been identified as the source of vibrations within this frequency range, at least for certainharmonics.

• The issue of stator winding damage is complex, and its root cause lies not only in the vibrations of the diesel engine or generator but also in the natural frequencies of the winding or its fixtures.

**REFERENCES**

1. Kozyaruk A.E., Kamyshyan A.M. Improving the Energy Efficiency of the Electromechanical Transmission of an Open-pit Dump Truck. *Journal of Mining Institute.* 2019. Vol. 239, p. 576-582. DOI: 10.31897/PMI.2019.5.576

2. Patterson S.R., Kozan E., Hyland P. Energy efficient scheduling of open-pit coal mine trucks. *European Journal of Operational Research*. 2017. Vol. 262. Iss. 2, p. 759-770. DOI: 10.1016/j.ejor.2017.03.081

3. Dubinkin D., Sadovets V., Syrkin I., Chicherin I. Assessment of the Need to Create Control Sytem of Unmanned Dump Truck. *E3S Web of Conferences*. 2020. Vol. 177. N 03022. DOI: 10.1051/e3sconf/202017703022

4. Kuznetsov D., Kosolapov A. Dynamic of performance of open-pit dump trucks in ore mining in severe climatic environment. *Transportation Research Procedia*. 2022. Vol. 63, p. 1042-1048. DOI: 10.1016/j.trpro.2022.06.104

5. Zhuravlev A.G., Isakov M.V. Experimental testing of open pit dump trucks in operating conditions. *Mining Informational and Analytical Bulletin*. 2020. N 3-1, p. 530-542 (in Russian). DOI: 10.25018/0236-1493-2020-31-0-530-542

6. Kuzin E.G., Pudov E.Yu., Dubinkin D.M. Analysis of failures of mining dump truck components under operating conditions. *Mining equipment and electromechanics.* 2021. N 2, p. 55-61 (in Russian). DOI: 10.26730/1816-4528-2021-2-55-61

7. Vlasov Yu.A., Spirin E.N., Lyapin A.N. Analysis of the reasons of low operational reliability of career dump trucks. *Scientific review. Technical sciences.* 2016. N 5, p. 37-44 (in Russian).

8. Semykina A., Zagorodnii N., Novikov A. Study of the effectiveness of the organization of the system of maintenance and repair of quarry transport of mining and processing plants. *Transportation Research Procedia*. 2022. Vol. 63, p. 983-989. DOI: 10.1016/j.trpro.2022.06.097

9. Dubinkin D.M., Kartashov A.B., Arutyunyan G.A. et al. Development of a program and methodology for preliminary testing of an autonomous quarry dump truck. *Mining equipment and electromechanics.* 2021. N 6, p. 59-65. DOI: 10.26730/1816-4528-2021-6-59-65

10. Zhen Wang, Lihui Zhao, Zhiguo Kong et al. Development of accelerated reliability test cycle for electric drive system based on vehicle operating data. *Engineering Failure Analysis*. 2022. Vol. 141. N 106696. DOI: 10.1016/j.engfailanal.2022.106696

11. Makharatkin P.N., Abdulaev E.K., Vishnyakov G.Yu. et al. Increase of efficiency of dump trucks functioning on the basis of justification of their rational speed by means of simulation modeling. *Mining Informational and Analytical Bulletin.* 2022. N 6-2, p. 237-250 (in Russian). DOI: 10.25018/0236_1493_2022_62_0_237

12. Yanbiao Feng, Zuomin Dong. Integrated design and control optimization of fuel cell hybrid mining truck with minimized lifecycle cost. *Applied Energy*. 2020. Vol. 270. N 115164. DOI: 10.1016/j.apenergy.2020.115164

13. Bolshunova O.M., Korzhev A.A., Kamyshyan A.M. Adaptive control system of dump truck traction electric drive. IOP Conference Series: Materials Science and Engineering. 2018. Vol. 327. Iss. 5. N 052007. DOI: 10.1088/1757-899X/327/5/052007

14. Yanbiao Feng, Qiang Liu, Yong Li et al. Energy efficiency and $CO_2$ emission comparison of alternative powertrain solutions for mining haul truck using integrated design and control optimization. *Journal of Cleaner Production*. 2022. Vol. 370. N 133568. DOI: 10.1016/j.jclepro.2022.133568

15. Seifoori S., Parrany A.M., Khodayari M. A high-cycle fatigue failure analysis for the turbocharger shaft of BELAZ 75131 mining dump truck. *Engineering Failure Analysis*. 2020. Vol. 116. N 104752. DOI: 10.1016/j.engfailanal.2020.104752

16. Klebanov A.F., Sizemov D.N., Kadochnikov M.V. Integrated Approach to Remote Monitoring of Technical and Operating Conditions of Mine Dump Trucks. *Russian Mining Industry*. 2020. N 2, p. 75-81 (in Russian). DOI: 10.30686/1609- 9192-2020-2-75-81

17. Koteleva N., Korolev N., Zhukovskiy Yu., Baranov G. A Soft Sensor for Measuring the Wear of an Induction Motor Bearing by the Park's Vector Components of Current and Voltage. *Sensors*. 2021. Vol. 21. Iss. 23. N 7900. DOI: 10.3390/s21237900

18. Kundu P., Darpe A.K., Kulkarni M.S. Weibull accelerated failure time regression model for remaining useful life prediction of bearing working under multiple operating conditions. *Mechanical Systems and Signal Processing*. 2019. Vol. 134. N 106302. DOI: 10.1016/j.ymssp.2019.106302

19. Jinjiang Wang, Peilun Fu, Laibin Zhang et al. Multilevel Information Fusion for Induction Motor Fault Diagnosis. *IEEE/ASME Transactions on Mechatronics*. 2019. Vol. 24. Iss. 5, p. 2139-2150. DOI: 10.1109/TMECH.2019.2928967

20. Minakova T. E., Malarev V. I., Korzhev A. A. Method to identify operating regimes of asynchronous drivers by sub-harmonic parameters in mining. *Mining Informational and Analytical Bulletin*. 2022. N 11, p. 96-108 (in Russian). DOI: 10.25018/0236_1493_2022_11_0_96

21. Zhukovskiy Yu.L., Vasilev B.Y., Korolev N.A., Malkova Y.M. Analysis of the behavior of asynchronous electric drive with a closed scalar control system when changing the inductance of the magnetizing circuit. *Indonesian Journal of Science and Technology*. 2023. Vol. 8. N 1, p. 65-78. DOI: 10.17509/ijost.v8i1.51983

22. Glowacz A., Glowacz W., Kozik J. et al. Detection of Deterioration of Three-phase Induction Motor using Vibration Signals. *Measurement Science Review*. 2019. Vol. 19. N 6, p. 241-249. DOI: 10.2478/msr-2019-0031

23. Barański M. New vibration diagnostic method of PM generators and traction motors – detecting of vibrations caused by unbalance. IEEE International Energy Conference (Energycon), 13-16 May 2014, Cavtat, Croatia. IEEE, 2014. P. 28-32. DOI: 10.1109/ENERGYCON.2014.6850401

24. Salomon C.P., Ferreira C., Sant'Ana W.C. et al. A Study of Fault Diagnosis Based on Electrical Signature Analysis for Synchronous Generators Predictive Maintenance in Bulk Electric Systems. *Energies*. 2019. Vol. 12. Iss. 8. N 1506. DOI: 10.3390/en12081506

25. Korolev N., Kozyaruk A., Morenov V. Efficiency Increase of Energy Systems in Oil and Gas Industry by Evaluation of Electric Drive Lifecycle. *Energies*. 2021. Vol. 14. Iss. 19. N 6074. DOI: 10.3390/en14196074

26. Qi Gong, Bingzhi Chen, Yonghua Li, Pengpeng Zhi. Reliability Assessment Based on GO Method of Metro Traction System.*Advances in Materials Science and Engineering*. 2020. Vol. 2020. N 2829084, p. 1-13. DOI: 10.1155/2020/2829084

27. Jianqiang Liu, Shi Li, Yong Jiang, Krishnamurthy M. Reliability Evaluating for Traction Drive System of High-speed Electrical Multiple Units. IEEE Transportation Electrification Conference and Expo (ITEC), 16-19 June 2013, Detroit, USA. IEEE, 2013, p. 1-6. DOI: 10.1109/ITEC.2013.6574491

28. Shuai Lin, Xiaochun Fang, Fei Lin et al. Reliability of rail transit traction drive system – A review. *Microelectronics Reliability*. 2018. Vol. 88-90, p. 1281-1285. DOI: 10.1016/j.microrel.2018.07.037

29. Kabikenov S.J., Buyalich G.D., Sembayev N.S. Ways to Upgrade the Utilisation Efficiency of Open-Pit Dump Trucks. *PalArch's Journal of Archaeology of Egypt/Egyptology*. 2020. Vol. 17. N 3, p. 602-614. DOI: 10.48080/jae.v17i3.138

30. Andreeva L.I., Ushakov Yu.Yu. Research of operational reliability of quarry dump trucks. *News of the Ural State Mining University*. Iss. 3 (43), p. 74-77 (in Russian). DOI: 10.21440/2307-2091-2016-3-74-77

31. Vinogradov A.B., Gnezdov N.E., Chistoserdov V.L., Korotkov A.A. Mining Dump Trucks Electrical Traction Equipment Improvement // XI International Conference on Electrical Power Drive Systems (ICEPDS), 04-07 October 2020, St. Petersburg, Russia. IEEE, 2020, p. 1-4. DOI: 10.1109/ICEPDS47235.2020.9249279

32. Ziran Guo, Ming Yang, Xu Huang. Bearing fault diagnosis based on speed signal and CNN model. *Energy Reports*. 2022. Vol. 8. S. 13, p. 904-913. DOI: 10.1016/j.egyr.2022.08.041

33. Tsyglianu P.P., Romasheva N.V., Fadeeva M.I., Petrov I.V. Engineering projects in the Russian fuel and energy complex: Actual problems, factors and recommendations for development. *Ugol*. 2023. N 3, p. 45-51. DOI: 10.18796/0041-5790-2023-3-45-51

34. Borisenko A.N., Oleinikov A.V., Semenov M.N. Improving maintenance and preventive over-haul programs for open pit dump trucks at SUEK-Khakassia. *Mining Informational and Analytical Bulletin*. 2021. N 6, p. 104-119 (in Russian). DOI: 10.25018/0236_1493_2021_6_0_104

35. Khalturin A.A., Parfenchik K.D., Shpenst V.A. Features of Oil Spills Monitoring on the Water Surface by the Russian Federation in the Arctic Region. *Journal of Marine Science and Engineering*. 2023. Vol. 11. Iss. 1. N 111. DOI: 10.3390/jmse11010111

36. Petrov D.S., Korotaeva A.E., Pashkevich M.A., Chukaeva M.A. Assessment of heavy metal accumulation potential of aquatic plants for bioindication and bioremediation of aquatic environment. *Environmental Monitoring and Assessment*. 2023. Vol. 195. N 122. DOI: 10.1007/s10661-022-10750-0

37. Jin Woo Oh, Dogun Park, Jongpil Jeong. Fault Detection for Lubricant Bearing with CNN. 2nd International Conference on Intelligent Autonomous Systems (ICoIAS), 28 February – 02 March 2019, Singapore. IEEE, 2019, p. 142-145. DOI: 10.1109/ICoIAS.2019.00031

38. Karpat F., Kalay O.C., Dirik A.E. et al. Convolutional Neural Networks Based Rolling Bearing Fault Classification Under Variable Operating Conditions. International Conference on INnovations in Intelligent SysTems and Applications (INISTA), 25-27 August 2021, Kocaeli, Turkey. IEEE, 2021, p. 1-6. DOI: 10.1109/INISTA52262.2021.9548378

39. Ehya H., Lyng Rødal G.L., Nysveen A., Nilssen R. Condition Monitoring of Wound Field Synchronous Generator under Inter-turn Short Circuit Fault utilizing Vibration Signal. 23rd International Conference on Electrical Machines and Systems (ICEMS), 24-27 November 2020, Hamamatsu, Japan. IEEE, 2020. P. 177-182. DOI: 10.23919/ICEMS50442.2020.9291088

40. Andreeva L.I. Machinery availability evaluation in mining. *Mining Informational and Analytical Bulletin*. 2018. N 5, p. 136-143 (in Russian). DOI: 10.25018/0236-1493-2018-5-0-136-143

41. Rudakov M.L., Duka N.E. Analysis of properties of deafeners to design personal ear protectors. *Mining Informational and Analytical Bulletin*. 2022. N 3, p. 165-180 (in Russian). DOI: 10.25018/0236_1493_2022_3_0_165

42. Ustinov D., Nazarychev A., Pelenev D. et al. Investigation of the Effect of Current Protections in Conditions of Single-Phase Ground Fault through Transient Resistance in the Electrical Networks of Mining Enterprises. *Energies*. 2023. Vol. 16. Iss. 9. N 3690. DOI: 10.3390/en16093690

43. Gendler S.G., Prokhorova E.A. Assessment of the cumulative impact of occupational injuries and diseases on the state of labor protection in the coal industry. *Mining Informational and Analytical Bulletin.* 2022. N 10-2, p. 105-116. DOI: 10.25018/0236_1493_2022_102_0_105

44. Gendler S.G., Fazylov I.R., Abashin A.N. The results of experimental studies of the thermal regime of oil mines in the thermal method of oil production. *Mining Informational and Analytical Bulletin.* 2022. N 6-1, p. 248-262 (in Russian). DOI: 10.25018/0236_1493_2022_61_0_248

45. Babyr K.V., Ustinov D.A., Pelenev D.N. Improving Electrical Safety of the Maintenance Personnel in the Conditions of Incomplete Single-Phase Ground Faults. *Occupational Safety in Industry.* N 8, p. 55-61 (in Russian). DOI: 10.24000/0409-2961-2022-8-55-61

46. Xihui Liang, Ming J. Zuo, Zhipeng Feng. Dynamic modeling of gearbox faults: A review. *Mechanical Systems and Signal Processing*. 2018. Vol. 98, p. 852-876. DOI: 10.1016/j.ymssp.2017.05.024

47. Haijun Zhang, Mingjie Zhang, Xin Wang. Fracture failure analysis of insulation with initial crack defect for stator end-winding in induction motor by using magnetic-structural coupling model. *Engineering Failure Analysis*. 2023. Vol. 149. N 107239. DOI: 10.1016/j.engfailanal.2023.107239

48. Yetgin A.G. Effects of induction motor end ring faults on motor performance. Experimental results. *Engineering Failure Analysis*. 2019. Vol. 96, p. 374-383. DOI: 10.1016/j.engfailanal.2018.10.019

***Authors:*** **Alexander N. Nazarychev,** *Doctor of Engineering Sciences, Deputy Vice-Rector, https://orcid.org/0000-0001-6223-4150* (*Saint Petersburg Mining University, Saint Petersburg, Russia*), **Grigory V. Dyachenok,** *Postgraduate Student, s205027@stud.spmi.ru, https://orcid.org/0000-0002-6828-4252* (*Saint Petersburg Mining University, Saint Petersburg, Russia*), **Yuriy A. Sychev,** *Doctor of Engineering Sciences, Professor, https://orcid.org/0000-0003-0119-505X* (*Saint Petersburg Mining University, Saint Petersburg, Russia*).

*The authors declare no conflict of interests.*

ISSN 2411-3336; e-ISSN 2541-9404

JOURNAL OF MINING INSTITUTE

Zapiski Gornogo instituta

Journal homepage: pmi.spmi.ru

*Research article*

# Evaluation of the influence of the hydraulic fluid temperature on power loss of the mining hydraulic excavator

**Maxim G. RAKHUTIN**[1], **Giang Quoc KHANH**[2], **Aleksandr E. KRIVENKO**[1]✉, **Tran Van HIEP** [1]
[1] *National University of Science and Technology "MISiS", Moscow, Russia*
[2] *Quang Ninh University of Industry, Quang Ninh, Vietnam*

***How to cite this article:*** Rakhutin M.G., Giang Quoc Khanh, Krivenko A.E., Tran Van Hiep. Evaluation of the influence of the hydraulic fluid temperature on power loss of the mining hydraulic excavator. Journal of Mining Institute. 2023. Vol. 261, p. 374-383. EDN OKWKUF

***Abstract.*** In the steady state of operation, the temperature of a mining excavator hydraulic fluid is determined by the ambient temperature, hydraulic system design, and power losses. The amount of the hydraulic system power loss depends on the hydraulic fluid physical and thermodynamic properties and the degree of wear of the mining excavator hydraulic system working elements. The main causes of power losses are pressure losses in pipelines, valves and fittings, and leaks in pumps and hydraulic motors. With an increase in the temperature of hydraulic fluid, its viscosity decreases, which leads, on the one hand, to a decrease in power losses due to pressure losses in pipelines, valves and fittings, and, on the other hand, to an increase in volumetric leaks and associated power losses. To numerically determine the level of power losses occurring in the hydraulic system on an example of the Komatsu PC750-7 mining excavator when using Shell Tellus S2 V 22, 32, 46, 68 hydraulic oils with the corresponding kinematic viscosity of 22, 32, 46, 68 cSt at 40 °C, the developed calculation technique and software algorithm in the MatLab Simulink environment was used. The power loss coefficient, obtained by comparing power losses at the optimum temperature for a given hydraulic system in the conditions under consideration with the actual ones is proposed. The use of the coefficient will make it possible to reasonably select hydraulic fluids and set the values of the main pumps limit state and other hydraulic system elements, and evaluate the actual energy efficiency of the mining hydraulic excavator. Calculations have shown that the implementation of measures that ensure operation in the interval with a deviation of 10 % from the optimal temperature value for these conditions makes it possible to reduce energy losses from 3 to 12 %.

***Keywords:*** mining hydraulic excavator; hydraulic system; power loss; viscosity; temperature; hydraulic fluid leakage; hydraulic losses

***Received: 16.03.2023*** ***Accepted: 20.06.2023*** ***Online: 19.07.2023*** ***Published: 19.07.2023***

**Introduction.** It is well known that in most hydraulic systems, the efficiency does not exceed 75 %. In this case, the input power is spent on overcoming mechanical friction, pressure losses in pipelines, valves and fittings, and internal leakage of the hydraulic fluid. All power losses are converted into heat absorbed by the hydraulic fluid [1-3]. An increase in the temperature of the working fluid above a certain limit is accompanied by an increase in the aging rate, deterioration of its working properties and significantly affects both the performance of the excavator and the durability of the hydraulic system. Power losses during the operation of mining hydraulic excavators are of particular importance, since they operate in changing external conditions, primarily ambient temperature, and have a powerful drive, which gives large absolute values of the losses of electric energy or diesel fuel [4-6].

The calculation of power losses will allow you to select the appropriate drive power when designing new equipment, find the conditions for thermal equilibrium, determine the maximum possible oil temperature in the excavator hydraulic system, and correctly select the oil cooler parameters, taking into account the power, mode, and equipment operating conditions. An accurate calculation of the total power losses of a mining excavator hydraulic system is difficult due to the large amount of

*Journal of Mining Institute.* 2023. Vol. 261. P. 374-383


calculations and the need to take into account the variability of the physical parameters of the substances involved in the process.

**Methods.** The hydraulic system of the Komatsu PC750-7 excavator was chosen as the object of study. Hydraulic fluids Shell Tellus S2 V 22, 32, 46, 68 with the corresponding kinematic viscosity of 22, 32, 46, 68 cSt at 40 °C. Mechanical losses in friction units are assumed to be constant and were not taken into account in the calculations [7, 8].

In a mining excavator hydraulic system, energy losses depend on the operations performed and the temperature of the hydraulic fluid. This is a power expended to overcome resistance in hydraulic lines, fittings, valves etc. and hydraulic fluid leakage in the components of the hydraulic system. To accurately assess the energy loss in the excavator hydraulic system, it is necessary to take into account the dependence of the density and viscosity of the hydraulic fluid on temperature. In manual calculations, it was customary to average the hydraulic fluid physical parameters, since taking into account density and viscosity changes on temperature greatly complicated the calculations.

A change in the hydraulic fluid density and viscosity over a wide temperature range affects the energy intensity of the energy transfer and conversion processes occurring in the hydraulic system of a mining excavator, and to obtain accurate results, these changes should be taken into account. As the temperature changes, the magnitude of each type of power loss changes. With an increase in the temperature of the working fluid, its viscosity decreases, which entails a decrease in power losses due to pressure losses in pipelines, valves and fittings and, at the same time, an increase in power losses due to an increase in the volume of leaks in the elements of the hydraulic system.

A change in the density of the hydraulic fluid in the operating temperature range affects the magnitude of power losses, is linear in nature and can be determined by the formula [9-11]

$$\rho_t = \frac{\rho_0}{1 + \alpha_t \Delta t},$$

where $\rho_0$, $\rho_t$ are the hydraulic fluid density at a temperature of $t_0$ and $t$ respectively, kg/m$^3$; $\Delta t$ is the temperature increment, °C; $\alpha_t$ is the thermal expansion coefficient of the material, °C$^{-1}$.

The change in the hydraulic fluid viscosity, when the temperature changes in the range 40-110 °C, is determined from the expression

$$\nu_t = \nu_0^{\left(\frac{t_0}{t}\right)^n},$$

where $\nu_0$, $\nu_t$ are the kinematic viscosity at temperature $t_0$ and $t$, m$^2$/s; $n$ is a coefficient depending on the type and brand of the hydraulic fluid, temperature $t_0$, and viscosity $\nu_0$ [9, 10, 12].

In the temperature range from 0 to 40 °C the expression for calculating the kinematic viscosity takes the following form:

$$\nu_t = at^2 + bt + c,$$

where $a$, $b$, $c$ are the coefficients depending on the temperature and characteristics of the hydraulic fluid are determined from the reference literature or experimentally. Their values for the hydraulic fluid Shell Tellus S2 V 46 in the temperature range up to 40 °C are presented in Table 1.

*Table 1*

**Values of coefficients for hydraulic liquid Shell Tellus S2 V 46**

| Temperature range $t$ | Coefficients | | |
|---|---|---|---|
| | $a$ | $b$ | $c$ |
| 0-10 | 0.9 | –30.5 | 430 |
| 10-20 | 0.6 | –28 | 435 |
| 20-30 | 0.14 | –11.3 | 285 |
| 30-40 | 0.04 | –5.4 | 198 |

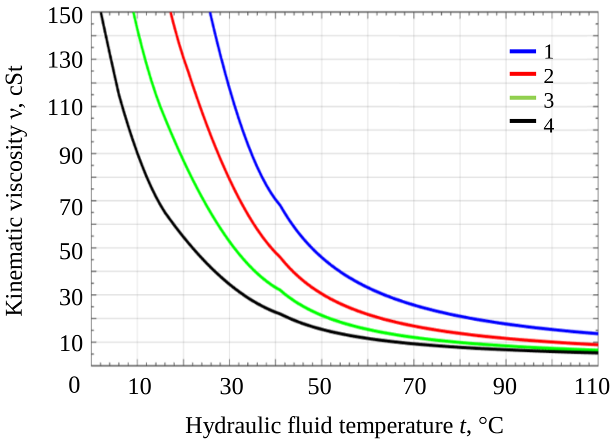


Fig.1. Viscosity curves for hydraulic fluids according to temperature
1 – Shell Tellus S2 V 68; 2 – S2 V 46; 3 – S2 V 32; 4 – S2 V 22

The dependence of the viscosity of Shell Tellus hydraulic fluids used in mining hydraulic excavators on temperature is shown in Fig.1.

The calculation of power losses during the operation of a mining hydraulic excavator involves the calculation of pressure losses in hydraulic components (pipelines, valves and fittings), power losses due to hydraulic fluid leaks, primarily of the main pumps and hydraulic motors. The total pressure losses by pipe length are determined by the Darcy – Weisbach formula for a viscous fluid flow

$$\sum \Delta p_{ln} = \rho g \sum_{i=1}^{n} \left( \lambda_i \frac{L_i}{d_i} \frac{v_i^2}{2g} \right) = \frac{\rho}{2} \sum_{i=1}^{n} \left( \lambda_i \frac{L_i}{d_i} v_i^2 \right),$$

where $i$ is the number of straight sections of the hydraulic pipe; $\lambda_i$ is the flow coefficient for the corresponding hydraulic line; $L_i$, $d_i$ are the length and internal diameter of the $i$-th pipeline respectively; $v_i$ is the average flow rate of the hydraulic fluid of the $i$-th pipeline [10, 13, 14].

The value of the flow coefficient depends on the type of fluid flow (Laminar and Turbulent). After a long downtime, immediately after starting the hydraulic system, when the fluid has not yet warmed up, laminar flow can be observed in the channels and the flow coefficient is usually calculated using the Poiseuille formula [10, 14, 15]

$$\lambda = \frac{64}{\mathrm{Re}}.$$

Further, in a turbulent flow, the Blausius formula is used [14-16]

$$\lambda = 0.3164 \mathrm{Re}^{-0.25},$$

where Re is the Reynolds number of the hydraulic fluid flow in the pipeline.

Losses also occur when the fluid passes through local resistances – fittings, valves, hydraulic control devices. The magnitude of these pressure losses is calculated using the following formula [14, 17]

$$\sum \Delta p_{lr} = \sum_{j=1}^{J} \rho g K_j \left( \frac{v_j^2}{2g} \right) = \frac{\rho}{2} \sum_{j=1}^{J} K_j v_j^2,$$

where $K$ is the pressure drop coefficient. Values are determined from reference literature or experimentally.

The work cycle of the piston chamber of an axial piston pump consists of the processes suction and discharge of the hydraulic fluid. The reason for the hydraulic fluid leakage in the pump is a large pressure difference between the piston chamber and the casing. Volume losses occur when liquid is forced into the pressure line. Fluid leakage from the working chamber consists of the following four components: leakage through the gap between the piston and the piston chamber wall $Q_{pc}$, through the gap between the piston and the slipper $Q_{ps}$, through the gap between the slipper and the swash plate $Q_{ss}$ and through the gap between the cylinder block and valve plate $Q_{cv}$ (Fig.2, *a*).

Hydraulic fluid leakage through the annular gap between the piston and the piston chamber wall is determined by the expression [10, 17, 18]

$$Q_{pc} = \frac{\pi d_p h_{pc}^3 (P_1 - P_0)}{12 \mu l} \left(1 + 1.5 \eta^2\right) - \frac{\pi d_p h_{pc} v}{2}, \quad (1)$$

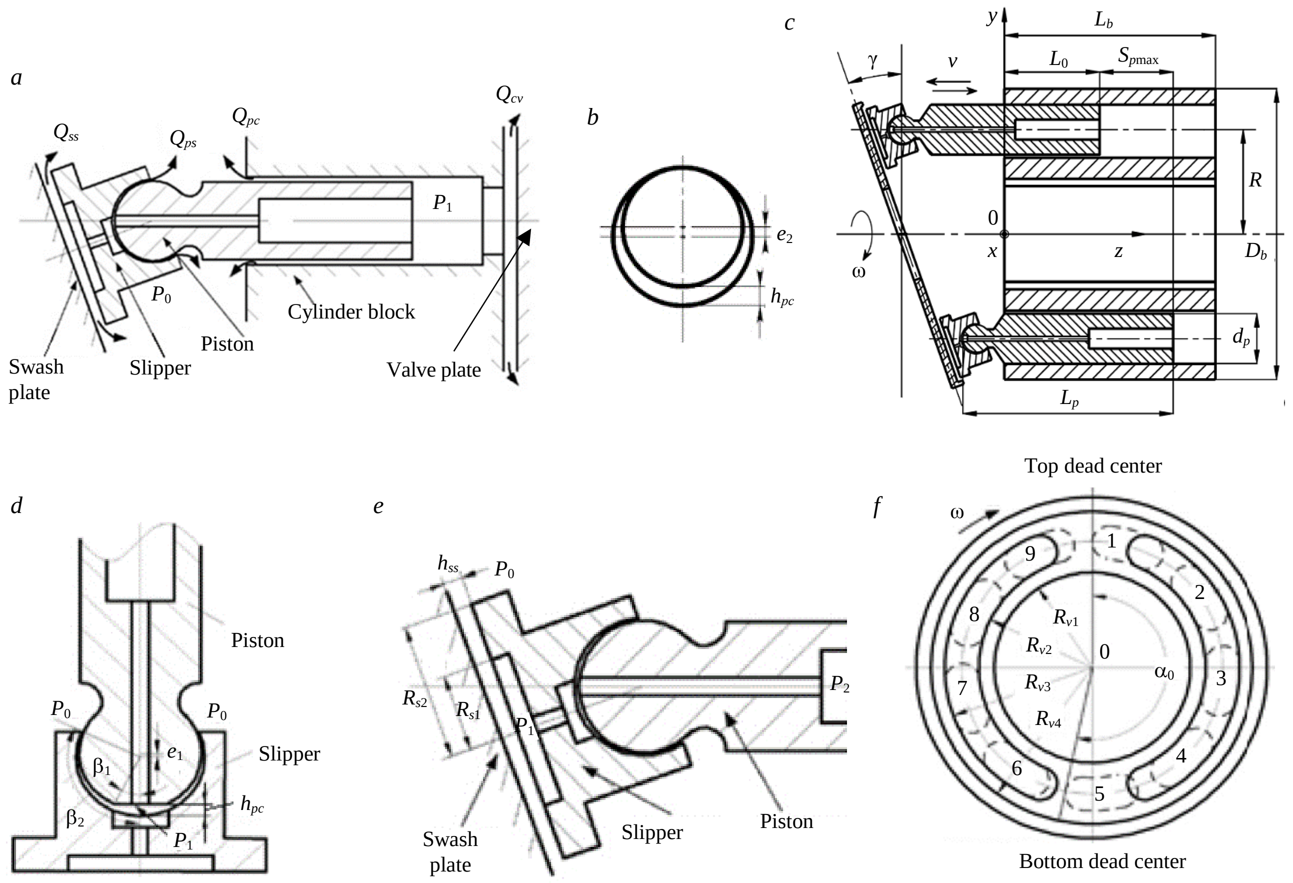


Fig.2. Leakage of hydraulic fluid in the axial plunger pump and hydraulic motor

where $d_p$ is the piston diameter, m; $h_{pc}$ is the gap width between the piston and the piston chamber wall, m; $P_1$, $P_0$ are the pressure in the piston chamber and in the casing respectively, Pa; μ is the hydraulic fluid dynamic viscosity, Pa·s; $l$ is the length of the piston part in the piston chamber, m; $\eta = e/h_{pc}$ is the relative eccentricity; $e$ is the eccentricity of the piston relative to the cylinder, m; $v$ – is the speed of the piston in the piston chamber, m/s (Fig.2, *b*, *c*) [10].

Hydraulic fluid leaks in the spherical hinge between the piston and the slipper are determined by the expression [10, 17, 18]

$$Q_{ps} = \frac{\pi h_{ps}^3 \left(P_1 - P_0\right)}{3\mu \left( \mathrm{tg}^2\beta_2 - \mathrm{tg}^2\beta_1 + 2\ln\left|\frac{\mathrm{tg}\beta_2}{\mathrm{tg}\beta_1}\right| \right)}, \qquad (2)$$

where $h_{ps}$ is the spherical hinge gap width, m; $P_1$, $P_0$ are the pressure in the slipper chamber and in the pump casing, respectively, Pa; $\beta_1$, $\beta_2$ are design angles of the spherical joint of the piston and slipper, rad (Fig.2, *d*).

Hydraulic fluid leaks through the gap between the slipper and the swash plate are determined by the formula [10, 18, 19]

$$Q_{ss} = \frac{\pi h_{ss}^3 \left(P_1 - P_0\right)}{6\mu \ln\left(R_{s2} / R_{s1}\right)}, \qquad (3)$$

where $h_{ss}$ is the width of the gap between the slipper and the swash plate, m; $R_{s1}$ is the groove and $R_{s2}$ is the outer radius of piston slipper, m (рис.2, *e*).

Hydraulic fluid leaks through the gap between the cylinder block and the valve plate, is determined by the expression [10, 18, 20]

$$Q_{cv} = \frac{\alpha_0 h_{cv}^3 (P_s - P_0)}{12\mu}\left[\frac{1}{\ln(R_{v2}/R_{v1})} + \frac{1}{\ln(R_{v4}/R_{v3})}\right], \quad (4)$$

where $h_{cv}$ is the width of the gap between the cylinder block and the valve plate, m; $R_{v1}$, $R_{v2}$, $R_{v3}$, $R_{v4}$ are the valve plate dimensions, m (Fig.2, *f*).

Summing up the results of formulas (1)-(4), taking into account the operating cycle of the piston chambers and the pump construction, we obtain

$$Q_{s1} = \frac{z}{2}(Q_{pc} + Q_{ps} + Q_{ss} + Q_{cv}),$$

where $z$ is the number of piston chambers.

Taking into account the assumptions made, the total power loss in the hydraulic system of a mining excavator can be written [21-23]

$$\Delta N = \frac{Q_w \Delta p + Q_{s1} p}{1000},$$

where $Q_w$ is the hydraulic fluid flow rate, m$^3$/s; $\Delta p$ is the pressure loss in the hydraulic system, Pa; $Q_{s1}$ is the total leakage of the hydraulic fluid in pumps and hydraulic motors, m$^3$/s; $p$ is the hydraulic system pressure, Pa.

The mathematical model used for programming calculations in the MatLab Simulink software is based on the considered equations and expressions. The main parameters used in calculations and modeling are the actual parameters of Komatsu PC750-7 mining excavator hydraulic system according to the manufacturer's catalog (Table 2).

*Table 2*

**Initial parameters for modeling**

| Hydraulic system component | Parameters |
|---|---|
| Hydraulic fluid Shell Tellus S2 V 440 | Density at $t$ = 15 °C: $\rho$ = 872 kg/m$^3$ |
| Main pump HPV160+160 2 pc. | Piston diameter $d_p$ = 22.5 mm<br>Piston length $L_p$ = 100 mm<br>Piston pitch radius $R_p$ = 49.5 mm<br>Swash plate angle $\gamma$ = 19.5°<br>Minimum piston length in piston chamber $l_0$ = 45 mm<br>Number of piston chambers $z$ = 9<br>Shaft speed $n$ = 2400 min$^{-1}$<br>Piston chamber working pressure $P_s$ = 31 MPa<br>Pump casing pressure $P_0$ = 1.5 MPa<br>Piston slipper design dimensions $R_{s1}$ = 8 mm; $R_{s2}$ = 13°<br>Design angles of the piston and slipper spherical $\beta_1$ = 14°; $\beta_2$ = 119°<br>Valve plate design dimensions $R_{v1}$ = 29 mm; $R_{v2}$ = 38 mm;<br>$R_{v3}$ = 50 mm; $R_{v4}$ = 60 mm; $\alpha_0$ = 193° |
| Swing motors<br>(axial piston) 2 pc. | Displacement $q_1$ = 255 cm$^3$<br>Shaft speed 260 min$^{-1}$<br>Working pressure 28.4 MPa<br>Power 31.4 kWt<br>Mechanical efficiency $\eta_{mc}$ = 0.98<br>Volumetric efficiency $\eta_{vl}$ = 0.96 |
| Boom lift cylinders 2 pc. | Flow rate at:<br>digging 0.0018 m$^3$/s<br>swing load 0.0013 m$^3$/s<br>loading 0.0014 m$^3$/s<br>swing empty 0.00144 m$^3$/s<br>Hydraulic pipe inner diameter $d_{pBlin}$ = 19.05 mm<br>Hose length $L_{pBl}$ = 13.4 m |

Second part of Table 2

| Hydraulic system component | Parameters |
|---|---|
| Arm cylinders 2 pc. | Flow rate at:<br>digging 0.002 $m^3/s$<br>swing load 0.00014 $m^3/s$<br>loading 0.00105 $m^3/s$<br>swing empty 0.001903 $m^3/s$<br>Hydraulic pipe inner diameter $d_{pAcin}$ = 19.05 mm<br>Hose length $L_{pAc}$ = 23 m |
| Bucket cylinders 1 pc. | Flow rate at:<br>digging 0.00191 $m^3/s$<br>swing load 0.001804 $m^3/s$<br>loading 0.0021 $m^3/s$<br>swing empty 0.00115 $m^3/s$<br>Hydraulic pipe inner diameter $d_{pBcin}$ = 19.05 mm<br>Hose length $L_{pBc}$ = 23 m |
| Oil cooler 1 pc. | Oil cooler oval pipes dimensions: $a$ = 22.1 mm; $b$ = 6 mm; $\delta_{pp}$ = 0.75 mm<br>Number of pipe rows $z_{row}$ = 3<br>Number of pipes in a row $m_{row}$ = 51<br>Hose length $L_{pOc}$ = 1290 mm |
| Filters 5 pc.<br>Directional control valves 3 pc.<br>Throttle valves 3 pc.<br>Elbows 90° 34 pc.<br>Check valves 5 pc.<br>Pump suction line dimensions | Pressure drop coefficients 5-12<br>Pressure drop coefficients 3-5<br>Pressure drop coefficients 0-100<br>Pressure drop coefficients 1<br>Pressure drop coefficients 1-5<br>Diameter 35 mm<br>Length 2.5 m |

Numerical modeling of physical processes has found wide application in the field of studying the processes of mining hydraulic excavators, since it allows taking into account a large number of quantities that change according to nonlinear dependencies and solving previously considered problems with much greater accuracy [24-26]. For computer simulation of power losses in a hydraulic system, the developed calculation method and a software algorithm implemented in the MatLab Simulink environment were used.

**Discussion of the results.** The preparation of a numerical experiment required an analysis of the Komatsu PC750-7 mining hydraulic excavator operating cycle [27-29]. The accurate values of flow rates in various sections of the hydraulic lines, as well as in individual devices of the hydraulic system of the excavator, were calculated, which is important for accurately determining energy losses [30-32]. As a result of the simulation, the values of power losses during the execution of work operations at various temperatures were obtained, presented in Table 3.

*Table 3*

**Power loss during work operations, kWt**

| Hydraulic fluid temperature $t$, °C | Digging | Swing load | Loading | Swing empty | Volumetric leakages |
|---|---|---|---|---|---|
| 0 | 390.2 | 110.3 | 269.3 | 222.5 | 1.6 |
| 20 | 126.3 | 41.73 | 90.08 | 76.23 | 5.99 |
| 30 | 90.78 | 32.44 | 65.92 | 56.42 | 9.64 |
| 40 | 71.43 | 27.51 | 52.34 | 45.74 | 15.2 |
| 50 | 58.41 | 24.34 | 43.69 | 38.73 | 24 |
| 55 | 54.66 | 23.39 | 41.16 | 36.68 | 28.71 |
| 60 | 51.87 | 22.69 | 39.28 | 35.15 | 33.56 |
| 70 | 48.04 | 21.71 | 36.69 | 33.04 | 43.51 |
| 80 | 45.54 | 21.07 | 35.02 | 31.67 | 53.62 |
| 90 | 43.8 | 20.61 | 33.85 | 30.71 | 63.76 |
| 110 | 41.52 | 20.02 | 32.33 | 29.45 | 83.78 |

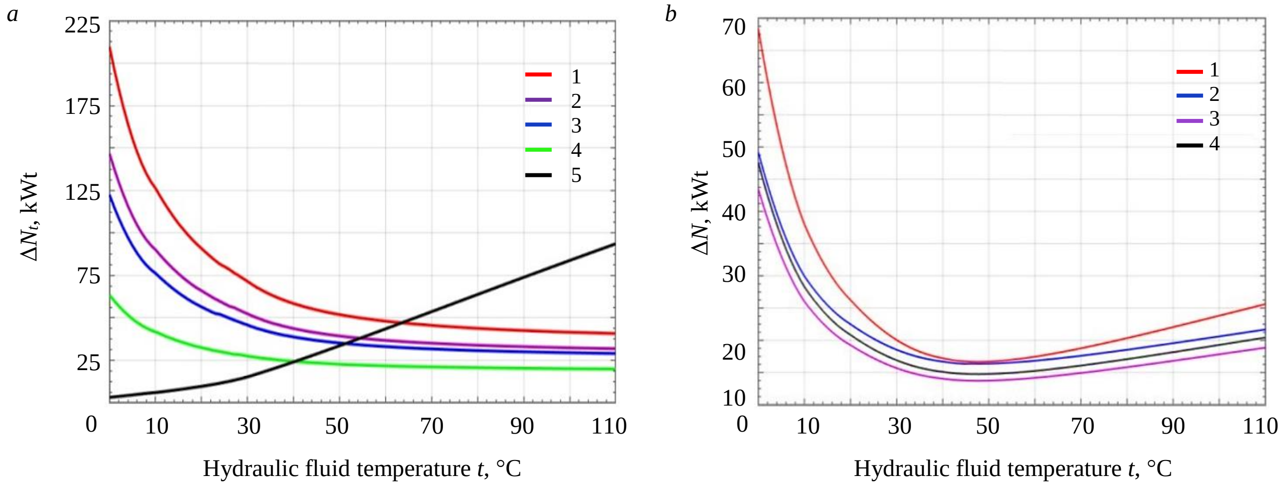


Fig.3. Power loss depending on the hydraulic fluid temperature:
*a* – due to hydraulic fluid leaks, pressure losses in hydraulic components (lines, valves etc.)
(1 – digging; 2 – swing load; 3 – swing empty; 4 – loading; 5 – main pumps)
*b* – total power losses during the implementation of work processes
(1 – digging; 2 – swing load; 3 – loading; 4 – swing empty)

Figure 3 shows power losses due to hydraulic fluid leakage and pressure losses in hydraulic components (lines, valves etc.) depending on the hydraulic fluid temperature for the working cycle operations: digging, swing load, loading, swing empty.

From the presented graphical dependences it is clearly seen that the energy losses during various working operations differ significantly from each other, which does not contradict the previously published results [33-35]. As the temperature of the liquid increases, the power loss caused by to hydraulic losses due to the properties of pipelines and associated resistances will decrease, while the increase in power due to the volume of leaks increases.

The values of the total power loss Δ*N* for different operations of the excavator working cycle differ in value, but they all have a common feature, which is that the total power loss decreases with an increase in the hydraulic fluid temperature from 0 to 30-35 °C, reaching the lowest value in the temperature range from 35 to 55 °C. After 55 °C, the power loss increases rapidly with the temperature rise. Since leaks in the control devices of the hydraulic system were not taken into account at this stage of the research, power losses with increasing temperature in the example under consideration will be the lower limit of values.

The total power loss versus temperature for various hydraulic fluids is shown in Fig.4. The presented graphic dependences clearly show a significant energy overspending when working on unheated hydraulic oil and the need to warm it up to 30-40 degrees before starting work.

It follows from these dependencies that when the excavator is operating in winter conditions, it is more advisable to use hydraulic fluids with a lower viscosity, and when working in a hot climate, for example, in the conditions of the Socialist Republic of Vietnam, it is advisable to use hydraulic fluids with increased viscosity. The optimal temperature value depends on the viscosity and other characteristics of the fluid, but it also depends on the hydraulic system elements technical condition and mining operating factors that affect the duration of the working cycles. Therefore, absolute value of power losses in certain conditions, are not an informative indicator.

To assess the energy efficiency of the mining excavator hydraulic system, a power loss coefficient is proposed. It is defined as the ratio of the minimum possible power losses in the hydraulic system in the considered operating conditions to the actual ones:

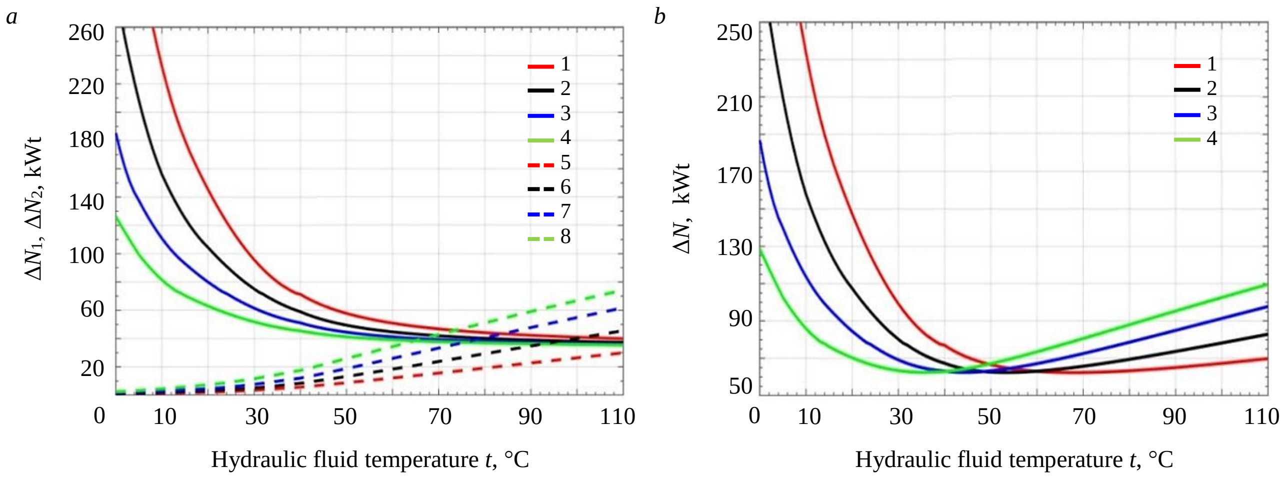


Fig.4. Power loss depending on temperature for various hydraulic fluids:
*a* – due to hydraulic fluid leaks, pressure losses in hydraulic components (lines, valves etc.)
(1, 5 – $\Delta N_1$ и $\Delta N_2$ using Shell Tellus S2 V 68; 2, 6 – $\Delta N_1$ и $\Delta N_2$ using Shell Tellus S2 V 46;
3, 7 – $\Delta N_1$ и $\Delta N_2$ using Shell Tellus S2 V 32; 4, 8 – $\Delta N_1$ и $\Delta N_2$ using Shell Tellus S2 V 22)
*b* – general power losses during the work processes
(1 – $\Delta N$ using Shell Tellus S2 V 68; 2 – using Shell Tellus S2 V 46; 3 – using Shell Tellus S2 V 32; 4 – using Shell Tellus S2 V 22)

$$K_{pl} = \frac{\Delta N_{min}}{\Delta N_f},$$

where $\Delta N_{min}$ is the minimum possible power loss in given conditions; $\Delta N_f$ is the actual power loss.

The value of the power loss coefficients when using various hydraulic fluids is shown in Fig.5. The concept of “temperature range of power loss – $T_{rpl}$” is proposed – the temperature interval between the minimum and maximum temperatures, corresponding to the value of the power loss coefficient.

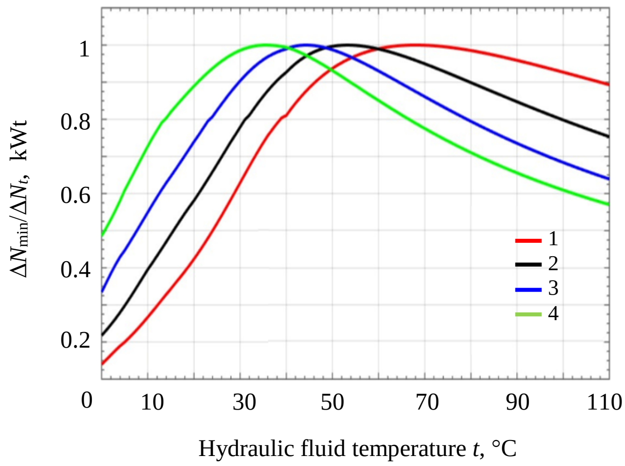


Fig.5. Change in the values of the power loss factor depending on the temperature
1 – $\Delta N_{min}/\Delta N_t$ using Shell Tellus S2 V 68;
2 – using Shell Tellus S2 V 46; 3 – using Shell Tellus S2 V 32;
4 – using Shell Tellus S2 V 22

The temperature range at the value of the power loss coefficient of 0.8; 0.9; 0.95 for liquids with different viscosities in the conditions under consideration is presented in Table 4: ν is the hydraulic fluid kinematic viscosity; $t_{opt}$ is the temperature value for the lowest energy losses; $t_{-A}$, $t_{+A}$ are the smallest and largest temperature values in the interval under consideration; $t_{-Ot}$, $t_{+Ot}$ are the value of the temperature interval from $t_{opt}$ to $t_{-A}$, $t_{+A}$; $t_+$-$t_-$ are the value of the temperature interval from $t_{-A}$ to $t_{+A}$.

*Table 4*

**The value of the temperature range for different viscosities of hydraulic fluids**

| ν, cSt | $t_{opt}$ | $K_{pl}$ = 0.8 | | | | | $K_{pl}$ = 0.9 | | | | | $K_{pl}$ = 0.95 | | | | |
|---|---|---|---|---|---|---|---|---|---|---|---|---|---|---|---|---|
| | | $t_{-A}$ | $t_{-Ot}$ | $t_{+A}$ | $t_{+Ot}$ | $t_+$-$t_-$ | $t_{-A}$ | $t_{-Ot}$ | $t_{+A}$ | $t_{+Ot}$ | $t_+$-$t_-$ | $t_{-A}$ | $t_{-Ot}$ | $t_{+A}$ | $t_{+Ot}$ | $t_+$-$t_-$ |
| 22 | 35 | 12 | 23 | 68 | 33 | 56 | 20 | 15 | 52 | 17 | 32 | 25 | 10 | 45 | 10 | 15 |
| 32 | 44 | 24 | 20 | 79 | 35 | 55 | 30 | 14 | 62 | 18 | 32 | 32 | 12 | 53 | 9 | 21 |
| 46 | 55 | 30 | 25 | 100 | 45 | 70 | 38 | 17 | 80 | 35 | 42 | 42 | 13 | 70 | 15 | 28 |
| 68 | 68 | 40 | 28 | > 110 | > 45 | 80 | 48 | 20 | 108 | 50 | 60 | 52 | 16 | 95 | 27 | 43 |

From the graphical dependencies and the data presented in Table 4, it follows that with an increase in viscosity, the difference in the values of the high and optimal temperatures increases, as well as the value of the "power loss interval" corresponding to the specified $K_{pl}$ value.

**Conclusion.** A method for calculating power losses in the hydraulic system of a mining hydraulic excavator depending on temperature is proposed. The method is implemented using the MatLab Simulink program on the example of Shell Tellus SV 2 46 hydraulic fluid and the hydraulic system of the Komatsu PC750-7 excavator.

• In the range from zero to 30-50 degrees, 70-80 % of power losses are pressure losses in hydraulic components (lines, valves etc.), which decrease in a quadratic relationship with a decrease in the hydraulic fluid viscosity caused by an increase in temperature. After 30-50 degrees, with a further decrease of hydraulic fluid viscosity, due to an increase in hydraulic fluid leaks in pumps and hydraulic motors, the main power losses increase according to a dependence close to a straight line, the angle of inclination of which is determined by the technical condition of the hydraulic motors and pumps, primarily the main pumps, the parameters of the hydraulic fluid, and mining factors of operation.

• A criterion for estimating energy losses in the hydraulic system of a mining hydraulic excavator depending on the hydraulic fluid temperature is proposed – the power loss coefficient $K_{pl}$, obtained by comparing the minimum possible losses at the optimum temperature in given conditions with energy losses at the actual temperature. The use of the proposed coefficient will allow estimating "excessive" energy losses when deviating from a range close to the optimal temperature of the hydraulic fluid in the conditions under consideration and hydraulic systems of other machines.

• The concept of "temperature range of power loss – $T_{rpl}$" is proposed – the temperature interval between the minimum and maximum temperatures, corresponding to the value of the power loss coefficient.

• Calculations have shown that the implementation of measures that ensure operation in the interval with a deviation of 10 % from the optimal temperature value ($K_{pl} \geq 0.9$) for these conditions, can reduce energy losses from 3 to 12 %.

**REFERENCES**

1. Pudov E.Yu., Zang K.K., Kuzin E.G., Krivenko A.E. Assessment of the impact of operating conditions on the performance of the hydraulic mining hydraulic excavator working fluid cooling system. *Mining Equipment and Electromechanics.* 2021. N 1, p. 51-58 (in Russian). DOI: 10.26730/1816-4528-2021-1-51-58

2. Özmen Ö., Sınanoğlu C., Batbat T., Güven A. Prediction of Slipper Pressure Distribution and Leakage Behaviour in Axial Piston Pumps Using ANN and MGGP. *Mathematical Problems in Engineering*. Vol. 2019. N 7317520, p. 1-13. DOI: 10.1155/2019/7317520

3. Bergada J.M., Kumar S., Davies D.L., Watton J. A complete analysis of axial piston pump leakage and output flow ripples. *Applied Mathematical Modelling*. 2012. Vol. 36. Iss. 4, p. 1731-1751. DOI: 10.1016/j.apm.2011.09.016

4. Komissarov A.P., Lagunova Yu.A., Shestakov V.S., Ivanov I.Yu. Single-bucket excavator energy demand. *Gornyi zhurnal.* 2018. N 1, p. 73-77 (in Russian). DOI: 10.17580/gzh.2018.01.13

5. Juza M., Hermanek P. Study of the energy efficiency of the UDS 214 excavator hydraulic system. *MM Science Journal*. 2022. Iss. 3, p. 5768-5774. DOI: 10.17973/MMSJ.2022_10_2022077

6. Casoli P., Scolari F., Vescovini C.M. et al. Excavator hydraulic circuit solution to reduce dissipations and fuel consumption. *E3S Web of Conferences*. 2021. Vol. 312. N 05004. DOI: 10.1051/e3sconf/202131205004

7. Balakhnina E., Vykhodtseva G., Sizova E. et al. Theoretical interpretation of the function of changing the tractive effort of a quarry locomotive in the starting mode. AIP Conference Proceedings. International Conference on Modern Trends in Manufacturing Technologies and Equipment 2021, 6-10 September 2021, Sevastopol, Russia. AIP Publishing, 2022. Vol. 2503. Iss. 1. N 050049. DOI: 10.1063/5.0100861

8. Balakhnina E., Sizova E., Vykhodtseva G., Mishedchenko O. Investigation of the Dependence of the Friction Coefficient Change on the Speed under Rational Starting Modes of a Quarry Locomotive. AIP Conference Proceedings, International Conference on Modern Trends in Manufacturing Technologies and Equipment 2021, 6-10 September 2021, Sevastopol, Russia. AIP Publishing, 2022. Vol. 2503. Iss. 1. N 050048. DOI: 10.1063/5.0100597

9. Pudov E.Yu., Zang K.K., Kuzin E.G. et al. Influence of ambient temperature and type of working fluid on thermodynamic equilibrium of hydraulic system of excavators. *Mining Equipment and Electromechanics.* 2021. N 1, p. 45-50 (in Russian). DOI: 10.26730/1816-4528-2021-1-45-50

10. Zang K.K. Justification and selection of the hydraulic system oil cooler parameters of a mining hydraulic excavator when operating in the conditions of the Republic of Vietnam: Avtoref. dis. … kand. tekhn. nauk. Moscow: MISiS, 2021, p. 21 (in Russian).

11. Abduazizov N.A., Muzaffarov A., Toshov J.B. et al. A complex of methods for analyzing the working fluid of a hydrostatic power plant for hydraulic mining machines. *International Journal of Advanced Science and Tehnology*. 2020. Vol. 29. SI5, p. 852-855.

12. Abduazizov N.A., Dzhuraev R.U., Zhuraev A.Sh. Study of the effect of temperature and viscosity of the hydraulic fluid of hydraulic systems on the reliability of mining equipment. *Gornyi vestnik Uzbekistana*. 2018. N 3 (74), p. 58-60 (in Russian). DOI: 10.13140/RG.2.2.11942.96329

13. Xia Lianpeng, Quan Long, Cao Donghui et al. Research on Energy Saving Characteristics of Large Hydraulic Excavator Boom Driven by Dual Hydraulic-gas Energy Storage Cylinder. *Journal of Mechanical Engineering*. 2019. Vol. 55. Iss. 20, p. 240-248. DOI: 10.3901/JME.2019.20.240

14. Yusuf S.I., Ejeh S., Olayiwola R.O. Analytical Study of Leakage of Viscous Flow in a Cylindrical Pipe. *International Journal of Scientific Engineering and Applied Science*. 2022. Vol. 8. Iss. 3, p. 74-93.

15. Siddique M.A.A., Yong-Joo Kim, Wan-Soo Kim et al. Effects of Temperatures and Viscosity of the Hydraulic Oils on the Proportional Valve for a Rice Transplanter Based on PID Control Algorithm. *Agriculture*. 2020. Vol. 10. Iss. 3. N 73. DOI: 10.3390/agriculture10030073

16. Lukashuk O.A., Komissarov A.P., Letnev K.Y. Increasing power efficiency of open-pit excavators. IOP Conference Series: Materials Science and Engineering. 2020. Vol. 709. Iss. 2. N 022083. DOI: 10.1088/1757-899X/709/2/022083

17. Ruichuan Li, Jilu Liu, Xinkai Ding, Qi Liu. Study on the Influence of Flow Distribution Structure of Piston Pump on the Output of Pulsation Pump. *Processes*. 2022. Vol. 10. Iss. 6. N 1077. DOI: 10.3390/pr10061077

18. Haocen Hong, Chunxiao Zhao, Bin Zhang et al. Flow Ripple Reduction of Axial-Piston Pump by Structure Optimizing of Outlet Triangular Damping Groove. *Processes*. 2020. Vol. 8. Iss. 12. N 1664. DOI: 10.3390/pr8121664

19. Shishlyannikov D., Zverev V., Ivanchenko A., Zvonarev I. Increasing the Time between Failures of Electric Submersible Pumps for Oil Production with High Content of Mechanical Impurities. *Applied Sciences*. 2022. Vol. 12. Iss. 1. N 64. DOI: 10.3390/app12010064

20. Xingjian Wang, Siru Lin, Shaoping Wang et al. Remaining useful life prediction based on the Wiener process for an aviation axial piston pump. *Chinese Journal of Aeronautics*. 2016. Vol. 29. Iss. 3, p. 779-788. DOI: 10.1016/j.cja.2015.12.020

21. Yingxiao Yu, Tri Cuong Do, Bifeng Yin, Kyoung Kwan Ahn. Improvement of Energy Saving for Hybrid Hydraulic Excavator with Novel Powertrain. *International Journal of Precision Engineering and Manufacturing-Green Technology*. 2023. Vol. 10. Iss. 2, p. 521-534. DOI: 10.1007/s40684-022-00437-9

22. Hidayat H., Aviva D., Muis A. et al. Failure analysis of excavator hydraulic pump. IOP Conference Series: Materials Science and Engineering. 2022. Vol. 1212. Iss. 1. N 012052. DOI: 10.1088/1757-899X/1212/1/012052

23. Makarova V.V., Lagunova Yu.A., Kovyazin R.A., Nesterov V.I. A new approach to creation of hydraulic excavators. *Mining Equipment and Electromechanics.* 2021. N 6, p. 9-14 (in Russian). DOI: 10.26730/1816-4528-2021-6-9-14

24. Litvin O.I., Markov S.O., Khoreshok A.A. et al. Determination of the area of energy-efficient position of working equipment and effective digging radius of hydraulic excavators at open pit mining. *Mine surveying and subsurface use.* 2022. N 4 (120), p. 38-44 (in Russian). DOI: 10.56195/20793332_2022_4_38

25. Kujundžić T., Klanfar M., Korman T., Briševac Z. Influence of Crushed Rock Properties on the Productivity of a Hydraulic Excavator. *Applied Sciences*. 2021. Vol. 11. Iss. 5. N 2345. DOI: 10.3390/app11052345

26. Holt G.D., Edwards D. Analysis of interrelationships among excavator productivity modifying factors. *International Journal of Productivity and Performance Management*. 2015. Vol. 64. N 6, p. 853-869. DOI: 10.1108/IJPPM-02-2014-0026

27. Komissarov A.P., Lagunova Yu.A., Lukashuk O.A., Shestakov V.S. Software management of the rock excavation process by a quarry excavator. *Mining Equipment and Electromechanics.* 2020. N 5, p. 28-33 (in Russian). DOI: 10.26730/1816-4528-2020-5-28-33

28. Litvin O.I., Khoreshok A.A., Dubinkin D.M. et al. Analysis of methods for calculating the productivity of open-pit hydraulic shovels and backhoes. *Russian Mining Industry.* 2022. N 5, p. 112-120 (in Russian). DOI: 10.30686/1609-9192-2022-5-112-120

29. Komissarov A.P., Lagunova Yu.A., Nabiullin R.Sh., Khoroshavin S.A. Digital model of shovel work process. *Mining Informational and Analytical Bulletin.* 2022. N 4, p. 156-168 (in Russian). DOI: 10.25018/0236_1493_2022_4_0_156

30. Litvin O., Litvin Y. Evaluation of Effect of the Excavator Cycle Duration on its Productivity. *E3S Web of Conferences*. Vol. 174. N 01010, p. 1-5. DOI: 10.1051/e3sconf/202017401010

31. Sobolevskyi R., Korobiichuk V., Levytskyi V. et al. Optimization of the process of efficiency management of the primary kaolin excavation on the curved face of the conditioned area. *Rudarsko-geološko-naftni zbornik*. 2020. Vol. 35. N 1, p. 123-138. DOI: 10.17794/rgn.2020.1.10

32. Klanfar M., Herceg V., Kuhinek D., Sekulić K. Construction and testing of the measurement system for excavator productivity. *Rudarsko-geološko-naftni zbornik*. 2019. Vol. 34. N 2, p. 51-58. DOI: 10.17794/rgn.2019.2.6

33. Cheol-Gyu Park, Seungjin Yoo, Hyeonsik Ahn et al. A coupled hydraulic and mechanical system simulation for hydraulic excavators. *Proceedings of the Institution of Mechanical Engineers, Part I: Journal of Systems and Control Engineering*. 2019. Vol. 234. Iss. 4, p. 527-549. DOI: 10.1177/0959651819861612

34. Ng F., Harding A.J., Glass J. An eco-approach to optimise efficiency and productivity of a hydraulic excavator. *Journal of Cleaner Production*. 2016. Vol. 112. Part 5, p. 3966-3976. DOI: 10.1016/j.jclepro.2015.06.110

35. Juraev A. Study of the Effect of Hydraulic Systems Operation on the General Performance of a Hydraulic Excavator. *The American Journal of Engineering and Technology*. 2021. Vol. 3. Iss. 10, p. 36-42. DOI: 10.37547/tajet/Volume03Issue10-07

***Authors*: Maxim G. Rakhutin,** *Doctor of Engineering Sciences, Professor, https://orcid.org/0000-0001-5873-5550* (*National University of Science and Technology* "*MISiS*", *Moscow, Russia*), **Giang Quoc Khanh,** *Candidate of Engineering Sciences, Lecturer, https://orcid.org/0009-0006-8589-5609* (*Quang Ninh University of Industry, Quang Ninh, Vietnam*), **Aleksandr E. Krivenko,** *Candidate of Engineering Sciences, Associate Professor, https://orcid.org/0000-0001-7198-4447* (*National University of Science and Technology* "*MISiS*", *Moscow, Russia*), **Tran Van Hiep,** *Postgraduate Student, https://orcid.org/0000-0003-0962-5835* (*National University of Science and Technology* "*MISiS*", *Moscow, Russia*).

*The authors declare no conflict of interests.*

ISSN 2411-3336; e-ISSN 2541-9404

JOURNAL OF MINING INSTITUTE

Zapiski Gornogo instituta

Journal homepage: pmi.spmi.ru

Research article

# Improvement of energy efficiency of ore-thermal furnaces in smelting of alumosilicic raw materials

**Vladimir Yu. BAZHIN**[1], **Yana V. USTINOVA**[1]✉, **Sergei N. FEDOROV**[2], **Mokhamed E. Kh. SHALABI**[3]

[1] *Saint Petersburg Mining University, Saint Petersburg, Russia*

[2] *Irkutsk National Research Technical University, Irkutsk, Russia*

[3] *Central Metallurgical Research Institute, Cairo, Egypt*

***How to cite this article*****:** Bazhin V.Yu., Ustinova Ya.V., Fedorov S.N., Shalabi M.E.Kh. Improvement of energy efficiency of ore-thermal furnaces in smelting of alumosilicic raw materials. Journal of Mining Institute. 2023. Vol. 261, p. 384-391. EDN RTQXSE

***Abstract.*** The issues of energy saving in pyrometallurgical production during processing of mineral raw materials in ore-thermal furnaces are particularly important for the development of new energy-efficient technologies. The reduction of the specific power consumption during melting at different stages of heating and melting of charge materials when modeling is related to obtaining kinetic curves in the process of kyanite concentrate regeneration in polythermal conditions. Based on practical data of carbo-thermal reduction the mathematical modeling of reduction processes from alumosilicic raw materials – kyanite was carried out. In this work, the nonisothermal method based on a constant rate of charge heating (i.e. a linear dependence between time and temperature) was used for the reduction of kyanite charge, which saves electrical energy. The experiments were carried out on a high-temperature unit with a heater placed in a carbon-graphite crucible. Based on the obtained kinetic dependences of nonisothermal heating of enriched kyanite concentrates in plasma heating conditions we obtained a number of kinetic anamorphoses of the linear form which point to the possibility of describing the reaction rate using the modified Kolmogorov – Erofeev equation for given heating conditions and within a narrow temperature range. The complex of mathematical modeling makes it possible to create a control algorithm of technological process of reduction of kyanite concentrate to a metallized state within the specified temperature range for the full flow of reaction exchange and to reduce the specific power consumption by 15-20 %. With the help of the received kinetic dependences, taking into account the thermodynamics of processes and current state of the art it is possible to create a universal thermal unit for the optimal carbothermal reduction of charge to a metallized state (alloy) with minimum power inputs compared to existing technologies.

***Keywords*****:** energy saving; energy efficient technologies; mining and metallurgical complex; aluminosilicate minerals; aluminum; silicon; oxide reduction; kinetics; specific energy consumption

***Received: 12.01.2023*** ***Accepted: 20.06.2023*** ***Online: 19.07.2023*** ***Published: 19.07.2023***

**Introduction.** Energy saving in production during processing of metallurgical and anthropogenic raw materials is paramount for solving both local [1, 2], and global environmental problems [3, 4]. So the development of new technologies based on fundamental scientific approaches is of great practical importance for the strategic energy-efficient development of the metallurgical industry [5-7]. The development strategy for ferrous and non-ferrous metallurgy of the Russian Federation until 2030 includes a large complex of measures for energy saving and the reduction of specific energy intensity of products, resource intensity, and emissions of harmful substances. The national mining and metallurgical complex [8-10] has already taken a number of measures to improve the energy efficiency of production. However, shortages of some resources or partial inaccessibility lead to significant economic and industrial problems [11-13] and risks [14-16], as well as to the reduced efficiency in the use of fuel and energy resources, sometimes complete losses in the supply of enterprises [17-19].

The production of aluminum silicon alloys, the most popular type of aluminum alloys, requires the organization of primary aluminum production in electrolysis cells, while the production of silicon requires the carbothermic method of reduction from quartz raw materials in ore-thermal furnaces [20-22]. In the production of primary aluminum, only alumina is used as an aluminum-containing raw material, and in Russia there are significant difficulties in providing enterprises with their own raw materials due to a shortage of high quality bauxite [23, 24]. The shortage of alumina for electrolytic production, which has developed as a result of the shutdown of some plants and the reduction in the share of exports for political reasons, leads to a search for innovative, energy-saving technologies for aluminum and aluminum silicon alloy production from alternative raw materials, which could be kyanite [25, 26]. After the reduction of unprofitable capacity and the mothballing of several plants with obsolete electrolysis cells, raw material shortages amount to approximately 45 % of all alumina production in the Russian Federation [27-29].

Systematic research is being conducted using aluminum and silicon industries wastes [10-15] in order to provide new types of aluminum-containing raw materials [30, 31]. Ore reserves of aluminum-silicon raw materials are studied as well in order to use them in processing [31, 32]. The end products of these technologies satisfy only a certain narrow demand of the industries due to the specific properties of the raw material and technological solutions. However, these studies are not focused on one of the promising areas, the direct production of aluminum silicon alloys, containing aluminum and silicon oxides by means of carbothermic reduction.

At present, the use of kyanite ores in various branches of industry is a highly topical issue due to the considerable number of reserves and simplicity of their development [33] in the Urals [36] and Keivy [34, 35] Mountains. Besides the production of refractories and ceramics, this type of raw materials can be used for production of alumina and silicon oxide after beneficiation and separation of the concentrate [37-39]. However, calculations show that the technology of kyanite disintegration is economically unprofitable in current conditions of traditional alumina production by the method of Bayer-sintering [40, 41].

Several attempts to study kyanite ores of the Kola Peninsula were made during the 20th century. The first study carried out by V.S.Artamonov, P.A.Borisov, and N.A.Volotovskaya dates back to 1929. The Mekhanobr Institute received preliminary data on beneficiation of kyanite-quartz material in 1939. All-Russian Aluminium-Magnesium Institute tested kyanite ore to produce kyanite concentrate by the flotation method in industrial conditions in 1949. In parallel, the geological aspects of kyanite deposits were studied, and 27 deposits were identified. A preliminary assessment of ore reserves showed 966 million tons located at depths of up to 100 m. The total volume of the deposits was 11 billion tons. Favorable geological conditions of ore occurrence make it possible to develop them by open-pit mining with high performance.

In this regard, the studies on the issues of direct reduction of the kyanite charge for the production of hypereutectic aluminum silicon alloys are of high scientific and practical interest (28 % of silicon in the final alloy). There are studies on the carbothermal reduction of alumina for production of aluminum [42-45]. Thus, calculations of technical and economic indicators in the work [43] confirmed the promising nature of this technology. The environmental analysis carried out in this work indicates a low ecological impact by the production of aluminum and its alloys compared to the current production. The analysis of the literature shows that methods of direct processing of charge materials [41, 46] without the use of fluorine-containing and carcinogenic substances (as in the electrolysis of molten salts according to Hall – Eru method) are promising, which is certainly a favorable positive factor. On the other hand, the carbothermal method of aluminum production had many difficulties in the implementation of the technological process in the 1970s and 1980s due to the formation of carbide compounds. The presence of these compounds reduces aluminum yield and with an increase of silicon content the production process was more active from the thermodynamic point of view. The low level of technology, insufficient study of the issues associated with reduction of charge, and the use of inadequate thermal aggregates could not have created the conditions for a wide distribution of industrial carbothermal production of aluminum.

Despite the existing scientific background and practical experience in the studies of the reduction of aluminosilicate charges, the issues of the direct reduction of the charge to the metallized state remain unresolved. There are no data on the kinetics and mechanism of interaction in the Si-Al-O-C system, which is an important technological factor and scientific justification for the implementation of the carbothermal process of aluminum silicon alloy production from kyanite concentrates or similar charge materials. The solution of this problem is especially important for improving the energy efficiency of the production of basic aluminum alloys.

**Methods.** Metallurgical processes based on the reduction of metals from their compounds by carbon and carbon-containing materials take place in ore-thermal furnaces at elevated temperatures and have high energy losses (part of the heat is waste, partly spent in the assembly units and on the reduction of impurity elements and incorrectly composed charge material). In the course of this work we considered a method that allows us to study more extensively the chemistry of the carbothermal reduction of kyanite charge materials when producing aluminum silicon alloy and eliminate energy losses in the metallurgical process. A non-isothermal method was used for the reduction of the kyanite charge in this work. The method is usually based on a constant heating rate of the charge, i.e., in the presence of a linear relationship between time and temperature, the following equations are valid

$$dT = mdt \text{ and } \frac{da}{d\tau} = m\frac{da}{dT},$$

where $m$ – heating rate, °C/min; $a$ – degree of conversion the metallic phase (reactivity).

The experiments were carried out on a high-temperature unit with a carbon-graphite heater with an additional element – a directed arc. A directed plasma arc is required for intensive heating and implementation of the non-isothermal method of processing the kianite charge to the specified temperatures (2000-2300 °C).

A sample of beneficiated kyanite concentrate with a minimum content of titanium oxide and iron (Table 1) with a molar ratio of $SiO_2:Al_2O_3 = 0.73$ was used in the conducted experiments. The carbon content in the sample was 110 % of the theoretically required amount for the reduction of oxides to metal (aluminum silicon alloy). The reduction was carried out using a directed plasma arc (controlled plasma flow) at heating rates of 10, 20, and 40 °C/min in the temperature range from 1100 to 2200 °C. The total heating rate and process kinetics were estimated by the rate of gas releasing during the reduction reaction (Fig.1) and by the amount of carbon dioxide registered by the MGL-98 gas analyzer. The temperature data were recorded by the WRe-5/20 tungsten-rhenium thermocouple connected to the OVEN TRM1 thermostat.

*Table 1*

**Results of X-ray spectral analysis of kyanite samples, %**

| Fraction | $Na_2O$ | MgO | $Al_2O_3$ | $SiO_2$ | $P_2O_5$ | S | $K_2O$ | CaO | $TiO_2$ | MnO | $Fe_2O_3$ |
|---|---|---|---|---|---|---|---|---|---|---|---|
| Non-magnetic | 0.2 | < 0.01 | 51.33 | 37.63 | 0.12 | 0.013 | 0.5 | 0.05 | 0.6 | < 0.01 | 0.18 |
| Magnetic | 0.25 | 0.21 | 50.98 | 35.64 | 0.19 | 0.029 | 0.49 | 0.25 | 0.67 | 0.054 | 1.85 |

For thermodynamic calculation of the process in a given temperature range, possible reactions are considered in wider values of 1400-1900 °C according to the following group of equations:

$$SiO_2 + C_{charge} = SiO + CO; \quad (1)$$

$$SiO + 2C_{charge} = SiC_{charge} + CO; \quad (2)$$

$$SiO_2 + 2C_{graphite} = SiO_2 + CO; \quad (3)$$

$$SiO + 2C_{graphite} = SiC_{graphite} + CO; \quad (4)$$

EDN RTQXSE
**Journal of Mining Institute.** 2023. Vol. 261. P. 384-391


$$3Al_2O_3 + C_{charge} = 2Al_2O_3 + CO; \quad (5)$$

$$2Al_2O_3 + 3C_{charge} = Al_4O_4C + 2CO, \quad (6)$$

where equations (3) and (4) refer to the interaction of oxides with fine fractions of carbon in the graphite environment of the furnace, and the rest of the equations refer to the interaction of oxides with solid carbon in the charge.

The kinetics of reduction of silicon dioxide in the given temperature range of 1100-1900 °C was studied at a constant heating rate of 20 °C/min. The studied sample was quenched every 100 °C, then the change in mass was determined, and the chemical analysis of the resulting material was carried out (Table 1).

The results of calculations are shown in Fig.2, as well as in Table 2. The flow of reactions in the temperature range 1400-1900 °C according to the analysis of waste gases was not recorded.

The most expedient way to carry out kinetic studies of the reactions (1) and (2) in conditions of polythermal heating (prompt-burst plasma heating) is to apply the generalized Kolmogorov – Erofeev topokinetic equation [8]:

$$\alpha = 1 - e^{-k\tau^n},$$

where $k$ and $n$ are constants and Erofeev, respectively, and the rate constant can be calculated by the ratio

$$K = nk^{1/n}.$$

**Results and discussion.** Since the reduction occurs in a narrower temperature range at a relatively high temperature, the most preferable option is to set heating temperature $T_s$ so that at $T = T_s(\theta = 0)$ $\frac{da}{dT} = \max$ or $\frac{d^2a}{dT^2} = 0$, defining it for solving the problem as the temperature of the reaction maximum for the energy-efficient melting mode.

The graphs $a = f(T)$ and $\upsilon_a = f(T)$ were plotted based on the obtained kinetic dependencies for the reaction (1) and (2) and defined $a_s$, $T_s$ и $\upsilon_{a_S}$. The calculated kinetic parameters $n$, $E$ и $K_0$ prove that the reaction is valid and the production of metallic charge (hypereutectic aluminum silicon alloy) is possible.

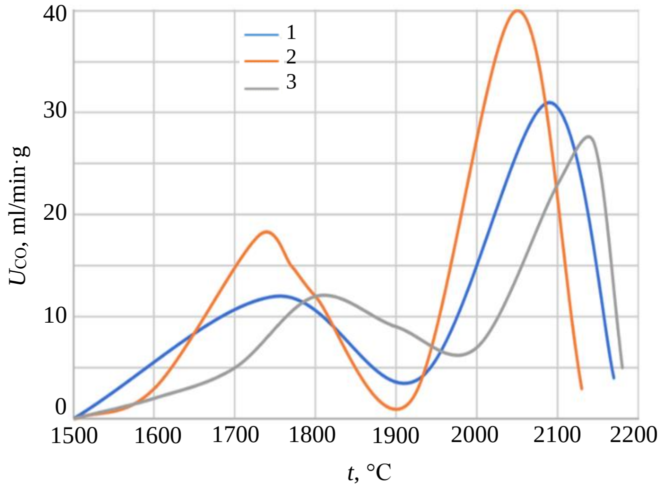


Fig.1. The kinetic curves of the reduction of kyanite concentrate in polythermal conditions
1 – 10 °C/min; 2 – 20 °C/min; 3 – 30 °C/min

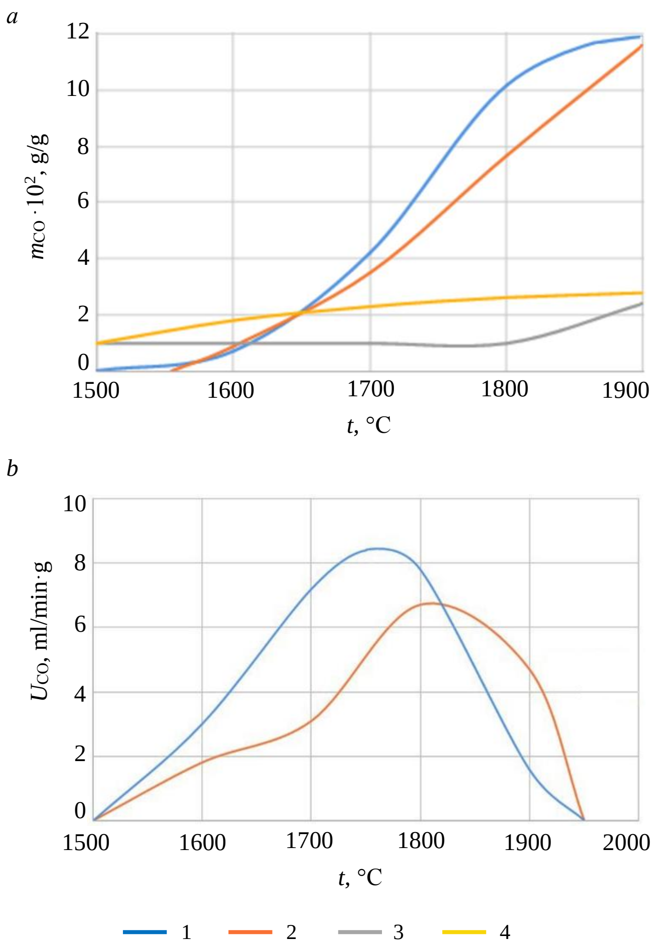


Fig.2. The dependences of the amount of carbon monoxide, evolved by reactions (1), (2), (4) and (5) (*a*) and gas release rate for reaction (1) and (2) (*b*) on temperature at a heating rate of kyanite charge 20 °C/min
1 – reaction (2); 2 – reaction (1); 3 – reaction (4); 4 – reaction (5)

*Table 2*

**The results of the reduction of the kyanite sample at the constant heating rate of 20 °C/min**

| Final temperature, °C | Sample mass, g | | CO, g | Chemical analysis of residues, % | | | | |
|---|---|---|---|---|---|---|---|---|
| | Before test | After test | | $SiO_{2gen}$ | $Al_2O_{3gen}$ | $Al_2O_{3sol}$ | SiC | C |
| 1100 | – | – | – | 25.92 | 42.32 | – | – | 28.62 |
| 1500 | 8.85 | 8.69 | 0.185 | 25.98 | 41.81 | 1.56 | – | 28.46 |
| 1600 | 8.93 | 8.60 | 0.305 | 26.29 | 45.42 | 1.34 | – | 28.08 |
| 1700 | 9.05 | 8.11 | 0.861 | 38.73 | 48.2 | 0.77 | 5.33 | 24.83 |
| 1800 | 8.87 | 6.96 | 1.737 | 30.37 | 53.50 | 1.30 | 1.87 | 21.04 |
| 1900 | 8.49 | 6.29 | 2.081 | 31.28 | 58.33 | 0.56 | 17.3 | 18.33 |

By substituting the expression for $K_0$, we obtain the equation and the dependence shown in Fig.3:

$$\ln\left[-\ln\left(1-a\right)\right]=\frac{nE}{RT_s^2}\theta. \tag{7}$$

The equation (7) is the equation of anamorphosis of the kinetic curve modified for conditions of linear polythermal heating by controlled plasma arc. Therefore, the graph of the dependence ln[–ln(1 – $a$)] depends on θ or $T$, and results in the linear relationship based on the equation $\theta = T - T_s$ with the slope of $\text{tg}\varphi = \frac{nE}{RT_s^2}$. In this case is the heating and melting time of the charge is decisive, which affects the energy mode of melting.

Thus, the linear form of the kinetic anamorphoses (Fig.3) indicates the possibility of describing the reaction rate in considered heating conditions and in a narrower temperature range by the modified Kolmogorov – Erofeev equation. This has a positive effect on the overall energy consumption of the unit – there is the most efficient use of the heat received, both in terms of process time and in absolute values of energy consumption.

The obtained mathematical model provides data for development of an algorithm for controlling the technological process of reduction of kyanite concentrate to a metallized state in the set temperature range for the complete cycle of the reaction ex-change and creates prerequisites for the justification and development of the modern energy efficient technology.

It is possible to create a universal thermal unit using the obtained dependencies and considering the thermodynamics of the processes and current technological level in order to optimize the process of carbothermal reduction of the charge to a metallized state (alloy).

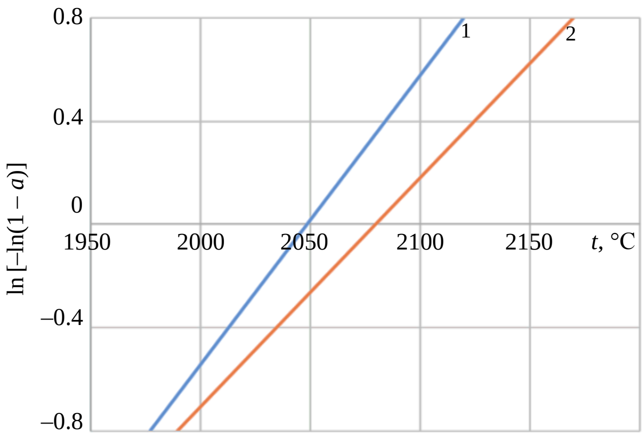


Fig.3. The anamorphoses of the kinetic curves for reactions (1) and (2) and heating rate
1 – reaction (2); 2 – reaction (1)

Description of the reaction rate using the modified Kolmogorov – Erofeev equation has an in-depth character of increasing the efficiency of aluminum silicon alloys production. General technical and economic comparative characteristics with the existing methods of aluminum silicon alloy production are not mentioned, since there is no need to produce aluminum and silicon separately. It enables to decrease considerably energy consumption for aluminum silicon alloy production, operating costs, and capital expenses. The advantages of the method of direct processing of silicon-aluminum ores for aluminum silicon alloy production are the following:

• combining energy-intensive aluminum and silicon production in a single smelter and the ability to process raw materials with high Al and Si content (up to 60-70 % in total), in particular, kyanite;

• in comparison with industrial electrolysis cells, orethermal or plasma furnaces are characterized by a substantially higher specific capacity, low capital and operating costs, and high environmental friendliness.

**Conclusion.** The non-isothermal method was used for the reduction of kyanite charge in the ore-thermal furnace, which is based on a constant rate of charge heating, i.e. with a linear relationship between time and temperature, which greatly saves electrical energy.

The expediency of using kyanite raw materials for energy-saving production of aluminum- and silicon-based alloys and aluminum silicon alloy has been substantiated.

The research on the kinetics and interaction mechanism in the Si-Al-O-C system was carried out on a high-temperature installation with a graphite heater in conditions of controlled plasma flow with symmetrical heating, focused on stabilization and energy losses reduction. A sample with the molar ratio of $SiO_2:Al_2O_3 = 0.73$ was used in the experiments. The carbon content in the sample was 90 % of the amount theoretically required for the reduction of the mineral oxide to metal. The sample consisted of kyanite ore subjected to electromagnetic separation and a complex reduction agent. The reduction was carried out at heating rates of 10, 20, and 40 °C/min in the temperature range from 1100 to 2200 °C. Calculations and obtained dependencies indicate a favorable operating mode of the furnace at the temperature of 1450 to 1650 °C.

The non-isothermal method was used for the reduction of kyanite charge.

The linear type of kinetic anamorphosis testifies to the possibility of describing the reduction reaction rate in the process of carbothermic reduction of aluminosilicon ore required for energy-saving technological melting regimes. This makes it possible to reduce specific power consumption for reduction smelting of kyanite ore by 15-20 % as compared to the existing indicators for ore-thermal furnaces. The solution of this problem is especially important for increasing the energy efficiency of the production of basic aluminum alloys.

A promising direction for the development of the aluminum industry is the use of plasma flow in the carbothermic reduction of pre-enriched kyanite concentrate. A large volume of kyanite deposits in the Murmansk region, the existing infrastructure, and an excess of cheap electric power create favorable logistics for organizing large-scale production of aluminum alloys.

A positive factor is the presence of the Kandalaksha aluminum smelter (United Company "RUSAL"), the only aluminum smelter in the world producing primary aluminum, located beyond the Arctic Circle, which, unlike the productions of the Western division, has maintained the full production volumes.

The development of technologies for deep, environmentally safe, and energy-efficient processing of kyanite ore in high-tech melting plants and furnaces is of great scientific and technical interest. These technologies ensure a high degree of aluminum silicon alloys extraction and obtaining multi-purpose commercial products, which will increase the competitiveness of the aluminum industry.

### REFERENCES

1. Litvinenko V.S., Tsvetkov P.S., Molodtsov K.V. The social and market mechanism of sustainable development of public companies in the mineral resource sector. *Eurasian Mining*. 2020. N 1, p. 36-41. DOI: 10.17580/em.2020.01.07

2. Litvinenko V., Bowbrick I., Naumov I., Zaitseva Z. Global guidelines and requirements for professional competencies of natural resource extraction engineers: Implications for ESG principles and sustainable development goals. *Journal of Cleaner Production*. 2022. Vol. 338. N 130530. DOI: 10.1016/j.jclepro.2022.130530

3. Litvinenko V.S., Petrov E.I., Vasilevskaya D.V. et al. Assessment of the role of the state in the management of mineral resources. *Journal of Mining Institute*. 2023. Vol. 259, p. 95-111. DOI: 10.31897/PMI.2022.100

4. Yurak V.V., Dushin A.V., Mochalova L.A. Vs sustainable development: scenarios for the future. *Journal of Mining Institute*. 2020. Vol. 242, p. 242-247. DOI: 10.31897/PMI.2020.2.242

5. Shklyarskiy Ya.E., Shklyarskiy A.Ya., Zamyatin E.O. Analysis of distortion-related electric power losses in aluminum industry. *Tsvetnye metally*. 2019. N 4, p. 84-91 (in Russian). DOI: 10.17580/tsm.2019.04.11

6. Timonina V.I. Energy conservation and efficiency as indicators for achieving energy security in the country. *Teoreticheskaya ekonomika*. 2022. N 1, p. 111-119 (in Russian). DOI: 10.52957/22213260_2022_1_111

7. Turysheva A.V., Gulkov Y.V., Krivenko A.V. Improving energy performance of the oil and gas industry by applying technologies for the use of associated petroleum gas. *Topical Issues of Rational Use of Natural Resources*. CRC Press, 2019. Vol. 1, p. 442-447. DOI: 10.1201/9781003014577-56

8. Kopteva A., Kalimullin L., Tcvetkov P., Soares A. Prospects and Obstacles for Green Hydrogen Production in Russia. *Energies*. 2021. Vol. 14. Iss. 3. N 718. DOI: 10.3390/en14030718

9. Cherepovitsyn A., Solovyova V. Prospects for the Development of the Russian Rare-Earth Metal Industry in View of the Global Energy Transition – A Review. *Energies*. 2022. Vol. 15. Iss. 1. N 387. DOI: 10.3390/en15010387

10. Zhukovskiy Yu.L., Kovalchuk M.S., Batueva D.E., Senchilo N.D. Development of an Algorithm for Regulating the Load Schedule of Educational Institutions Based on the Forecast of Electric Consumption within the Framework of Application of the Demand Response. *Sustainability*. 2021. Vol. 13. Iss. 24. N 13801. DOI: 10.3390/su132413801

11. Catalán-Vázquez M., Riojas-Rodríguez H., Cortez-Lugo M. et al. Social representations of mining activity after an environmental improvement program in the manganese district of Molango, in Mexico, and their implications for risk management. *Journal of Environmental Planning and Management*. 2019. Vol. 62. Iss. 10, p. 1714-1735. DOI: 10.1080/09640568.2018.1512475

12. Abramkin S.E., Shisterov G.A., Dushin S.E. et al. The problems of complex algorithms development for gas industy objects. *Automation, telemechanization and communication in oil industry*. 2019. N 5 (550), p. 27-32 (in Russian). DOI: 10.33285/0132-2222-2019-5(550)-27-32

13. Zinovieva O.M., Kolesnikova L.A., Merkulova A.M., Smirnova N.A. Environmental risk management at mining enterprises. *Ugol'*. 2022. N 3, p. 76-80 (in Russian). DOI: 10.18796/0041-5790-2022-3-76-80

14. Zgheib H. Concept of environmental risk management in the system of sustainable environmental economics. *Proceedings of BSTU. Iss. 5. Economics and Management*. 2018. N 2, p. 111-115.

15. Litvinenko V.S. Technological Progress Having Impact on Coal Demand Growth. XVIII International Coal Preparation Congress, 28 June – 01 July 2016, Saint-Petersburg, Russia. Cham: Springer, 2016, p. 3-16. DOI: 10.1007/978-3-319-40943-6_1

16. Abramkin S.E., Dushin S.E., Ilyushin Yu.V. et al. Automation and control of technological processes: status and prospects. Problems of Training of Specialists. Pyatigorsk: Izd-vo Pyatigorskogo instituta (filiala) Severo-Kavkazskogo federalnogo universiteta, 2019, p. 140 (in Russian).

17. Iakovleva E., Guerra D., Tcvetkov P., Shklyarskiy Ya. Technical and Economic Analysis of Modernization of Solar Power Plant: A Case Study from the Republic of Cuba. *Sustainability*. 2022. Vol. 14. Iss. 2. N 822. DOI: 10.3390/su14020822

18. Shklyarskiy Ya.E., Batueva D.E. Operation mode selection algorithm development of a wind-diesel power plant supply complex. *Journal of Mining Institute*. 2022. Vol. 253, p. 115-126. DOI: 10.31897/PMI.2022.7

19. Pyagay I.N., Kremcheev E.A., Pasechnik L.A., Yatsenko S.P. Carbonization processing of bauxite residue as an alternative rare metal recovery process. *Tsvetnye metally*. 2020. N 10, p. 56-63 (in Russian). DOI: 10.17580/tsm.2020.10.08

20. Shklyarskiy Y., Skamyin A., Vladimirov I., Gazizov F. Distortion Load Identification Based on the Application of Compensating Devices. *Energies*. 2020. Vol. 13. Iss. 6. N 1430. DOI: 10.3390/en13061430

21. Boduen A.Ya., Petrov G.V., Kobylyansky A.A., Bulaev A.G. Sulfide leaching of high-grade arsenic copper concentrates. *Obogashchenie rud*. 2022. N 1, p. 14-19 (in Russian). DOI: 10.17580/or.2022.01.03

22. Sizyakov V.M., Kononenko E.S., Snegurova A.I. Intensification of carbon aluminates technology of superdeep desilication on the basis of the catalytic properties of the hydro granate sludge. *Journal of Mining Institute*. 2013. Vol. 202, p. 27-30 (in Russian).

23. Shepelev I.I., Sakhachev A.Yu., Zhyzhaev A.M. et al. Extraction of valuable components from alumosilicate natural and technogenic materials under alumina production by sintering. *Proceedings of Irkutsk State Technical University*. 2018. Vol. 22. N 4, p. 203-214 (in Russian). DOI: 10.21285/1814-3520-2018-4-202-214

24. Dubovikov O.A., Yaskelyainen E.E. Processing of low-quality bauxite feedstock by thermochemistry-Bayer method. *Journal of Mining Institute*. 2016. Vol. 221, p. 668-674. DOI: 10.18454/PMI.2016.5.668

25. Pasechnik L.A., Medyankina I.S., Yatsenko S.P. Scandium extraction from multicomponent systems by crystallization of complex sulfates. IOP Conference Series: Materials Science and Engineering. 2020. Vol. 848. N 012064. DOI: 10.1088/1757-899x/848/1/012064

26. Koteleva N.I., Zhukovskiy Y.L., Valnev V. Augmented reality technology as a tool to improve the efficiency of maintenance and analytics of the operation of electromechanical equipment. *Journal of Physics: Conference Series*. 2021. Vol. 1753. N 012058. DOI: 10.1088/1742-6596/1753/1/012058

27. Mann V., Buzunov V., Frantsev Y. et al. The Development of RUSAL's Prebake Anode Production in Support of the Company's Green Initiatives. Light Metals 2022. Cham: Springer, 2022, p. 890-900. DOI: 10.1007/978-3-030-92529-1_117

28. Brough D., Jouhara H. The aluminium industry: A review on state-of-the-art technologies, environmental impacts and possibilities for waste heat recovery. *International Journal of Thermofluids*. 2020. Vol. 1-2. N 100007. DOI: 10.1016/j.ijft.2019.100007

29. Farjana S.H., Huda N., Parvez Mahmud M.A. Impacts of aluminum production: A cradle to gate investigation using life-cycle assessment. *Science of the Total Environment*. 2019. Vol. 663, p. 958-970. DOI: 10.1016/j.scitotenv.2019.01.400

30. Nemchinova N.V., Mineev G.G., Tyutrin A.A., Yakovleva A.A. Utilization of Dust from Silicon Production. *Steel in Translation*. 2017. Vol. 47. Iss. 12, p. 763-767. DOI: 10.3103/S0967091217120087

31. Kuzmin M.P., Ivanov N.A., Kondratev V.V. et al. Preparation of aluminum-carbon nanotubes composite material by hot pressing. *Metallurgist*. 2018. Vol. 61. N 9-10, p. 815-821. DOI: 10.1007/s11015-018-0569-2

32. Romanov A.D., Romanova E.A., Vilkov I.V. et al. Technology for Producing Aluminum-Matrix Composite Material Reinforced with Multi-Wall Carbon Nanotubes. *Metallurgist*. 2022. Vol. 66, p. 681-687. DOI: 10.1007/s11015-022-01376-1

33. Evans K. The History, Challenges, and New Developments in the Management and Use of Bauxite Residue. *Journal of Sustainable Metallurgy*. 2016. Vol. 2, p. 316-331. DOI: 10.1007/s40831-016-0060-x

34. Akcil A., Akhmadiyeva N., Abdulvaliyev R. et al. Overview On Extraction and Separation of Rare Earth Elements from Red Mud: Focus on Scandium. *Mineral Processing and Extractive Metallurgy Review*. 2018. Vol. 39. Iss. 3, p. 145-151. DOI: 10.1080/08827508.2017.1288116

35. Voytyuk I.N., Pantyushin I.V. Automated Measurement of Oil-gas-water Mixture Component Composition in Pipeline. 3rd International Conference on Control Systems, Mathematical Modeling, Automation and Energy Efficiency (SUMMA), 10-12 November 2021, Lipetsk, Russian Federation. IEEE, 2021, p. 935-939. DOI: 10.1109/SUMMA53307.2021.9632165

36. Grishin N.N., Ivanova A.G., Neradovskii Yu.N., Kalinnikov V.T. Integrated recovery of kyanite ore from the Keivskoye deposit. *Tekhnologiya metallov*. 2013. N 7, p. 3-9 (in Russian).

37. Salama E.I., Abbas A., Esawi A.M.K. Preparation and properties of dual-matrix carbon nanotube-reinforced aluminum composites. Composites Part A: Applied Science and Manufacturing. 2017. Vol. 99, p. 84-93. DOI: 10.1016/j.compositesa.2017.04.002

38. Kuskov V.B., Lvov V.V., Yushina T.I. Increasing the recovery ratio of iron ores in the course of preparation and processing. *CIS Iron and Steel Review*. 2021. Vol. 21, p. 4-8. DOI: 10.17580/cisisr.2021.01.01

39. Qing-chun Yu, Hai-bin Yuan, Fu-long Zhu et al. Carbothermic reduction of alumina with carbon in vacuum. *Journal of Central South University*. 2012. Vol. 19. Iss. 7, p. 1813-1816. DOI: 10.1007/s11771-012-1213-0

40. Baisong Guo, Xinming Zhang, Xi Cen et al. Enhanced mechanical properties of aluminum based composites reinforced by chemically oxidized carbon nanotubes. *Carbon*. 2018. Vol. 139, p. 459-471. DOI: 10.1016/j.carbon.2018.07.026

41. Khairul M.A., Zanganeh J., Moghtaderi B. The composition, recycling and utilisation of Bayer red mud. *Resources, Conservation and Recycling*. 2019. Vol. 141, p. 483-498. DOI: 10.1016/J.RESCONREC.2018.11.006

42. Vozniakovskii A.A., Kidalov S.V., Koltsova T.S. Development of composite material aluminum-carbon nanotubes with high hardness and controlled thermal conductivity. *Journal of Composite Materials*. 2019. Vol. 53. Iss. 21, p. 2959-2965. DOI: 10.1177/0021998319829894

43. Choate W., Green J. Technoeconomic Assessment of the Carbothermic Reduction Process for Aluminum Production. Essential Readings in Light Metals. Cham: Springer, 2016, p. 1070-1075. DOI: 10.1007/978-3-319-48156-2_156

44. Qingchun Yu, Yong Deng, Yuebin Feng, Ziyong Li. Phase Transformation of Alumina, Silica and Iron Oxide during Carbothermic Reduction of Fly Ash for Ceramics Production. *Metals*. 2021. Vol. 11. Iss. 8. N 1165. DOI: 10.3390/met11081165

45. Litvinova T., Kashurin R., Lutskiy D. Complex Formation of Rare-Earth Elements in Carbonate-Alkaline Media. *Materials.* 2023. Vol. 16. Iss. 8. N 3140. DOI: 10.3390/ma16083140

46. Bazhin V.Yu., Masko O.N., Martynov S.A. Automatic burden balance monitoring and control in the production of metallurgical silicon. *Tsvetnye metally*. 2023. N 4, p. 53-59. DOI: 10.17580/tsm.2023.04.07

***Authors*: Vladimir Yu. Bazhin,** *Doctor of Engineering Sciences, Professor, https://orcid.org/0000-0001-8231-3833* (*Saint Petersburg Mining University, Saint Petersburg, Russia*), **Yana V. Ustinova,** *Candidate of Engineering Sciences, Associate Professor, yana.kuskova@gmail.com, https://orcid.org/0000-0002-4382-3301* (*Saint Petersburg Mining University, Saint Petersburg, Russia*), **Sergei N. Fedorov,** *Candidate of Engineering Sciences, Associate Professor, https://orcid.org/0000-0003-4654-4364* (*Irkutsk National Research Technical University, Irkutsk, Russia*), **Mokhamed E. Kh. Shalabi,** *Doctor of Engineering Sciences, Professor* (*Central Metallurgical Research Institute, Cairo, Egypt*).

*The authors declare no conflict of interests.*

ISSN 2411-3336; e-ISSN 2541-9404

JOURNAL OF MINING INSTITUTE

Zapiski Gornogo instituta

Journal homepage: pmi.spmi.ru

Research article

# Forecasting planned electricity consumption for the united power system using machine learning

**Roman V. KLYUEV**[1], **Angelika D. MORGOEVA**[2]✉, **Oksana A. GAVRINA**[2], **Igor I. BOSIKOV**[2], **Irbek D. MORGOEV**[2]

[1] *Moscow Polytechnic University, Moscow, Russia*

[2] *North Caucasian Institute of Mining and Metallurgy (State Technological University), Vladikavkaz, Russia*

***How to cite this article*:** Klyuev R.V., Morgoeva A.D., Gavrina O.A., Bosikov I.I., Morgoev I.D. Forecasting planned electricity consumption for the united power system using machine learning. Journal of Mining Institute. 2023. Vol. 261, p. 392-402. EDN FJGZTV

***Abstract.*** The paper presents the results of studies of the predictive models development based on retrospective data on planned electricity consumption in the region with a significant share of enterprises in the mineral resource complex. Since the energy intensity of the industry remains quite high, the task of rationalizing the consumption of electricity is relevant. One of the ways to improve control accuracy when planning energy costs is to forecast electrical loads. Despite the large number of scientific papers on the topic of electricity consumption forecasting, this problem remains relevant due to the changing requirements of the wholesale electricity and power market to the accuracy of forecasts. Therefore, the purpose of this study is to support management decisions in the process of planning the volume of electricity consumption. To realize this, it is necessary to create a predictive model and determine the prospective power consumption of the power system. For this purpose, the collection and analysis of initial data, their preprocessing, selection of features, creation of models, and their optimization were carried out. The created models are based on historical data on planned power consumption, power system performance (frequency), as well as meteorological data. The research methods were: ensemble methods of machine learning (random forest, gradient boosting algorithms, such as XGBoost and CatBoost) and a long short-term memory recurrent neural network model (LSTM). The models obtained as a result of the conducted studies allow creating short-term forecasts of power consumption with a fairly high precision (for a period from one day to a week). The use of models based on gradient boosting algorithms and neural network models made it possible to obtain a forecast with an error of less than 1 %, which makes it possible to recommend the models described in the paper for use in forecasting the planned electricity power consumption of united power systems.

***Keywords:*** electricity power consumption; forecasting; gradient boosting; artificial neural network; machine learning

***Received: 14.03.2023*** ***Accepted: 20.06.2023*** ***Online: 19.07.2023*** ***Published: 19.07.2023***

**Introduction.** Energy-saving approaches occupy an important place in the modern world. One of the areas of research in the field of energy saving, which has a high practical and scientific significance, is the forecasting of electricity consumption. This is primarily due to the fact that electrical energy is a resource necessary to ensure all spheres of society. Especially large electricity power consumption is observed in industry, in particular, at the enterprises of the mineral resource complex. At the same time, power consumption forecasting is used in solving various problems, each of which is necessarily subject to one goal – the optimal management of power consumption, i.e. minimization of electricity consumption while maintaining the required level of quality of performance of the main functional processes.

In line with the concept of price-dependent electricity consumption, known under the term "demand response" [1, 2], it has become possible to create economically beneficial conditions for the production, distribution, and consumption of electricity for all participants in the electricity market: generating companies, electricity power grid companies, large consumers of electricity, etc. Wholesale electricity and capacity markets (WECM) are currently operating in many countries. In WECM various conditions for the purchase of electricity are offered. The day-ahead market and the balancing market are segments of the WECM. The main condition necessary for participation in them is the availability of a reliable forecast of electricity consumption. In this regard, forecasting is an actual production and scientific problem, which solution determines the economic efficiency for all participants in the WECM and contributes to the development of forecasting methods in general.

The efficiency of energy saving by forecasting of electricity power consumption is represented in many scientific papers [3-5]. At the same time, researchers use various methods for predicting power consumption, such as methods of classical and deep machine learning [6-8], mathematical models with fuzzy logic [9], as well as models that take into account the seasonality of power consumption time series [10] and other approaches [11, 12]. The review [13] presents the results of a comparative analysis of methods for forecasting electricity power consumption in accordance with the classification of the methods used depending on the forecast horizon. It should be noted that despite the wide variety of methods for forecasting electricity power consumption, there are no universal approaches that allow obtaining a reliable forecast of electricity power consumption for each subject area. This is mainly due to changing requirements for forecasting precision, the need to take into account a large number of factors that characterize the specifics of the subject area, for which forecasting is carried out, as well as progress in the field of data mining technologies which makes it more efficient than traditional methods of mathematical statistics (exponential smoothing, moving average, etc.) to process large data arrays, and for other reasons. Therefore, it was decided to conduct an applied research, which consists in forecasting electricity consumption using modern data mining tools for the united energy system with a large share of enterprises of the mineral resource complex. Thus, the purpose of this work is to predict planned electricity consumption, assess the precision of forecasting, and develop recommendations for the practical application of some of the proposed forecasting methods, as well as for the need to take into account the factors that characterize electricity consumption.

Forecasting of electricity consumption was carried out on the example of the united energy system of the Ural – a region with a large concentration of enterprises of the mineral resource complex, which are large consumers of electricity in the wholesale electricity and capacity market. Figure 1 shows the structure of electricity consumption for 2021 according to the Unified Interdepartmental Information and Statistical System* for the Ural Federal District (UFD). The largest consumption of electricity falls on the extraction of minerals (70888.4 GW·h) is shown at Fig.1.

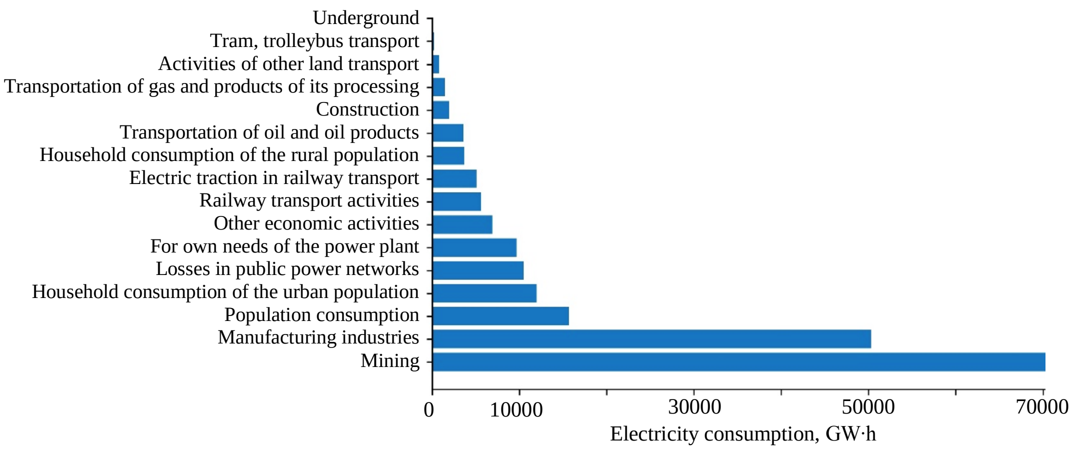


Fig.1. Structure of electricity consumption in the Ural Federal District in 2021

* Unified Interdepartmental Information and Statistical System. URL: https://www.fedstat.ru/indicator/43277 (accessed 12.03.2023).

The deviation of actual values from the planned ones leads to an increase in costs for all participants in the wholesale electricity market [14-16]. Therefore, the purpose of this study is to support management decisions in the process of determining the optimal values of electricity generation and consumption through hourly forecasting of planned consumption and generation of electricity for a period from a day to a week. The goal was achieved in several stages: the previous world experience in applying various approaches to forecasting electricity power consumption was analyzed; retrospective data on planned electricity power consumption, weather data, and data of indicators of the work of the energy system under consideration were obtained, and their analysis was carried out; predictive models were built and their reliability was assessed, and the main conclusions of the study were formulated. The scientific novelty of the work lies in the study of factors affecting the amount of electricity consumption of the integrated energy system, as well as in the creation of predictive models based on modern gradient boosting algorithms and artificial neural networks, and their optimization. The end result of the study, which is of scientific value, is recommendations on the use of economic and meteorological factors in the development of predictive models for large energy systems with consumers – enterprises of the mineral resource complex, as well as the experience of using specific machine learning algorithms and the configuration parameters of the models obtained as a result of the study.

**Methods.** Before description of the specific methods used in this study, we will note some of the most modern approaches used to forecast electricity power consumption.

For this purpose, a search has been carried out in the database of scientific publications on the websites ScienceDirect.com and ResearchGate.net by the keywords: forecasting, energy power consumption, machine learning, deep learning, modeling, short-term forecasting, mining industry, etc. Search results contain more than 1000 scientific publications. A part of these papers, most corresponding to the objectives of this study, was considered and the table was also compiled with the results of the analysis of some of the existing forecasting methods (Table 1), in which the analyzed studies are grouped according to the forecasting methods used, which also reflects such quantitative and qualitative characteristics of the research results as forecast depth, input and output data, brief description of the object, the forecasting of electricity consumption of which is carried out, the forecast error.

*Table 1*

**Analysis of methods for forecasting power consumption**

| Forecast method | Object of study | Forecast depth | Forecast quality | Input/output data | Reference |
|---|---|---|---|---|---|
| Long Short Term Memory Model (LSTM) | Port of Busan, South Korea | 1 month | $R^2$ = 0.973<br>RMSE = 107105 | Input data: forecast of the monthly throughput of the port.<br>Forecast value: electricity consumption | [17] |
| Hybrid: seasonal and trend decomposition using locally weighted regression, XGBoost gradient boosting and support vector regression | Australian Wholesale Electricity Market Operator | 12 h<br>24 h | sMAPE = 0.75-3.18 %<br>sMAPE = 1.56-7.72 % | Input data: electrical load time series.<br>Predicted value: electrical load | [18] |
| Ensemble model: LSTM, GRU and TCN | Data from Bejaia Electricity Company, Algeria | 1 month | $MAPE_{min}$ = 0.64 %<br>$MAPE_{max}$ = 10.16 % | Input data: power consumption data for the previous 12 months.<br>Output data: electricity consumption | [19] |

Various forecasting methods were used in the papers presented in Table 1. In papers [18, 19], retrospective data on electricity consumption were used as predictors, in article [17], a factor that significantly affects the amount of electricity consumption was studied. However, these works do not present a study of exogenous factors that nonlinearly affect the amount of electricity consumption, such as meteorological, social, economic, etc.

The paper [20] presents the results of electricity sales forecasting based on a Deep Spatio-Temporal Residual Network (ST-ResNet). Sales forecasting is directly related to the planning of power generation, so this actual problem was effectively solved. The use of the artificial neural network ST-ResNet made it possible to reduce the value of the mean absolute percentage error of prediction by more than 2.5 % compared to the use of various forecasting models (recurrent neural networks, moving average, exponential smoothing, etc.) in the short-term (1 day) and medium-term forecasting (1 week). When forecasting, the authors used weather data, a binary sign of the type of the day of the week (workday/day off), data on sales of electricity consumption 1 hour ago.

Forecasting allows you to optimally control the operating modes of electricity storage devices, which contributes to a more rational use of electricity. In research paper [21] presents the results of forecasting electricity power consumption by means of a decision tree model using exogenous variables. The results of forecasting are used in the decision support system in the process of determining the optimal capacity of an electric power storage device on an industrial scale.

The results of a comparative analysis of machine learning methods and traditional methods for forecasting electricity power consumption, carried out in paper [22], confirm the significant superiority of machine learning methods in terms of forecast accuracy, which, in turn, indicates the relevance of developing predictive models based on neural networks and algorithms of classical machine learning. However, as noted in paper [23], the main disadvantage of using these methods is computational complexity, which makes the task of improving the efficiency of data mining algorithms especially relevant.

In research paper [24], machine learning models were built to predict the power consumption of a small industrial facility. The model based on the gradient boosting algorithm of the CatBoost library turned out to be the best model.

In study [25], a hybrid model was developed that combines the use of singular spectrum analysis for partitioning the time series of power consumption and a fully connected neural network. The model described in paper [25] made it possible to improve the results of forecasting the electricity power consumption of a mining and metallurgical plant compared to using a neural network (without singular spectrum analysis) for forecasting. The application of data mining methods and best practices for their implementation are given in paper [26]. A promising direction is the use of hybrid forecasting models using a combination of several mining methods [27-29]. However, even when using the most modern approaches for forecasting power consumption [30] scientists note limitations in the application of some methods [31]. This only confirms the need for research to modernize and expand the methodological arsenal used in solving the problem of forecasting electricity power consumption. As applied to mining enterprises, the research results are given in papers [32, 33].

Therefore, it is advisable to conduct systematic reviews, such as in papers [13, 34], reflecting the current state of research in the field of electricity power consumption forecasting. Taking into account the undying interest of the scientific community in the issues of energy saving, the progress of means and methods of intelligent data processing, and the high practical significance of the development of energy-saving technologies, it is necessary to conduct applied research in order to develop recommendations on the possibility of using various forecasting methods.

The study was carried out in the Python programming language (v. 3.10.0) in the Jupyter Notebook programming environment. The NumPy and Pandas libraries were used for calculations and data manipulation, Matplotlib, Seaborn (for data visualization), SKLearn, XGBoost and CatBoost – for data preprocessing and loading regression model instances, tensorFlow.keras – for creating artificial neural networks . The choice of algorithms is justified by the recommendations in the literature [8, 19, 24] and the need to conduct a comparative analysis of the application of different algorithms in the same conditions. The advantages of ensemble approaches and neural networks are high generalizing ability, low overfitting of models. Linear regression and *k*-nearest neighbors algorithms were chosen to validate the non-linearity of the original data and compare the results with more sophisticated methods.

The initial data for the study were hourly data for the period from 04.03.2020 to 04.03.2023: on the planned electricity consumption of the united power system of the Ural; the power system operation indicator (frequency); production calendar data on the type of day (workday/day off/a day before holiday); data on the heating period. All data are taken from open sources. Since the study [35] analyzed the influence of climatic factors, confirming their significant impact on the magnitude of power consumption, it was decided to add the actual meteorological data of the administrative center – Ekaterinburg, as the initial ones.

The following assumptions were made when creating forecast models: the actual meteorological factors of the administrative center were used, despite the fact that the district occupies a vast territory belonging to various climatic zones; the data on the frequency in the power system were also taken actual.

A schedule of the planned electricity consumption is shown on Fig.2 and Fig.3 shows an example of a weekly schedule of planned electricity power consumption. On Fig.3, the index (serial number) of the time interval is plotted along the abscissa axis, the magnitude of the planned power consumption is plotted along the ordinate axis. Analysis of the graphs allows us to conclude that the amount of electricity power consumption depends on the time of day and the season.

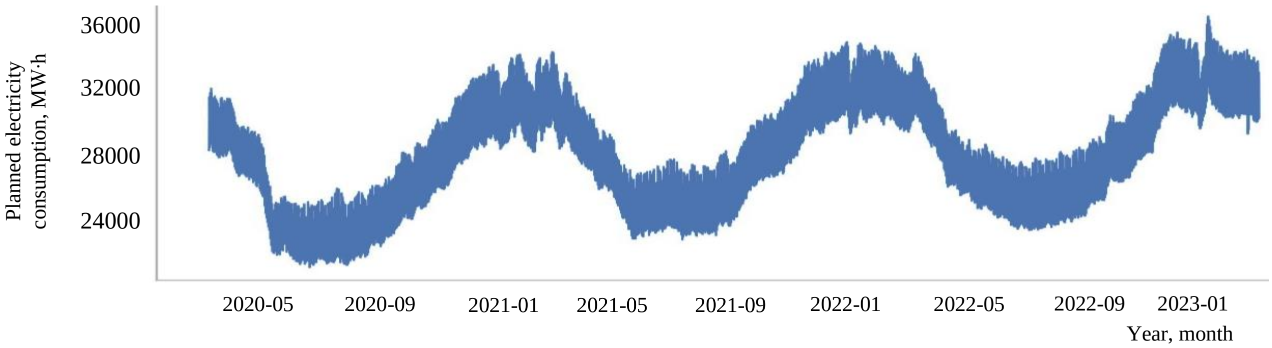


Fig.2. Schedule of planned electricity power consumption

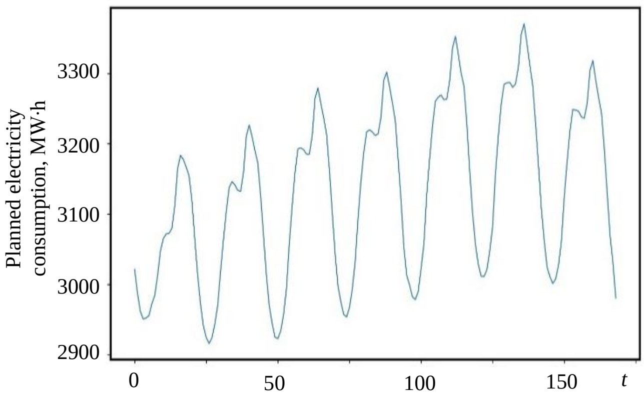


Fig.3. Weekly schedule of planned electricity power consumption

A correlation analysis was carried out in order to assess the influence of meteorological factors and the possibility of their further use in creating forecasting models. According to the Pearson paired correlation coefficient, the correlation coefficients between the features and the target variable were calculated. The notation and description of the factors and the target variable is shown in Table 2, correlation matrix is shown in Fig.4:

$$r_{xy} = \frac{\overline{xy} - \overline{x}\,\overline{y}}{\sigma(x)\sigma(y)},$$

where *x* and *y* are pairwise enumerated features and the target variable.

*Table 2*

**Description of the target variable and factors**

| Name | Units | Designation |
|---|---|---|
| Volume of planned electricity consumption | MW·h | *y* |
| Frequency | Hz | X1 |
| Index of equilibrium prices for the purchase of electricity | rub./MW·h | X2 |
| Index of equilibrium prices for the sale of electricity | rub./MW·h | X3 |
| Maximum equilibrium price index | rub./MW·h | X4 |
| Minimum equilibrium price index | rub./MW·h | X5 |
| Heating season in Ekaterinburg (yes 1/no 0) | – | X6 |
| Type of day (working 0 / non-working 1 / pre-holiday 2) | – | X7 |
| Temperature | °C | X8 |
| Relative humidity | % | X9 |
| Direction of the wind | rhumbs | X10 |
| Wind speed | m/s | X11 |
| General cloudiness | % | X12 |
| Horizontal line of sight | km | X13 |
| Dew point temperature | °C | X14 |
| Day | – | X15 |
| Month | – | X16 |
| Year | – | X17 |
| Hour | – | X18 |

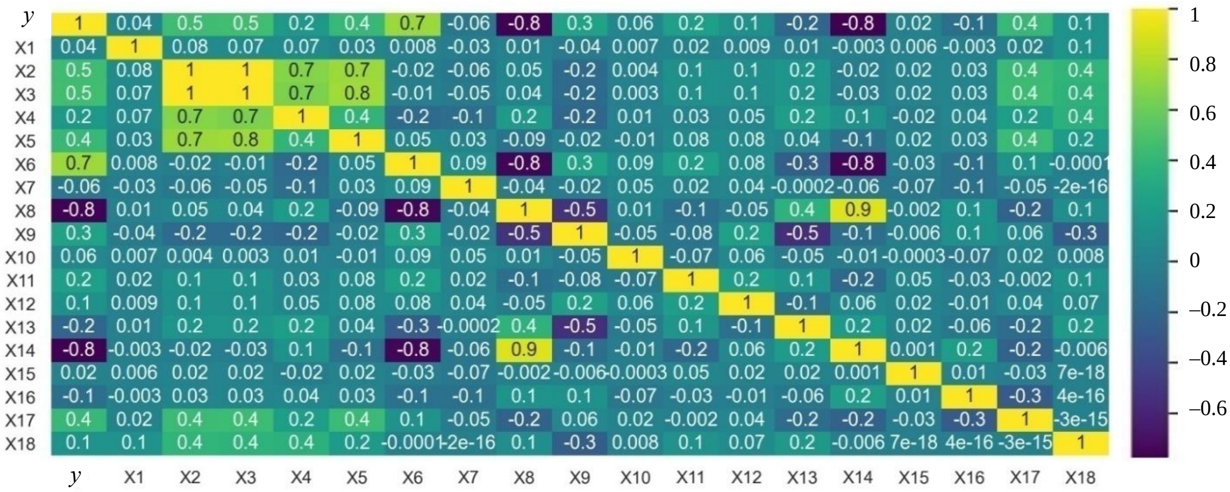


Fig.4. Correlation matrix of features and target variable

As a result of the analysis of the correlation matrix, it was decided to exclude the factors X3-X6, X14 from further research due to the presence of multicollinearity of features. All the other factors were used as input features in forecast models.

The next step was the normalization of features using the MinMaxScaler function of the SKLearn library. Using normalization, the values of all features were brought to the same scale

$$x_{\text{norm}} = \frac{x - x_{\min}}{x_{\max} - x_{\min}},$$

where *x* is the actual value of the attribute; $x_{\min}$ and $x_{\max}$ are the minimum and maximum values.

The following algorithms of the SKLearn library were used to create forecast models: Linear Regression (LR), *k*-nearest neighbors KNeighborsRegressor (KNN), random forest Random-ForestRegressor (RFR). Ensemble methods were also applied (XGBRegressor extreme gradient boosting and CatBoostRegressor gradient boosting) and a Long short-term memory (LSTM) recurrent neural network model was created in tensorFlow.keras. The algorithms of various complexity were used: from linear regression to ensemble methods and neural networks. The choice of these machine learning algorithms is due to the need to conduct a comparative analysis of algorithms applied in the same conditions. The reliability of some of the methods used is confirmed in some works, such as [12, 24, 36].

The neural network model was created by performing a series of experiments on the selection of parameters and the choice of the optimal network structure. The best-fitted network configuration is as follows: two LSTM layers of 30 and 25 neurons, respectively, with an activation function of hyperbolic tangent (tanh), one linear layer, including 25 neurons, the output layer. The Adam optimization algorithm was used as an optimizer, and the root mean square error was used as a loss function. The training of the neural network model took place with partitioning into batches, the optimal batch size turned out to be 5, the convergence of the result is observed at 1000 iterations.

The mean absolute error in percent (MAPE) and the coefficient of determination ($R^2$) were chosen as forecast quality metrics:

$$\mathrm{MAPE}(y,\hat{y}) = \frac{1}{n}\sum_{i=0}^{n-1}\frac{|y_i-\hat{y}_i|}{y_i}\cdot 100\ \%;$$

$$\mathrm{R}^2(y,\hat{y}) = 1-\frac{\sum_{i=1}^{n}(y_i-\hat{y}_i)^2}{\sum_{i=1}^{n}(y_i-\bar{y})^2},$$

where $y$ and $\hat{y}$ are the actual and forecast values of the volume of planned electricity power consumption, $n$ is the length of the time series.

The training and test data (datasets) were divided in a ratio of 80:20. The corresponding values of the quality of predictive models are shown in Table 3. Selection of parameters for RFR, KNN, XGBoost, and CatBoost models was performed using the cross-validation tool GridSearchCV.

*Table 3*

**Assessment of the predictive models quality**

| Model | Forecast quality metrics | | | | | | | | | | |
|---|---|---|---|---|---|---|---|---|---|---|---|
| | Training dataset | | Test dataset | | MAPE of forecast for $n$ days, % ($n = \overline{1.7}$) | | | | | | |
| | MAPE, % | $R^2$ | MAPE, % | $R^2$ | $n$ = 1 | $n$ = 2 | $n$ = 3 | $n$ = 4 | $n$ = 5 | $n$ = 6 | $n$ = 7 |
| LR | 3.37 | 0.86 | 3.39 | 0.86 | 2.08 | 2.09 | 1.93 | 1.79 | 1.89 | 2.16 | 2.22 |
| KNN | 1.26 | 0.97 | 1.66 | 0.96 | 1.10 | 1.25 | 1.50 | 1.55 | 1.79 | 1.93 | 1.84 |
| RFR | 0.41 | 0.99 | 0.78 | 0.99 | 1.39 | 1.31 | 1.41 | 1.37 | 1.59 | 1.64 | 1.59 |
| XGBoost | 0.73 | 0.99 | 0.82 | 0.99 | 0.47 | 0.63 | 0.71 | 0.74 | 1.07 | 1.20 | 1.17 |
| CatBoost | 0.17 | 0.99 | 0.36 | 0.99 | 0.42 | 0.86 | 0.75 | 0.71 | 0.71 | 0.68 | 0.64 |
| LSTM | 0.36 | 0.99 | 0.40 | 0.99 | 0.36 | 0.74 | 0.64 | 0.62 | 0.59 | 0.59 | 0.55 |

For these models the forecasting was carried out for a period from one day to a week. The values of forecast errors for each period ($n$) of forecasting are shown in Table 3. So, with $n$ = 1 24 forecast values (1 day) were obtained, with $n$ = 2, the forecast was made for 48 points (2 days), etc. up to 7 days. As can be seen from Table 3, with an increase in the forecasting horizon, the accuracy of the forecast decreases, but the error does not exceed 1-2 %. The best forecast was shown by the LSTM recurrent neural network model, the mean absolute percentage error (MAPE) of which is less than 1 % for a weekly lead period. The results obtained allow us to consider the model reliable.

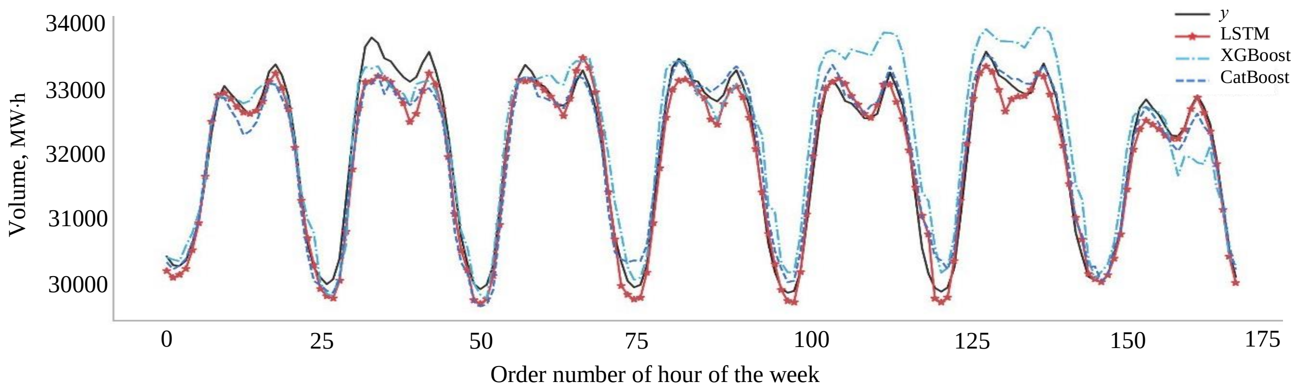


Fig.5. Actual and forecast values

Graphs of volumes of planned electricity power consumption (*y*) and its forecasted values obtained by different models for the week ahead are shown on Fig.5. As can be seen from Fig.5, the largest deviations of the forecasted values from the actual ones are observed in the XGBoost model with a forecast for a period of 4 to 7 days. With a forecast horizon of up to 4 days, the error is comparable to other methods. Therefore, it can be assumed that for a weekly period it is better to use LSTM neural network models and the CatBoost ensemble algorithm. It is possible that combining the analyzed models using the stacking technology will make it possible to obtain the smallest forecast error.

The results of forecasting electricity power consumption using the Holt – Winters method for two days ahead are presented in paper [33]. At the same time, MAPE was 1.08 %. In the mathematical modeling of power consumption based on the maximum likelihood sample, described in [14], the forecast error was 2.19 %. In addition, when forecasting electricity consumption using a multifactorial regression model, the forecasting error turned out to be 3.32 % [37].

Using the models reviewed in this study, it is possible to reduce the forecast error (when forecasting two days ahead, using the XGBoost model, the MAPE value was 0.63 %, when using the model based on the CatBoost algorithm, 0.86 %, when using the neural model LSTM network 0.74 %). All of this confirms the effectiveness of ensemble methods and deep learning methods for forecasting electricity power consumption.

**The discussion of the results.** During the study, the machine learning models were created that made it possible to obtain a short-term forecast of planned electricity power consumption (from a day to a week) with an error of 0.63 %. The results obtained will make it possible to take into account the forecast data obtained using the models described in this study in the process of making managerial decisions when forming applications for the production and consumption of electricity, which will allow making more in-formed decisions when planning the volume of electricity consumption. Thus, the presence of a reliable forecast should help to reduce the deviation of actual volumes of electricity consumption from the planned ones due to the intellectual analysis of retrospective data and taking into account a large number of weather (X8-X13), technical (X1, X7), economic (X2) factors, etc. It should be noted that without the assumption made in this study regarding weather factors, the forecast error may change. On the one hand, when using more detailed climatic data, for example, several settlements with different climatic conditions, the forecast error should probably decrease. On the other hand, the study used actual climate data rather than predictive ones. Therefore, in the presence of forecast data, the magnitude of the error in the forecast of electricity consumption will increase due to the error in the weather forecast. In this reason, one of the promising areas is the further study of meteorological factors and their influence on the target result.

Economic factors are subject to the influence of macro- and microeconomic indicators. In particular, it is worth assessing the risks of unforeseen situations related to the concept of the so-called "black swan" (accidents, sanctions, etc.). The forecasting of electricity consumption is based on past events and established correlations between factors, new events can be taken into account based on the detection of a large mismatch error at the moment when the "black swan" appears. In this case, the error will occur immediately, and by detecting it, it is possible to investigate the influence of a new factor caused by an unforeseen situation and evaluate its relationship to the forecast of power consumption directly. Then, taking into account the new factor, the model is reset. If there is a sharp change in the economic factor (X2) or any other factor already existing in the model, caused by sharp changes in the economic situation, then it is necessary to update the weights in the models, select the optimal hyperparameters and retrain the models.

Since one of the problems in forecasting electricity consumption is the lack of the universal models suitable for all subject areas and different forecast lead times, a promising direction of research is the search for universal approaches to creating predictive models. Thus, the results of this study, in particular, the structure of input forecast features, can be used in similar researches. In addition, the recommendations obtained in this study include the effectiveness of using gradient boosting models and neural networks in forecasting electricity consumption.

**Conclusion.** The conclusions of a practical and theoretical nature were obtained as a result of the study. Prognostic models were developed, their comparative analysis was carried out according to the quality metrics of predictive values. It can be argued that the use of ensemble (gradient boosting algo-rithms CatBoost and XGBoost) and the LSTM neural network model showed close results. However, with a better generalizing ability of the neural network and, as a result, more precise results, the disadvantage of this method compared to the ensemble ones is the high computational complexity and the time spent on training the model. The direction of future research is to increase the forecasting horizon, compare forecasting methods in terms of the forecast execution time, and optimize model parameters. The practical significance of the study lies in the use of forecasting results in making managerial decisions in the process of drawing up applications for the WECM. The models developed in this study can be implemented in the decision support system for participants in the whole-sale electricity markets, in particular, JSC "Administrator of the Trading System", who are involved in the calculation of the volume of the total planned electricity consumption. In addition, the results of this study can be used in the development of decision support subsystems for generating companies when forecasting demand for electricity and for large industrial enterprises when calculating planned electricity consumption.

## REFERENCES

1. Faria P., Vale Z. Demand Response in Smart Grids. *Energies*. 2023. Vol. 16. Iss. 2. N 863. DOI: 10.3390/en16020863

2. Zhukovskiy Yu.L., Kovalchuk M.S., Batueva D.E., Senchilo N.D. Development of an Algorithm for Regulating the Load Schedule of Educational Institutions Based on the Forecast of Electric Consumption within the Framework of Application of the Demand Response. *Sustainability*. 2021. Vol. 13. Iss. 24. N 13801. DOI: 10.3390/su132413801

3. Iftikhar H., Bibi N., Canas Rodrigues P., López-Gonzales J.L. Multiple Novel Decomposition Techniques for Time Series Forecasting: Application to Monthly Forecasting of Electricity Consumption in Pakistan. *Energies*. 2023. Vol. 16. Iss. 6. N 2579. DOI: 10.3390/en16062579

4. Almuhaini S.H., Sultana N. Forecasting Long-Term Electricity Consumption in Saudi Arabia Based on Statistical and Machine Learning Algorithms to Enhance Electric Power Supply Management. *Energies*. 2023. Vol. 16. Iss. 4. N 2035. DOI: 10.3390/en16042035

5. Weijie Zhou, Huihui Tao, Jiaxin Chang et al. Forecasting Chinese Electricity Consumption Based on Grey Seasonal Model with New Information Priority. *Sustainability*. 2023. Vol. 15. Iss. 4. N 3521. DOI: 10.3390/su15043521

6. Sayed H.A., William A., Said A.M. Smart Electricity Meter Load Prediction in Dubai Using MLR, ANN, RF, and ARIMA. *Electronics*. 2023. Vol. 12. Iss. 2. N 389. DOI: 10.3390/electronics12020389

7. Lin Pan, Sheng Wang, Jiying Wang et al. Research on Central Air Conditioning Systems and an Intelligent Prediction Model of Building Energy Load. *Energies*. 2022. Vol. 15. Iss. 24. N 9295. DOI: 10.3390/en15249295

8. Alsharekh M.F., Habib S., Dewi D.A. et al. Improving the Efficiency of Multistep Short-Term Electricity Load Forecasting via R-CNN with ML-LSTM. *Sensors*. 2022. Vol. 22. Iss. 18. N 6913. DOI: 10.3390/s22186913

9. Poczeta K., Papageorgiou E.I. Energy Use Forecasting with the Use of a Nested Structure Based on Fuzzy Cognitive Maps and Artificial Neural Networks. *Energies*. 2022. Vol. 15. Iss. 20. N 7542. DOI: 10.3390/en15207542

10. Vyalkova S.A., Nadtoka I.I. Analysis of the noise component of the daily schedules of active power energy systems and meteofactors at short-term forecasting. *Smart Electrical Engineering*. 2018. N 4, p. 25-34 (in Russian). DOI: 10.46960/2658-6754_2018_4_25

11. Yotov K., Hadzhikolev E., Hadzhikoleva S., Cheresharov S. Neuro-Cybernetic System for Forecasting Electricity Consumption in the Bulgarian National Power System. *Sustainability*. 2022. Vol. 14. Iss. 17. N 11074. DOI: 10.3390/su141711074

12. Xin Hu, Keyi Li, Jingfu Li et al. Load forecasting model consisting of data mining based orthogonal greedy algorithm and long short-term memory network. *Energy Reports*. 2022. Vol. 8. S. 5, p. 235-242. DOI: 10.1016/j.egyr.2022.02.110

13. Klyuev R.V., Morgoev I.D., Morgoeva A.D. et al. Methods of Forecasting Electric Energy Consumption: A Literature Review. *Energies*. 2022. Vol. 15. Iss. 23. N 8919. DOI: 10.3390/en15238919

14. Mokhov V.G., Demyanenko T.S. Forecasting of consumption of electric energy on the wholesale market of energy and power. *Bulletin of the South Ural State University Series* "*Economics and Management*". 2014. Vol. 8. N 2, p. 86-92 (in Russian).

15. Karpenko S.M., Karpenko N.V., Bezginov G.Y. Forecasting of power consumption at mining enterprises using statistical methods. *Russian Mining Industry*. 2022. N 1, p. 82-88 (in Russian). DOI: 10.30686/1609-9192-2022-1-82-88

16. Poluyanovich N.K., Dubyago M.N. Assessment of influencing factors and forecasting of power consumption in the regional power system, taking into account its operating mode. *Izvestiya SFedU. Engineering sciences*. 2022. N 2, p. 31-46 (in Russian). DOI: 10.18522/2311-3103-2022-2-31-46

17. Geunsub Kim, Gunwoo Lee, Seunghyun An, Joowon Lee. Forecasting future electric power consumption in Busan New Port using a deep learning model. *The Asian Journal of Shipping and Logistics*. 2023. Vol. 39. Iss. 2, p. 78-93. DOI: 10.1016/j.ajsl.2023.04.001

18. Ribeiro M.H.D.M., Gomes da Silva R., Ribeiro G.T. et al. Cooperative ensemble learning model improves electric short-term load forecasting. *Chaos, Solitons & Fractals*. 2023. Vol. 166. N 112982. DOI: 10.1016/j.chaos.2022.112982

19. Hadjout D., Torres J.F., Troncoso A. et al. Electricity consumption forecasting based on ensemble deep learning with application to the Algerian market. *Energy*. 2022. Vol. 243. N 123060. DOI: 10.1016/j.energy.2021.123060

20. Min Cao, Jinfeng Wang, Xiaochen Sun et al. Short-Term and Medium-Term Electricity Sales Forecasting Method Based on Deep Spatio-Temporal Residual Network. *Energies*. 2022. Vol. 15. Iss. 23. N 8844. DOI: 10.3390/en15238844

21. Senchilo N.D., Ustinov D.A. Method for Determining the Optimal Capacity of Energy Storage Systems with a Long-Term Forecast of Power Consumption. *Energies*. 2021. Vol. 14. N 21. N 7098. DOI: 10.3390/en14217098

22. Habbak H., Mahmoud M., Metwally K. et al. Load Forecasting Techniques and Their Applications in Smart Grids. *Energies*. 2023. Vol. 16. Iss. 3. N 1480. DOI: 10.3390/en16031480

23. Szczepaniuk H., Szczepaniuk E.K. Applications of Artificial Intelligence Algorithms in the Energy Sector. *Energies*. 2023. Vol. 16. Iss. 1. N 347. DOI: 10.3390/en16010347

24. Morgoeva A.D., Morgoev I.D., Klyuev R.V., Gavrina O.A. Forecasting of electric energy consumption by an industrial enterprise using machine learning methods. *Bulletin of the Tomsk Polytechnic University. Geo Assets Engineering*. 2022. Vol. 333. N 7, p. 115-125 (in Russian). DOI: 10.18799/24131830/2022/7/3527

25. Vyalkova S.A., Morgoeva A.D., Gavrina O.A. Development of a hybrid model for predicting the consumption of electrical energy for a mining and metallurgical enterprise. *Sustainable development of mountain territories*. 2022. Vol. 14. N 3 (53), p. 486-493 (in Russian). DOI: 10.21177/1998-4502-2022-14-3-486-493

26. Yuhan Xie, Yunfei Yang, Lifeng Wu. Power Consumption Forecast of Three Major Industries in China Based on Fractional Grey Model. *Axioms*. 2022. Vol. 11. Iss. 8. N 407. DOI: 10.3390/axioms11080407

27. Qingyong Zhang, Changwu Li, Conghui Yin et al. A Hybrid Framework Model Based on Wavelet Neural Network with Improved Fruit Fly Optimization Algorithm for Traffic Flow Prediction. *Symmetry*. 2022. Vol. 14. Iss. 7. N 1333. DOI: 10.3390/sym14071333

28. Zichao He, Chunna Zhao, Yaqun Huang. Multivariate Time Series Deep Spatiotemporal Forecasting with Graph Neural Network. *Applied Sciences*. 2022. Vol. 12. Iss. 11. N 5731. DOI: 10.3390/app12115731

29. Qiang Xiao, Hongshuang Wang. Prediction of WEEE Recycling in China Based on an Improved Grey Prediction Model. *Sustainability*. 2022. Vol. 14. Iss. 11. N 6789. DOI: 10.3390/su14116789

30. Narwariya J., Verma C., Malhotra P. et al. Electricity Consumption Forecasting for Out-of-Distribution Time-of-Use Tariffs. *Computer Sciences & Mathematics Forum*. 2022. Vol. 3. Iss. 1. N 1. DOI: 10.3390/cmsf2022003001

31. Frikha M., Taouil K., Fakhfakh A., Derbel F. Limitation of Deep-Learning Algorithm for Prediction of Power Consumption. *Engineering Proceedings*. 2022. Vol. 18. Iss. 1. N 26. DOI: 10.3390/engproc2022018026

32. Zhukovskiy Y.L., Semenyuk A.V., Alieva L.Z., Arapova E.G. Blockchain-based digital plat-forms to reduce the carbon footprint of mining. *Mining Informational and Analytical Bulletin*. 2022. N 6-1, p. 361-378 (in Russian). DOI: 10.25018/0236_1493_2022_61_0_361

33. Senchilo N., Babanova I. Improving the Energy Efficiency of Electricity Distribution in the Mining Industry Using Distributed Generation by Forecasting Energy Consumption Using Machine Learning. International Multi-Conference on Industrial Engineering and Modern Technologies (Far East Con), 06-09 October 2020, Vladivostok, Russia. IEEE, 2020, p. 1-7. DOI: 10.1109/FarEastCon50210.2020.9271335

34. Aguiar-Pérez J.M., Pérez-Juárez M.Á. An Insight of Deep Learning Based Demand Forecasting in Smart Grids. *Sensors*. 2023. Vol. 23. Iss. 3. N 1467. DOI: 10.3390/s23031467

35. Shklyarskiy J.E., Batueva D.E. The influence of external climatic factors on the accuracy of the forecast of energy consumption. E3S Web of Conferences. 2019. Vol. 140. N 04014. DOI: 10.1051/e3sconf/201914004014

36. Aseeri A.O. Effective RNN-Based Forecasting Methodology Design for Improving Short-Term Power Load Forecasts: Application to Large-Scale Power-Grid Time Series. *Journal of Computational Science*. 2023. Vol. 68. N 101984. DOI: 10.1016/j.jocs.2023.101984

37. Mokhov V.G., Demyanenko T.S. Definition of the significant factors for consumption volume forecasting of the electric energies for the united energy system of the Ural based on regression analysis. *Bulletin of Ural Federal University. Series Economics and Management.* 2017. Vol. 16. N 4, p. 642-662 (in Russian). DOI: 10.15826/vestnik.2017.16.4.031

***Authors*: Roman V. Klyuev,** *Doctor of Engineering Sciences*, *Professor*, *https://orcid.org/0000-0003-3777-7203* (*Moscow Polytechnic University*, *Moscow*, *Russia*), **Angelika D. Morgoeva,** *Postgraduate Student*, *m.angelika-m@yandex.ru*, *https://orcid.org/0000-0003-2949-1993* (*North Caucasian Institute of Mining and Metallurgy* (*State Technological University*), *Vladikavkaz*, *Russia*), **Oksana A. Gavrina,** *Candidate of Engineering Sciences*, *Associate Professor*, *https://orcid.org/0000-0002-9712-9075 (North Caucasian Institute of Mining and Metallurgy* (*State Technological University*), *Vladikavkaz*, *Russia*), **Igor I. Bosikov,** *Candidate of Engineering Sciences*, *Head of the Department*, *https://orcid.org/0000-0001-8930-4112* (*North Caucasian Institute of Mining and Metallurgy* (*State Technological University*), *Vladikavkaz*, *Russia*), **Irbek D. Morgoev,** *Postgraduate Student*, *https://orcid.org/0000-0003-4390-5662* (*North Caucasian Institute of Mining and Metallurgy* (*State Technological University*), *Vladikavkaz*, *Russia*).

*The authors declare no conflict of interests.*

ISSN 2411-3336; e-ISSN 2541-9404

JOURNAL OF MINING INSTITUTE

Zapiski Gornogo instituta

Journal homepage: pmi.spmi.ru

*Research article*

# Application of the cybernetic approach to price-dependent demand response for underground mining enterprise electricity consumption

**Aleksandr V. NIKOLAEV**[1]✉, **Stefan VÖTH**[2], **Aleksey V. KYCHKIN**[3]

[1] *Perm National Research Polytechnic University, Perm, Russia*

[2] *George Agricola Graduate School of Technical Sciences, Bochum, Germany*

[3] *National Research University Higher School of Economics, Branch in Perm, Perm, Russia*

***How to cite this article*:** Nikolaev A.V., Vöth S., Kychkin A.V. Application of the cybernetic approach to price-dependent demand response for underground mining enterprise electricity consumption. Journal of Mining Institute. 2023. Vol. 261, p. 403-414. EDN CJGQKP. DOI: 10.31897/PMI.2022.33

***Abstract.*** The article considers a cybernetic model for the price-dependent demand response (DR) consumed by an underground mining enterprise (UGME), in particular, the main fan unit (MFU). A scheme of the model for managing the energy consumption of a MFU in the DR mode and the implementation of the cybernetic approach to the DR based on the IoT platform are proposed. The main functional requirements and the algorithm of the platform operation are described, the interaction of the platform with the UGME digital model simulator, on which the processes associated with the implementation of the technological process of ventilation and electricity demand response will be simulated in advance, is shown. The results of modeling the reduction in the load on the MFU of a mining enterprise for the day ahead are given. The presented solution makes it possible to determine in advance the necessary power consumption for the operation of the main power supply unit, manage its operation in an energy-saving mode and take into account the predicted changes in the planned one (e.g., when men hoisting along an air shaft) and unscheduled (e.g., when changing outdoor air parameters) modes. The results of the study can be used to reduce the cost of UGME without compromising the safety of technological processes, both through the implementation of energy-saving technical, technological or other measures, and with the participation of enterprises in the DR market. The proposed model ensures a guaranteed receipt of financial compensation for the UGME due to a reasonable change in the power consumption profile of the MFU during the hours of high demand for electricity, set by the system operator of the Unified Energy System.

***Keywords:*** demand response; cybernetic approach; system architecture; Internet of Things platform; underground mining enterprise; short-term load forecasting; digital twin

***Acknowledgment.*** The study was carried out with the financial support of the Government of the Perm Territory within the framework of the International Research Group “Development of a digital model for forecasting and price-dependent demand response for electricity consumed by the underground mining enterprises” project, 2020 (agreement N C-26/506 dated 09.03.2021)

***Received*: *12.05.2021*** ***Accepted*: *11.05.2022*** ***Online*: *13.07.2022*** ***Published: 19.07.2023***

**Introduction.** Underground mining is associated with a significant energy costs for production, almost half of which (according to some sources, up to 70 %) is spent on ventilation of an underground mining enterprise [1-3]. The main fan unit (MFU) has the highest energy consumption in the ventilation system. In this regard, underground mining enterprises, in order to reduce the cost of mined and processed products, actively introduce various technical and technological solutions into production, which make it possible to reduce the cost of electricity for the operation of the MFU and the ventilation system in total. These solutions include: struggling with the external air leaks [4, 5], air recirculation usage [6, 7], application of energy efficient air conditioning technologies [8-10], etc.

EDN CJGQKP
DOI: 10.31897/PMI.2022.33

However, in the field of electric power industry, in addition to the cost of electricity, there is a problem of power balance in the form of generated and consumed electricity comparison, since most of the power plants in industrial areas continuously produce it during the day, while energy consumption is of the cyclical nature, tied to a 24-hour time interval. This leads to the fact that the electrical power produced during low demand hours is not demanded, while there is a shortage during peak demand hours [11]. The inability to automatically respond to demand dynamics leads to a decrease in the flexibility of the power system and, as a result, high operating costs [12-14].

The world practice of creating flexible energy systems shows the high efficiency of price-dependent electricity demand response methods in the day-ahead load planning mode. The method provides for the analysis of historical data on energy consumption, the identification of the most repeated (predicted with high accuracy) energy consumers, the assessment of the expected demand for the day ahead and, the formation of a plan for the generation of electric power on their basis [15-17].

Russian demand response technologies are theoretically well developed and presented by a number of publications by Russian scientists; the papers present algorithms for regulating the load schedule of educational institutions based on the forecast of energy consumption [18-20]; the papers [21, 22] describe the proposed ways to accumulate electricity during hours of low demand (flexible systems). Despite this, the scientific and practical experience of their use in the real market has not been fully formed. This is largely due to the fact that the demand response market is new for Russia, regulated by regulatory documentation approved by Decree of the Government of the Russian Federation dated March 20, 2019 N 287. To implement these measures, the Electricity Response Management Aggregator was introduced – an electric power industry entity that combines the resources of retail consumers to provide services for managing the demand for electricity consumers to provide electricity demand response services. The aggregator is a participant in the wholesale electricity market that manages the change in the load of a group of consumers (for example, at mine or a shaft), in order to sell the set of regulation capabilities as a single object as a product/service on the wholesale market and/or on the system services market.

Despite the opening of the market, the processes associated with the automation of the participation of an underground mining enterprise have not been fully explored and are promising for reducing the cost of mining raw materials.

**Formulation of problem.** The cybernetic approach to price-dependent demand response for mines and shafts involves the use of a calculation model for the analysis of energy consumption and automatic reduction during the hours set by the system operator (SO) of the Unified Energy System (UES) of Russia. The reduction is achieved by reducing the productivity of the MFU, which, in turn, can be planned and unplanned. Thus, the performance of the MFU can be reduced when workers descend or ascend the ventilation shaft. These actions are known in advance, and the results of a decrease in productivity at such moments can be used in energy planning in day-ahead mode [23].

It is more difficult to reduce the productivity, and hence the energy consumption of the MFU outside of the planned technological processes. This is due to the fact that a large number of random factors affect the ventilation process [24]. For example, in the process of ventilation between mine shafts, the so-called "general mine natural draft" acts – the phenomenon of convective heat transfer, when warm air tends up and cold air goes down [25]. In this regard, the value and the direction of the general mine natural draft will depend on the parameters of the outside air. In this case, the resulting thrust can be directed in the direction of air movement, i.e. will contribute to ventilation (the so-called positive natural draft), or, vice-versa, may act in the opposite direction – interfere with the operation of the MFU ("negative" natural draft). Consequently, the ventilation mode will depend on the parameters of the air entering the mine shafts.

EDN CJGQKP
DOI: 10.31897/PMI.2022.33




In [26] a method for calculating the predicted general mine natural draft with possible changes in the parameters of the outside air is presented. Since the meteorological forecast in the short term has an accuracy of 85-90 % [25, 27], then it is possible to determine the value of the general mine natural draft a day ahead and set the required MFU operation mode. During the air preparation period, in addition to the MFU, it is necessary to control the mine air heaters (MAH) modes, which complicates the process. But, taking into account the dependence of the operation of the MAH on the parameters of the outside air, and taking into account the heat output of the heaters, it is possible to determine the parameters of the air in mine shafts and predict the magnitude and direction of the general mine natural draft. The MFU operation mode depends on the magnitude and direction of the general mine natural draft. Under the action of positive general mine natural draft, it is possible to reduce the productivity of the MFU by reducing the cost of electricity for ventilation.

The potential possibility of unloading the power supply system of an underground mining enterprise as a result of reducing electricity consumption during the general natural draft operation can be used in practice after the implementation of an electricity demand response cybernetic model as part of the Internet of things platform. There are limitations to the use of such a platform at facilities, since it is impossible to control the operation of the MFU in automatic mode according to security rules. In this case, a necessary condition for ensuring the operability of the proposed solution is the use of a digital twin of the shaft (mine) ventilation process, in which measurement information will be accumulated, simulation modeling of technological processes will be carried out, and forecasts of the MFU productivity will be made when external factors change [28]. The architecture of the Internet of Things (IoT) platform and its interaction with the digital twin of the ventilation process are given in [26].

**Methodology.** The research methodology is based on the structural-algorithmic organization of the process of demand response for electricity for underground mining enterprises.

In general terms, electricity demand response (DR) is understood as the process of reducing the energy consumption of an object relative to a certain base level at time points set by the energy system operator, followed by receiving a monetary reward for successfully implemented unloading events.

From the point of view of the technical effect, the energy system of the region where underground mining enterprises operate receives a balancing tool that replaces the commissioning of expensive sources of electricity with an equivalent unloading in terms of volume, i.e. if an underground mining enterprise participates in DR activities, the load profile in this industrial area and partially beyond it will be smoother. The effect of the participation of the enterprise in the process of managing the demand for electricity is shown in Fig.1 [29].

Electricity supply curve $S$ in the region increases sharply on the right side (Fig.1), which is due to the connection of backup energy sources, additional costs for planning, maintenance, etc. Reducing consumption during peak hours from the value $P_1$ to $P_2$ leads to a shift in the demand curve $D_1$ into a curve $D_2$ and a decrease in electricity prices by the amount $\Delta C_{12}$. Similarly, the decrease in consumption during peak hours from the value $P_2$ to $P_3$ leads to a shift in the demand curve $D_2$ into curve $D_3$ and a decrease in electricity prices by the amount $\Delta C_{23}$.

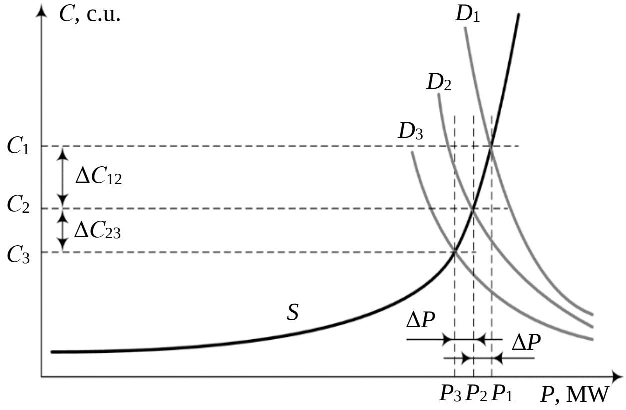

Fig.1. The dependence of the price on the electricity demand

It is important to note that with an equivalent decrease in the load of an underground mining enterprise $D_1 \rightarrow D_2$ and $D_2 \rightarrow D_3$ cost effect will vary. This indicates the expediency of strict observance of the unloading time. In order to ensure the timeliness of unloading within the framework of DR events, it is necessary to draw up an energy consumption plan in advance, in a day-ahead mode, coordinate this plan with the DR service operator, and on the day of the unloading event, implement a reduction in energy consumption in accordance with the previously adopted plan just in time (Fig.2).

In the presented model of process response for electricity of an underground mining enterprise, which is adapted for the Russian market, the following elements are distinguished:

• The system operator – body of operational and dispatching control, which, within the framework of the proposed DR model, forms a command for unloading for pre-selected aggregators and controls the fulfillment of obligations and pays for unloading.

• The aggregator – a power industry entity that acts as an intermediary between the system operator and the UGME, issues commands to reduce the energy consumption of the UGME after receiving unloading commands from the SO when the MFU is ready for unloading.

• The Internet of Things platform – an information product [30, 31], that monitors and manages the energy consumption of technological machines and equipment, in particular the MFU, generates notifications about the readiness to unload the UGME.

• Consumer – a UGME site that takes part in DR activities, for which it reduces energy consumption at certain hours of the day using manual, automated or automatic switching of the MFU operation modes.

• Controller – a device for measuring energy consumption at the input of the power receiving device of the ventilation system, in particular the MFU, as well as the implementation of control actions (in the event of receiving a control command from the Internet of Things platform), if necessary, automatic switching of the MFU operating modes.

• Load – a power receiving device that is involved in the technological processes of ventilation of the UGME, controlled by a controller.

Figure 2 shows several loads, since the demand response system itself involves other consumers in addition to the MFU. If there are several MFUs in the shaft (mine), then their work will be coordinated. The mechanism for managing the power consumption of the MFU in DR mode using the IoT platform is shown in detail in Fig.2.

An underground mining enterprise enters into a contract with a demand aggregator for the DR service. The contract is concluded for a fixed period of time, for example, one quarter. The aggregator

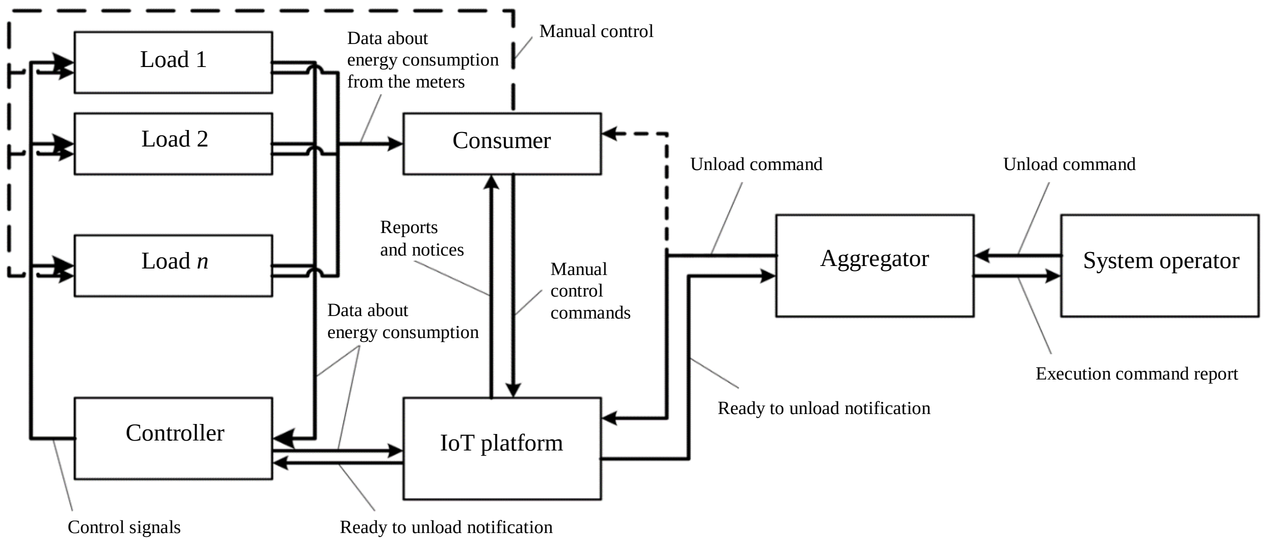


Fig.2. Power management model for MSU in DR mode using IoT platform

calculates the volume of unloading for each consumer within the organizational structure of the enterprise. Within the framework of the contract, the total volume of unloading, which the consumer must realize, is indicated. Every day, the consumer of an underground mining enterprise notifies the aggregator or system operator with whom he has concluded the contract for DR that unloading is ready for the next day.

As soon as the system operator identifies the possibility (forecast) of overloading the power system, he determines the need to reduce the load in the region. After that, the system operator sends this request to the aggregators with which there is an agreement. Aggregators must allocate the required amount of reduction in electricity consumption among the consumers of the UGME with whom they have an agreement, and notify them the day before reducing the load of the system. They can do it manually or with the help of an Internet of Things platform that connects through controllers to energy consumers [32, 33].

The aggregator, in turn, at the time of the load reduction event, undertakes to reduce energy consumption by the declared amount of electricity and, in case of successful fulfillment of the conditions, receive the remuneration established by the contract.

The consumer, receiving the appropriate signal, implements unloading, for example, by reducing the power consumption of the MFU. No more than five unloading signals per month are allowed. The signal contains information about the power unloading time and its value in kW (MW). The duration of the unloading period is two or four hours. At this time, the consumer must reduce his energy consumption (electrical power) by the specified amount. The consumer can implement this either manually or with the help of a controller and automation tools available at the enterprise.

**Discussion.** As part of the discussion, the following results of the authors' direct research were proposed:

1. Cybernetic scheme of price-dependent demand response at an underground mining enterprise with energy consumption forecasting.

2. Implementation results of a cybernetic approach to price-dependent demand response for an underground mining enterprise based on the Internet of Things platform.

When implementing a demand response strategy on the aggregator side, it becomes necessary to plan a reduction in energy consumption between UGME loads a day before the actual load reduction. At the same time, consumers also need to prepare in advance for unloading and know at what time it will be possible to reduce power. The magnitude and direction of the general mine natural draft depends on the parameters of the outside air, which may not change significantly in the required period. In this case, it will not be possible to achieve a reduction in the electricity consumed by the MFU, taking into account the general mine natural draft. The solution to the problem is short-term forecasting of energy consumption, which, in the absence of actual data, allows you to determine the load in terms of indicators based on past data that affect pricing and demand.

Figure 3 considers an algorithm for constructing a load reduction schedule in the process of managing demand for electricity for an underground mining enterprise based on the calculation of base load schedules offered by “System Operator of the Unified Energy System of Russia” JSC. The diagram illustrates the algorithm for determining the possible amount of load reduction during the hours indicated by the SO, and then plotting the load reduction schedule for one calculation day based on the actual energy consumption profiles of an underground mining enterprise for previous calculation periods.

The algorithm for scheduling unloading as part of the DR activities of an underground mining enterprise is as follows:

1. Construction of base load schedules for consumers, including MFU.

2. Construction of actual load curves for consumers.

EDN CJGQKP
DOI: 10.31897/PMI.2022.33

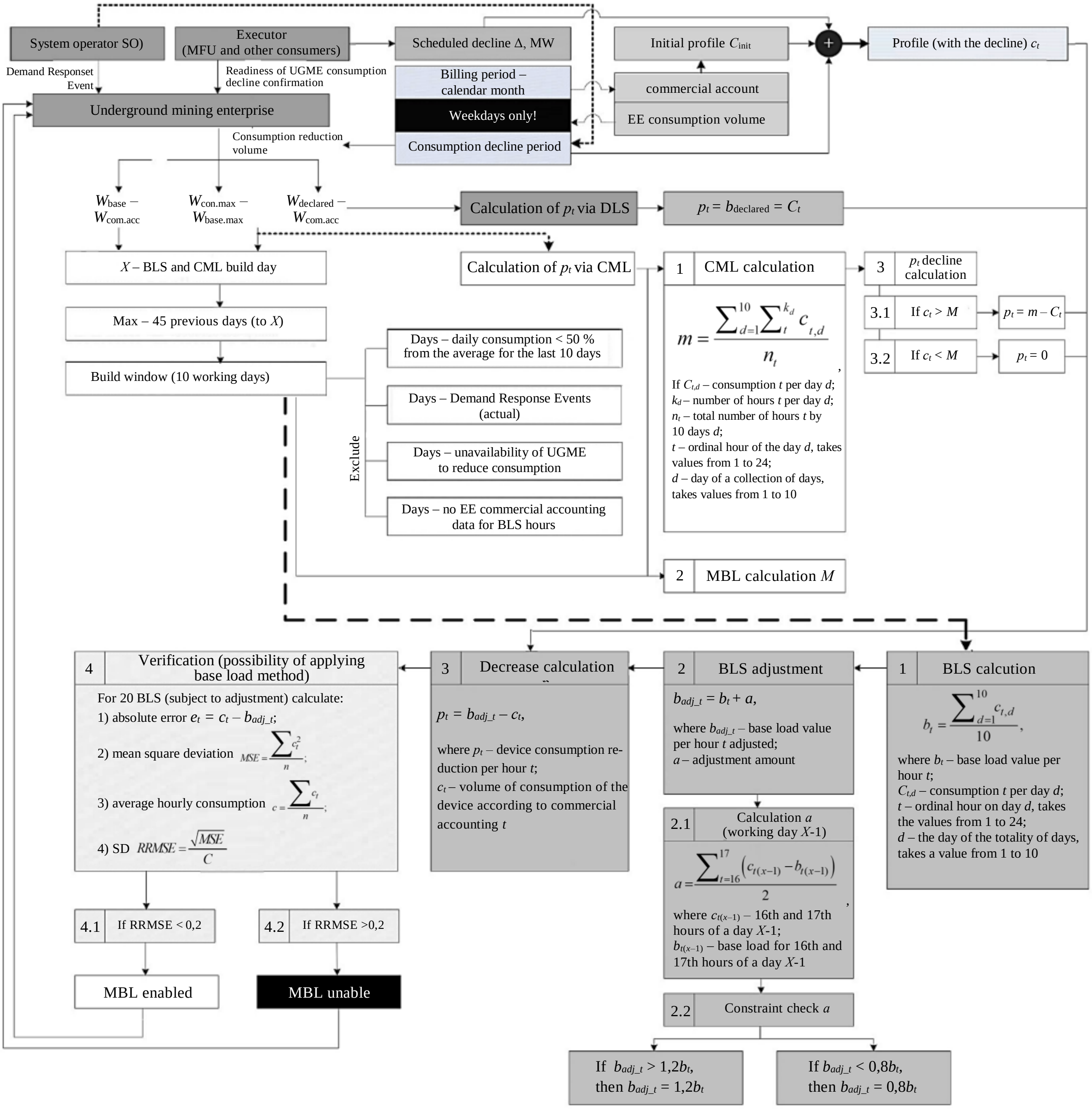


Fig.3. Scheme of price-dependent demand response for consumed electricity with UGME energy consumption forecasting

BLS – base load schedule; CML – conditional maximum load; MBL – maximum base load; DLS – declared load schedule; SO – system operator; P – performer; UGME – underground mining enterprise; SD – standard deviation; EE – electric energy

3. Calculation of the planned deviation of the actual from the base load with the determination of periods of excess / shortage of energy for each consumer (both planned and unplanned).

4. Distribution of consumers with excess productivity by hours of the settlement day.

5. Superposition (summation of values) of base load curves and actual load curves for consumers with excess power.

6. Calculation of excess productivity for a group of energy consumers of an enterprise by hours of the settlement day: calculation of the difference between the aggregated value of the basic load plan and the aggregated plan of the actual load (with a surplus);

• deviations sum calculation of the actual load from the base load with excess productivity for each hour of the settlement day (step 3-4).

7. Cases number estimation of load reduction $N_d$ for each for the current month (current settlement day); must be $N_d \leq 5$ for the whole month.

8. The choice of a specific consumer within the power system of an underground mining enterprise to reduce the load in order to fulfill the unloading volume set by the aggregator during the specified hours is based on the calculation of excess productivity (step 6) with an emphasis on those technological objects that comply with the established reduction restrictions load (number of load reductions for the billing month $N_d \leq 5$).

Service-oriented implementation of the cybernetic approach to DR based on the Internet of Things platform requires compliance with a number of functional requirements:

- formation of a detailed consumption structure at a mining enterprise; classification of power receivers installed at the facilities of the enterprise by type of activity and modes of operation;
- monitoring the dynamics of energy consumption of an underground mining enterprise technological equipment, including MFU, with fixation of critical deviations and registration of electric power indicators in real time;
- description and preparation of initial data for energy consumption analysis with specification of features for power receiver classes;
- differentiated analysis with clustering of consumers in the energy system of a mining enterprise by the level and mode of energy consumption with the identification of typical regularities (patterns) taking into account the days of the week and seasonality;
- intelligent analysis of energy consumption data with the identification of peak load zones as potential time intervals from the DR point of view;
- ensuring the repeatability of load profiles and reducing excess (peak) energy flows, developing scenarios for typical control actions on switching (off-off) loads to smooth out the daily profile;
- statistics on operation and maintenance, including the withdrawal of mining enterprise power receivers for repair, reporting on energy consumption reduction at DR hours;
- forecasting of energy consumption for certain categories of power receivers of the power system of an underground mining enterprise;
- stabilization of the demand and consumption ratio, taking into account the predicted values (DR-modeling);
- development of alternative and integrated solutions for managing the energy consumption of technological units, including the MFU, with the determination of the duration of the decrease, the sequence of automatic shutdown/switching of power receivers.

The presented requirements are implemented programmatically through the development of a typical Internet of Things platform, for example, Tibbo Aggregate, InfluxData, Siemens MindSphere, GE Predix, etc. Such platforms are designed specifically for the implementation of various services basedon IoT technologies, with the connection of many data sources, using analytics, including machine learning, time series databases. The architecture is based on the IoT technology stack, which allows developing various applications using tools for collecting, storing, visualizing and analyzing data (Fig. 4). The platform provides integration of all elements of the demand management system at a mining enterprise into a single cyber-physical system [11, 34], which includes various types of controllers, web servers, and application servers that collect power consumption data and implement DR logic. All communications of the underground mining enterprise with SO can be processed by the data collection and transmission unit, which also allows you to receive data from the demand aggregator. This implementation is capable of handling up to 1,000,000 controller connections. Information about energy consumption and the DR platform is available to end users in the personal accounts of the platform website.

The platform works as follows. The source of data is the controllers C*, which record the energy consumption of the mining enterprise during several settlement periods (at least 45 days preceding

**Journal of Mining Institute.** 2023. Vol. 261. P. 403-414
© Aleksandr V. Nikolaev, Stefan Vöth, Aleksey V. Kychkin, 2023
EDN CJGQKP
DOI: 10.31897/PMI.2022.33

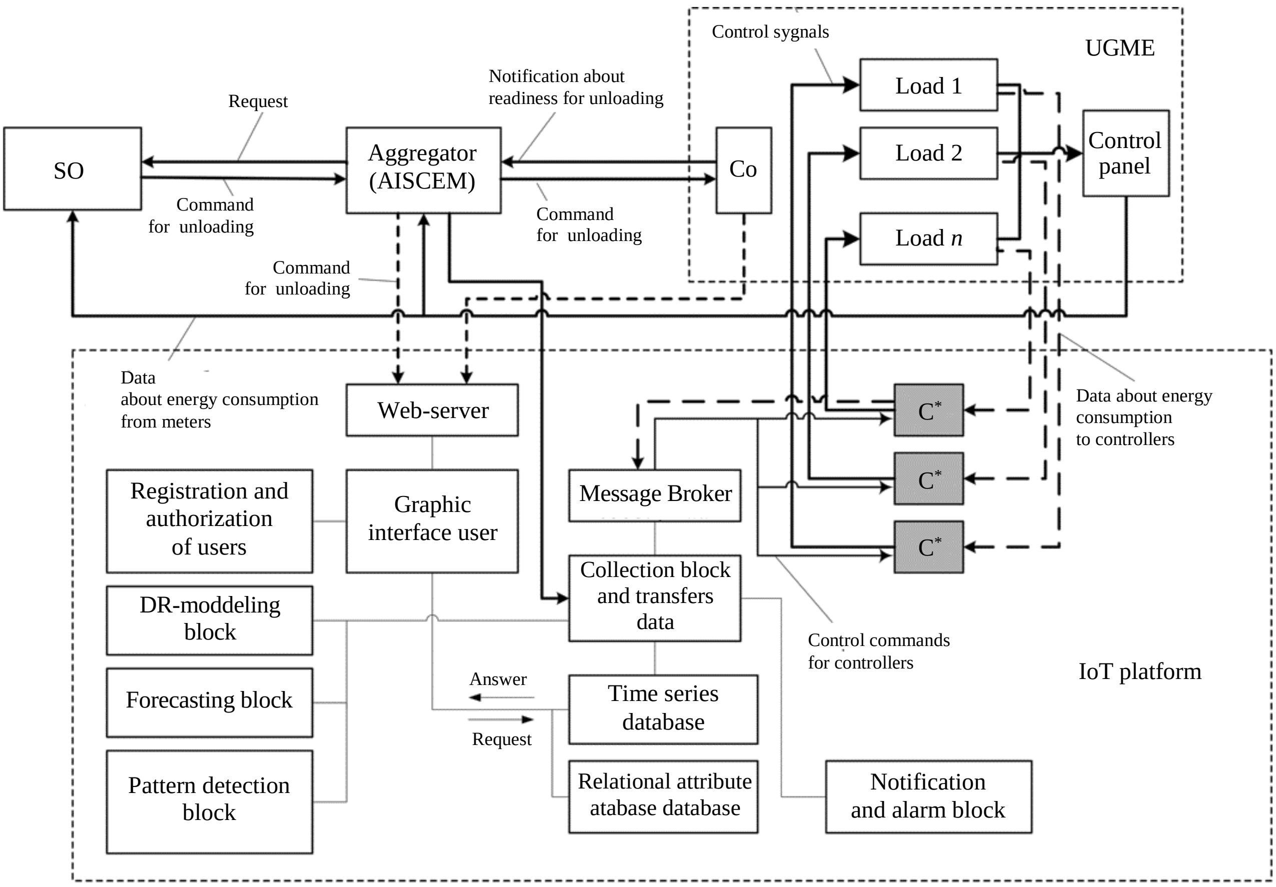


Fig.4. Scheme for the implementation of a cybernetic approach to DR of UGME based on the Internet of Things platform

the settlement day for which the analyzed load graph will be built). This implies that the enterprise includes one or more large loads in the form of local consumers (MFU in our case). The load profile is formed on the basis of electricity consumption indicators with a 30-minute interval and is stored in the energy monitoring process [35]. To simplify the demand response problem, the presented scheme does not take into account the reactive power flows when calculating the energy consumption indicators of the equipment of a mining enterprise.

For information interaction between the platform and real equipment, a message broker is used that supports the typical Internet of Things protocol, such as MQTT. Data from the broker, as well as from the automated information system for commercial electricity metering (AISCEM) of the demand aggregator, enters the data collection and transmission unit and then to the time series database. In online mode, these data are processed using the notification and alarm block, in case the parameters go beyond the required ranges, users are informed.

Calculation of energy consumption with the extraction of peak load zones is performed by typical days (working/weekend days of each month) in the pattern detection block. The DR-modeling block implements the calculation of hourly consumption statistics for the facilities of an underground mining enterprise; analysis of hourly statistics on the composition and modes of operation of the included equipment; calculation of the coefficients of the ratio of deficit and surplus of electricity (capacity) in the case of unloading; values of expected (preferred) restrictions on electricity consumption in case of participation in DR events.

The prediction block implements the construction of base load graphs for typical days. The predicted values of energy consumption for the objects of the mining enterprise are stored in the relational database of attributes for each calculation month (quarter). The results of unloadings are also

EDN CJGQKP
DOI: 10.31897/PMI.2022.33




stored there, deviations of the actual volumes of unloadings from the values specified in the framework of contractual obligations are additionally calculated.

Visualization of a summary graph of load reduction for a mining enterprise implemented using the graphical user interface of the IoT platform, available on the company's local network as a web server [36].

The presented cybernetic approach implies the possibility of introducing new analytical functions that improve the efficiency of estimating the total cost of electricity at a mining enterprise [37]. However, before using the above architecture scheme in practice, it is necessary to adapt the database and prediction blocks, taking into account the characteristics of specific enterprises. In particular, information security issues should be additionally considered, which are placed in the block of registration and authorization of users in the diagram.

**Conclusion.** The cybernetic approach to price-dependent demand response for electricity consumed by an underground mining enterprise involves providing the user with the following graphical screen forms:

• power consumption summary (including base load);

• report on the fulfillment of requests for unloading, logs of information exchange between the aggregator and consumers (statistics of requests, confirmation of readiness to fulfill requests);

• information on the calculation models for the distribution of SO commands by loads;

• base load forecasts, MFU unloading results, expected load energy profile calculations using Modelica Digital Twin [38, 39].

An example of a screen form showing the real power consumption of a MFU without unloading (*Active_power_Power_Station*) baseline plots (*demand response baseline*), base line with unloading (*demand response discharge*), predictive unloading profile (*demand response expected*) in the day ahead mode is shown in Fig.5.

It is proposed to build two types of reports for end users of the platform:

• PLAN report with predicted cumulative load reduction schedule according to the algorithm, which presents the baseline, predicted and expected load schedules, the RRMSE score as a metric for forecast accuracy, energy deficit and surplus. The following parameters are used: target day, time and duration of load shedding, total shedding volume (MW).

• FACT report that shows the actual graph of the cumulative load reduction. It shows base load curve, actual energy consumption, set load reduction commitments, RRMSE as a predictive accuracy metric, unload result (success/failure) by hour. The following parameters are used: target day, time


Fig.5. Modeling the load reduction on the MFU of a mining enterprise for the day ahead

EDN CJGQKP
DOI: 10.31897/PMI.2022.33

and duration of unloading, total amount of load shedding (MW), load shedding readiness indicator, electricity demand response event presence indicator.

Consumers of a mining enterprise can be connected to the IoT platform with an implemented price-dependent demand response service in the following ways:

• By installing hardware (master controllers) in the infrastructure of a mining enterprise. Controllers will allow you to receive data on energy consumption, as well as automatically control the load of the consumer based on pre-installed scenarios or commands through a user application.

• It is assumed that the consumer has a high level of energy management automation (EMS). Then the integration of the platform can be implemented by software (without installing additional hardware) – connecting the IoT platform to the consumer's EMS and receiving data on energy consumption from it.

The presented cybernetic model of electricity demand response can be built into the cyber-physical ventilation system of an underground mining enterprise, in which all kinds of scenarios for changing technological processes and parameters of the involved electrical equipment will be implemented.

The analysis of the information received will be carried out by the Internet of Things platform, as a result of which at least two possible scenarios for reducing load consumption will be developed:

• based on the analysis of the operating modes of all energy consumers obtained from the readings of electricity meters;

• based on an analysis of external factors (reduction of unplanned load), for example, on the basis of a change in the parameters of the outside air that enters the mine shafts and affects the distribution of air between them (the volumetric flow rate of the incoming air changes due to a change in the value of the general mine natural draft), and therefore for the work of the MFU.

When analyzing external factors, as a result of modeling technological processes in a digital twin, it is possible to predict in advance (for example, within a day) options for a possible decrease in the performance of the MFU and, consequently, the consumed electricity.

The architecture considered in the paper will allow underground mining enterprises to occupy a niche in the DR price-dependent energy demand response market, thereby achieving sustainable development and adhering to energy saving policies. From the point of view of achieving a financial result, an enterprise can reduce the cost of the mining process to 700 thousand rubles. per 1 MW as a result of a decrease in electric power during the hours established by the SO.

**REFERENCES**

1. Nikolaev A.V. The method for ventilating the slope blocks of oil mines enhancing the energy efficiency of the underground oil production. *Neftyanoe khozyaistvo*. 2016. N 11, p. 133-136 (in Russian).

2. Vilhena Costa de L., Silva da J.M. Cost-saving electrical energy consumption in underground ventilation by the use of ventilation on demand. *Mining Technology*. 2020. Vol. 129. Iss. 1, p. 1-8. DOI: 10.1080/25726668.2019.1651581

3. Wallace K., Prosser B., Stinnette J.D. The practice of mine ventilation engineering. *International Journal of Mining Science and Technology*. 2015. Vol. 25. Iss. 2, p. 165-169. DOI: 10.1016/j.ijmst.2015.02.001

4. Kamenskikh A.A. Development of methods to control and reduce surface air leakage in mines: Avtoref. dis. ... kand. tekhn. nauk. Perm: Gornyi institut Uralskogo otdeleniya RAN, 2011, p. 20 (in Russian).

5. Nikolaev A.V., Alymenko N.I., Sadykov R.I. Calculation of surface air leaks at potash mine. *Bulletin of Perm University. Geology*. 2012. N 5, p. 115-121 (in Russian).

6. Golovatyi I.I., Kruglov Yu.V., Levin L.Yu. Mine fan installation with automatic control system for recirculation ventilation of potash mines. *Gornyi Zhurnal*. 2010. N 8, p. 78-80 (in Russian).

7. Kruglov Yu.V., Levin L.Yu., Zaitsev A.V. Calculation method for the unsteady air supply in mine ventilation networks. *Journal of Mining Science*. 2011. Vol. 47. N 5, p. 651-659 (in Russian).

8. Zaitsev A.V. Scientific basis for calculating and managing the thermal regime of underground mines: Avtoref. dis. … d-ra tekhn. nauk. Perm: Permskii natsionalnyi issledovatel'skii politekhnicheskii universitet 2019, p. 44 (in Russian).

9. Gendler S.G., Kovshov S.V. Estimation and reduction of mining-induced damage of the environment and work area air in mining and processing of mineral stuff for the building industry. *Eurasian mining*. 2016. N 1, p. 45-49. DOI: 10.17580/em.2016.01.08

10. Nikolaev A.V. Energy-efficient air conditioning in shallow mines. *Gornyi Zhurnal*. 2017. Vol. 3, p. 71-74 (in Russian). DOI: 10.17580/gzh.2017.03.13

11. Kudzh S.A., Tsvetkov V.Ya. Network-centric control and cyber-physical systems. *Educational resources and technology*. 2017, p. 86-92 (in Russian). DOI: 10.21777/2500-2112-2017-2-86-92

12. Piette, M., Sezgen, O., Watson, D. et al. Development and evaluation of fully automated demand response in large facilities. Lawrence Berkeley National Laboratory, 2004.

13. Sezgen O., Goldman C.A., Krishnarao P. Option value of electricity demand response. *Energy*. 2007. Vol. 32. Iss. 2, p. 108-119. DOI: 10.1016/j.energy.2006.03.024

14. Valero S., Ortiz M., Senabre C. et al. Methods for customer and demand response policies selection in new electricity markets. *IET Generation, Transmission & Distribution*. 2007. Vol. 1. Iss. 1, p. 104-110. DOI: 10.1049/iet-gtd:20060183

15. Chasparis G.C., Pichler M., Spreitzhofer J., Esterl T. A cooperative demand-response framework for day-ahead optimization in battery pools. *Energy Informatics*. 2019. Vol. 2, p. 1-17. DOI: 10.1186/s42162-019-0087-x

16. Soares L.J., Medeiros M.C. Modeling and forecasting short-term electricity load: A comparison of methods with an application to Brazilian data. *International Journal of Forecasting*. 2008. Vol. 24. Iss. 4, p. 630-644. DOI: 10.1016/j.ijforecast.2008.08.003

17. Xu Y., Li N., Low S.H. Demand Response With Capacity Constrained Supply Function Bidding. *IEEE Transactions on Power Systems*. 2016. Vol. 31. N 2, p. 1377-1394. DOI: 10.1109/TPWRS.2015.2421932

18. Boikov A., Payor V., Savelev R., Kolesnikov A. Synthetic Data Generation for Steel Defect Detection and Classification Using Deep Learning. *Symmetry*. 2021. Vol. 13. Iss. 7. N 1176. DOI: 10.3390/sym13071176

19. Zhukovskiy Y.L., Kovalchuk M.S., Batueva D.E., Senchilo N.D. Development of an Algorithm for Regulating the Load Schedule of Educational Institutions Based on the Forecast of Electric Consumption within the Framework of Application of the Demand Response. *Sustainability*. 2021. Vol. 13 (24). N 13801. DOI: 10.3390/su132413801

20. Shabalov M.Yu, Zhukovskiy Yu.L., Buldysko A.D. et al. The influence of technological changes in energy efficiency on the infrastructure deterioration in the energy sector. *Energy Reports.* 2021. Vol. 7, p. 2664-2680. DOI: 10.1016/j.egyr.2021.05.001

21. Savard C., Iakovleva E., Ivanchenko D., Rassõlkin A. Accessible battery model with aging dependency. *Energies*. 2021. Vol. 14. Iss. 12. N 3493. DOI: 10.3390/en14123493

22. Senchilo N.D., Ustinov D.A. Method for determining the optimal capacity of energy storage systems with a long-term forecast of power consumption. *Energies.* 2021. Vol. 14. Iss. 21. N 7098. DOI: 10.3390/en14217098

23. Dicks F., Clausen E. Ventilation on Demand. *Mining Report*. 2017. Vol. 153. N 4, p. 334-341.

24. Nikolaev A.V., Alymenko N.I., Kamenskikh A.A. et al. Factors defining value and direction of thermal pressure between the mine shafts and impact of the general mine natural draught on ventilation process of underground mining companies. *IOP Conference. Series: Earth and Environmental Science*. 2017. Vol. 87. N 052020, p. 561-566. DOI: 10.2991/aime-17.2017.91

25. Rogers D.P., Tsirkunov V.V. Weather and Climate Resilience: Effective Preparedness through National Meteorological and Hydrological Services. World Bank Publications. Washington, DC: Directions in Development – Environment and Sustainable Development, 2013, p. 152.

26. Kychkin A., Nikolaev A. IoT-based Mine Ventilation Control System Architecture with Digital Twin. 2020 International Conference on Industrial Engineering, Applications and Manufacturing (ICIEAM). 2020. N 9111995, p. 5. DOI: 10.1109/ICIEAM48468.2020.9111995

27. Bedritskii A.I., Korshunov A.A., Khandozhko L.A., Shaimardanov M.Z. Hydrometeorological safety and sustainable development of Russia. *Pravo i bezopasnost*. 2007. N 1-2 (22-23), p. 7-13 (in Russian).

28. Nikolaev A., Alymenko N., Kamenskih A., Nikolaev V. The results of air treatment process modeling at the location of the air curtain in the air suppliers and ventilation shafts. *E3S Web of Conferences*. 2017. Vol. 15. N 02004, p. 7. DOI: 10.1051/e3sconf/20171502004

29. Andersen F.M., Jensen S.G., Larsen H.V. et al. Analyses of Demand Response in Denmark. Denmark. Roskilde: Riso National Laboratory Information Service Department, 2006, p. 100.

30. Xu B., Zheng J., Wang Q. Analysis and Design of Real-Time Micro-Environment Parameter Monitoring System Based on Internet of Things. IEEE International Conference on Internet of Things (iThings) and IEEE Green Computing and Communications (GreenCom) and IEEE Cyber, Physical and Social Computing (CPSCom) and IEEE Smart Data (SmartData), 15-18 December 2016. Chengdu, China, 2016, p. 368-371. DOI: 10.1109/iThings-GreenCom-CPSCom-SmartData.2016.87

31. Gubbi J., Buyya R., Marusic S., Palaniswamia M. Internet of Things (IoT): A vision, architectural elements, and future directions. *Future Generation Computer Systems*. 2013. Vol. 29. Iss. 7, p. 1645-1660. DOI: 10.1016/j.future.2013.01.010

32. Kychkin A., Deryabin A.S., Neganova E., Markvirer V. IoT-Based Energy Management Assistant Architecture Design. 2019 IEEE 21st Conference on Business Informatics (CBI). IEEE Computer Society. 2019. Vol. 1, p. 522-530. DOI:10.1109/CBI.2019.00067

33. Mijić D., Varga E. Unified IoT Platform Architecture Platforms as Major IoT Building Blocks. International Conference on Computing and Network Communications (CoCoNet). 2018, p. 6-13. DOI: 10.1109/CoCoNet.2018.8476881

34. Lu Hou, Shaohang Zhao, Xiong Xiong et al. Internet of Things Cloud: Architecture and Implementation. *IEEE Communications Magazine*. 2016. Vol. 54. Iss.12, p. 32-39. DOI: 10.1109/MCOM.2016.1600398CM

35. Kychkin A.V. Synthesizing a system for remote energy monitoring in manufacturing. *Metallurgist*. 2016. Vol. 59. N 9-10, p. 752-760. DOI: 10.1007/s11015-016-0170-5

36. Lyakhomskiy A., Perfileva E., Kychkin A., Genrikh N. A software- hardware system of remote monitoring and analysis of the energy data. *Russian Electrical Engineering*. 2015. Vol. 86 (6), p. 314-319. DOI: 10.3103/S1068371215060103

EDN CJGQKP
DOI: 10.31897/PMI.2022.33

37. Faizrakhmanov R.A., Frank T., Kychkin A.V., Fedorov A.B. Sustainable energy consumption control using the MY-JEVIS energy management data system. *Russian Electrical Engineering*. 2011. Vol. 82 (11), p. 607-611. DOI: 10.3103/S1068371211110022

38. Vöth S., Vasilyeva M. Potential of Modelica for the creation of digital twins. Advances in raw material industries for sustainable development goals. London: Taylor & Francis Group, 2020, p. 386-389. DOI: 10.1201/9781003164395

39. Vöth S., Bogdanov V., Pomazov D. Modeling of Efficiencies on Basis of Power Flow Directions using Modelica on the Example of Hoisting Systems. Project: Safety and Availability of Cranes. 2020, p. 6.

***Authors*: Aleksandr V. Nikolaev,** *Doctor of Engineering Sciences*, *Associate Professor*, *nikolaev0811@mail.ru*, *https://orcid.org/0000-0002-4601-5780* (*Perm National Research Polytechnic University*, *Perm*, *Russia*), **Stefan Vöth,** *Doctor of Engineering Sciences*, *Professor*, *Head of Department*, *https://orcid.org/0000-0002-0705-973X* (*George Agricola Graduate School of Technical Sciences*, *Bochum*, *Germany*), **Aleksey V. Kychkin,** *Candidate of Engineering Sciences*, *Associate Professor*, *Head of the Scientific and Educational Laboratory*, *https://orcid.org/0000-0003-0626-5803* (*National Research University Higher School of Economics*, *Branch in Perm*, *Perm*, *Russia*).

*The authors declare no conflict of interests*.

ISSN 2411-3336; e-ISSN 2541-9404

JOURNAL OF MINING INSTITUTE

Zapiski Gornogo instituta

Journal homepage: pmi.spmi.ru

Research article

# Enhancement of energy efficiency of the vacuum oil distillation unit using pinch analysis

**Ekaterina A. YUSHKOVA**✉, **Vladimir A. LEBEDEV**
*Saint Petersburg Mining University, Saint Petersburg, Russia*

***How to cite this article*****:** Yushkova E.A., Lebedev V.A Enhancement of energy efficiency of the vacuum oil distillation unit using pinch analysis. Journal of Mining Institute. 2023. Vol. 261, p. 415-427. EDN LXDVDP

***Abstract.*** The actual task of the state is to increase the energy efficiency of the oil refinery. The object of research is a vacuum distillation unit, including a preheating unit for raw materials and a furnace for heating fuel oil before the column. Pinch analysis allows to analyze and optimize a large number of heat flows. In this study the analysis and enhancement of efficiency of the research object is carried out by enthalpy pinch analysis. In order to reduce the heat load of the furnaces, the additional flows were introduced into the heat exchange system of the oil heating unit. Parametric optimization of the new heat exchange system was carried out. The minimum needs of the heat exchange system in external energy carriers are determined. An enthalpy cascade of the heat exchange system has been constructed, which clearly shows the distribution of heat between each heat flow of the system. In the analysis of the energy efficiency of a furnace, an important point is the determination of the optimal heat capacity of the combustion products. In this work, we have determined the optimal flow heat capacity, at which the heat loss with the exhaust gases is minimal. As a result of the studies carried out, the efficiency of the fuel oil preheating unit has been increased by maximizing heat recovery, and the cost of external energy carriers has been minimized. By reducing heat loss with flue gases, it was possible to increase the efficiency of the furnace.

***Keywords*****:** vacuum distillation unit; energy efficiency; pinch analysis; heat cascade; enthalpy

***Received: 10.03.2023*** ***Accepted: 20.06.2023*** ***Online: 19.07.2023*** ***Published: 19.07.2023***

**Introduction.** Increasing energy efficiency is the main factor in the economic growth of an enterprise and the state [1-3]. Energy efficient technologies can reduce the consumption of natural resources and reduce environmental damage [4-6]. Federal Law N 296-FZ of July 2, 2021 “On Limiting Greenhouse Gas Emissions” confirms the relevance of reducing emissions to the environment.

Scientists around the world create energy efficient technologies [7-9]. Modern research includes computer technology [10-12]. There are many different methods for assessing energy efficiency [13-15]. Current areas of research are the so-called 4-E [16]: enthalpy, exergy, exergoeconomics, and economic analysis. Research is moving forward and 4-E can be supplemented with environmental analysis [17-20].

One of the efficient methods for optimizing heat flows is pinch analysis [21]. Theoretical foundations in the field of integration of thermal processes and pinch analysis are presented in the work of R.Smith et al. [22, 23]. Pinch analysis makes it possible to work with a large number of heat flows. This method performs parametric and structural optimization of the heat exchange system.

The oil refining industry is energy intensive [20] – the plants have a large amount of heat flows with large potentials of thermal energy. Therefore, the use of pinch analysis is advisable in oil refineries [24-26].

The study [27] presents in detail a method for improving the energy efficiency of primary oil distillation units without making changes to the structure of the heat exchange network. Increasing the economic efficiency of process units is achieved through the use of mathematical programming methods. The authors of the study also achieved a reduction in carbon dioxide emissions into the environment.

A common method for designing heat exchange networks is the graphical method of process integration [28]. This method has a number of significant advantages, in particular, interactive visualization of the heat exchange network analysis is provided. This advantage can replace the use of various software products (Aspen Energy Analyser, etc.). This method was practically used in the modernization of an oil refinery in Kuwait [29]. However, this method is applicable only to heat exchange networks with one minimum temperature difference.

One of the main results of the study [30] is the development of a graphical tool for designing heat exchange networks with the simultaneous presence of several minimum temperature differences.

The work [31] gives an example of optimization of the heat exchange network of the primary oil distillation unit located in Bahrain. Particular attention is paid to the reduction of carbon dioxide emissions.

Pinch analysis includes various tools: parametric optimization, structural optimization, grand compound curve, and thermal cascades. There are various options for using pinch analysis: enthalpy, exergy, etc. [32-34]. The method of structural and parametric optimization based on exergy pinch analysis was described in previous studies [35]. The novelty of this study is the use of pinch analysis technology to analyze and develop measures to improve the energy efficiency of a vacuum distillation unit of fuel oil.

**Methods.** Vacuum tubular distillation unit of the fuel profile is designed for processing the fuel oil fraction and fraction of atmospheric gasoil from the atmospheric tubular plant AT-5 in order to obtain vacuum diesel fuel, light vacuum gasoil (LVG) and heavy vacuum gasoil (HVG). The general scheme of the investigated blocks of the vacuum distillation unit VT-1 is shown in Fig.1.

The objects of study are the fuel oil preheating unit VT-1 and the furnace for heating fuel oil before the column. The main stages of the study are:

• analysis of the existing heat exchange system of the fuel oil preheating unit using enthalpy pinch analysis;

• pinch analysis of the vacuum distillation unit:

– parametric optimization of the new heat exchange system of the preheating unit;

– construction and study of the enthalpy cascade, which shows what is the proportion of enthalpy in each temperature range;

– analysis of the heat exchange system using a grand composite curve, which will optimize the operation of the fuel oil preheating furnace.

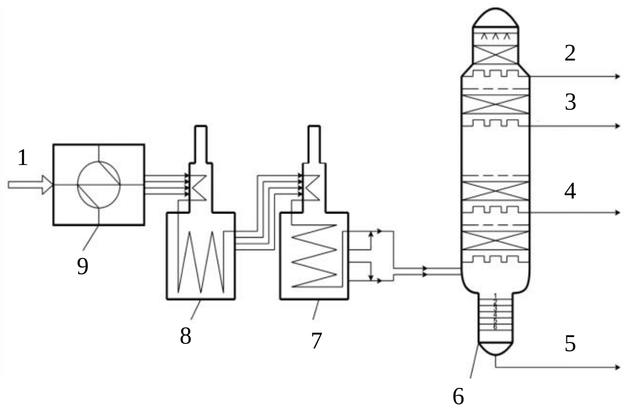


Fig.1. General scheme of the investigated blocks of the vacuum distillation unit

1 – fuel oil in HE-27/1.2; 2 – vacuum component of diesel fuel and the first pumparound in ACU-10/1.2; 3 – light vacuum gasoil in HE-22/1.2; 4 – heavy vacuum gasoil and the second pumparound in HE-26/3.4; 5 – tar and quench in HE-31/3.4; 6 – vacuum column C-4; 7 – furnace F-3; 8 – furnace F-3N; 9 – fuel oil preheating unit

*Analysis of the existing heat exchange system of the fuel oil preheating unit.* Before proceeding to the conversion of heat flows, namely their integration, it is necessary to understand the general structure of the fuel oil preheating unit. The heat exchange system of the vacuum unit for the distillation of fuel oil is shown in Fig.2. The raw material of the unit is fuel oil or a petroleum product similar in physical and chemical properties.

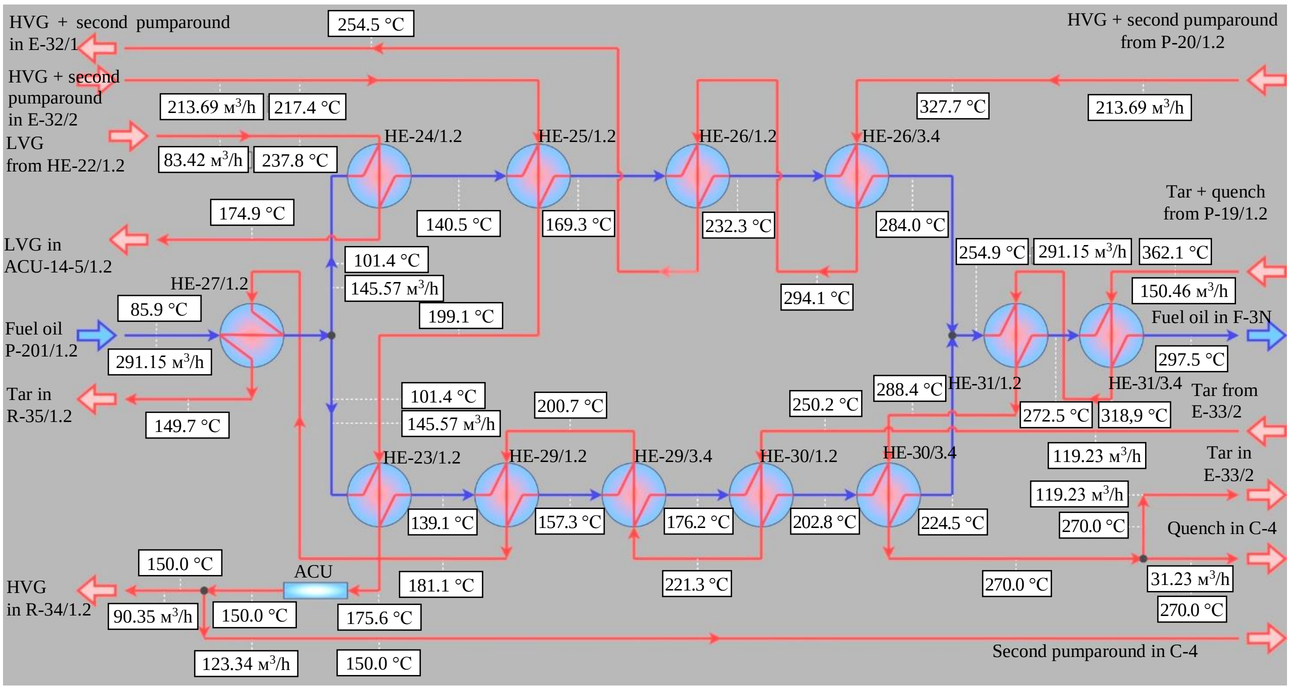


Fig.2. Heat exchange system of the fuel oil preheating unit

According to the set operating mode of the vacuum column, the temperature of the fuel oil entering the distillation column should be 393 °C. To achieve this temperature, fuel oil after the heat exchanger HE-31/3.4 enters the block of fire heating of raw materials (fuel oil), which consists of tubular furnaces for heating fuel oil F-3N and F-3. Fuel oil passes through the convection and radiant sections of the F-3N furnace, where it is heated to a temperature of 320 °C. At the same time, the F-3N furnace is four-flow. Fuel oil enters it in four flows and is also removed from it in four flows. Further, the fuel oil enters the F-3 furnace, where, when passing through the convection and radiant sections, it is heated to a temperature of 393 °C.

After passing through the fire heating unit, fuel oil with a temperature of 393 °C enters the vacuum column in two streams. Vacuum distillation column is designed for vacuum separation of fuel oil into fractions according to the following fuel scheme: vacuum diesel fraction; light and heavy vacuum gasoils; tar.

The cold flow of the unit is fuel oil. But for the construction of a cold composite curve, this flow will be represented as four separate cold flows. Hot flows are fuel oil fractions withdrawn from the distillation column for this technological scheme. After analyzing the technological scheme of the unit, five hot streams can be distinguished, which are used to heat fuel oil (cold streams) in the preheating unit. Heat flows are determined. The flow data are presented in Table 1.

The flow enthalpy change with a change in its temperature (at constant value of heat capacity within a given temperature interval) is determined according to the formula

$$\Delta H = CP\left[T_2 - T_1\right], \qquad (1)$$

where $CP$ – flow heat capacity, is the product of mass flow and specific heat capacity, W/°C; $T_1$ – initial temperature; $T_2$ – final temperature.

The hot compound curve combines flows that give off heat. Fuel oil flows that require heating are combined into a cold composite curve. Cold and hot composite curves are plotted using flow data (Fig.3, *a*).

*Table 1*

**Initial data of heat flows of the unit**

| Type | Flows | Temperature, °C | | Mass flow, kg/s | Specific heat capacity at constant pressure, kJ/(kg·°C) | Flow heat capacity, kW/°C | Flow enthalpy change, MW |
|---|---|---|---|---|---|---|---|
| | | Initial | Final | | | | |
| Hot flow 1 | Heavy vacuum gasoil and second pumparound from column to HE-26/3.4 | 328 | 255 | 56.0 | 2.8 | 154.1 | –11.2 |
| Hot flow 2 | Heavy vacuum gasoil and second pumparound from E-32/2 to HE-25/1.2 | 232 | 176 | 56.0 | 2.4 | 136.7 | –7.7 |
| Hot flow 3 | Tar and quench from P-19/1.2 to HE-31/3.4 | 362 | 270 | 44.2 | 2.7 | 118.5 | –10.9 |
| Hot flow 4 | Tar from E-33/2 to HE-30/1.2 | 250 | 150 | 35.0 | 2.3 | 81.5 | –8.2 |
| Hot flow 5 | Light vacuum gasoil from HE-22/1.2 to HE-24/1.2 | 238 | 175 | 21.0 | 2.5 | 52.9 | –3.3 |
| Cold flow 1 | Fuel oil from P-201/1.2 to HE-27/1.2 | 86 | 101 | 79.2 | 2 | 160.2 | 2.4 |
| Cold flow 2 | Fuel oil from HE-27/1.2 to HE-24/1.2 | 101 | 284 | 39.6 | 2.4 | 93.5 | 17.1 |
| Cold flow 3 | Fuel oil from HE-27/1.2 to HE-23/1.2 | 101 | 225 | 39.6 | 2.3 | 89.7 | 11.1 |
| Cold flow 4 | Fuel oil in HE-31/1.2 | 255 | 393 | 79.2 | 2.7 | 217.2 | 29.8 |

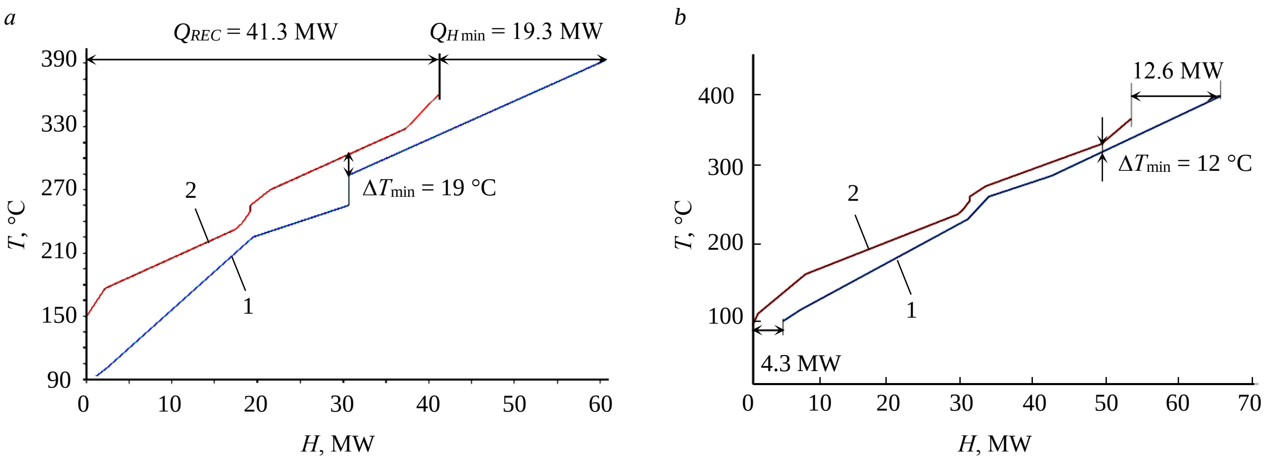


Fig.3. Flow composite curves before (*a*) and after (*b*) transformation
1 – cold; 2 – hot

The value of the minimum temperature difference in the heat exchange system is obtained by changing the position of the cold composite curve on the temperature-enthalpy plane. This is due to the fact that the initial and final temperatures of the flows must be preserved, but the enthalpy is a relative value. Only the change in the flow enthalpies is preserved, therefore, compound curves can be shifted along the x-axis on the *TH*-diagram [22].

Plotting hot and cold composite curves on the temperature-enthalpy diagram allows you to determine the values of heat recovery, the values of external hot and cold utilities.

We obtained the data by analyzing the composition of the curves:

• the minimum temperature difference is the distance between the compound curves along the temperature axis on the *TH*-diagram:

$$\Delta T_{\min} = 19\ °C;$$

• maximum heat recovery

$$Q_{REC} = 41.3 \text{ MW};$$

• hot utilities

$$Q_{H\min} = 60.6 - 41.3 = 19.3 \text{ MW};$$

• cold utilities

$$Q_{C\min} = 0 \text{ MW}.$$

The values of hot utilities $Q_{H\min}$ determine the amount of external thermal energy, that is, the energy of cold streams is not enough. This energy must be supplied from external energy sources. The external sources are the F-3N and F-3 furnaces.

The cold utility $Q_{C\min}$ values determine the amount of heat energy to be removed from the system. For a vacuum distillation unit, the residual heat of the hot flows is removed in refrigerators and air coolers. In order to reduce the required number of external hot utilities, it is necessary to investigate the possibility of post-cooling the existing hot flows in the fuel oil preheating unit before supplying them to refrigerators and air coolers. We will reduce the heat load of the F-3H and F-3 furnaces.

Consider the possibility of additional use of each of the hot streams presented in Table 1:

• Heavy vacuum gasoil and second pumparound from E-32/2 to HE-25/1.2. This flow passes through the heat exchangers HE-25/1.2, HE-23/1.2 and then enters the air-cooling units (ACU). After passing through the ACU, the flow is cooled from 176 to 150 °C. Although heavy vacuum gas oil must be cooled down to 80.4 °C before entering the park, the column's second circulating reflux must be cooled exactly to 150 °C, since this flow after the ACU enters the distillation column. Therefore, changing the temperature of the second circulating reflux of the column is unacceptable, as this may cause a change in the operating mode of the vacuum column. But it is possible to exclude ACU from work. We propose to cool this flow in heat exchangers HE-25/1.2 and HE-23/1.2 immediately to 150 °C. This will reduce the load on external hot utilities and reduce the power consumption of the ACU.

• Tar from E-33/2 to HE-30/1.2. This flow passes through the heat exchangers and enters the refrigerators, where it is cooled by heating the circulating water. This tar cooling is necessary. The temperature of the tar when entering the park or bitumen plant should be 96 °C. The temperature of the tar at the outlet of the preheating unit is 150 °C. We will consider the possibility of additional cooling of tar to 96 °C due to heat recovery. Thus, we exclude the operation of refrigerators R-35/1.2 and R-35/3.4.

• Light vacuum gasoil from HE-22/1.2 to HE-24/1.2. This flow passes through the heat exchanger HE-24/1.2. Then the flow enters the air coolers. Then the flow is discharged into the park or into the tar line into the park (depending on the requirements for the resulting products). The temperature of the light vacuum gas oil after the heat exchanger (HE-24/1.2) is 175 °C. The temperature of the light vacuum gasoil at the outlet of the unit should be 80 °C. We propose to cool this flow down to 80 °C in a preheating unit. We will exclude air coolers and reduce the heat load of furnaces (F-3N and F-3).

*Enthalpy pinch analysis of a fuel oil vacuum distillation unit.* Data flows after transformations are presented in Table 2. Parameters of other flows are not changed. Composite curves on the temperature-enthalpy plane are shown in Fig.3, *b*. These composite curves are approximated to $\Delta T_{\min}$ = 12 °C.

*Table 2*

**Data flows after transformations**

| Type | Flows | Temperature, °C | | Mass flow, kg/s | Specific heat capacity at constant pressure, kJ/(kg·°C) | Flow heat capacity, kW/°C | Flow enthalpy change, MW |
|---|---|---|---|---|---|---|---|
| | | Initial | Final | | | | |
| Hot flow 2 | Heavy vacuum gasoil and second pumparound from E-32/2 to HE-25/1.2 | 232 | 150↓ | 56.0 | 2.4 | 134.2 | –11 |
| Hot flow 4 | Tar from E-33/2 to HE-30/1.2 | 250 | 96↓ | 35.0 | 2.1 | 74.4 | –11.5 |
| Hot flow 5 | Light vacuum gasoil from HE-22/1.2 to HE-24/1.2 | 238 | 80↓ | 21.0 | 2.3 | 48.7 | –7.7 |

We obtained the data by analyzing the composition of the curves:

• the minimum temperature difference is the distance between the compound curves along the tem-perature axis on the *TH*-diagram $\Delta T_{\min}$ = 12 °C;

• the amount of heat recovered (maximum heat recovery), which is determined by the area of overlap of the flow composite curves along the enthalpy axis on the *TH*-diagram: $Q_{REC}$ = 48 MW;

• hot utilities $Q_{H\min}$ = 12.6 MW;

• cold utilities $Q_{C\min}$ = 4.3 MW.

The values of external hot and cold utilities were determined with the minimum temperature difference between the process flows ($\Delta T_{\min}$ = 12 °C).

Due to the construction of composite curves, it is possible to set the value of the minimum temperature difference in the heat exchange chemical-technological system. So, for shell-and-tube heat exchangers, the minimum temperature difference must be at least 10 °C. This requirement is due to the fact that at small values of $\Delta T_{\min}$, heat exchangers must operate only in counterflow mode. When designing a new or reconstructing an existing heat exchanger, the optimal value of $\Delta T_{\min}$ is chosen by achieving an economic compromise between the dependencies on the minimum temperature difference between process flows in heat exchange equipment, the cost of external utilities (energy carriers), and capital investments in the heat exchange system.

The next stage of research and optimization of the unit is the construction of a heat cascade. The cascade clearly shows the process of heat exchange between flows [22]. To construct a heat cascade, it is necessary that the shifted compound curves touch each other at the pinch point. Imagine that hot flows are colder by $\Delta T_{\min}/2$, and cold flows are colder by $\Delta T_{\min}/2$. As a result of such a shift of composite curves along the temperature axis, heat transfer becomes possible between flows containing composite curves in cold and hot within each temperature interval. Changing the boundaries of temperature intervals keeps the heat balance of the entire system.

The energy values of external utilities and the localization of the pinch point will be determined at $\Delta T_{\min}$ = 12 °C. To construct a heat cascade, it is necessary to obtain new temperatures shifted by $\Delta T_{\min}/2$. The changed values of the initial and final temperatures of the flows are presented in Table 3. The location of technological flows on the temperature axis after transformations is presented in Table 4.

EDN LXDVDP

*Journal of Mining Institute*. 2023. Vol. 261. P. 415-427


*Table 3*

**Shifted temperature intervals**

| Flow | Type | $T_{in}$, °C | $T_f$, °C | $T_{in}$, °C | $T_f$, °C |
|---|---|---|---|---|---|
| 1 | Cold | 86 | 101 | 92 | 107 |
| 2 | –"– | 101 | 284 | 107 | 290 |
| 3 | –"– | 101 | 225 | 107 | 231 |
| 4 | –"– | 255 | 393 | 261 | 399 |
| 5 | Hot | 328 | 255 | 322 | 249 |
| 6 | –"– | 232 | 150 | 226 | 144 |
| 7 | –"– | 362 | 270 | 356 | 264 |
| 8 | –"– | 250 | 96 | 244 | 90 |
| 9 | –"– | 238 | 80 | 232 | 74 |

*Table 4*

**Heat balance in shifted temperature intervals**

| Temperatures at the boundaries of the intervals $T$, °C | Flow distribution | Value of the temperature interval $T$, °C | $\Sigma CP_{cold} - \Sigma CP_{hot}$, kW/°C | Enthalpy change of the interval, MW | Excess/deficiency |
|---|---|---|---|---|---|
| 399 | | | | | |
| | | 43 | 217.2 | 9.339 | Deficiency |
| 356 | | | | | |
| | | 34 | 98.7 | 3.356 | Deficiency |
| 322 | | | | | |
| | | 32 | –55.4 | –1.773 | Excess |
| 290 | | | | | |
| | | 26 | 38.1 | 0.991 | Deficiency |
| 264 | | | | | |
| | | 3 | 156.6 | 0.469 | Deficiency |
| 261 | | | | | |
| | | 12 | –60.6 | –0.727 | Excess |
| 249 | | | | | |
| | | 5 | 93.5 | 0.468 | Deficiency |
| 244 | | | | | |
| | | 12 | 19.1 | 0.229 | Deficiency |
| 232 | | | | | |
| | | 1 | –29.6 | –0.029 | Excess |
| 231 | | | | | |
| | | 5 | 60.1 | 0.301 | Deficiency |
| 226 | | | | | |
| | | 82 | –74.1 | –6.076 | Excess |
| 144 | | | | | |
| | | 37 | 60.1 | 2.224 | Deficiency |
| 107 | | | | | |
| | | 15 | 37.1 | 0.557 | Deficiency |
| 92 | | | | | |
| | | 2 | –123.1 | –0.246 | Excess |
| 90 | | | | | |
| | | 16 | –48.7 | –0.779 | Excess |
| 74 | | | | | |

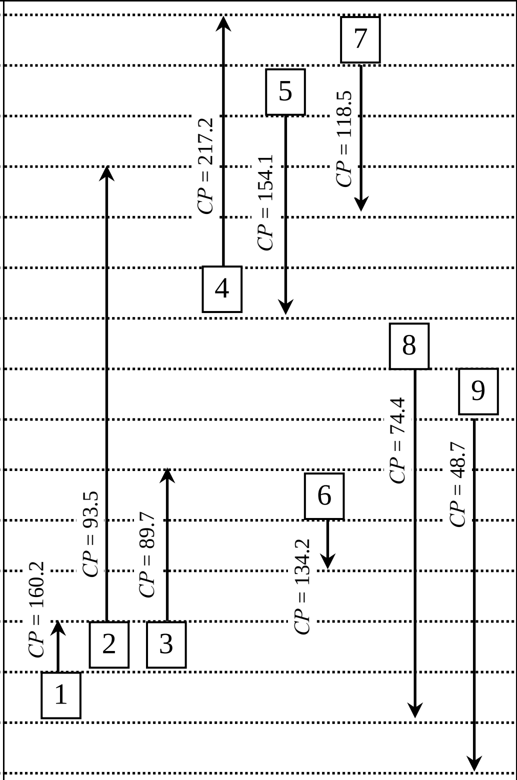


To solve the tabular problem, it is necessary to determine the energy balance for each shifted temperature interval. Formula for determining enthalpy change:

$$\Delta H_i = \left(\Sigma CP_{cold} - \Sigma CP_{hot}\right)_i \Delta T_i \,, \qquad (2)$$

where $\Sigma CP_{cold}$, $\Sigma CP_{hot}$ – the sum of the flow heat capacities of all cold and hot flows, respectively, W/°C; $\Delta T_i$ – value of the *i*-th temperature interval, °C.

In formula (2), $\Delta H_i$ is the change in enthalpy for each shifted temperature interval. A positive value of $\Delta H_i$ means that there is a shortage of thermal energy in the *i*-th interval. It is necessary to

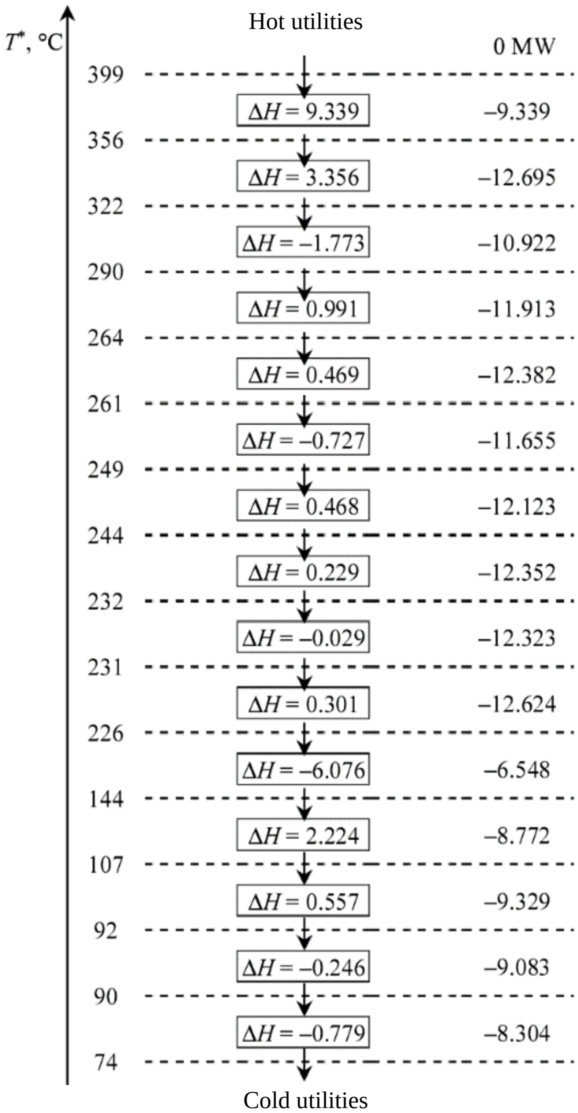


Fig.4. The enthalpy cascade at zero hot utilities

supply heat from external sources. A negative value of $\Delta H_i$ means that there is an excess of thermal energy in the *i*-th interval. Enthalpy changes of each temperature interval are presented in Table 4.

To consider the possibility of heat recovery between temperature intervals, it is necessary to build a cascade of heat flows (enthalpy cascade). The cascade sums up the enthalpy change from top to bottom. It is necessary to build two cascades. In the first case, the first temperature interval does not receive thermal energy from external energy carriers, i.e. $Q_{H\min} = 0$.The enthalpy cascade at zero hot utilities is shown in Fig.4.

Figure 4 shows that the first temperature interval has a net deficiency of thermal energy equal to –9.339 MW. This deficiency is transferred to the second temperature interval. The second interval also has a deficiency of thermal energy of hot streams 3.356 MW. As a result, the deficiency in the system is already –12.695 MW. The third temperature interval has an excess of thermal energy of hot flows –1.773 MW. The heat deficiency in the system decreases and becomes equal to –10.992 MW. According to this principle, an excess or deficiency of thermal energy is determined at each temperature interval. But the task of the study is to determine the location of the pinch, the values of hot and cold utilities using a heat flow cascade. It is necessary to build a second cascade, with non-zero hot utilities.

Heat flows cannot be negative because it is impossible to transfer energy up the temperature scale (from low temperatures to higher temperatures). There should be no negative flows. For this, the value of the largest negative value is brought to the first interval. In this study –12.69 MW (Fig.4). The resulting heat flow cascade is shown in Fig.5.

From the constructed cascade, we can conclude that in this case there are no negative heat fluxes. This indicates the possibility of transferring heat from one temperature interval to another. In this case, the heat flux is zero in the temperature range 322-356 °C. It can be concluded that the values of hot and cold utilities are $Q_{H\min}$ = 12.6 and $Q_{C\min}$ = 4.39 MW, respectively. The data are equal to the values obtained when constructing flow composite curves on the *TH*-diagram (see Fig.3, *b*). The pinch temperature is 322 °C. At the pinch point, the heat flow at the boundary of the intervals is zero. The real values of hot and cold flows at the pinch point are equal to $T_{\text{pinch}}^{\text{hot}} = 328$ and $T_{\text{pinch}}^{\text{cold}} = 316$ °C respectively. Values are consistent with data obtained from hot and cold composite curves.

Thus, the thermal cascade algorithm makes it possible to simplify the calculation of external energy carriers and determine the localization of the pinch point. The construction of composite

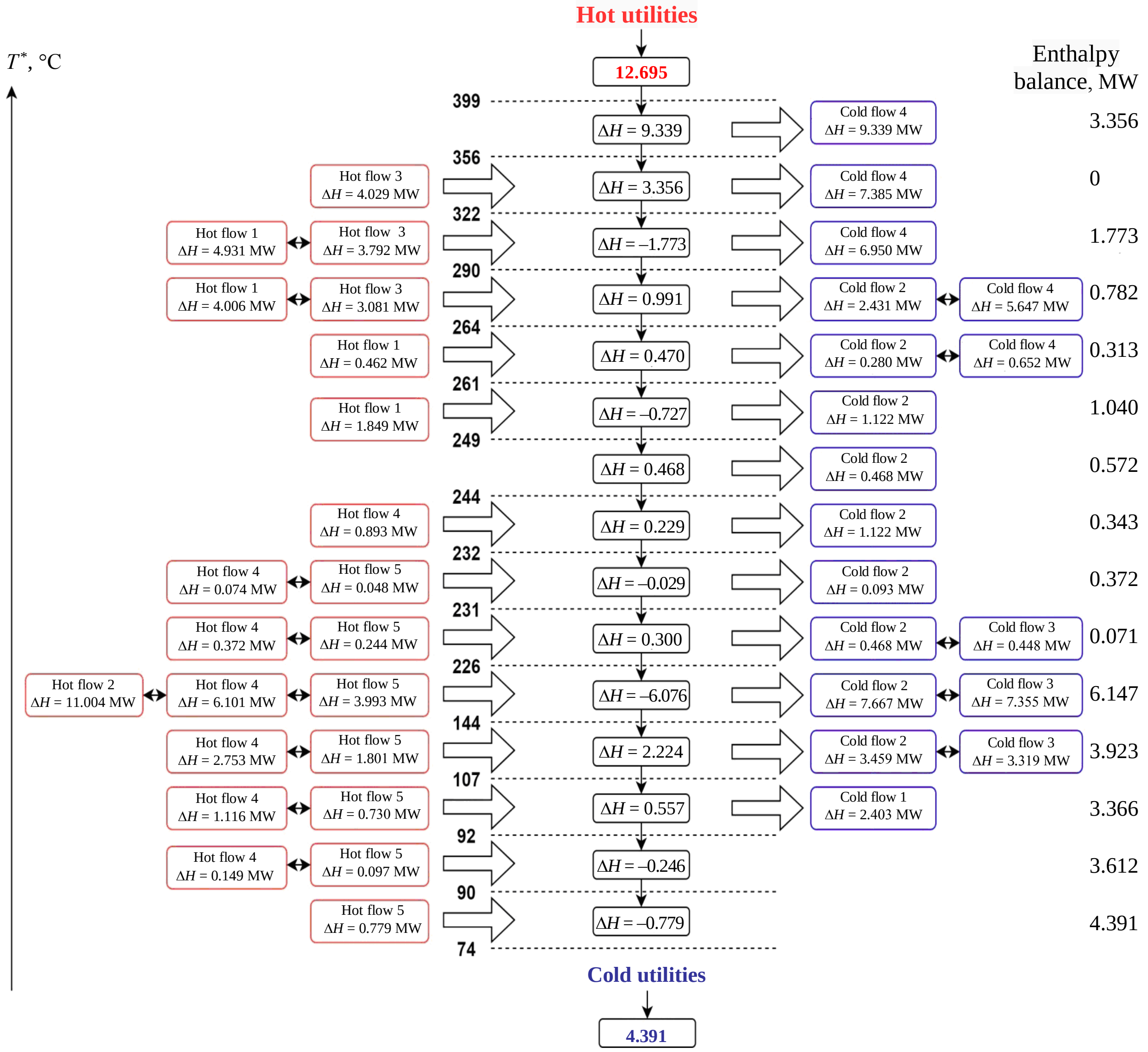


Fig.5. Thermal cascade of the heat exchange system of the fuel oil distillation unit
$T^*_{pinch}$ = 322 °C; $T^{hot}_{pinch}$ = 328 °C for hot flows; $T^{cold}_{pinch}$ = 326 °C for cold flows

flow curves makes it possible to visualize the relationship between hot and cold flows of a heat exchange system, i.e. this is necessary for a "conceptual understanding of the process". The heat transfer system is then analyzed using the third pinch analysis tool, the grand compound curve. This analysis will optimize the operation of the furnace, which is an external hot source.

The grand composite curve is built on the basis of the thermal cascade obtained earlier. It is a curve on the plane of shifted temperatures by $\Delta T_{min}/2$ and enthalpy. On the $x$-axis put down the value of the deficiency of thermal energy in a given temperature interval (Fig.6). Furnace efficiency before optimization was 80 %. To analyze the furnace, a graph of flue gas temperatures is plotted, which is an inclined straight line. The same graph shows a grand composite curve. The first point is the burning temperature ($T_{1furnace}$ = 2000 °C), the second point is the flue gas temperature.

In the unit for different heat exchangers – different value $\Delta T_{min}$. For the flows of the heat exchange system of the object of study, the shift in temperature intervals is defined and equal to 6 °C. For furnace flue gases, the shift will be equal to 25 °C. Then on recuperative flow heat exchangers $\Delta T_{min}$ = 12 °C, and on heat exchangers that transfer heat from flue gases to flows, $\Delta T_{min}$ = 6 + 25 = 31 °C.

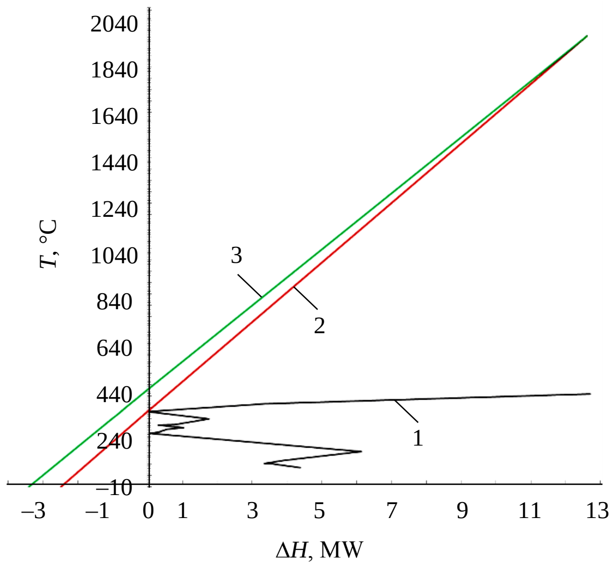


Fig.6. Grand compound curve and furnace flue gas profiles
1 – grand compound curve; 2 – flue gases N 1 $CP$ = 0.0076 MW/°C; 3 – flue gases N 2 $CP$ = 0.008 MW/°C

Since the ordinate shows shifted temperatures by $\Delta T/2$, the flue gas profile starts at temperature 2000 – 25 = 1975 °C. The slope of the straight line above the pinch is unrestricted. By changing the slope of the curve, fuel consumption is optimized. For comparison, Fig.6 shows two flue gas lines drawn from the starting point. Line graph N 1 passes through the pinch point, line graph N 2 passes through the maximum temperature of cold streams. After crossing the straight axis of ordinates, the heat of the flue gases is removed to the atmosphere, i.e. this is the loss of the furnace with flue gases.

It can be seen from the graph that flue gases N 1 for the furnace are more efficient: heat losses with exhaust gases are minimal and equal to 2.29 MW; flow heat capacity is minimal.

Actual flue gas temperature 322 + 25 = 347 °C, it is above the acid dew point, i.e. eliminates the possibility of formation of sulfuric acid, which adversely affects structural materials. Minimum hot utilities are $Q_{min}$ = 12.6 MW. Let us determine the optimal flow heat capacity of flue gases using the formula

$$CP_{\text{flue gases}} = \frac{Q_{H\min}}{T_2 - T_1} = \frac{12.69}{1975 - 322} = 0.0076 \text{ MW/°C}. \quad (3)$$

In the ideal case, the energy given up by the fuel $Q_{fuel}$, is equal to the energy that the flow gases gave up when cooled from the theoretical combustion temperature to the ambient temperature. Therefore, the formula is applied

$$Q_{\text{fuel}} = CP_{\text{flue gases}} \Delta T = 0.0076(2000 - 15) = 15 \text{ MW}. \quad (4)$$

The furnace efficiency is determined by the formula

$$\eta_{\text{furnace}} = \frac{Q_{H\min}}{Q_{\text{fuel}}} \cdot 100\,\% = \frac{12.69}{15} \cdot 100\,\% = 84\,\%. \quad (5)$$

**Discussion of the results.** Improving the energy efficiency of an oil refinery is an important and complex task. Pinch analysis allows you to analyze and optimize a large number of heat flows. Analysis and improvement of the energy efficiency of the objects of study were carried out by enthalpy pinch analysis.

Optimization measures are proposed:

• Change the final temperature of hot flow 2 from 176 to 150 °C, hot flow 4 from 150 to 96 °C, hot flow 5 from 175 to 80 °C. Thus, the enthalpy of hot flows increases and the costs for their cooling decrease.

• After parametric optimization, the values of the maximum heat recovery, the minimum values of external energy carriers were determined. In further studies, the structural optimization of the heat exchange system by pinch analysis will be carried out.

• The efficiency of the furnace can be increased by reducing heat loss with flue gases.

The technical characteristics of the furnace indicate that the flue gas temperature before optimization is 400 °C. Actual flow heat capacity of flue gases for heating cold flows 12.6 MW:

$$CP_{\text{flue gases}} = \frac{12.69}{1975 - 400} = 0.008 \text{ MW/°C}.$$

If take $Q_{\text{fuel}}$ for the ideal case:

$$Q_{\text{fuel}} = 0.008(2000 - 15) = 15.88 \text{ MW}.$$

The furnace efficiency before optimization is determined by the formula (5):

$$\eta_{\text{furnace}} = \frac{12.69}{15.88} \cdot 100\ \% = 80\ \%.$$

The calculated efficiency under design conditions is approximately the same. In this study, the furnace efficiency is increased by 4 %.

**Conclusion.** The existing heat exchange system of the fuel oil preheating unit was analyzed using enthalpy pinch analysis, the ways of optimization were determined. To reduce the heat load of the furnace, the additional flows were introduced into the heat exchange system of the fuel oil preheating unit.

The enthalpy pinch analysis of the fuel oil vacuum distillation unit and the parametric optimization of the new heat exchange system have been carried out. Hot and cold composite curves are plotted on the temperature-enthalpy plane. The minimum needs of the heat exchange system in external energy carriers are determined.

An enthalpy cascade at $\Delta T_{\text{min}} = 12$ °C is constructed, which confirms the correctness of pinch point determination and the values of external energy carriers determined by parametric optimization.

The heat exchange system is analyzed using a large compound curve. This step made it possible to optimize the operation of the fuel oil heating furnace. The search for the optimal flow heat capacity of the combustion products of the furnace is an important point in the analysis of the energy efficiency of the furnace. The optimal flow heat capacity is determined, at which heat losses with outgoing gases are minimal.

Measures are proposed to improve the efficiency of the fuel oil preheating unit. Heat recovery is maximized and external energy costs are minimized. By reducing heat loss with flue gases, it was possible to increase the efficiency of the furnace from 80 to 84 %. The results of the study can be used to improve the energy efficiency of existing and projected facilities of the oil refining industry.

*The authors are grateful to D.D.Tupikov for help in collecting information on the object of study and to Yu.V.Borisova for informational support.*

**REFERENCES**

1. Rudko V.A., Derkunskii I.O., Gabdulkhakov R.R. et al. Kinetics of various hydrocarbon groups formation in distillates obtained during the production of needle coke via the delayed coking of decantoil. *Egyptian Journal of Petroleum*. 2022. Vol. 31. Iss. 1, p. 33-38. DOI: 10.1016/j.ejpe.2022.02.002

2. König W., Löbbe S., Büttner S., Schneider C. Establishing Energy Efficiency – Drivers for Energy Efficiency in German Manufacturing Small- and Medium-Sized Enterprises. *Energies*. 2020. Vol. 13. Iss. 19. N 5144. DOI: 10.3390/en13195144

3. Muraveinikov S.S., Sulin A.B., Baranov I.V., Nikitin A.A. Average annual efficiency evaluation in the design of life support systems. *AIP Conference Proceedings*. 2019. Vol. 2141. Iss. 1. N 030019. DOI: 10.1063/1.5122069

4. Xinxiao Chen, Paprouschi A., Elveny M. et al. A laboratory approach to enhance oil recovery factor in a low permeable reservoir by active carbonated water injection. *Energy Reports*. 2021. Vol. 7, p. 3149-3155. DOI: 10.1016/j.egyr.2021.05.043

5. Pyagai I., Zubkova O., Babykin R. et al. Influence of Impurities on the Process of Obtaining Calcium Carbonate during the Processing of Phosphogypsum. *Materials*. 2022. Vol. 15. Iss. 12. N 4335. DOI: 10.3390/ma15124335

6. Tsvetkov O.B., Laptev Yu.A., Nikitin A.A. et al. Energy and environment options of working fluid alternative for different refrigeration configurations. IOP Conference Series: Materials Science and Engineering. 2020. Vol. 826. N 012017. DOI: 10.1088/1757-899X/826/1/012017

7. Kondrasheva N.K., Eremeeva A.M., Nelkenbaum K.S. et al. Development of environmentally friendly diesel fuel. *Petroleum Science and Technology*. 2019. Vol. 37. Iss. 12, p. 1478-1484. DOI: 10.1080/10916466.2019.1594285

8. Tcvetkov P. Climate Policy Imbalance in the Energy Sector: Time to Focus on the Value of $CO_2$ Utilization. *Energies*. 2021. Vol. 14. Iss. 2. N 411. DOI: 10.3390/en14020411

9. Kopteva A., Kalimullin L., Tcvetkov P., Soares A. Prospects and Obstacles for Green Hydrogen Production in Russia. *Energies*. 2021. Vol. 14. Iss. 3. N 718. DOI: 10.3390/en14030718

10. Malarev V., Kopteva A., Koptev V., Gotsul Yu. Improvement of Efficiency of Steam-Thermal Treatment of High-Viscous Oil Formations Using Downhole Electric Steam Generators. *Journal of Ecological Engineering*. 2021. Vol. 22. Iss. 2, p. 17-24. DOI: 10.12911/22998993/130630

11. Morenov V., Leusheva E., Buslaev G., Gudmestad O.T. System of Comprehensive Energy-Efficient Utilization of Associated Petroleum Gas with Reduced Carbon Footprint in the Field Conditions. *Energies*. 2020. Vol. 13. Iss. 18. N 4921. DOI: 10.3390/en13184921

12. Zhukovskiy Yu.L., Korolev N.A., Malkova Ya.M. Monitoring of grinding conditionin drum mills based on resulting shaft torque. *Journal of Mining Institute.* 2022. Vol. 256, p. 686-700. DOI: 10.31897/PMI.2022.91

13. Shabalov M.Yu., Zhukovskiy Yu.L., Buldysko A.D. et al. The influence of technological changes in energy efficiency on the infrastructure deterioration in the energy sector. *Energy Reports*. 2021. Vol. 7, p. 2664-2680. DOI: 10.1016/j.egyr.2021.05.001

14. Rogachev M.K., Nguyen Van T., Aleksandrov A.N. Technology for Preventing the Wax Deposit Formation in Gas-Lift Wells at Offshore Oil and Gas Fields in Vietnam. *Energies*. 2021. Vol. 14. Iss. 16. N 5016. DOI: 10.3390/en14165016

15. Resniova E., Ponomarenko T. Sustainable Development of the Energy Sector in a Country Deficient in Mineral Resources: The Case of the Republic of Moldova. *Sustainability*. 2021. Vol. 13. Iss. 6. N 3261. DOI: 10.3390/su13063261

16. Kumar R. A critical review on energy, exergy, exergoeconomic and economic (4-E) analysis of thermal power plants. *Engineering Science and Technology, an International Journal*. 2017. Vol. 20. Iss. 1, p. 283-292. DOI: 10.1016/j.jestch.2016.08.018

17. Sciubba E. Exergy-based ecological indicators: From Thermo-Economics to cumulative exergy consumption to Thermo-Ecological Cost and Extended Exergy Accounting. *Energy*. 2019. Vol. 168. P. 462-476. DOI: 10.1016/j.energy.2018.11.101

18. Aghbashlo M., Tabatabaei M., Hosseinpour S. On the exergoeconomic and exergoenvironmental evaluation and optimization of biodiesel synthesis from waste cooking oil (WCO) using a low power, high frequency ultrasonic reactor. *Energy Conversion and Management*. 2018. Vol. 164, p. 385-398. DOI: 10.1016/j.enconman.2018.02.086

19. Nami H., Mahmoudi S.M.S., Nemati A. Exergy, economic and environmental impact assessment and optimization of a novel cogeneration system including a gas turbine, a supercritical $CO_2$ and an organic Rankine cycle (GT-HRSG/$SCO_2$). *Applied Thermal Engineering*. 2017. Vol. 110, p. 1315-1330. DOI: 10.1016/j.applthermaleng.2016.08.197

20. Kondrasheva N.K., Rudko V.A., Nazarenko M.Yu., Gabdulkhakov R.R. Influence of parameters of delayed asphalt coking process on yield and quality of liquid and solid-phase products. *Journal of Mining Institute.* 2020. Vol. 241, p. 97-104. DOI:10.31897/PMI.2020.1.97

21. Hon Huin Chin, Varbanov P.S., Fengqi You et al. Plastic Circular Economy Framework using Hybrid Machine Learning and Pinch Analysis. *Resources, Conservation and Recycling*. 2022. Vol. 184. N 106387. DOI: 10.1016/j.resconrec.2022.106387

22. Smith R., Klemesh J., Tovazhnyansky L.L. et al. Basics of integration of thermal processes. Kharkov: NTU "KhPI", 2000, p. 458.

23. Ibrahim D., Jobson M., Jie Li, Guillén-Gosálbez G. Optimal design of flexible heat-integrated crude oil distillation units using surrogate models. *Chemical Engineering Research and Design*. 2021. Vol. 165, p. 280-297. DOI: 10.1016/j.cherd.2020.09.014

24. Ndunagu P.U., Alaike E.E., Megueptchie T. A Practical Approach to Energy Optimization Using Pinch Analysis: A Case Study of an Oil Refinery. SPE Nigeria Annual International Conference and Exhibition, 2-4 August 2021, Lagos, Nigeria. OnePetro, 2021. N SPE-207096-MS. DOI: 10.2118/207096-MS

25. Yong Zheng. Optimization of Chenzhuang Combined Station through Pinch Analysis. *Journal of Physics: Conference Series*. 2023. Vol. 2442. N 012036. DOI: 10.1088/1742-6596/2442/1/012036

26. Bayomie O.S., Abdelaziz O.Y., Gadalla M.A. Exceeding Pinch limits by process configuration of an existing modern crude oil distillation unit – A case study from refining industry. *Journal of Cleaner Production*. 2019. Vol. 231, p. 1050-1058. DOI: 10.1016/j.jclepro.2019.05.041

27. Kunru Yang, Shirun Liu, Chang He et al. Improving energy saving of crude oil distillation units with optimal operations. *Journal of Cleaner Production*. 2020. Vol. 263. N 121340. DOI: 10.1016/j.jclepro.2020.121340

28. Gadalla M.A. A new graphical method for Pinch Analysis applications: Heat exchanger network retrofit and energy integration. *Energy*. 2015. Vol. 81, p. 159-174. DOI: 10.1016/j.energy.2014.12.011

29. Alhajri I.H., Gadalla M.A., Abdelaziz O.Y., Ashour F.H. Retrofit of heat exchanger networks by graphical Pinch Analysis – A case study of a crude oil refinery in Kuwait. *Case Studies in Thermal Engineering*. 2021. Vol. 26. N 101030. DOI: 10.1016/j.csite.2021.101030

30. Dianliang Fu, Zeting Yu, Yanhua Lai. Linking pinch analysis and shifted temperature driving force plot for analysis and retrofit of heat exchanger network. *Journal of Cleaner Production*. 2021. Vol. 315. N 128235. DOI: 10.1016/j.jclepro.2021.128235

31. Mrayed S., Bin Shams M., Al-Khayyat M., Alnoaimi N. Application of pinch analysis to improve the heat integration efficiency in a crude distillation unit. *Cleaner Engineering and Technology*. 2021. Vol. 4. N 100168. DOI: 10.1016/j.clet.2021.100168

32. Konur O., Saatcioglu O.Y., Korkmaz S.A. et al. Heat exchanger network design of an organic Rankine cycle integrated waste heat recovery system of a marine vessel using pinch point analysis. *International Journal of Energy Research*. 2020. Vol. 44. Iss. 15, p. 12312-12328. DOI: 10.1002/er.5212

33. Qi Zhang, Jin Xu, Xiaoyu Zhao, Yujie Wang. Energy and exergy analyses of an integrated iron and steel making process. *International Journal of Exergy*. 2018. Vol. 26. N 4, p. 454-480. DOI: 10.1504/IJEX.2018.093190

34. Goodarzvand-Chegini F., GhasemiKafrudi E. Application of exergy analysis to improve the heat integration efficiency in a hydrocracking process. *Energy & Environment*. 2017. Vol. 28. Iss. 5-6, p. 564-579. DOI: 10.1177/0958305X17715767

35. Lebedev V.A., Yushkova E.A. Exergy pinch analysis of all elements of the boiler unit and the boiler unit as a whole. *Bulletin of the Tomsk Polytechnic University, Geo Assets Engineering.* 2020. Vol. 331. N 8, p. 92-98. DOI: 10.18799/24131830/2020/8/2771

***Authors*: Ekaterina A. Yushkova,** *Candidate of Engineering Sciences*, *Assistant Lecturer*, *atenoks@mail.ru*, *https://orcid.org/0000-0002-8492-0159* (*Saint Petersburg Mining University*, *Saint Petersburg*, *Russia*), **Vladimir A. Lebedev**, *Candidate of Engineering Sciences*, *Head of Department*, *https://orcid.org/0000-0003-0956-5772* (*Saint Petersburg Mining University*, *Saint Petersburg*, *Russia*).

*The authors declare no conflict of interests.*

ISSN 2411-3336; e-ISSN 2541-9404

JOURNAL OF MINING INSTITUTE

Zapiski Gornogo instituta

Journal homepage: pmi.spmi.ru

Research article

# The wireless charging system for mining electric locomotives

**Valery M. ZAVYALOV**[1], **Irina Yu. SEMYKINA**[2]✉, **Evgeniy A. DUBKOV**[1], **Amet-han S. VELILYAEV**[1]

[1] *Sevastopol State University, Sevastopol, Russia*

[2] *T.F.Gorbachev Kuzbass State Technical University, Kemerovo, Russia*

***How to cite this article***: Zavyalov V.M., Semykina I.Yu., Dubkov E.A., Velilyaev A.S. The wireless charging system for mining electric locomotives. Journal of Mining Institute. 2023. Vol. 261, p. 428-442. EDN JSNTAQ

***Abstract***. The electric vehicles development has a high potential for energy saving: an energy-saving traffic control can reduce energy resource consumption, and integration with the power grid provides the ability of daily load pattern adjustment. These features are also relevant for underground mining. The critical element of vehicle-to-grid integration is the charging infrastructure, where wireless charging is promising to develop. The implementation of such systems in underground mining is associated with energy efficiency issues and explosion safety. The article discusses the development and research of a wireless charging system for mining electric locomotive A-5.5-600-U5. The analytic hierarchy process is used for justification of the circuitry and design solution by a comparison of different technical solutions based on energy efficiency and safety criteria. A complex computer model of the wireless charging system has been developed that gives the transients in the electrical circuit of a wireless charging system and the high-frequency field density distribution near the transmitting and receiving coils in a 3D setting. An approach to ignition risk evaluation based on the analysis of high-frequency field density in the charging area between the coils of the wireless charging system is proposed. The approach using a complex computer model is applied to the developed system. The study showed that the wireless charging system for mining electric locomotives operating in the gaseous-and-dusty mine is technically feasible and there are designs in which it is explosion safe.

***Keywords***: mining electric locomotives; wireless charger; analytic hierarchy process; effectiveness; explosion safety; integrated computer model; field density

***Acknowledgment.*** The study was supported by the state assignment of Ministry of Science and Higher Education of the Russian Federation N 075-03-2021-138/3.

***Received: 14.03.2023*** ***Accepted: 20.06.2023*** ***Online: 19.07.2023*** ***Published: 19.07.2023***

**Introduction.** Energy saving and reduction of anthropogenic load on the environment is a global trend in the development of science and technology [1]. This research area includes the development of electric transport that has significant potential for energy saving. For instance, in China, where the fleet of electric vehicles accounts for more than 50 % of the world's total [2], replacing internal combustion engines with electric vehicles can reduce fossil fuel consumption by 50-60 % [3], which is estimated at 40.99 million tons of reference fuel savings by 2025 [4].

A prominent position in this area is occupied by the concept of integrating electric vehicles into the power grid known as V2G (vehicle-to-grid), which allows to reduce the peak demand for electricity and adjust the power consumption profile [5, 6]. The V2G concept consists of many components that provide energy saving, for example, electric vehicle traffic control systems [7], car battery monitoring systems [8], complex charging infrastructure, etc. [9]. Charging infrastructure is a key link between electric vehicles and the power grid and can be implemented using wired and wireless technologies [10].

Compared to wired ones, in addition to affecting energy efficiency wireless chargers, in addition to affecting energy efficiency, also contribute to increasing the autonomy of electric vehicles, since they do not require human participation in the charging of their batteries [11]. These advantages allow us to consider wireless charging systems for industrial electric vehicles operating in the conditions of increased danger to personnel. A similar industry is underground mining, for which unmanned technologies are actively developing. The study [12] describes the experience of introducing unmanned technologies at a Chinese underground mine, where diesel underground mining trucks were used to transport minerals, although at this time there is a trend in underground mining to switch from diesel transport to electric battery analogs [13]. Wireless charging is a promising solution for these tasks.

In Russia, at the underground mining enterprises, a common type of battery electric transport is electric locomotive haulage. Wireless charging for mining electric locomotives can reduce operating costs and the duration of the charging procedure since this technology phases out the prescribed safety requirements need to disconnect the battery and transfer it to the surface for charging in a specially equipped room [14]. The joining of the charging procedure with the technological operations of loading and unloading ensures a consistently high level of mining electric locomotive battery charge. As a result, wireless charging facilitates the automatic control systems operation for traction electric drives, supporting the required traction force with high accuracy, which can vary significantly depending on the track profile, the friction coefficient with the rails, and other factors [15].

An important detail of wireless chargers for the batteries of mining electric locomotives is their operating conditions since a significant part of underground mines in Russia is hazardous because of the explosive gaseous-and-dusty atmosphere. The studies [16, 17] assess factors affecting the increased risk of overheating at the wireless charger elements. The development of such a device for mining electric locomotives should include an assessment of explosion safety. The objective of this study is to scientifically substantiate the technical solution for the wireless charger for mining electric locomotives, which simultaneously provides high energy efficiency and explosion safety.

**Methods.** *The wireless charging principle and its main components*. The wireless charging (Fig.1, *a*) is based on the principle of inductive coupling and magnetic resonance coupling between a stationary transmitting coil and an onboard receiving coil installed on a mining electric locomotive (Fig.1, *b*) [18, 19]. The transmitting and receiving coils in combination with compensation capacitors are the resonant circuit compensation topology. The resonant circuit is supplied by a high-frequency inverter. The high-frequency magnetic field induces the electric field in receiving coil, and the receiving voltage is transmitted through a DC power converter to the battery. When the wireless charging system operates in resonant mode, wireless power transfer is highly efficient. In the power range from 5 to 100 kW, wireless chargers have a distance between the coils from 50 to 200 mm and an efficiency above 90 % [20]. The energy efficiency of wireless chargers is mostly determined by their circuitry, and their explosion safety mainly depends on design solutions.

On the mining electric locomotive, all the elements of the receiving circuit, excluding the receiving coil, are placed in the battery container, and the elements of the transmitter is placed in a special cabinet. This allows for explosion protection of the “flameproof enclosure” type for all elements of the system, except for coils, for which such placement will act as a screen preventing wireless power transfer [21]. The coils can be insulated or encapsulated with a compound for explosion protection. However, the charging area between them remains located in the explosive atmosphere, and therefore, the impact on the explosion safety of the electromagnetic field is subject to analysis.

*Justification of the circuitry and design solution.* Analysis of specific circuitry for the wireless charger under consideration can be performed using the analytic hierarchy process [22]. This method supposes to make paired comparisons for each of the possible circuit solutions with respect to all

*Journal of Mining Institute*. 2023. Vol. 261. P. 428-442 EDN JSNTAQ


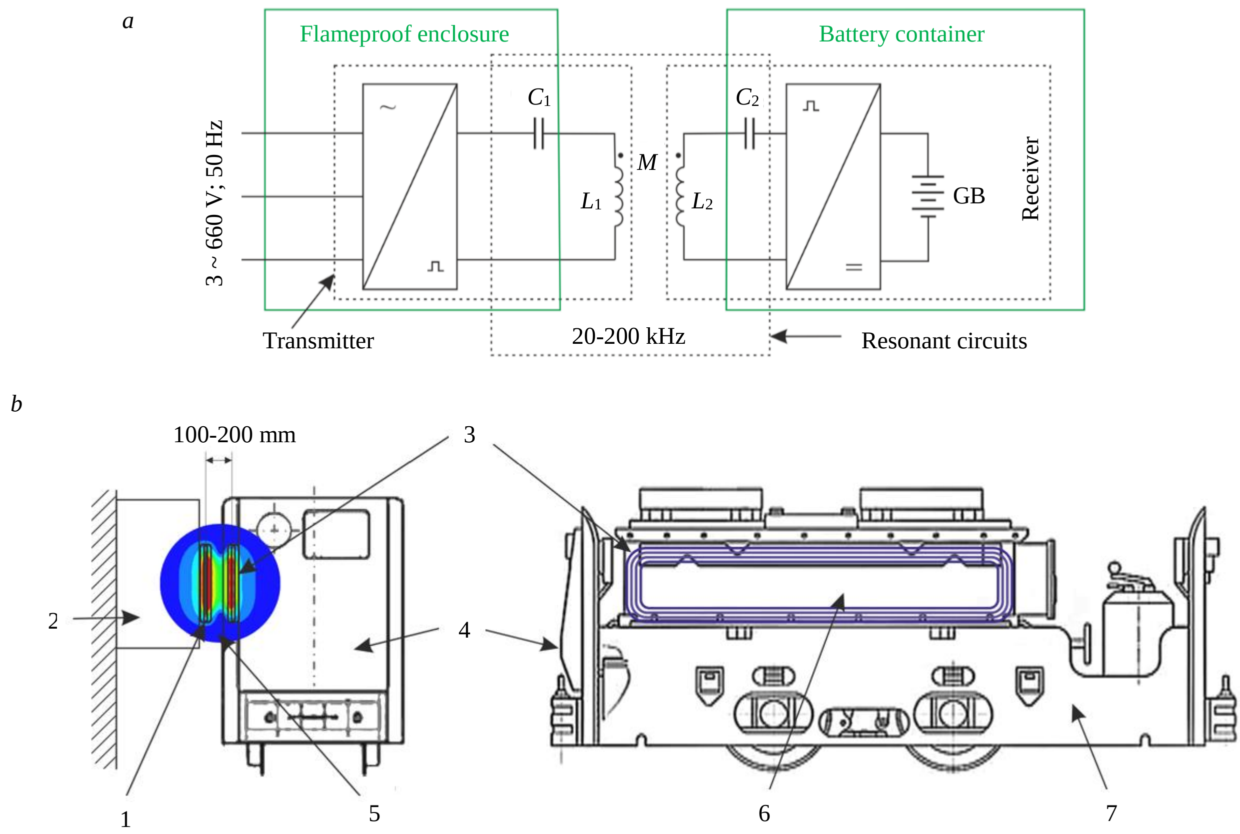


Fig.1. Wireless charging system for mining electric locomotive A-5.5-600-U5:
*a* – block diagram of the wireless charger; *b* – possible design

1 – transmitting coil; 2 – transmitter enclosure; 3 – receiving coil; 4 – mining electric locomotive;
5 – charging area; 6 – battery container; 7 – frame

decision criteria, then determine the local priorities of the decisions that show the weight of solutions with respect to each decision criterion, and finally determine the global priorities that indicate the final circuitry.

The following decision criteria were considered: surface temperature K1; electromagnetic radiation energy K2; transferred power K3; efficiency K4 [23]. The two-level hierarchy that describes the main components of the wireless charging system was considered as possible circuit solutions (Table 1).

*Table 1*

**Hierarchy of solutions**

| First level | | Second level | |
|---|---|---|---|
| Designation | Component of the wireless charging system | Designation | Circuit solutions |
| R1 | High-frequency inverter | R1.1 | Matrix converter |
| | | R1.2 | Current-source inverter |
| | | R1.3 | Voltage-source inverter |
| R2 | DC power converter | R2.1 | Diode-bridge rectifier |
| | | R2.2 | Active rectifier |
| | | R2.3 | Synchronous rectifier |
| R3 | Compensation topology | R3.1 | Series |
| | | R3.2 | Parallel |
| | | R3.3 | Hybrid |
| R4 | Coil type | R4.1 | Circular |
| | | R4.2 | Rectangular |
| | | R4.3 | Polarized |

For high-frequency inverters R1, there is a high variability of circuitry [24, 25]. They are divided into single-stage and dual-stage power converters. The first ones are matrix converters R1.1 and, as there is no intermediate DC link, they have smaller dimensions and higher total efficiency, but the second-order harmonic appears in the receiving circuit, and, consequently, in the battery charging current. Dual-stage converters, despite some loss in weight and overall dimensions, are much more common, since they are used in a wide range of electrical applications, are well debugged and, in addition, have a high potential for optimizing components and parameters, which can level out the difference in efficiency.

In the dual-stage converters, a current-source inverter R1.2 and a voltage-source inverter R1.3 can be employed. The current-source inverters are usually used for the resonant circuits with parallel compensation topology to mitigate current loading and overvoltages, as well as improve the harmonic content of the transmitting current. Compared to other inverter types, they have a lower current stress on all elements, which leads to lower losses in semiconductor switches. This effect is achieved by using a powerful inductor with large dimensions, so such inverters are inferior voltage-source inverters in terms of weight and overall dimensions.

The DC power converter R2 provides the battery charging current and can be a diode-bridge rectifier R2.1 or an active rectifier R2.2, or a synchronous rectifier 2.3. The diode-bridge rectifier is the most common due to its simplicity and minimal dimensions, however, in a wide load range due to its nonlinearity, it provokes a significant decrease in the coupling coefficient [26]. Diodes in the active rectifier are replaced by transistors, and due to the adjustable phase shift, this rectifier provides impedance matching but requires a relatively complex control system [27, 28]. An alternative to the active rectifier that also provides impedance matching is the synchronous rectifier, consisting of a diode bridge and a boost converter [29]. The active rectifier and the synchronous rectifier cannot operate without a closed-loop control system.

The compensation topology R3 of the resonant circuit differs in the placement of additional inductors and capacitors relative to the transmitting and receiving coils [30, 31]. The basic compensation topologies are series R3.1 and parallel R3.2. Series topology is usually used in conjunction with voltage sources. It has a higher power transfer coefficient and less sensitivity to misalignment between the transmitting and receiving coils [32]. Parallel topology is typically used with current sources and requires an additional series inductor, which makes the system more complex. This topology provides more impedance and is easier to control.

In addition to series and parallel, there are also hybrid topologies R3.3 that can have a parallel compensating capacitor in the transmitting circuit and a series one in the receiving circuit or the use of several compensating inductors and capacitors simultaneously in different connection options. They are used to reduce the misalignment sensitivity [33], to provide switching the battery charging mode from current charging to voltage charging [34], to reduce sensitivity to load changes [35], and in other specific tasks.

The coil type R4 for transmitting and receiving coils is fundamentally divided into non-polarized coils (circular R4.1 and rectangular R4.2), and polarized coils R4.3 (solenoid, flat bipolar coil, “double D”, etc.) [36, 37]. Circular ones provide the highest coupling coefficient and efficiency for a comparable active mass and coil area. Rectangular coils are somewhat inferior to circular, but they are better than polarized coils with respect to leakage flux in both vertical and lateral directions. Polarized ones are more resistant to misalignment of the coils compared to circular and rectangular coils.

Since it is difficult to quantify the described hierarchy of solutions, to compose paired comparison matrixes (PCM) the seventeen-digit Saaty scale* was used. In addition to the above characteristics of the particular circuit solutions, the design limitations were also taken into account. For example, if the compared solutions differ in size, given the volume limit of the flameproof enclosure it becomes necessary to reduce the power for the larger alternative. The PCMs for the first-level solutions R1-R4 relating to criterion K1 are composed, and the local priorities were found.

Let us consider in detail the PCM for the high-frequency inverter R1 relating to the surface temperature K1. Since the second-level solution R1.1 has smaller dimensions and higher efficiency, the heating losses are less, consequently, the surface temperature is lower than for R1.2 and R1.3. Solutions R1.2 and R1.3 were taken as equivalent. Thus,

$$C_{\mathrm{K1,R1}} = \begin{pmatrix} 1 & 2 & 2 \\ 1/2 & 1 & 1 \\ 1/2 & 1 & 1 \end{pmatrix} \begin{vmatrix} \mathrm{R1.1} \\ \mathrm{R1.2} \\ \mathrm{R1.3} \end{matrix}.$$

Arguing similarly, the PCMs for R2-R4 relating to K1 were obtained:

$$C_{\mathrm{K1,R2}} = \begin{pmatrix} 1 & 1/2 & 1/2 \\ 2 & 1 & 1 \\ 2 & 1 & 1 \end{pmatrix} \begin{vmatrix} \mathrm{R2.1} \\ \mathrm{R2.2} \\ \mathrm{R2.3} \end{matrix}; \; C_{\mathrm{K1,R3}} = \begin{pmatrix} 1 & 5 & 3 \\ 1/5 & 1 & 2 \\ 1/3 & 1/2 & 1 \end{pmatrix} \begin{vmatrix} \mathrm{R3.1} \\ \mathrm{R3.2} \\ \mathrm{R3.3} \end{matrix}; \; C_{\mathrm{K1,R4}} = \begin{pmatrix} 1 & 1 & 3 \\ 1 & 1 & 3 \\ 1/3 & 1/3 & 1 \end{pmatrix} \begin{vmatrix} \mathrm{R4.1} \\ \mathrm{R4.2} \\ \mathrm{R4.3} \end{matrix}.$$

All PCMs are highly aligned. The consistency indices $k_{\mathrm{CIK1R1}}$-$k_{\mathrm{CIK1R4}}$ and the consistency ratios $k_{\mathrm{CRK1R1}}$-$k_{\mathrm{CRK1R4}}$ for the given PCMs are:

$$k_{\mathrm{CIK1R1}} = 0 \le 0.1; \; k_{\mathrm{CIK1R2}} = 0 \le 0.1; k_{\mathrm{CIK1R3}} = 0.08 \le 0.1; k_{\mathrm{CIK1R4}} = 0 \le 0.1;$$

$$k_{\mathrm{CRK1R1}} = 0 \le 0.2; \; k_{\mathrm{CRK1R2}} = 0 \le 0.2; k_{\mathrm{CRK1R3}} = 0.14 \le 0.2; k_{\mathrm{CRK1R4}} = 0 \le 0.2,$$

which indicates the correctness of the assessment made.

The general solution R comprises a combination of one second-level solution from each of the first-level solutions R1-R4. Taking that the paired comparison is the ratio of the weights for the considered solutions relating to a particular criterion, and the weight of the combinational solution is determined by the product of the weights of its constituents, the PCM for the general solution R is defined as the Kronecker product of the PCMs for R1, R2, R3, and R4:

$$C_{\mathrm{K1,R}} = C_{\mathrm{K1,R1}} \otimes C_{\mathrm{K1,R2}} \otimes C_{\mathrm{K1,R3}} \otimes C_{\mathrm{K1,R4}}.$$

For clarity, let us expand the Kronecker product for the last two factors, which demonstrates the increase in the dimension of matrices:

$$C_{\mathrm{K1,R3}} \otimes C_{\mathrm{K1,R4}} = \left( C_{\mathrm{K1,R3}_{(i,j)}} C_{\mathrm{K1,R4}} \right) = \left( C_{\mathrm{K1,R3}_{(i,j)}} \begin{pmatrix} C_{\mathrm{K1,R4}_{(1,1)}} & C_{\mathrm{K1,R4}_{(1,2)}} & C_{\mathrm{K1,R4}_{(1,3)}} \\ C_{\mathrm{K1,R4}_{(2,1)}} & C_{\mathrm{K1,R4}_{(2,2)}} & C_{\mathrm{K1,R4}_{(2,3)}} \\ C_{\mathrm{K1,R4}_{(3,1)}} & C_{\mathrm{K1,R4}_{(3,2)}} & C_{\mathrm{K1,R4}_{(3,3)}} \end{pmatrix} \right),$$

and therefore $C_{\mathrm{K1,R}}$ is an 81×81 matrix.

It should be taken that not all the second-level solutions are compatible. For example, it is inefficient to combine the current-source inverter R1.2 with the series compensation topology R3.1. This means that the hierarchy is not complete, and therefore the assessment of unrealizable combinations and their reciprocals should be replaced by zero. Further, from the obtained PCM, the local priorities vector was calculated

* Saaty T. Decision making. Analytic hierarchy process. Moscow: Radio and communication, 1993. 278 p.

$$V_{K1,R} = \left(V_{K1,R_{(i)}}\right) = \frac{\sqrt[n]{\prod_{j=1}^{n} C_{K1,R_{(i,j)}}}}{\sum_{k=1}^{n}\sqrt[n]{\prod_{j=1}^{n} C_{K1,R_{(k,j)}}}},$$

where $n = 81$.

Similarly, the PCMs $C_{K2,R}$-$C_{K4,R}$ for general solutions R relating to each criterion K2-K4 were sequentially obtained. Further, based on these PCMs, the local priorities vectors $V_{K2,R}$-$V_{K4,R}$ were calculated. By combining $V_{K1,R}$-$V_{K4,R}$, a general local priorities vector $V_R$ was obtained from which the global priorities vector was determined:

$$G_R = V_R V_K = \left(V_{K1,R}, V_{K2,R}, V_{K3,R}, V_{K4,R}\right) V_K,$$

where $V_K$ was taken equal to [23]

$$V_K = (0.133;\quad 0.147;\quad 0.125;\quad 0.127)^T.$$

The global priority is the solution where the value of $G_{R(i)}$ is maximum. The obtained global priorities vector has the maximum at the solution $R_{(56)} = R1.3 \cup R2.1 \cup R3.1 \cup R4.2$ with $G_{R(56)} = 0.102$.

The electrical circuit for this solution is shown in Fig.2. Let us determine the parameters of the circuit elements for the mining electric locomotive A-5.5-600-U5 that is equipped with a lithium-ion battery LIAB-70 TRV-BK. This battery has a nominal voltage of 130 V and a maximum charging current of 270 A. To ensure the system reliability, the nominal charging current was assumed to be 260 A, because short-term in-rush currents are possible. Thus, the equivalent load resistance $R_{load}$ is equal to 0.5 Ohm.

The parameters of the transmitting and receiving coils were determined based on a given design (according to P.L.Kalantarov and L.A.Tsejtlin). The coils have the same design, which means coil inductances are equal $L_1 = L_2 = L$ and their internal resistances are equal $R_1 = R_2 = R$ too. The receiving coil dimensions are 3000×700 mm as the coil is limited by the external surface of the battery container at the electric locomotive. The coil-to-coil distance was assumed to be 100 mm, which sufficiently guarantees a gap between the transmitter when the electric locomotive is moving, on the one hand, but on the other hand, it provides a high enough coupling coefficient. Then the inductances of the transmitting and receiving coils are determined as follows:

$$L = \frac{1}{\pi}\mu_0 w^2 (b+c)\left[\ln\frac{2bc}{r} - \frac{c}{b+c}\ln\left(c+\sqrt{b^2+c^2}\right) - \frac{b}{b+c}\ln\left(b+\sqrt{b^2+c^2}\right) + \frac{2\sqrt{b^2+c^2}}{b+c} - \frac{1}{2} + 0.447\frac{r}{c+b}\right],$$

where $\mu_0$ is the vacuum magnetic permeability; $w$ is the number of turns; $b$ and $c$ are the length and width of the coil outer boundary; $r$ is the width of the winding pitch, which was taken equal to 15 mm. Mutual inductance $M$ is calculated as

$$M = w^2\frac{\mu_0}{\pi}\left[c\ln\left(\frac{c+\sqrt{c^2+x^2}}{c+\sqrt{c^2+b^2+x^2}}\frac{\sqrt{b^2+x^2}}{x}\right) + b\ln\left(\frac{b+\sqrt{b^2+x^2}}{b+\sqrt{c^2+b^2ex^2}}\frac{\sqrt{c^2+x^2}}{x}\right) +\right.$$

$$\left. +2\left(\sqrt{c^2+b^2+x^2} - \left(\sqrt{c^2+x^2} - \sqrt{b^2+x^2} + x\right)\right)\right],$$

where $x$ is the coil-to-coil distance.

Internal resistances are determined as

$$R = w\rho_m\frac{2(b+c)-2rw}{S},$$

 

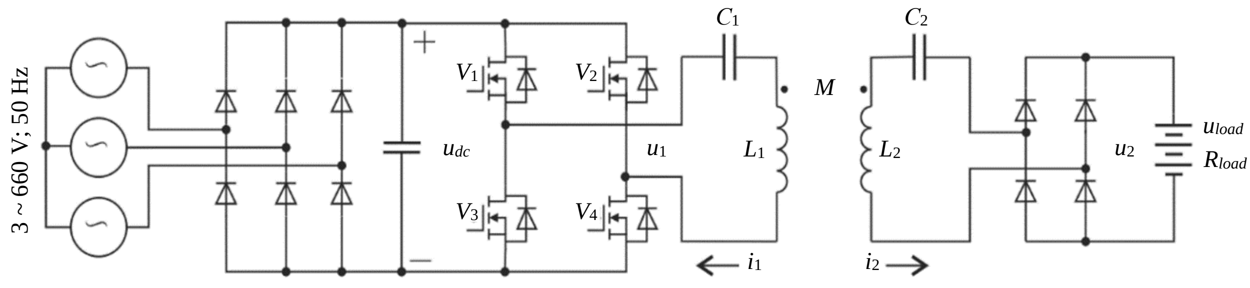


Fig.2. The electrical circuit of the wireless charger

where $S$ is the cross-section of the winding wire; $\rho_m$ is its resistivity. The high-voltage high-frequency wire "LELOR-E" with a nominal cross-section of 50 mm$^2$ and a maximum diameter of 15 mm was chosen as the winding wire.

The parameters of the coils and the load at a given resonant frequency determine the capacitance of the compensation topology capacitors. Owing to the resonant circuit symmetry, the capacitances of the transmitting and receiving circuit capacitors are also considered equal, i.e. $C_1 = C_2 = C$. It is difficult to determine an analytical expression for $C$, since the equation describing the resonant frequency $f_r$ for the wireless charger shown in Fig.2 has a high dimension. Therefore, the capacitance $C$ was determined by numerical methods using a specially written computer program. The resonant frequency was selected according to the recommendations of the SAE J2954 standard, and $f_r$ = 90 kHz.

The design values of the wireless charger electrical parameters are given in Table 2 for a different number of turns. The efficiency design value for the wireless charging system was obtained as the possible maximum over the entire operating frequency range. It does not consider switching and conductive losses in semiconductor switches as well as dielectric losses in capacitors. The efficiency was used only to compare the different designs for one device. The data obtained show that the highest efficiency of the wireless charger is provided for $w$ = 1, and such a design is the simplest. Therefore, the transmitting and receiving coils with the number of turns of 1 were accepted for further consideration. The resulting circuitry and design solution is the basis to analyze the impact on the explosion safety of the electromagnetic field in the charging area of the wireless charger in an explosive gas-and-dust atmosphere.

*Table 2*

**The design values of the wireless charger electrical parameters**

| $w$, u | $L$, μH | $M$, μH | $R$, Ohm | $C$, μF | η | $i_2/u_1$, A/V |
|---|---|---|---|---|---|---|
| 1 | 16.6 | 2.7 | 0.003 | 0.162 | 0.994 | From 0.606 to 2 |
| 2 | 43.7 | 10.5 | 0.006 | 0.058 | 0.988 | From 0.15 to 1.96 |
| 3 | 78.7 | 23.2 | 0.009 | 0.031 | 0.983 | From 0.07 to 1.93 |

*Determining the conditions for the safe operation.* Given the flameproof enclosures for all the components of the wireless charger except the transmitting and receiving coils, the only potential ignition source is the charging area between the coils. Simulation of temperature distribution shows that under normal operation, the high-frequency alternating magnetic field is not a heat source, and the heating of the explosive atmosphere in the charging area occurs mainly due to the laws of heat-and-mass transfer from ohmic losses in winding wires [38, 39]. But the situation fundamentally changes if there is a foreign metal object between the coils as in this object the eddy currents are induced. Since the specific heat capacity of metals is generally low, the heating losses from the eddy currents can significantly increase the surface temperature.

To evaluate the ignition risk from the foreign metal object heating, it was assumed that in the metal object with the limited volume, the heating power from eddy currents cannot exceed the power of the inducing magnetic field. Given that the high-frequency alternating magnetic field at each point of the charging area changes sinusoidally with an angular frequency ω, and the magnetic induction distributes over the metal object volume $V$ is uniform, the power of the magnetic field converting into heating power is determined as follows

$$P_m = \frac{\omega B_{\max}^2 V}{\mu_0 \mu}, \tag{1}$$

where μ is the magnetic permeability; $B_{\max}$ is the magnetic induction amplitude.

The temperature to which the foreign metal object will be heated is determined by thermal equilibrium. Assuming that the thermal field potential is uniformly distributed over the metal object volume, and the heat is transferred due to natural convection, the temperature exceedance over the ambient temperature is determined as (according to S.S.Kutateladze, V.M.Borishanskiy)

$$\tau = \frac{P_m}{\alpha}, \tag{2}$$

where α is thermal diffusivity, depending on the shape and size of the heated metal object, as well as the product of the Prandtl number Pr and the Grashof number Gr.

The temperature exceedance τ was determined based on GOST 31610.0-2019 standard. It precepts that for equipment of group I, i.e. for equipment in explosive atmospheres of underground mines, the maximum surface, on which coal dust is unlikely to be deposited in the form of a layer, the temperature should be no higher than 450 °C, and the ambient temperature is taken equal to 40 °C.

Analyzing (1) and (2) together, we determine the limiting value of the magnetic induction amplitude as:

$$\begin{cases} B_{\max} = \sqrt{\dfrac{\mu_0 \mu \tau}{\omega l^3} A_1 \sqrt[8]{\dfrac{\tau}{l^5}}} \text{ if } l \le 2.574 \text{ mm}; \\ B_{\max} = \sqrt{\dfrac{\mu_0 \mu \tau}{\omega l^3} A_2 \sqrt[4]{\dfrac{\tau}{l}}} \text{ if } 2.574 < l < 88.044 \text{ mm}; \\ B_{\max} = \sqrt{\dfrac{\mu_0 \mu \tau}{\omega l^3} A_3 \sqrt[3]{\tau}} \text{ if } l \ge 88.044 \text{ mm}, \end{cases}$$

where $A_1$, $A_2$, $A_3$ are coefficients depending on air temperature; $l$ is the length of the cube edge.

If the magnetic induction is lower than $B_{\max}$, the maximum possible surface temperature of the foreign metal object heated by the eddy currents does not exceed 450 °C with a guarantee.

The dependence of $B_{\max}$ on $l$ for the conditions under consideration is shown in Fig.3. Considering that the distance $x$ was assumed to be 100 mm, the length of the cube edge of the foreign metal object cannot exceed this value. Consequently, the magnetic induction amplitude of the wireless charger at any point in the charging area should not exceed

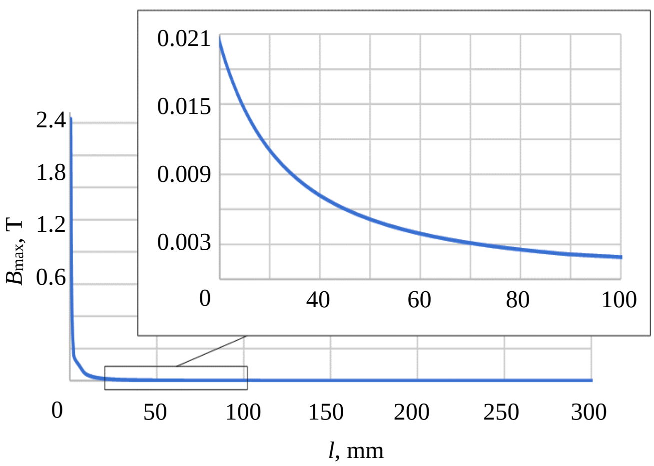


Fig.3. The limiting value of the magnetic induction amplitude

1.929 mT. It is possible to determine whether this condition is met for the wireless charging system under consideration using computer simulation.

*Complex computer model*. Computer simulation of the wireless charger under consideration can determine the magnetic induction of the magnetic field at the charging area in a 3D formulation, taking into account the physical properties of the transmitting and receiving coils' materials and the environment. Using a finite element model in combination with a dynamic model of the wireless charger electrical circuit describes the transients in the system, including changes in the electromagnetic radiation energy. Such a complex computer model was implemented employing the MatLab Simulink and Altair Flux.

The MatLab Simulink model of the wireless charger has the following assumptions: the rectifier in the dual-stage voltage-source inverter is ideal, and the DC link voltage is constant; semiconductor switches of the inverter and the rectifier are idealized and do not describe their switching losses and conductive losses; the compensation topology capacitors are idealized and do not describe their dielectric losses. The model is made using the SimPowerSystems library which ensures a high level of its adequacy since the elements of this library have been widely tested (Fig.4).

The Altair Flux model of the transmitting and receiving coils and the charging area is based on a 3D drawing consisting of two elements shaped as curved cylinders with a cross-section of 50 mm$^2$ which are rectangular in plan with dimensions of 3000×700 mm, placed at the distance of 100 mm between the cylinders axes with no misalignment. In the simulation, a dynamic mesh was used with automatic selection of finite elements size, providing an error of no more than $1 \cdot 10^{-6}$ T at each calculation step.

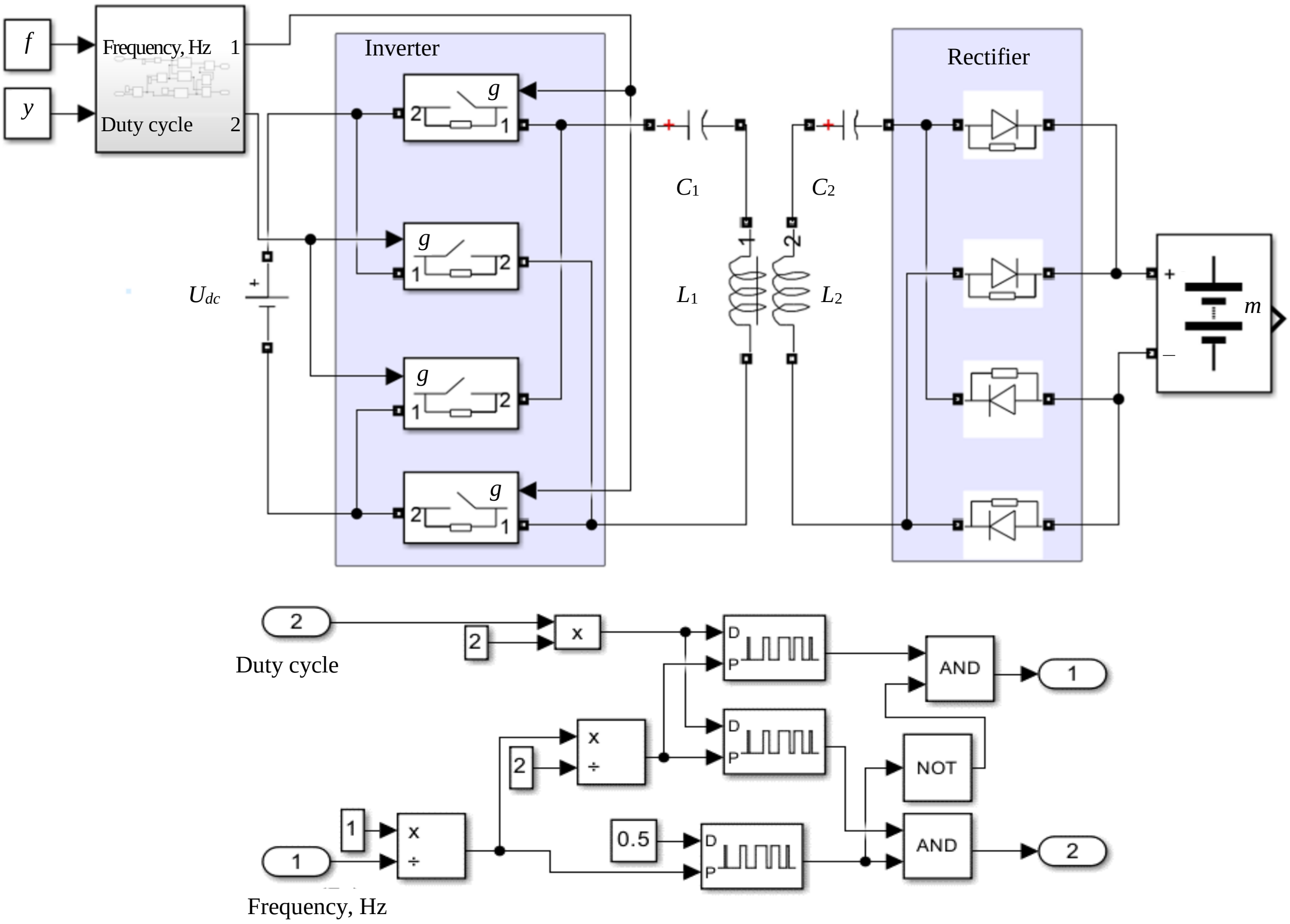


Fig.4. The MatLab Simulink model of the wireless charger

EDN JSNTAQ
**Journal of Mining Institute.** 2023. Vol. 261. P. 428-442


**Results and discussion.** *Prototype test.* To demonstrate the feasibility of the wireless charger with the described design and to confirm the adequacy of the computer model used, the electric locomotive prototype was made on a scale of 1:10, equipped with the wireless charging system having the following parameters: $L_1 = L_2 = 100$ μH; $M = 10$ μH; $R_1 = R_2 = 0.01$ Ohm; $C_1 = C_2 = 33$ nF; $R_{load} = 6$ Ohm (Fig.5). The high-frequency inverter is built on IRFP90N20DPBF transistors with the nominal voltage of 200 V and the nominal current of 94 A, and the DC power converter is based on Schottky diodes of VS-80CPQ150-N3 with the nominal current of 40 A and the nominal voltage of 150 V. The Delta Elektronika SM330-AR-22 DC power supply with a power of 3300 W was used as a power source. A Fluke TiS20 thermal imager and a DS1074Z-S oscilloscope were used as measuring equipment for the prototype test.

The prototype test was carried out at a power supply voltage of 24 V, an operating frequency of 91 kHz, and a duty cycle of 0.28. During the tests, voltages $u_{L1}$, $u_{C1}$, and $u_{L2}$, $u_{C2}$ were measured on the coils and the capacitors of the transmitting and receiving circuits respectively. The same parameters for the same conditions were simulated using MatLab Simulink. The obtained results are shown in Fig.6.

The thermogram demonstrates the operation of the wireless charging system, and it is an indirect tool showing the magnetic field distribution between the coils (Fig.6, *a*). The heating source at the charging area is the heating losses in the coils' wire caused by flowing currents as the central region of the coils has a significantly lower temperature.

The oscillograms show the measured voltages, where the division values are 100 V on the voltage scale and 2 μs on the time scale (Fig.6, *b*, *d*, *f*). The corresponding voltages obtained by simulation are shown in Fig.6, *c*, *e*, *g*. Comparison of the simulation and experiment results indicates that, except for micro transients, when semiconductor switches activate, there is a quantitative and qualitative correspondence of the considered voltages in both the amplitude and the phase. The maximum discrepancy between the simulation and experiment results is 3.28 % which indicates a high adequacy of the computer model (see Fig.4). This result justifies using the above-described complex computer model to analyze the explosion safety of the wireless charging system for the mining electric locomotive A-5.5-600-U5.

*Simulation results.* The complex computer model gives the high-frequency field density distribution in the charging area of the wireless charging system for mining electric locomotive A-5.5-600-U5. The simulation was carried out in two stages. In the first stage, the transients were simulated, including the current of the transmitting and receiving coils that were subsequently used in the second stage as the input data for the magnetic field simulation.

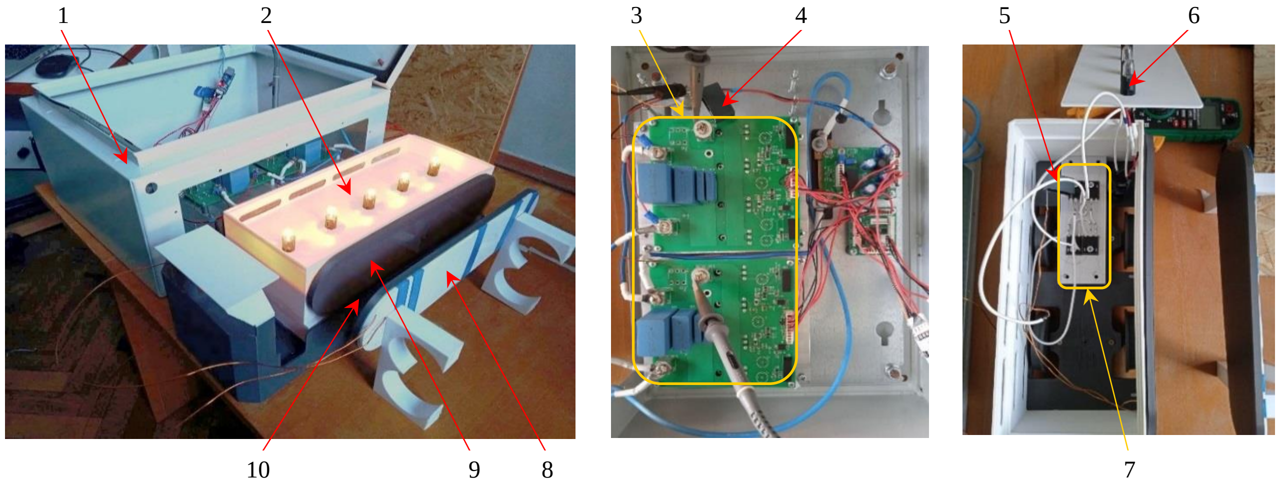


Fig.5. The electric locomotive prototype equipped with the wireless charging system

1 – transmitter; 2 – electric locomotive prototype; 3 – high-frequency inverter; 4 – transmitting circuit capacitor; 5 – receiving circuit capacitor; 6 – load; 7 – DC power converter; 8 – transmitting coil; 9 – receiving coil; 10 – charging area

*a*


Fig.6. The prototype test results:
*a* – thermogram;
*b* – experiment $u_{L_1}$, $u_{C_1}$;
*c* – simulation $u_{L_1}$, $u_{C_1}$;
*d* – experiment $u_{L_2}$, $u_{C_2}$;
*e* – simulation $u_{L_2}$, $u_{C_2}$;
*f* – experiment $u_{C_1}$, $u_{C_2}$;
*g* – simulation $u_{C_1}$, $u_{C_2}$

*b*

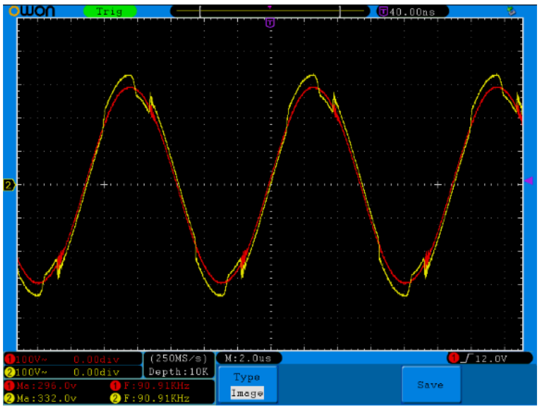

*c*

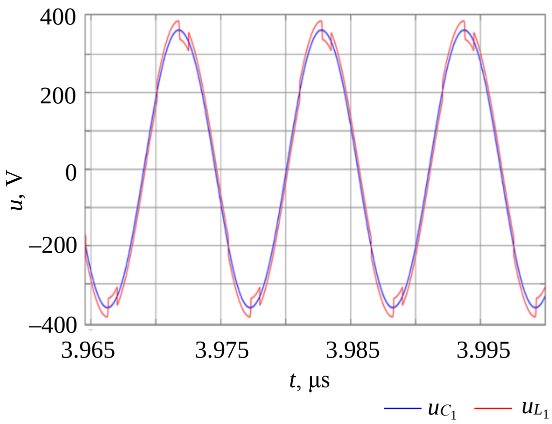


*d*

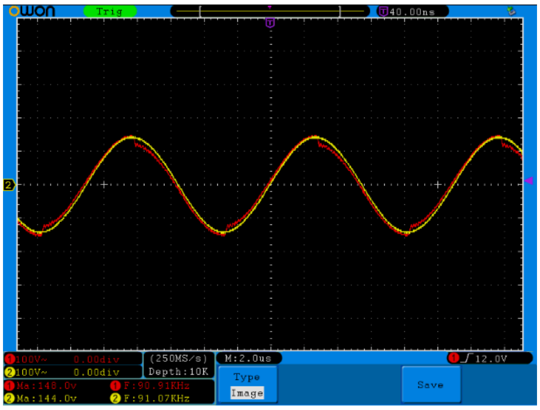

*e*

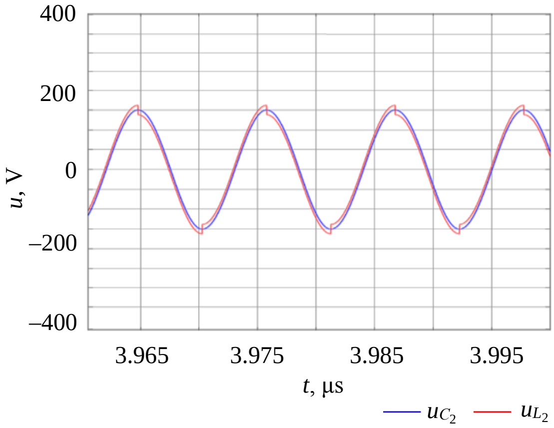


*f*

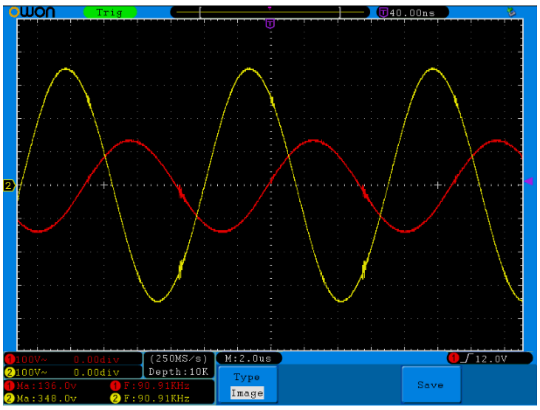

*g*

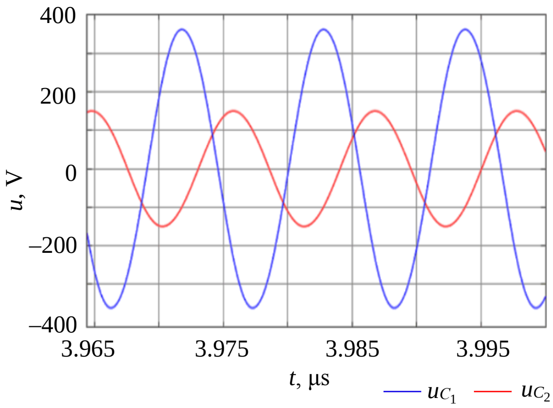

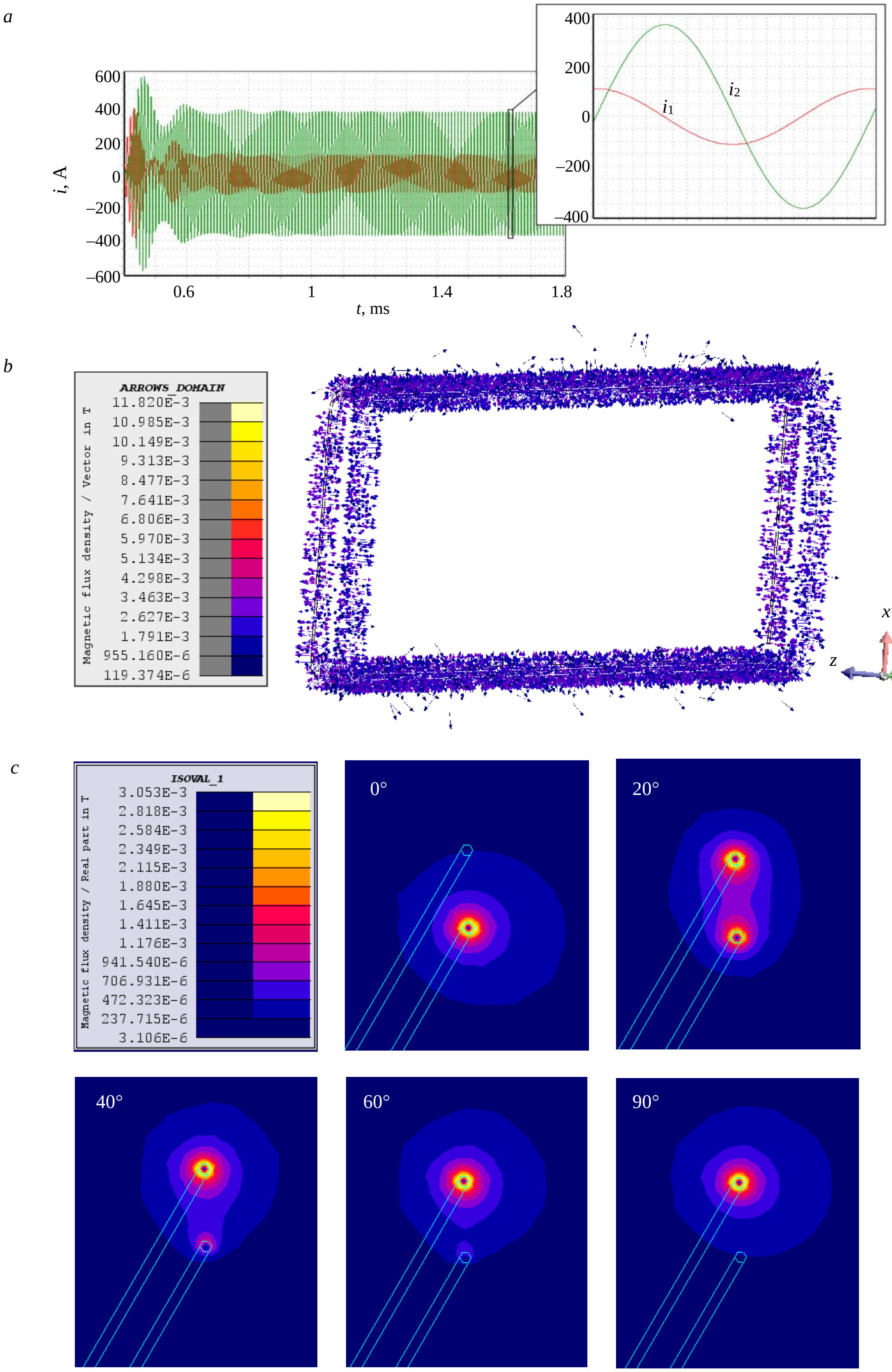


Fig.7. Simulation results: *a* – transients of $i_1$ and $i_2$; *b* – the field of the magnetic induction distribution vectors for a phase value of 20°; *c* – distribution of magnetic induction in the winding wire vicinity for phase values of 0, 20, 40, 60 and 90°

When working with the model in MatLab Simulink, the operating frequency and duty cycle were set at the input of the system. It should be noted that when the wireless charger parameters were calculated the resonant frequency was set at 90 kHz. Hence, the receiving current $i_2$ has the maximum at this frequency, where in case the resonant circuit input voltage $u_1$ is constant, the current transfer coefficient $i_2/u_1 = 2$ A/V. The efficiency of wireless power transfer at this frequency is 0.988, while the theoretical maximum is 0.994. Therefore, it is advisable to set the operating frequency differing from the resonant one to find a balance between striving for maximum efficiency and providing the required charging current.

In the case under consideration, the charging current is 260 A, so the current amplitude of $i_2$ is 368 A. The theoretical minimum of the current transfer coefficient $i_2/u_1 = 0.606$ A/V, hence the voltage amplitude of $u_1$ should be no lower than 607 V. As the effective phase to neutral voltage of three-phase mains is 660 V, the DC link voltage is 891 V, and the required charging current can be provided at any operating frequency. Based on this, the operating frequency was set at 97.1 kHz where the efficiency has the maximum. The duty cycle that provides the resonant circuit input voltage of 607 V is 0.68.

The currents $i_1$ and $i_2$ obtained from the MatLab Simulink model for the described conditions are shown in Fig.7, *a*. The amplitudes of these currents, as well as the phase shift between them, were used as the input data for the Altair Flux model that determines the magnetic induction distribution vectors in the charging area during the period of current change. The simulation results of the magnetic field distribution in the charging area are shown in Fig.7, *b*, *c*. They show that the induction of the high-frequency magnetic field outside the winding wire vicinity of the transmitting and receiving coils is negligible and is equal to zero in the center of the 3000×700 rectangle. This indicates fairly high electromagnetic compatibility and safety for people according to the criteria of SanPiN 1.2.3685-21 sanitary norms.

Analyzing the magnetic field in the winding wire vicinity, it was found that the maximum magnetic induction amplitude outside the winding wire is 3.548 mT, whereas as early as the distance of 18 mm, the magnetic induction amplitude does not exceed 1.929 mT. Since it was initially supposed to use encapsulation as the coils' protection, with an insulation layer of 20 mm thick, the ignition risk could be neglected for any metal object between the transmitting and receiving coils. As an additional measure, the charging current reduction can be used. It proportionally slows down the charging process of the mining electric locomotive battery but increases the system reliability against explosion.

**Conclusion.** The study showed that the wireless charging system for mining electric locomotives operating in the gaseous-and-dusty mine is technically feasible and there are such designs and operation modes in which it is explosion safe. The obtained circuitry and design solutions provide the basis for developing the detailed engineering drawings and a set of technological documentation necessary for the manufacture of a prototype wireless charging system and its subsequent submission to the certification authority for proof-of-compliance tests according to the requirements of the Customs Union technical regulation TR CU 012/2011.

The implementation of the considered wireless charging system for mining electric locomotives and other similar mine transports can increase mining efficiency by reducing operating costs that are caused by the need to turn off the batteries and charge them outside the hazardous area. In the case of the implementation of integrating the wireless chargers with the power grid on large mine transport systems, the wireless chargers can be used to adjust the load, ensuring an increase in the energy efficiency of the entire enterprise.

Further study of the wireless charging system under consideration includes modernization of its dynamic model so that switching losses and conduction losses in semiconductor switches as well as dielectric losses in the compensation topology capacitors are taken into account. It allows us to evaluate not just the efficiency of wireless power transfer but the efficiency of the entire wireless charger.

It is advisable to analyze the high-frequency field density distribution near the transmitting and receiving coils in the conditions of their misalignment, such as coil-to-coil distance deviations, as well as horizontal and angular misalignment. Additionally, as a development of the system, it is possible to optimize its parameters, as well as to introduce a closed control system.

**REFERENCES**


1. Weilong Wang, Xiaodong Yang, Jianhong Cao et al. Energy internet, digital economy, and green economic growth: Evidence from China. *Innovation and Green Development*. 2022. Vol. 1. Iss. 2. N 100011. DOI: 10.1016/j.igd.2022.100011

2. Jie Xiong, Shuyan Zhao, Yan Meng et al. How latecomers catch up to build an energy-saving industry: The case of the Chinese electric vehicle industry 1995-2018. *Energy Policy*. 2022. Vol. 161. N 112725. DOI: 10.1016/j.enpol.2021.112725

3. Zhifeng Que, Shixue Wang, Weiyi Li. Potential of energy saving and emission reduction of battery electric vehicles with two type of drivetrains in China. *Energy Procedia*. 2015. Vol. 75, p. 2892-2897. DOI: 10.1016/j.egypro.2015.07.584

4. Hong-Mei Deng, Yun-Peng Zhang, Jing Li et al. Research on energy saving potential and countermeasures in China's transport sector. *Energy Reports*. 2022. Vol. 8. S. 6, p. 300-311. DOI: 10.1016/j.egyr.2022.03.098

5. Bibak B., Tekiner-Mogulkoc H. Influences of vehicle to grid (V2G) on power grid: An analysis by considering associated stochastic parameters explicitly. *Sustainable Energy, Grids and Networks*. 2021. Vol. 26. N 100429. DOI: 10.1016/j.segan.2020.100429

6. Gough R., Dickerson C., Rowley P., Walsh C. Vehicle-to-grid feasibility: A techno-economic analysis of EV-based energy storage. *Applied Energy*. 2017. Vol. 192, p. 12-23. DOI: 10.1016/j.apenergy.2017.01.102

7. Laiqing Xie, Yugong Luo, Donghao Zhang et al. Intelligent energy-saving control strategy for electric vehicle based on preceding vehicle movement. *Mechanical Systems and Signal Processing*. 2019. Vol. 130, p. 484-501. DOI: 10.1016/j.ymssp.2019.05.027

8. Augello A., Gallo P., Sanseverino E.R. et al. Certifying battery usage for V2G and second life with a blockchain-based framework. *Computer Networks*. 2023. Vol. 222. N 109558. DOI: 10.1016/j.comnet.2023.109558

9. Mastoi M.S., Shenxian Zhuang, Munir H.M. et al. An in-depth analysis of electric vehicle charging station infrastructure, policy implications, and future trends. *Energy Reports*. 2022. Vol. 8, p. 11504-11529. DOI: 10.1016/j.egyr.2022.09.011

10. Mohammed S.A.Q., Jin-Woo Jung. A Comprehensive State-of-the-Art Review of Wired/Wireless Charging Technologies for Battery Electric Vehicles: Classification/Common Topologies/Future Research Issues. *IEEE Access*. 2021. Vol. 9, p. 19572-19585. DOI: 10.1109/ACCESS.2021.3055027

11. Cirimele V., Diana M., Freschi F., Mitolo M. Inductive power transfer for automotive applications: state-of-the-art and future trends. *IEEE Transactions on Industry Applications*. 2018. Vol. 54. N 5, p. 4069-4079. DOI: 10.1109/TIA.2018.2836098

12. Jian-guo Li, Kai Zhan. Intelligent Mining Technology for an Underground Metal Mine Based on Unmanned Equipment. *Engineering*. 2018. Vol. 4. Iss. 3, p. 381-391. DOI: 10.1016/j.eng.2018.05.013

13. Jäderblom N. From Diesel to Battery Power in Underground Mines. A Pilot Study of Diesel Free LHDs: Master of Science Thesis in Industrial Design Engineering. Luleå: Luleå University of Technology, 2017, p. 75.

14. Semykina I., Zavyalov V., Dubkov E., Veliliaev A.-H. On the possibility of wireless battery charging in a gaseous-and-dusty mine. *E3S Web of Conferences*. 2021. Vol. 303. N 01032. DOI: 10.1051/e3sconf/202130301032

15. Borisov S.V., Koltunova E.A., Kladiev S.N. Traction asynchronous electric drive of mine electric locomotivesimulation model structure improvement. *Journal of Mining Institute*. 2021. Vol. 247, p. 114-121. DOI: 10.31897/PMI.2021.1.12

16. Songyan Niu, Hang Yu, Shuangxia Niu, Linni Jian. Power loss analysis and thermal assessment on wireless electric vehicle charging technology: The over-temperature risk of ground assembly needs attention. *Applied Energy*. 2020. Vol. 275. N 115344. DOI: 10.1016/j.apenergy.2020.115344

17. Lijuan Xiang, Ze Zhu, Jindong Tian, Yong Tian. Foreign Object Detection in a Wireless Power Transfer System Using Symmetrical Coil Sets. *IEEE Access*. 2019. Vol. 7, p. 44622-44631. DOI: 10.1109/ACCESS.2019.2908866

18. Ahmad A., Alam M.S., Chabaan R. A Comprehensive Review of Wireless Charging Technologies for Electric Vehicles. *IEEE Transactions on Transportation Electrification*. 2018. Vol. 4. N 1, p. 38-63. DOI: 10.1109/TTE.2017.2771619

19. Abou Houran M., Xu Yang, Wenjie Chen. Magnetically Coupled Resonance WPT: Review of Compensation Topologies, Resonator Structures with Misalignment, and EMI Diagnostics. *Electronics*. 2018. Vol. 7. Iss. 11. N 296. DOI: 10.3390/electronics7110296

20. Foote A., Onar O.C. A review of high-power wireless power transfer. IEEE Transportation Electrification Conference and Expo (ITEC), 22-24 June 2017, Chicago, USA. IEEE, 2017, p. 234-240. DOI: 10.1109/ITEC.2017.7993277

21. Semykina I.Yu., Zavyalov V.M., Krylov V.N. Research of the Laboratory Prototype for the Battery Charging System Based on Wireless Power Transfer. 21th International Conference of Young Specialists on Micro/Nanotechnologies and Electron Devices (EDM), 29 June – 3 July 2020, Chemal, Russia. IEEE, 2020, p. 324-330. DOI: 10.1109/EDM49804.2020.9153521

22. Qizhi Liu. Identifying and correcting the defects of the Saaty analytic hierarchy/network process: A comparative study of the Saaty analytic hierarchy/network process and the Markov chain-based analytic network process. *Operations Research Perspectives*. 2022. Vol. 9. N 100244. DOI: 10.1016/j.orp.2022.100244

23. Semykina I.Yu., Dubkov E.A., Zavyalov V.M. Substantiation of criteria for technical solutions evaluating for wireless charging systems for mining electric vehicles. Sbornik trudov VIII Mezhdunarodnoi nauchno-prakticheskoi konferentsii "Perspektivy innovatsionnogo razvitiya ugolnykh regionov Rossii", 13-14 aprelya 2022 g., Prokopevsk, Rossiya. Prokopevsk: filial KuzGTU v g. Prokopevske, 2022. C. 88-93.

24. Huynh P.S., Ronanki D., Vincent D., Williamson S.S. Overview and Comparative Assessment of Single-Phase Power Converter Topologies of Inductive Wireless Charging Systems. *Energies*. 2020. Vol. 13. Iss. 9. N 2150. DOI: 10.3390/en13092150

25. Kripalakshmi T., Deepa T. A Comprehensive Review of High-frequency Transmission Inverters for Magnetic Resonance Inductive Wireless Charging Applications in Electric Vehicles. *IETE Journal of Research*. 2021, p. 1-11. DOI: 10.1080/03772063.2021.1905089

26. Bing Cheng, Liangzong He, Le Li et al. Improved wireless power transfer system utilizing a rectifier with nonlinear resistance compression characteristic. *Applied Energy*. 2023. Vol. 331. N 120365. DOI: 10.1016/j.apenergy.2022.120365

27. Zhong W.X., Hui S.Y.R. Maximum Energy Efficiency Tracking for Wireless Power Transfer Systems. *IEEE Transactions on Power Electronics*. 2015. Vol. 30. N 7, p. 4025-4034. DOI: 10.1109/TPEL.2014.2351496

28. Di Capua G., Femia N., Lisi G. Impact of losses and mismatches on power and efficiency of Wireless Power Transfer Systems with controlled secondary-side rectifier. *Integration*. 2016. Vol. 55, p. 384-392. DOI: 10.1016/j.vlsi.2016.04.005

29. Hongchang Li, Jie Li, Kangping Wang et al. A Maximum Efficiency Point Tracking Control Scheme for Wireless Power Transfer Systems Using Magnetic Resonant Coupling. *IEEE Transactions on Power Electronics*. 2015. Vol. 30. N 7, p. 3998-4008. DOI: 10.1109/TPEL.2014.2349534

30. Shuyu Cao, Htet Ye Yint Naing, Naayagi R.T. et al. Wireless Charging Resonant Converter Topology Study Based On Analytical Design Computation. 3rd International Conference on Energy, Power and Environment: Towards Clean Energy Technologies, 5-7 March 2021, Shillong, Meghalaya, India. IEEE, 2021, p. 1-6. DOI: 10.1109/ICEPE50861.2021.9404462

31. Mude K.N., Aditya K. A Comprehensive Review and Analysis of Two-Element Resonant Compensation Topologies for Wireless Inductive Power Transfer Systems. *Chinese Journal of Electrical Engineering*. 2019. Vol. 5. N 2, p. 14-31. DOI: 10.23919/CJEE.2019.000008

32. Jayalath S., Khan A. Design, Challenges, and Trends of Inductive Power Transfer Couplers for Electric Vehicles: A Review. *IEEE Journal of Emerging and Selected Topics in Power Electronics*. 2021. Vol. 9. N 5, p. 6196-6218. DOI: 10.1109/JESTPE.2020.3042625

33. Jianwei Mai, Yijie Wang, Yousu Yao, Dianguo Xu. Analysis and Design of High-Misalignment-Tolerant Compensation Topologies With Constant-Current or Constant-Voltage Output for IPT Systems. *IEEE Transactions on Power Electronics*. 2021. Vol. 36. N 3, p. 2685-2695. DOI: 10.1109/TPEL.2020.3014687

34. Xiaohui Qu, Hongdou Han, Siu-Chung Wong et al. Hybrid IPT Topologies With Constant Current or Constant Voltage Output for Battery Charging Applications. *IEEE Transactions on Power Electronics*. 2015. Vol. 30. N 11, p. 6329-6337. DOI: 10.1109/TPEL.2015.2396471

35. Siqi Li, Weihan Li, Junjun Deng et al. A Double-Sided LCC Compensation Network and Its Tuning Method for Wireless Power Transfer. *IEEE Transactions on Vehicular Technology*. 2015. Vol. 64. N 6, p. 2261-2273. DOI: 10.1109/TVT.2014.2347006

36. Marques E.G., Mendes A.M.S. Optimization of transmitter magnetic structures for roadway applications. IEEE Applied Power Electronics Conference and Exposition (APEC), 26-30 March 2017, Tampa, USA. IEEE, 2017, p. 959-965. DOI: 10.1109/APEC.2017.7930812

37. Bandyopadhyay S., Venugopal P., Jianning Dong, Bauer P. Comparison of Magnetic Couplers for IPT-Based EV Charging Using Multi-Objective Optimization. *IEEE Transactions on Vehicular Technology*. 2019. Vol. 68. N 6, p. 5416-5429. DOI: 10.1109/TVT.2019.2909566

38. Chunbo Zhu, Chaoye Fu, Dean Wang et al. Thermal Simulation and Optimization Study for Magnetic Coupler of Static Electric Vehicle Wireless Power Transfer Systems. 22nd International Conference on Electrical Machines and Systems (ICEMS), 11-14 August 2019, Harbin, China. IEEE, 2019, p. 1-4. DOI: 10.1109/ICEMS.2019.8921715

39. Chunming Wen, Qing Xu, Minbo Chen et al. Thermal Analysis of Coupled Resonant Coils for an Electric Vehicle Wireless Charging System. *World Electric Vehicle Journal*. 2022. Vol. 13. Iss. 8. N 133. DOI: 10.3390/wevj13080133

***Authors*: Valery M. Zavyalov,** *Doctor of Engineering Sciences, Head of Department, https://orcid.org/0000-0001-8485-9864* (*Sevastopol State University, Sevastopol, Russia*), **Irina Yu. Semykina,** *Doctor of Engineering Sciences, Senior Researcher, arinasemykina@gmail.com, https://orcid.org/0000-0001-6874-1735* (*T.F.Gorbachev Kuzbass State Technical University, Kemerovo, Russia*), **Evgeniy A. Dubkov,** *Senior Lecturer, https://orcid.org/0000-0003-0065-8681* (*Sevastopol State University, Sevastopol, Russia*), **Amet-han S. Velilyaev,** *Assistant Lecturer, https://orcid.org/0000-0002-3944-4042* (*Sevastopol State University, Sevastopol, Russia*).

*The authors declare no conflict of interests.*

ISSN 2411-3336; e-ISSN 2541-9404

JOURNAL OF MINING INSTITUTE

Zapiski Gornogo instituta

Journal homepage: pmi.spmi.ru

Research article

# Determination of the grid impedance in power consumption modes with harmonics

**Aleksandr N. SKAMYIN**[1] ✉, **Vasiliy S. DOBUSH**[1], **Mohd Hatta JOPRI**[2]

[1] *Saint Petersburg Mining University, Saint Petersburg, Russia*

[2] *Universiti Teknikal Malaysia Melaka, Melaka, Malaysia*

***How to cite this article*****:** Skamyin A.N., Dobush V.S., Jopri M.H. Determination of the grid impedance in power consumption modes with harmonics. Journal of Mining Institute. 2023. Vol. 261, p. 443-454. EDN LPAYJO DOI: 10.31897/PMI.2023.25

***Abstract*****.** The paper investigates the harmonic impedance determination of the power supply system of a mining enterprise. This parameter is important when calculating modes with voltage distortions, since the determined parameters of harmonic currents and voltages significantly depend on its value, which allow the most accurate modeling of processes in the presence of distortions in voltage and current. The power supply system of subsurface mining is considered, which is characterized by a significant branching of the electrical network and the presence of powerful nonlinear loads leading to a decrease in the power quality at a production site. The modernization of the mining process, the integration of automated electrical drive systems, renewable energy sources, energy-saving technologies lead to an increase in the energy efficiency of production, but also to a decrease in the power quality, in particular, to an increase in the level of voltage harmonics. The problem of determining the grid harmonic impedance is solved in order to improve the quality of design and operation of power supply systems for mining enterprises, taking into account the peculiarities of their workload in the extraction of solid minerals by underground method. The paper considers the possibility of determining the grid impedance based on the measurement of non-characteristic harmonics generated by a special nonlinear load. A thyristor power controller based on phase regulation of the output voltage is considered as such a load. Simulation computer modeling and experimental studies on a laboratory test bench are used to confirm the proposed method. The recommendations for selecting load parameters and measuring device connection nodes have been developed.

***Keywords*****:** harmonics; power quality; nonlinear electrical load; thyristor power controller; distortion; grid harmonic impedance

***Received: 26.10.2022*** ***Accepted: 13.02.2023*** ***Online: 04.05.2023*** ***Published: 19.07.2023***

**Introduction.** The development of mining and processing technologies is characterized by an increase in energy consumption and in process automation. New technologies of electrothermal metallurgy are being introduced [1-3], renewable energy technologies are used to supply remote power plants in the oil and gas industry [4-6] and for autonomous power supply using hybrid plants [7, 8]. New technological installations are based on the use of power electronics devices, which are part of various semiconductor converters. This leads to harmonic currents injection into power supply system. The negative effects of voltage and current distortion are known and widely reported [9-11].

Underground mining power supply systems have such features as a high length of power lines and a dispersal of high power electrical installations [12-14]. This circumstance is one of the main reasons for the increase in voltage distortion levels, which depend on the equivalent impedance of the power supply system and on the harmonic currents. When modernizing energy-intensive installations in mining, such as drainage systems, fans, electric hoisting installations, etc., the automated converter technology is used [15-17]. Such installations increase the energy efficiency of the technological process, but they are sources of voltage and current distortions. The possibility of modeling such drives is studied in more detail in the works [18-20]. Predicting the voltage distortion levels, when modeling processes in an electrical grid in the presence of harmonics, is an important and urgent challenge for a design engineer or researcher. The paper [18] confirms the importance of taking into account the power quality indicators when calculating electrical loads and choosing the parameters of the main equipment at mining enterprises.

The impedance of the power supply system is widely used in the calculation of the electrical grid operating modes, including non-sinusoidal conditions [21-23]. It was shown in [23] that, depending on the measured values of the system impedance, it is possible to determine the dominant harmonic source at the point of common coupling of consumers. One of the features of underground mining power supply systems is the remoteness of electrical loads from the power source, and hence the high impedance value of the system. As a result, the levels of voltage distortion can significantly exceed the requirements of regulations. The efficiency of harmonic distortion compensation devices, such as passive harmonic filters, directly depends on the impedance of the supply system. Therefore, when choosing the parameters of such devices, it is necessary to know the value of the harmonic system impedance. The impedance of the power supply system can help in determining the harmonic source, i.e. settle disputes between the supplier of electrical energy and the consumer [24-26].

The harmonic system impedance can be determined by calculation or by measurement. The determination of the harmonic impedance using calculations is based on the assumption of its inductive nature and linear dependence on frequency:

$$X_S^{(n)} = nX_S^{(1)},$$

where $n$ – harmonic order; $X_S^{(1)}$ – inductive impedance at the fundamental frequency.

This method is simple and does not require the use of additional equipment. However, when modeling the operating modes of the power system, the accuracy of determining the harmonic levels decreases. This is due to the fact that the energy system impedance includes resistive and capacitive components, and has a nonlinear character [27, 28]. The application of an analytical method for estimating system impedance for wind turbines is shown in the work [29]. Also, the impedance of the power supply system can change over time, i.e. it can be non-stationary due to the connection of various additional loads upstream of the point of common coupling [30, 31]. On the other hand, the application of the measuring method is more laborious, but gives more accurate results [32, 33].

Measuring methods can be invasive and non-invasive. Invasive methods are based on the use of harmonic current generators, non-invasive methods are based on the measurement of harmonic currents and voltages for two consecutive times. A comparison of various methods for determining the system impedance is given in the article [34]. Using the method based on harmonic generators requires additional expensive equipment, as well as preliminary measurement of current harmonics in the power supply system in order to generate a special signal that excludes the existing ones. The method of two consecutive measurements is easier to apply. However, its principle is based on changing the parameters of nonlinear loads from the grid side or from the consumer side relative to the point of common coupling. It does not allow accurate measurement of the grid harmonic impedance in the condition of simultaneous changes in the load parameters from the grid side and from the consumer side. Error estimation of the system impedance measurement method based on load fluctuations is given in [35].

Another problem when investigating the impedance of an underground mining power supply system is that the loads can be highly variable at many connection points, and the harmonic system impedance can also be a non-stationary value. Approaches to determining harmonic system impedance in real time are described in [36, 37].

This paper proposes a method for measuring the harmonic system impedance based on connecting an additional nonlinear load with a certain range of harmonics, which does not require large implementation costs. However, nonlinear loads may have significant internal impedance in their composition, which may depend on frequency, thus being comparable in magnitude to the harmonic system impedance. Therefore, it is necessary to study the influence of the internal impedance of an additionally connected nonlinear load, the parameters of its power consumption and operating modes.

**Methods.** To determine the harmonic system impedance by the method under consideration, it is necessary to use a nonlinear electrical load that satisfies two conditions. Firstly, the nonlinear load should generate harmonic currents that are uncharacteristic for the power supply system. Non-characteristic harmonics of the nonlinear load are understood as harmonics that are absent or extremely small in the voltage spectrum when this nonlinear load is not connected. Secondly, this nonlinear load should have no internal harmonic impedance. So, it can be represented in the equivalent circuit as a set of parallel-connected current sources without additional impedances. The presence of internal impedance in the nonlinear load also distorts the value of the harmonic system impedance, since the internal impedance in the equivalent circuit is connected in parallel with the system impedance and therefore the calculated value of the system impedance is less than its real value. These conditions should be observed in order to accurately determine the harmonic system impedance. For example, in the equivalent circuit, the presence of voltage harmonics of the same frequency as the current harmonic of an additionally connected nonlinear load leads to an error in calculating the harmonic system impedance, because it is necessary to take into account the influence of this voltage source on the calculation.

Let us consider a simplified power supply scheme for underground mining associated with the extraction of solid minerals (Fig.1).

The power supply of underground consumers depends on many factors: the depth of the developed horizons, the voltage of underground electrical system, the overall load and type of power receivers, the method of mining, etc. However, all this is associated with an increase in the length of the distribution feeders and the dispersal of power receivers. The majority of mining machines and mechanisms are driven by asynchronous motors with a squirrel-cage rotor. Variable electrical drives are widely used in the mining and developing areas of coal mines. Often, six-pulse semiconductor frequency converters are used to control the rotation speed of motors. For energy-intensive customers where speed control is not required (main ventilation fans, compressors), synchronous motors are widely used. Recently, even for energy-intensive hoists, high-power frequency-controlled asynchronous motors are increasingly being used, which leads to problems in the field of power quality in terms of harmonics. Applications are found for soft starters made according to the scheme of thyristor voltage regulators, in particular, for conveyor installations. It should be noted that there are developments and tools that allow minimizing the influence of semiconductor converters of individual installations on the power supply system (active rectifier, input power active and passive filters). The high cost of such devices is one of the main reasons for the low rate of their implementation.

Thus, from the point of view of the goal set, it is possible to highlight the main positions. In underground mining power supply systems, there is a nonlinear load with the harmonics order $n = 6k \pm 1$, where $k = 1, 2, 3, \ldots$; that is characteristic for sixpulse rectifiers. In the current spectrum there are also even harmonics, which are characterized by a short duration of presence in starting

EDN LPAYJO
DOI: 10.31897/PMI.2023.25

modes of electrical equipment. The power supply system is an extensive radial grid and a sharply variable load at different points of connection to the grid.

As a nonlinear load that is necessary to determine the harmonic impedance of the power supply system, a specialized semiconductor device that generates uncharacteristic for an external power supply system harmonic currents can be used. It should be loaded with linear resistive elements, the parameters of which do not depend on frequency. According to the results of the experiments, it was revealed that such loads are, for example, a thyristor power controller (TPC) and an uncontrolled rectifier without a capacitive DC filter [38]. The uncontrolled rectifier has a spectrum that includes harmonics $6k\pm1$, which can often be found in the external power supply grid. The TPC current consumption spectrum contains even harmonics, which in most cases are absent in the external grid. Therefore, TPC was chosen as the generator of uncharacteristic harmonics. This choice has some disadvantages. Firstly, TPC creates other harmonics in addition to uncharacteristic ones, including the current at the fundamental frequency, the value of which in all modes is greater than other harmonics. Secondly, to increase the accuracy of the measurement results, it is necessary to increase the TPC load power, therefore, the overall dimensions of the installation also increase.

Thus, to measure the harmonic system impedance, it is necessary to:

• Make sure that there are no uncharacteristic voltage harmonics in the supply grid when the uncharacteristic harmonics generator is turned off. If there are devices that generate even harmonics, they should be turned off. This is possible due to the small number of such devices in

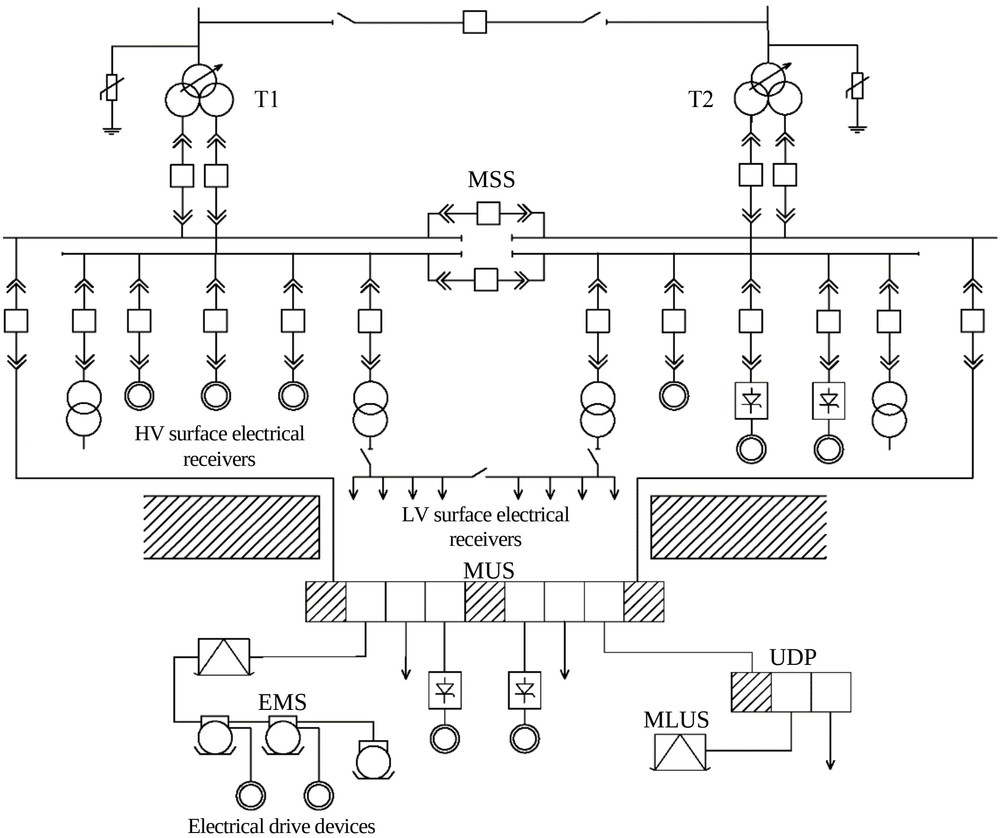


Fig.1. Simplified power supply scheme for mining production

MSS – main step-down substation; MUS – main underground substation;
T – power transformers; HV – high voltage; LV – low voltage;
UDP – underground distribution point; MLUS – mobile local underground substation;
EMS – explosion-proof mine starters

EDN LPAYJO
DOI: 10.31897/PMI.2023.25




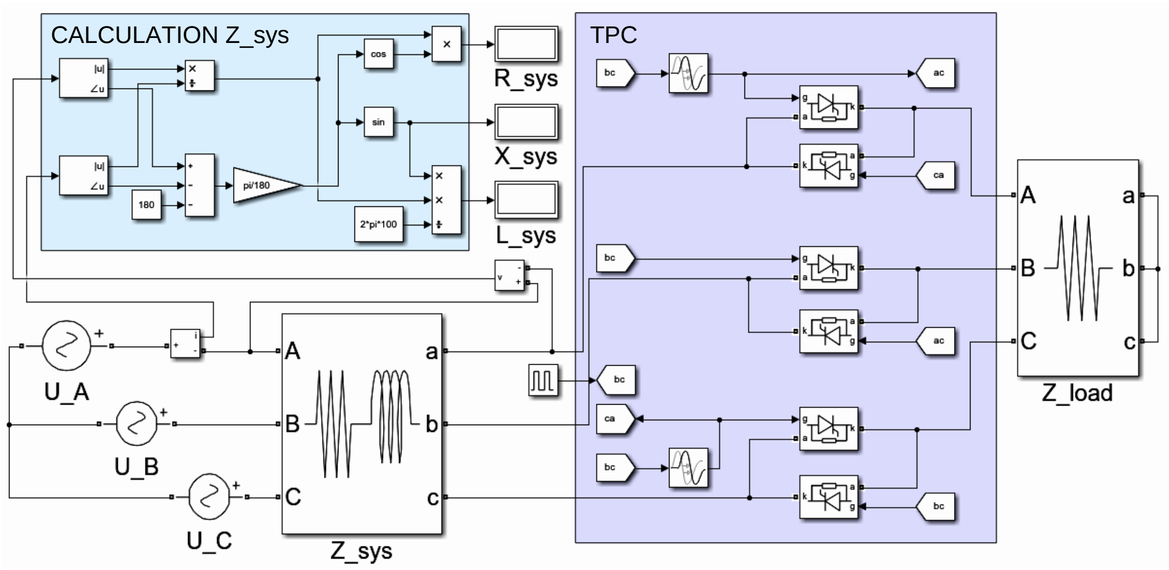


Fig.2. Simulation model in Matlab/Simulink

subsurface mining power supply systems. In the case of a short-term activation of such devices (for example, in the starting modes of engines), preliminary measurements can be carried out without turning them off with the control of such periods of switching on engines.

• Turn on the generator of uncharacteristic harmonics. Devices generating even harmonics can also be included in the work. In this case, it is necessary to take into account the location of such a load during measurements.

• Measure current and voltage waveforms at the connection point of the harmonic generator.

• Obtain the current and voltage spectrum at the input of the generator.

• Calculate the system impedance at uncharacteristic harmonics.

To verify the proposed method for calculating the harmonic system impedance, a simulation model was created in the Matlab/Simulink (Fig.2). The simulation model consists of a three-phase symmetrical source (sources of sinusoidal voltage U_A, U_B, U_C), a thyristor power controller with a control system (TPC unit), thyristor regulator loads (Z_load unit), a system impedance (Z_sys unit) and a measurement and calculation of the system impedance unit (CALCULATION Z_sys). The TPC unit consists of three pairs of an inverse-parallel thyristors and operates in the phase regulation mode of the output voltage. CALCULATION Z_sys unit performs the calculations of the harmonic system impedance based on phase voltage and TPC current waveforms. The developed model was used to determine the harmonic system impedance with different value and type of the system impedance.

The verification of the computer model was carried out on a laboratory test bench (Fig.3), which consists of a three-phase symmetric voltage source (1), a TPC (2), loads in the form of electrical heating tubes (3), three induction coils (4) and voltage and current meter (5). As a registration device, an oscilloscope Rigol 1202 and a power quality analyzer Resource PQA were used. The obtained waveforms were processed in Matlab.

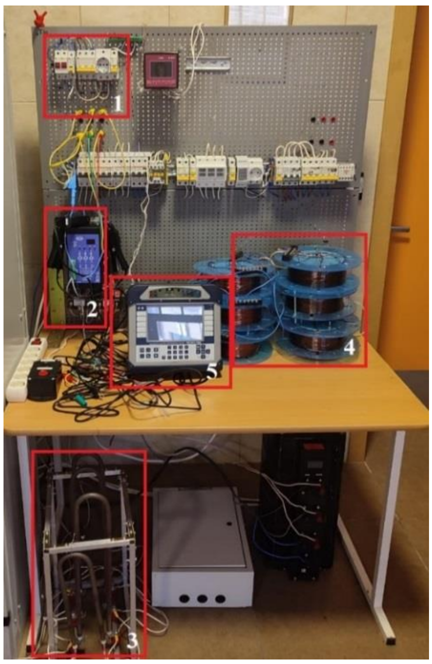

Fig.3. Laboratory test bench

EDN LPAYJO
DOI: 10.31897/PMI.2023.25

The parameters of the TPC and the system impedance are shown in the Table. All parameters of the model are identical to the parameters of the laboratory bench, and the algorithm for the TPC model operation is fully consistent with the operation of the real device.

**Laboratory equipment parameters**

| Name of equipment | Parameters |
|---|---|
| System impedance | |
| Stage 1 | $R$ = 0.45 Ω; $L$ = 1 mH |
| Stage 2 | $R$ = 1.12 Ω; $L$ = 4.1 mH |
| Stage 3 | $R$ = 1.84 Ω; $L$ = 8.8 mH |
| Load of thyristor controller | $R$ = 96 Ω |
| Thyristor power controller | $I_{rated}$ = 30 A |
| Three-phase supply grid | $U_{rated}$ = 380 V; $f$ = 50 Hz |
| Short circuit power | |
| Stage 1 | 263 kVA |
| Stage 2 | 85 kVA |
| Stage 3 | 44 kVA |
| System resistance | 10 Ω |
| System capacitance | 2350 μF |

Induction coils have three stages of regulation, its parameters are shown in the Table. The magnitude-frequency characteristic of inductance is linear, which has been confirmed using a laboratory source of a variable frequency from 0 to 500 Hz. As an assumption, it is accepted that the impedance of 10 kV grid and above is not taken into account, since its value is much smaller than laboratory linear inductance.

The system impedance can have a complex dependence on the frequency and consist of different types of impedances. Experiments with various types of the system impedance, which depend on the frequency differently, have been conducted. In addition, a test of the proposed method on these types of impedance has been carried out.

**Discussions.** The simulation model in Matlab/Simulink has been verified using laboratory equipment with various TPC loading (from 0 to 50 %). TPC waveforms obtained during modeling and as a result of measurement on a laboratory test bench have been compared. This is confirmed by the waveforms presented in Fig.4. In Fig.4, *a* a comparison of waveforms obtained by modeling (1)

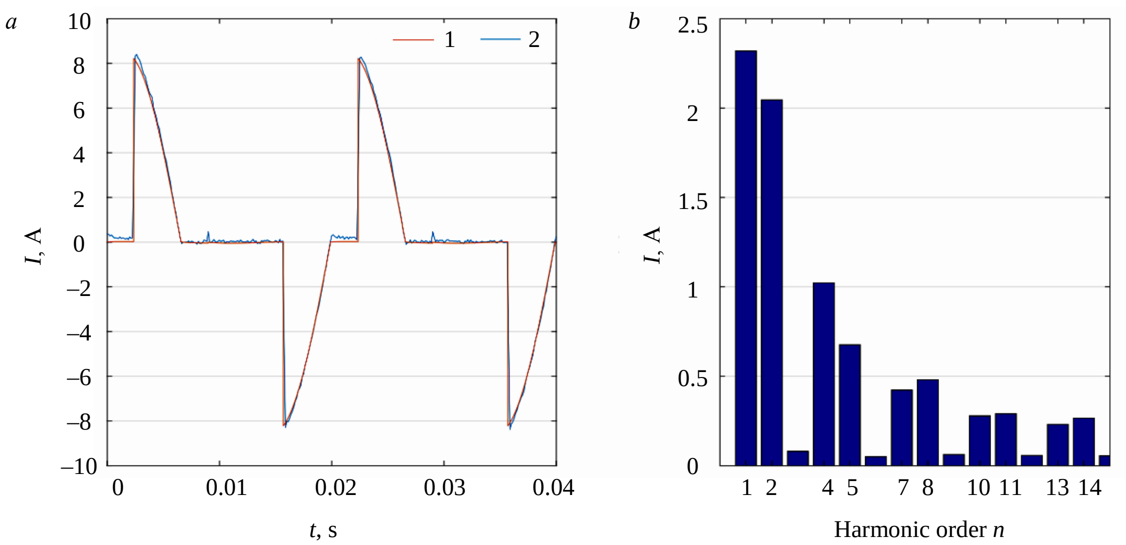


Fig.4. Waveform (*a*) and current spectrum (*b*) of TPC

and by an experiment on equipment (2) is presented. In Fig.4, *b* a spectrum of TPC current is presented.

The computer model under consideration has fully confirmed its performance for all even harmonics, i.e. the active and reactive impedance of the system have been determined. The error in determining the harmonic system impedance was less than 1 %. Thus, it is confirmed that equivalent circuit for uncharacteristic harmonics consists only of harmonic current sources and the system impedance. Therefore, the *n*th harmonic vector voltage of the system can be found according to the equation:

$$Z_S^{(n)} = \frac{\dot{U}^{(n)}}{\dot{I}^{(n)}},$$

where $\dot{U}^{(n)}$ – the *n*th harmonic vector voltage; $\dot{I}^{(n)}$ – the *n*th harmonic vector current.

To verify the proposed method, an experiment on a laboratory stand has been conducted. The TPC has worked in the phase control mode and its load has changed from 0 to 50 %. With a 100 % load, current distortions are zero and the load operates in a completely sinusoidal mode, so this mode

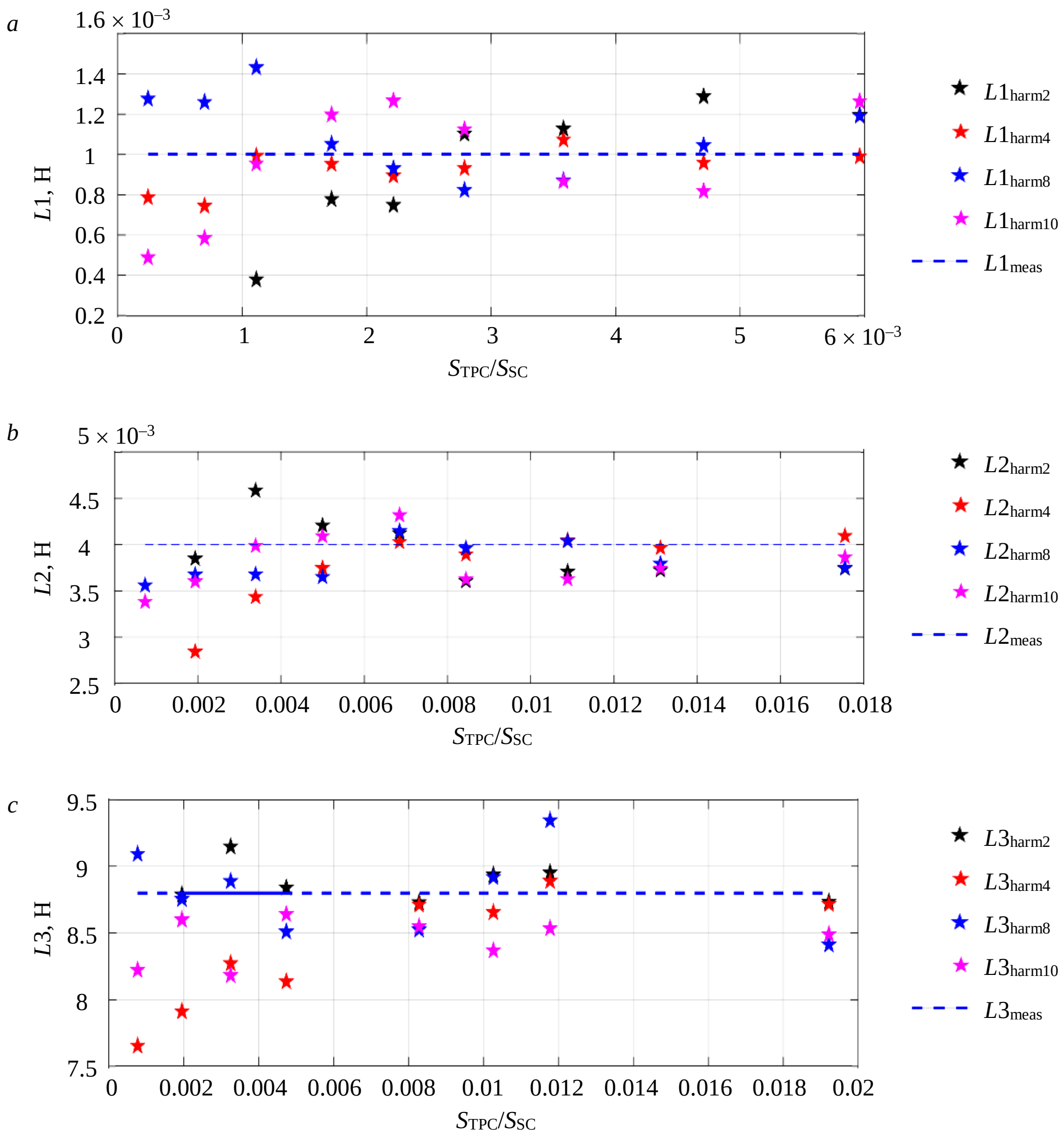


Fig.5. Calculated coil inductance values *L*1 (*a*), *L*2 (*b*), *L*3 (*c*)
for harmonics 2, 4, 8, 10 and different power of TPC

is not considered. Figure 5 presents the calculated values of the L1, L2, L3 coils inductance for the 2nd, 4th, 8th and 10th harmonics with various TPC load. An important parameter when determining the harmonic system impedance using the proposed method is the short circuit power. This is due to the fact that with various harmonic currents, the corresponding voltage drop in the harmonic system impedance occurs, which may be within the meter error. In order to achieve the required values of harmonic currents and voltages, it is necessary to determine the range of corresponding TPC power values depending on the short circuit power of the system when performing calculations.

The characteristics presented in Fig.5 reflect the values of the calculated inductance for the 2nd, 4th, 8th and 10th harmonics depending on the TPC power and the short circuit power at the connection point of receivers. The dotted line shows the value of the inductance measured using a programmable laboratory source. The ratio of TPC power to short circuit power can serve as a criterion for selecting the TPC power that is suitable for the grid under study. Based on the dependencies obtained, the following conclusions can be drawn:

• TPC operating modes with minimum load (5-15 %) can be attributed to outliers, since in this case the values of the second harmonic of current and voltage are insignificant and the inductance calculation has a large error. The rest of the TPC operating modes are suitable for measuring and calculating inductance and have negligible error;

• taking into account the other modes of TPC operation (20-50 %), the average deviation from the measured value of the inductance is less than 5 %;

• the TPC harmonic equivalent circuit can be represented as parallel-connected current sources without internal impedance;

• when a TPC power value is 0.2 % of the short circuit power then the inductance of the power system is determined with the required accuracy.

Further, experiments have been carried out for the active and capacitive system impedances in order to verify the previously obtained conclusions for these types of impedances. The measurement results for active and capacitive impedances are presented in Fig.6.

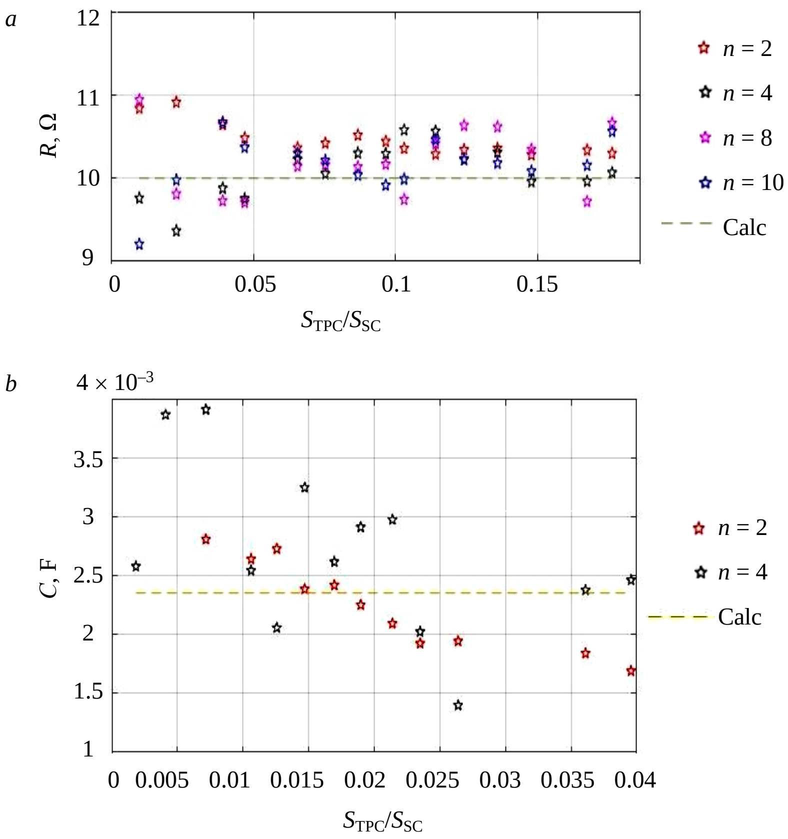


Fig.6. Measured impedance values with active (*a*) and capacitive (*b*) character

According to the experiment data, the measurement of the active impedance takes place with an error of less than 10 % in comparison with value of the real resistance (Fig.6, *a*). Moreover, when loading TPC in the range of 25-45 %, the measurement error does not exceed 5 %. The measurement error of the active system resistance is practically independent of the harmonic number. Resistance was measured in the range of 1-18 % of the short-circuit power, i.e. the TPC was one of the dominant loads. Figure 6, *b* shows the dependence of the

EDN LPAYJO
DOI: 10.31897/PMI.2023.25

Journal of Mining Institute. 2023. Vol. 261. P. 443-454


calculated system capacity at different frequencies on the ratio of the TPC power to the short circuit power of the system. Using the described method, the system capacitance can only be determined with an error of 50 % at low-frequency harmonics, which can be explained as follows. Firstly, the TPC power does not exceed 4 % of the grid short-circuit power in laboratory conditions due to the low system impedance. Secondly, the capacitance becomes even smaller at higher frequencies, so it is not possible to reliably measure currents and voltages at these harmonics and calculate the system capacitance on their basis in laboratory conditions.

In most cases, for subsurface mining power supply systems, the impedance of the power system is active-inductive, especially for medium and low voltage grids. Therefore, the proposed method can be implemented without significant increases in the power of an additionally connected nonlinear load. The methodology for applying the developed method for determining the power supply system impedance of the subsurface mining consists of the following steps:

1. The analysis of the underground mining power supply system for the presence of uncharacteristic harmonics in the supply voltage is carried out on the basis of preliminary measurements of power quality indicators with the uncharacteristic harmonic generator turned off. An analysis of the types of power semiconductor converters in production is also carried out. If there are semiconductor converters that generate uncharacteristic even harmonics, they should also be turned off for the duration of the measurements. In the case of a short switching on of such devices (for example, in the starting modes of engines), preliminary measurements are possible without turning them off, with control and exclusion of such periods from the measured data. In the absence of uncharacteristic harmonics in the supply voltage, the transition to the next step is carried out. The presence of uncharacteristic harmonics in the supply voltage leads to an additional error in the calculation of the harmonic system impedance. This error was not evaluated in this work.

2. The selection of TPC power is determined based on the short circuit power at the investigated point of connection:

$$\frac{S_{\mathrm{SC}}}{S_{\mathrm{TPC}}} \le 500.$$

When measuring in a low-voltage electrical grid of a mining enterprise, which is characterized by the worst indicators in terms of distortion in comparison with grids of medium and high voltage class, the TPC power will be an insignificant value from ones to tens of kilowatts.

3. Selection of connection points for measuring devices. The section of the grid (substation) is determined where it is necessary to solve the required problem. Namely, it is the calculation of distortion levels at the connection point of new nonlinear consumers, at the connection point of consumers when the load parameters and reactive power compensation devices change, at the connection point of consumers when installing harmonic reduction devices, etc. Figure 7 shows a simplified single-line electrical diagram, which considers the connection of the TPC and measurement circuits to the selected section of the grid.

If the power quality standards are exceeded and it is necessary to select the parameters of harmonic reduction devices, for example, on the buses of

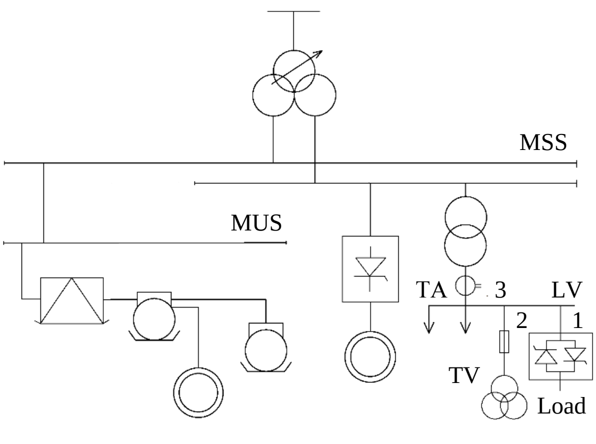


Fig.7. Simplified electrical single-line scheme
TA – current transformer; TV – voltage transformer

EDN LPAYJO
DOI: 10.31897/PMI.2023.25

a low-voltage (LV) substation, it is necessary to determine the harmonic grid impedance at this node. The TPC connection is carried out on the LV substation buses (point 1), the measurement of the harmonic phase voltage is also carried out on the LV buses (point 2). The presence of internal impedance of such a nonlinear load can be minimized by correctly connecting the current measuring circuits. In this case, the measurement of harmonic currents is carried out at the input feeder of the substation (point 3). This choice of connection points for measuring circuits also applies to other voltage levels.

If there are additional devices on the LV substation buses that generate the same spectrum of non-characteristic harmonics, the same connection of the measuring current circuits on the input feeder is necessary. The presence of such devices only increases the uncharacteristic harmonic currents flowing through the impedance of the upstream grid. Consequently, the uncharacteristic harmonic voltages at this point and the accuracy of calculating the harmonic system impedance increase. If the enterprise has devices in the HV grid that also generate a spectrum of non-characteristic harmonics, it is necessary to connect measuring devices at such a substation (for example, main step-down substation). Then based on the measurements, the harmonic system impedance from the bus of main step-down substation is determined. At the LV substation, the harmonic system impedance will differ only by the parameters of the supply line from LV to the main step-down substation.

4. Calculation of the harmonic system impedance based on the measured data of non-characteristic harmonic currents and voltages.

**Conclusion.** The conducted studies confirm the possibility of measuring the harmonic impedance of the system based on determining the response to uncharacteristic current harmonics generated using the proposed device in the form of a TPC. The use of such a device as a source of non-characteristic harmonics can be implemented to determine the system impedance at harmonic frequencies, which is confirmed by studies on physical and mathematical models in the absence of non-characteristic harmonics in the supply voltage. The TPC is a simpler and cheaper device than expensive harmonic generators.

The ratio of the short circuit power of the grid to the TPC power connected at the same node should be used as a selection criterion for the TPC power to determine the harmonic impedance of the system. Based on the analysis of short circuit power values in underground mining power supply systems, it was found that the TPC power will be from units to tens of kilowatts, depending on its connection node location. A technique for applying the proposed method to underground mining power supply systems is presented, which contains a preliminary analysis of the network and load, the selection of the required TPC parameters and the places for connecting the measuring circuits of current and voltage in the presence and absence of additional devices that generate a spectrum of characteristic and non-characteristic harmonics in the internal power supply system of the enterprise.

There are several directions for further research. First, thyristor controller improvement to amplify only non-characteristic harmonics and reduce the current magnitude at the fundamental frequency. Second, an assessment of the influence of uncharacteristic harmonics generated from the grid side. Third, the application of the proposed method for field measurements in order to measure the harmonic system impedance and develop a methodology for processing the measured data.

## REFERENCES

1. Baake E., Shpenst V.A. Recent scientific research on electrothermal metallurgical processes. *Journal of Mining Institute*. 2019. Vol. 240, p. 660-668. DOI: 10.31897/PMI.2019.6.660

2. Shklyarskiy Ya.E., Shklyarskiy A.Ya., Zamyatin E.O. Analysis of distortion-related electric power losses in aluminum industry. *Tsvetnye metally*. 2019. N 4, p. 84-91 (in Russian). DOI: 10.17580/tsm.2019.04.11

3. Khalifa A.A., Bazhin V.Yu., Ustinova Ya.V., Shalabi M.E.Kh. Study of the kinetics of the process of producing pellets from red mud in a hydrogen flow. *Journal of Mining Institute.* 2022. Vol. 254, p. 261-270. DOI: 10.31897/PMI.2022.18

4. Kroposki B., Johnson B., Yingchen Zhang et al. Achieving a 100% Renewable Grid: Operating Electric Power Systems with Extremely High Levels of Variable Renewable Energy. *IEEE Power and Energy Magazine*. 2017. Vol. 15. Iss. 2, p. 61-73. DOI: 10.1109/MPE.2016.2637122

5. Nikulin A.N., Epifancev K.V., Kovshov S.V., Korshunov G.I. The research of possibility to use the machine for biofuel production as a mobile device for poultry farm waste recycling. *Life Science Journal*. 2014. Vol. 11. N 4, p. 464-467.

6. Zhukovskiy Y.L., Vasilev B.Y., Korolev N.A., Malkova Y.M. Analysis of the behavior of asynchronous electric drive with a closed scalar control system when changing the inductance of the magnetizing circuit. *Indonesian Journal of Science and Technology*. 2022. Vol. 8. N 1, p. 65-78. DOI: 10.17509/ijost.v8i1.51983

7. Morenov V., Leusheva E., Lavrik A. et al. Gas-Fueled Binary Energy System with Low-Boiling Working Fluid for Enhanced Power Generation. *Energies*. 2022. Vol. 15. Iss. 7, p. 1-15. DOI: 10.3390/en15072551

8. Shklyarskiy Y.E., Guerra D.D., Iakovleva E.V., Rassõlkin A. The influence of solar energy on the development of the mining industry in the Republic of Cuba. *Journal of Mining Institute.* 2021. Vol. 249, p. 427-440. DOI: 10.31897/PMI.2021.3.12

9. Benaouadj M., Boumous Z., Boumous S. Active Harmonic Filtering for Improving Power Quality of an Electrical Network. *Journal Européen des Systèmes Automatisés*. 2022. Vol. 55. N 3, p. 397-403. DOI: 10.18280/jesa.550312

10. Ruuskanen V., Koponen J., Kosonen A. et al. Power quality and reactive power of water electrolyzers supplied with thyristor converters. *Journal of Power Sources*. 2020. Vol. 459. N 228075. DOI: 10.1016/j.jpowsour.2020.228075

11. Zhukovskiy Y., Tsvetkov P., Buldysko A. et al. Scenario Modeling of Sustainable Development of Energy Supply in the Arctic. *Resources*. 2021. Vol. 10. Iss. 12. № 124. DOI: 10.3390/resources10120124

12. Belsky A.A., Morenov V.A., Kupavykh K.S., Sandyga M.S. Wind Turbine Electrical Energy Supply System for Oil Well Heating. *Energetika. Proceedings of CIS higher education institutions and power engineering associations.* 2019. Vol. 62. N 2, p. 146-154 (in Russian). DOI: 10.21122/1029-7448-2019-62-2-146-154

13. Alexandrov V.I., Kopteva A.V., Serzan S.L. Effective Parameters of Tail Processing of Gold-Bearing Ore Hydrotransport for Verninskaya Processing Factory. *Key Engineering Materials.* 2020. Vol. 836, p. 25-35. DOI: 10.4028/www.scientific.net/KEM.836.25

14. Abdallah W.J., Hashmi K., Faiz M.T., Flah A., Channumsin S., Mohamed M.A., Ustinov D.A. A Novel Control Method for Active Power Sharing in Renewable-Energy-Based Micro Distribution Networks. *Sustainability*. 2023. Vol. 15. N 1579. DOI: 10.3390/su15021579

15. Munoz-Guijosa J.M., Kryltcov S.B., Solovev S.V. Application of an Active Rectifier Used to Mitigate Currents Distortion in 6-10 kV Distribution Grids. *Journal of Mining Institute.* 2019. Vol. 236, p. 229-238. DOI: 10.31897/PMI.2019.2.229

16. Abramovich B.N., Ustinov D.A., Abdallah W.J. Modified proportional integral controller for single ended primary inductance converter. *International Journal of Power Electronics and Drive Systems*. 2022. Vol. 13. N 2, p. 1007-1025. DOI: 10.11591/ijpeds.v13.i2.pp1007-1025

17. Raj L.R.L.V., Jidin A., Abdul Karim K. et al. Improved torque control performance of direct torque control for 5-phase induction machine. *International Journal of Power Electronics and Drive Systems*. 2013. Vol. 3. N 4, p. 391-399. DOI: 10.11591/ijpeds.v3i4.5249

18. Lingom P.M., Song-Manguelle J., Doumbia M.L. et al. Electrical Submersible Pumps: A System Modeling Approach for Power Quality Analysis with Variable Frequency Drives. *IEEE Transactions on Power Electronics*. 2022. Vol. 37. Iss. 6, p. 7039-7054. DOI: 10.1109/TPEL.2021.3133758

19. Yerbayev Y., Artyukhov I., Zemtsov A. et al. Negative Impact Mitigation on the Power Supply System of a Fans Group with Frequency-Variable Drive. *Energies*. 2022. Vol. 15. Iss. 23. N 8858. DOI: 10.3390/en15238858

20. Jopri M.H., Abdullah A.R., Manap M. et al. An Improved Of Multiple Harmonic Sources Identification In Distribution System With Inverter Loads By Using Spectrogram. *International Journal of Power Electronics and Drive Systems*. 2016. Vol. 7. N 4, p. 1355-1365. DOI: 10.11591/ijpeds.v7.i4.pp1355-1365

21. Shawon M.H., Barczentewicz S.H., Bień A., Hanzelka Z. Localization of Harmonic Sources in Power System – Simulation and Laboratory Study. *Renewable Energy and Power Quality Journal*. 2016. N 14, p. 546-551. DOI: 10.24084/repqj14.388

22. Martinez R., Castro P., Arroyo A. et al. Techniques to Locate the Origin of Power Quality Disturbances in a Power System: A Review. *Sustainability*. 2022. Vol. 14. Iss. 12. N 7428. DOI: 10.3390/su14127428

23. Srikanth P., Koley C. Deep learning and signal processing based algorithm for autorecognition of harmonic loads. *Journal of Intelligent and Fuzzy Systems*. 2022. Vol. 42. N 2, p. 1171-1184. DOI: 10.3233/JIFS-189780

24. Kasemuana S.M., De Beer A.S., Pretorius J.H.C. A Practical Method to Identify Contributions of Harmonics in Power Systems: Method and Application. *International Review of Electrical Engineering*. 2021. Vol. 16. N 4, p. 304-315. DOI: 10.15866/iree.v16i4.19194

25. Mokoena B., Eboule P.S.P., Pretorius J.H.C. Medium voltage consumers' cost evaluation connected to a micro-grid PV system. *Energy Reports*. 2022. Vol. 8. S. 10, p. 235-244. DOI: 10.1016/j.egyr.2022.05.105

26. Jopri M.H., Abdullah A.R., Sutikno T. et al. A Diagnostic Analytics of Harmonic Source Signature Recognition by Using Periodogram. *International Journal of Electrical and Computer Engineering*. 2018. Vol. 8. N 6, p. 5399-5408. DOI: 10.11591/ijece.v8i6.pp5399-5408

27. Ebadi M., Bayat M., Asadi H. Evaluating maximum permissible feeder current in capacitive compensated harmonic polluted networks introducing Apparent RMS Current Ratio Index (ACRI). *Electric Power Systems Research*. 2020. Vol. 187. N 106511. DOI: 10.1016/j.epsr.2020.106511

28. Yaqiong Li, Zhanfeng Deng, Tongxun Wang et al. Coupled Harmonic Admittance Identification Based on Least Square Estimation. *Energies*. 2018. Vol. 11. Iss. 10. N 2600. DOI: 10.3390/en11102600

29. Xia Zhou, Yishi Liu, Ping Chang et al. Voltage Stability Analysis of a Power System with Wind Power Based on the Thevenin Equivalent Analytical Method. *Electronics*. 2022. Vol. 11. Iss. 11. N 1758. DOI: 10.3390/electronics11111758

EDN LPAYJO
DOI: 10.31897/PMI.2023.25

30. Ahmed E.F., Said E.-S.S.A., Abdel Mageed H.M., Ammar A.A. A novel interactive technique for load current harmonic reduction for any randomly utilized household equipment. *International Journal of Power Electronics and Drive Systems*. 2022. Vol. 13. N 4, p. 2159-2171. DOI: 10.11591/ijpeds.v13.i4.pp2159-2171

31. Azebaze Mboving C.S., Hanzelka Z., Firlit A. Analysis of the Factors Having an Influence on the LC Passive Harmonic Filter Work Efficiency. *Energies*. 2022. Vol. 15. Iss. 5. N 1894. DOI: 10.3390/en15051894

32. Singh R.S., Ćuk V., Cobben S. Measurement-Based Distribution Grid Harmonic Impedance Models and Their Uncertainties. *Energies*. 2020. Vol. 13. Iss. 16. N 4259. DOI: 10.3390/en13164259

33. Wanjun Lei, Cheng Nie, Mingfeng Chen et al. A Fast-Transient Repetitive Control Strategy for Programmable Harmonic Current Source. *Journal of Power Electronics*. 2017. Vol. 17. Iss. 1, p. 172-180. DOI: 10.6113/JPE.2017.17.1.172

34. Kanálik M., Margitová A., Bena L., Kanáliková A. Power System Impedance Estimation Using a Fast Voltage and Current Changes Measurements. *Energies*. 2021. Vol. 14. Iss. 1. N 63. DOI: 10.3390/en14010063

35. Yang Wang, Wilsun Xu, Jing Yong. An Adaptive Threshold for Robust System Impedance Estimation. *IEEE Transactions on Power Systems*. 2019. Vol. 34. Iss. 5, p. 3951-3953. DOI: 10.1109/TPWRS.2019.2924349

36. Sommer S., Aabrandt A., Jóhannsson H. Reduce-factor-solve for fast Thevenin impedance computation and network. *IET Generation, Transmission & Distribution*. 2019. Vol. 13. Iss. 2, p. 288-295. DOI: 10.1049/iet-gtd.2018.5330

37. Ziteng Liu, Yonghai Xu, Haiwei Jiang, Shun Tao. Study on Harmonic Impedance Estimation and Harmonic Contribution Evaluation Index. *IEEE Access*. 2020. Vol. 8, p. 59114-59125. DOI: 10.1109/ACCESS.2020.2982950

38. Skamyin A., Shklyarskiy Y., Dobush V., Dobush I. Experimental Determination of Parameters of Nonlinear Electrical Load. *Energies*. 2021. Vol. 14. Iss. 22. N 7762. DOI: 10.3390/en14227762

***Authors*: Aleksandr N. Skamyin,** *Candidate of Engineering Sciences, Associate Professor, skamin_an@pers.spmi.ru, https://orcid.org/0000-0001-7738-7539* (*Saint Petersburg Mining University, Saint Petersburg, Russia*), **Vasiliy S. Dobush,** *Candidate of Engineering Sciences, Associate Professor, https://orcid.org/0000-0002-9401-5638* (*Saint Petersburg Mining University, Saint Petersburg, Russia*), **Mohd Hatta Jopri,** *PhD, Associate Professor, https://orcid.org/0000-0002-6902-0099* (*Universiti Teknikal Malaysia Melaka, Melaka, Malaysia*).

*The authors declare no conflict of interests.*

ISSN 2411-3336; e-ISSN 2541-9404

JOURNAL OF MINING INSTITUTE

Zapiski Gornogo instituta

Journal homepage: pmi.spmi.ru

*Research article*

# Integration of renewable energy at coal mining enterprises: problems and prospects

**Fedor S. NEPSHA**[1,2]✉, **Kirill A. VARNAVSKIY**[1], **Vyacheslav A. VORONIN**[1], **Ilya S. ZASLAVSKIY**[1], **Andrey S. LIVEN**[1]

[1] *T.F.Gorbachev Kuzbass State Technical University, Kemerovo, Russia*

[2] *National University of Oil and Gas "Gubkin University", Moscow, Russia*

***How to cite this article:*** Nepsha F.S., Varnavskiy K.A., Voronin V.A., Zaslavskiy I.S., Liven A.S. Integration of renewable energy at coal mining enterprises: problems and prospects. Journal of Mining Institute. 2023. Vol. 261, p. 455-469. EDN LNSCEY

***Abstract.*** This article addresses the issue of developing renewable energy in coal mining enterprises in the Russian Federation. The study presents a methodology for assessing the technical and economic efficiency of introducing renewable energy sources based on simulation modeling. An analysis of the potential of solar and wind energy for coal mining regions in Russia is conducted. The authors use a custom software developed by them to simulate the power supply system for various scenarios of renewable energy integration, including solar generation, wind generation, solar generation with energy storage, wind generation together with solar generation. Based on the example of the Rostov region, a feasibility study of the considered options is presented. Additionally, the research includes a sensitivity analysis of the investment project in the conditions of uncertainty in the development of Russian renewable energy. The research findings indicate that even in market conditions with $CO_2$ emission quotas and prices at the level of the Sakhalin experiment, renewable energy in coal mining enterprises in Russia remains unattractive and requires additional support.

***Keywords***: energy efficiency; renewable energy; distributed generation; decarbonization of coal mines; simulation modeling

***Acknowledgment.*** The research was supported by the state assignment of Ministry of Science and Higher Education of the Russian Federation (N 075-03-2021-138/3).

***Received: 02.04.2023*** ***Accepted: 20.06.2023*** ***Online: 19.07.2023*** ***Published: 19.07.2023***

**Introduction.** In accordance with the ratified Kyoto Protocol to the United Nations Framework Convention on Climate Change, the Paris Agreement, as well as the agreements adopted at the Climate Change Conference in Glasgow (2021) and Sharm el-Sheikh (2022), the Russian Federation took on commitments to reduce the carbon footprint by decarbonizing the economy [1]. Many countries are actively introducing carbon payments, declaring a complete phase-out of fossil energy resources, including coal, and setting the goal of achieving carbon neutrality in the period 2045-2060 [2]. Despite this, the coal industry continues to play a significant role in the global energy sector. As of 2021[1], coal provided about 27 % of global energy consumption (10.9 % in Russia), and the electric power industry accounted for 36.7 % of coal consumption in the world (17.3 % in Russia). The share of coal use is especially high in Asian countries: China – 62.93 %, India – 74.17 %, Indonesia – 61.46 %. According to EIA and IEA analytical reports, coal will retain a significant role in the power industry until 2050. Thus, despite the active lobbying for measures to decarbonize the economy and the constant increase in the use of renewable energy sources (RES), the coal industry remains an important component of the global energy balance.

[1] Ritchie H., Roser M., Rosado P. Energy. URL: https://ourworldindata.org/energy (accessed 14.04.2023).

However, the implementation of the economy decarbonization strategy is not the only challenge for the Russian coal industry. Unprecedented sanctions pressure, reorientation to new sales markets in the countries of Southeast Asia and the Indian Ocean, increase in the logistics chain and transportation costs, export price volatility are also serious external shocks for the Russian coal industry [3]. Of particular importance is the increase in the competitiveness of Russian coal companies through the introduction of modern technologies such as IoT (Internet of Things) and Big Data, as well as the energy efficiency of power supply to coal enterprises [4]. The introduction by coal companies of highly efficient technologies, including digital ones, in the processes of coal mining and processing is provided for by the Program for the Development of the Russian Coal Industry for the period up to 2035. Large investments are also aimed at creating a set of technologies that increase the efficiency of coal mining and coal processing[2].

One of the ways to reduce the carbon footprint of Russia without harming the coal industry is to "green" the internal power consumption of coal mines through the introduction of the distributed generation. Studies [5, 6] noted the possibility of reducing the cost of purchasing electricity from the power grid and the volume of carbon dioxide emissions by coal mines when using their own generation on coal mine methane. The relevance and necessity of RES in the conditions of enterprises of the mineral resource complex (MRC) is substantiated in the work [7]. The article [8] considers the possibilities of integrating distributed generation based on RES for MRC enterprises, gives a positive assessment of the use of RES to provide electricity and heat supply. The work [9] is devoted to the study of the effectiveness of the use of hybrid energy systems based on solar, wind and diesel power plants, as well as the replacement of diesel transport with hydrogen for coal mines in Northern China. A high potential for reducing $CO_2$ emissions and reducing diesel fuel consumption was noted. The study [10] evaluated the effectiveness of the introduction of cogeneration on coal mine methane and noted a significant dependence of the investment attractiveness of the project on tariffs for $CO_2$ emissions. There are a number of projects on the use of RES at MRC enterprises: the introduction of mobile solar power plants by SunShift (Australia) at coal mines[3], 36 MW hybrid solar power plant at a gold mine in southwestern Mali[4], mining dump trucks with electric motors and the subsequent development of electric transport charging infrastructure as one of the business diversification options.

The studies mentioned above suggest that incorporating renewable energy into the power supply systems of MRC enterprises has the potential to reduce their carbon footprint, lower coal mining costs by reducing energy expenses, increase reliability, minimize financial losses from power outages, and create new high-tech employment opportunities.

**The problem statement.** The use of RES in industrial enterprises was considered by many scientists. The paper [11] considers the possibility of achieving energy independence of industrial enterprises through the use of RES. It is noted that the introduction of renewable energy sources (RES) in power utilities may present certain challenges, such as potential increases in electricity prices, complexities in managing power systems, and a reduction in reliability. Simultaneously, the study concluded that there are promising opportunities for utilizing renewable energy sources as decentralized energy sources within the power supply systems of industrial enterprises. This approach involves energy sources exclusively for the enterprise's consumers, without the possibility of transferring power to the grid. In the study [12], a system for managing energy flexibility in industrial enterprises

[2] The Order of the Government of the Russian Federation N 1144-r dated 11.05.2022 "On approval of the comprehensive scientific and technical program of the full innovation cycle "Development and implementation of a set of technologies in the areas of exploration and production of solid minerals, ensuring industrial safety, bioremediation, creating new products of deep processing from coal raw materials while consistently reducing the environmental impact on the environment and risks to the life of the population".

[3] SunSHIFT Global Fleet of Modular Moveable Megawatt Scale Solar Assets. URL: https://www.climatefinancelab.org/ideas/ sunshift-global-fleet-of-modular-moveable-megawatt-scale-solar-assets/ (accessed 20.06.2023).

[4] Takouleu J.M. MALI: Reuniwatt to buid weather forecasting system for Fekola solar hybrid power plant. URL: https://www.afrik21.africa/en/mali-reuniwatt-to-buid-weather-forecasting-system-for-fekola-solar-hybrid-power-plant/ (accessed 11.03.2023).

is proposed. The findings indicate that the RES integration in industrial enterprises can have a positive impact on the development of the energy flexibility market. In the paper [13] the conclusion that there is a high potential for renewable sources in the territory of the Russian Federation was made based on an assessment of solar activity and wind speed data in different regions. It notes a mismatch between the periods of maximum solar radiation and wind speed for several regions in Russia throughout the day. Considering this, it is recommended to use hybrid solar-wind power plants to minimize the installed generation capacity in microgrids. Similar conclusions were made by foreign researchers in [14], who considered the application of a hybrid power plant (solar-wind power plant). This option has resulted in a reduction in electricity costs from $5,300,000 to $2,400,000 per year and the generation of additional income from selling electricity to the grid, amounting to $1,300,000 per year. As a result, the project has an estimated payback period of approximately six years.

Researchers from Tsinghua University [15] are studying the problem of selecting the optimal combination of solar generation, wind generation, and biogas generation for rural electrification. This research examines numerous grid development options involving different combinations of renewable energy generation. The most feasible approach is a hybrid system whereby the village's grid can operate both in parallel with and independently from the external grid. The study emphasizes the favorable impact of distributed energy resources on the environment and social factors.

As a solution to improve the reliability of power supply of the oil sector, the paper [16] considers the use of wind-diesel power plants for power supply of submersible electric motors of electric centrifugal pumps in oil wells. The article [17] considers the introduction of a cogeneration plant at oil production facilities with the possibility of additional power generation with a low demand for heat. Such a system could be promising in coal mines utilizing methane as the primary energy source.

In [18], Chinese researchers presented a hybrid power supply system, including wind and solar generating sources, as well as a pumped storage power plant (PSPP). PSPP acts as a backup power source on windless days and periods of increased cloud cover, ensuring the stability of the power supply system. It is proposed to use spent underground mine workings of coal mines in the Ningxia Hui Autonomous Region of China as reservoirs for water storage. A similar approach has been proposed by Spanish scientists [19] for the spent coal mines in the Asturian coal basin in Spain. Hydrodynamic models are presented that reflect the movement of mine water flows. It is noted that the absence of such models hinders the implementation of projects for the creation of PSPP in underground workings due to the impossibility of assessing their effectiveness. In the research [20], the same researchers analyze the technical and economic feasibility of using mine water from flooded coal mines to provide thermal and electrical energy to consumers located in nearby areas. The developed economic model shows that the performance of such a power supply system depends on many factors, but with proper development of implementation options, it can be very effective and will optimize consumers' power supply costs, as well as reduce carbon dioxide emissions into the environment.

The article [21] considers the problem of determining the optimal location of a PSPP in underground workings using the example of the Chinese province of Shanxi. The study is based on a multi-criteria decision-making method, four assessment criteria are given, and a number of quantitative indicators for real examples are presented. The necessity of improving the method by introducing additional assessment criteria is noted.

Another study on the problem of the optimal location of PSPP in the underground workings of closed mines, conducted by European scientists, is presented in [22]. A mathematical model is proposed to estimate the impact of hydrogeological factors, rock chemical composition, and other variables when selecting an appropriate location for an underground PSPP.

The article [23] shows the analysis of the current state and trends in usage of RES by Australian mining enterprises. The study highlights the factors that encourage mining enterprises to adopt RES, as well as the challenges that hinder their widespread implementation. However, the article notes that due to inadequate scientific and technical research on RES implementation in MRC enterprises, only approximately 7 % of Australian mining enterprises currently utilize RES.

The research [24] is devoted to the study of the possibilities of optimizing energy consumption using RES on the example of Zimbabwean mines. It is shown that the use of traditional methods for improving energy efficiency (optimization of the operating mode, increasing the power factor, etc.) without RES is the best option in terms of economic efficiency. Nevertheless, RES can prove to be beneficial in developing mechanisms for their own payback.

The article [25] proposes the developed multicriteria algorithm for the operation of the dispatch center of an integrated energy system that uses coal mine methane, mine water, etc. as primary energy sources. The algorithm has been tested in a coal mine and allows solving a wide range of problems from optimizing energy consumption and increasing the reliability of energy supply to reducing greenhouse gas emissions.

The study [26] presents the model of an integrated power supply system for a coal mine including energy storage devices and RES. Using this model and real data from one of the coal mines in Western China, the algorithm for two-stage optimization of the power supply system in the conditions of uncertainty was worked out. The algorithm application results in optimal loading of power equipment, enhancing the energy efficiency and reliability of the coal mine power supply system.

Researchers from the University of Virginia in [27] proposed the concept of using spent oil and gas wells, as well as spent underground workings of coal mines as compressed air accumulators, which can be used to stabilize the operation of nearby wind farms on windless days. The complexity of the implementation of such projects is noted, but at the same time, it points at a significant socio-economic effect from the development of infrastructure, the creation of new jobs, as well as an impetus in the development of mining science in the direction of finding and substantiating alternative approaches to the operation of mine workings.

The article [28] investigates the possibility of using low-potential heat sources typical for coal industry enterprises. A schematic diagram of the complex processing of mine waters with the production of thermal energy, drinking and technical water (suitable, for example, for the agro-industrial complex) is presented. According to the authors, the use of the proposed scheme will improve the reliability of heat supply to industrial and domestic consumers, as well as reduce the negative impact of the coal industry on the environment.

The paper [29] presents a thematic study on the possibilities of utilizing underground workings of coal mines as PSPP, compressed air energy storage systems, and geothermal energy sources. It is noted that the energy potential of underground excavations amounts to approximately 197 GW·h/year, with a significant reduction in $CO_2$ emissions.

In the article [30], the results of utilizing mine water from a flooded copper mine in the state of Michigan, USA, as a source of thermal energy for nearby consumers, are presented. The study concludes that the proposed solutions exhibit high efficiency. Additionally, the research indicates that the knowledge gained from implementing these technologies can be applied not only in the USA but also in other mining regions worldwide.

The topic of the optimal use of mine water as an energy source in the conditions of the closed mine Markham Colliery (Great Britain) is presented in [31], where the chemical composition of mine water is studied, measures are proposed to improve the efficiency of power equipment, as well as to increase its service life.

The article [32] is devoted to the study of the control algorithm for an electrical engineering complex, including a wind power plant, batteries, and a diesel generator. The study emphasizes that incorporating climatic factors and energy consumption forecast data for the upcoming day into the control algorithm enhances the efficiency of the power supply system. The findings are pertinent in analyzing models of power supply systems with RES for domestic MRC enterprises since the climatic conditions in Russia's mineral deposit regions can vary significantly.

Despite a considerable amount of research on RES implementation in industrial enterprises, the effectiveness of RES in coal mining enterprises in the Russian Federation remains inadequately explored. Further study is necessary to assess the feasibility of introducing RES during the construction and modernization stages of these enterprises. The assessment of renewable generation efficiency and its integration into coal mine power supply systems is conducted using a custom computer program developed in Python programming language, along with specialized libraries such as pvlib and windpowerlib.

**Methodology.** There are several foreign software available for simulating hybrid power supply systems, including HOMER, iHOGA, PVsyst, SAM, RETScreen Expert, EnergyPlan, and many others [33]. The most efficient and convenient tool is HOMER PRO, which surpasses other available options with similar functionality [34]. However, HOMER PRO does not consider the special features of the Russian electricity and capacity market. Therefore, there is a need to develop domestic software that could account for these features and subsequently be used for preliminary testing and developing control systems for distributed energy facilities. The authors have developed a computer program that performs following functions:

- forming a profile of RES generation using location data while taking into account seasonality and installed capacity;
- forming an annual balance for a hybrid power supply system using optimal control algorithms;
- creation of a financial and economic model that allows assessing the sensitivity of an investment project and the risks of its implementation.

It is worth noting that foreign software has the potential to address these issues. However, challenges arise when it comes to implementing the financial and economic model in the context of the Russian electricity market. Furthermore, the optimization algorithms used are not sufficiently described to enable their integration within an actual control system. According to the authors of the software, in order to select the optimal equipment composition, the hybrid power supply system and its automated control system should be interconnected using common control algorithms. This will ensure a high degree of certainty that the results obtained during the equipment optimization process correspond to the actual operating experience of the control system.

*Simulation model structure*. Figure 1 provides a diagram of the power supply system model for the mining enterprise, which takes into account the integration of renewable energy sources. This model comprises the following components:

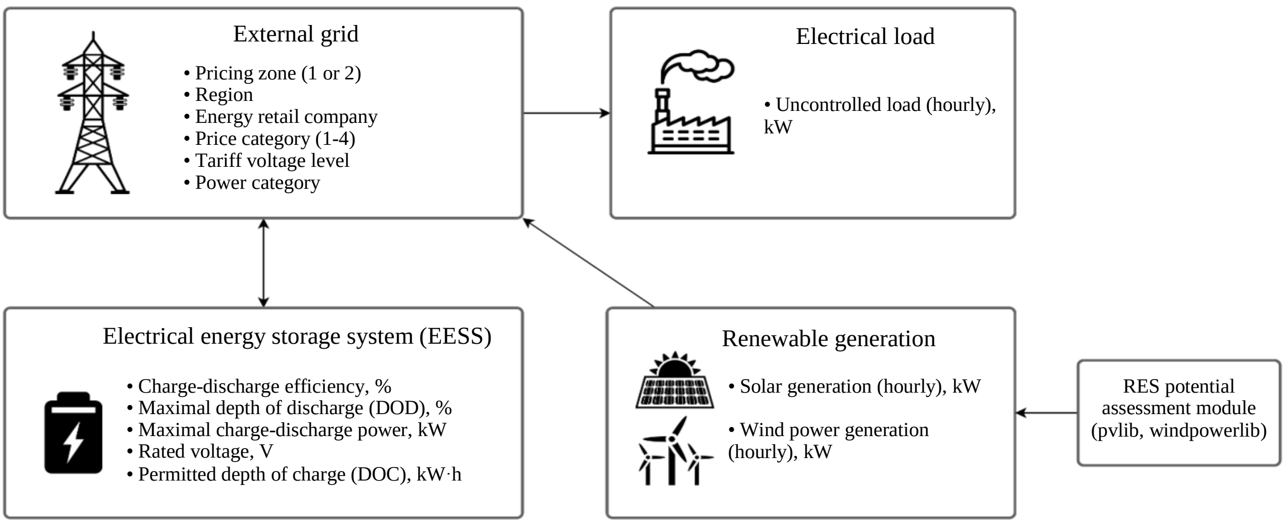


Fig.1. Block scheme of the simulation model for a hybrid power supply system

• external grid the parameters of which are determined by the region of connection of the mining enterprise, as well as the contract for the sale of electrical energy and the contract for services for the transmission of electrical energy. In some cases, small enterprises may only need to sign one energy supply contract with an energy retail company;

• electrical load represented by mining equipment and the own needs of distributed energy facilities. The simulation model uses the load profile of a Kuzbass coal mine to set the consumption profile, which is assumed to be similar to the load schedule for coal mines in other regions due to their round-the-clock mode of operation;

• RES generation comprises a wind power plant (WPP) and/or a photovoltaic power plant (PVP). The generation profile is first generated using the pvlib and windpowerlib libraries and then used in the calculations to generate the annual profiles of wind and solar generation;

• electric energy storage system (EESS) is represented by the accumulation (storage) and power conversion subsystems.

*Algorithm for feasibility study of the RES integration at the mining enterprise* is shown in Fig.2 and includes the following steps:

• Setting a location. The coordinates of the object in question are entered, which are used in the formation of requests to external services.

• Loading data from external services. Data requests are generated for meteorological parameters (solar insolation, air temperature, atmospheric pressure, wind speed) using the NASA POWER API.

• Setting the power consumption profile. The power consumption profiles of mining equipment are entered.

• Setting the parameters of the generation equipment. The parameters of the main equipment of the hybrid energy complex are being entered: PVP, WPP, EESS.

• Formation of the RES generation profile. It is carried out based on data on the location of the object and the specified parameters for the nominal capacities of the PVP, WPP, and EESS. To calculate the generation profiles of solar and wind power plants, the pvlib and windpowerlib python libraries are used, which allow considering the main characteristics of photovoltaic panels with inverters and the parameters of wind turbines.

• Simulation modeling and balance calculation involve calculating the power balances, which include power consumption profiles from the external grid using the obtained RES generation profiles and a given electrical load profile. In the presence of EESS, its optimal management is ensured to reduce power consumption during peak load hours and absorb excess RES generation.

• NPV and LCOE calculation. To assess the energy efficiency of the considered hybrid power supply system, the net present value (NPV) and the levelized cost of electricity (LCOE) are calculated:

$$\mathrm{NPV} = \sum_{n=1}^{N} \frac{CF_n}{(1+i)^n} - \mathrm{CAPEX}, \tag{1}$$

where $CF_n$ – cash flow for the $n$-th tear; CAPEX – capital expenditures; $N$ – duration of the project, years; $i$ – discount rate, which is taken at a level of 7.5 %

In terms of income, the economic model considers the savings achieved by reducing the amount of electricity purchased from the grid, as well as penalties for indirect carbon dioxide emissions into the atmosphere. In terms of expenses, the model considers capital investments in the purchase of equipment and operating expenses, including regular maintenance.

To evaluate the profitability of RES generation, the present value of electricity is calculated. This represents the cost of producing one kilowatt-hour of electricity throughout the entire life cycle of the project:

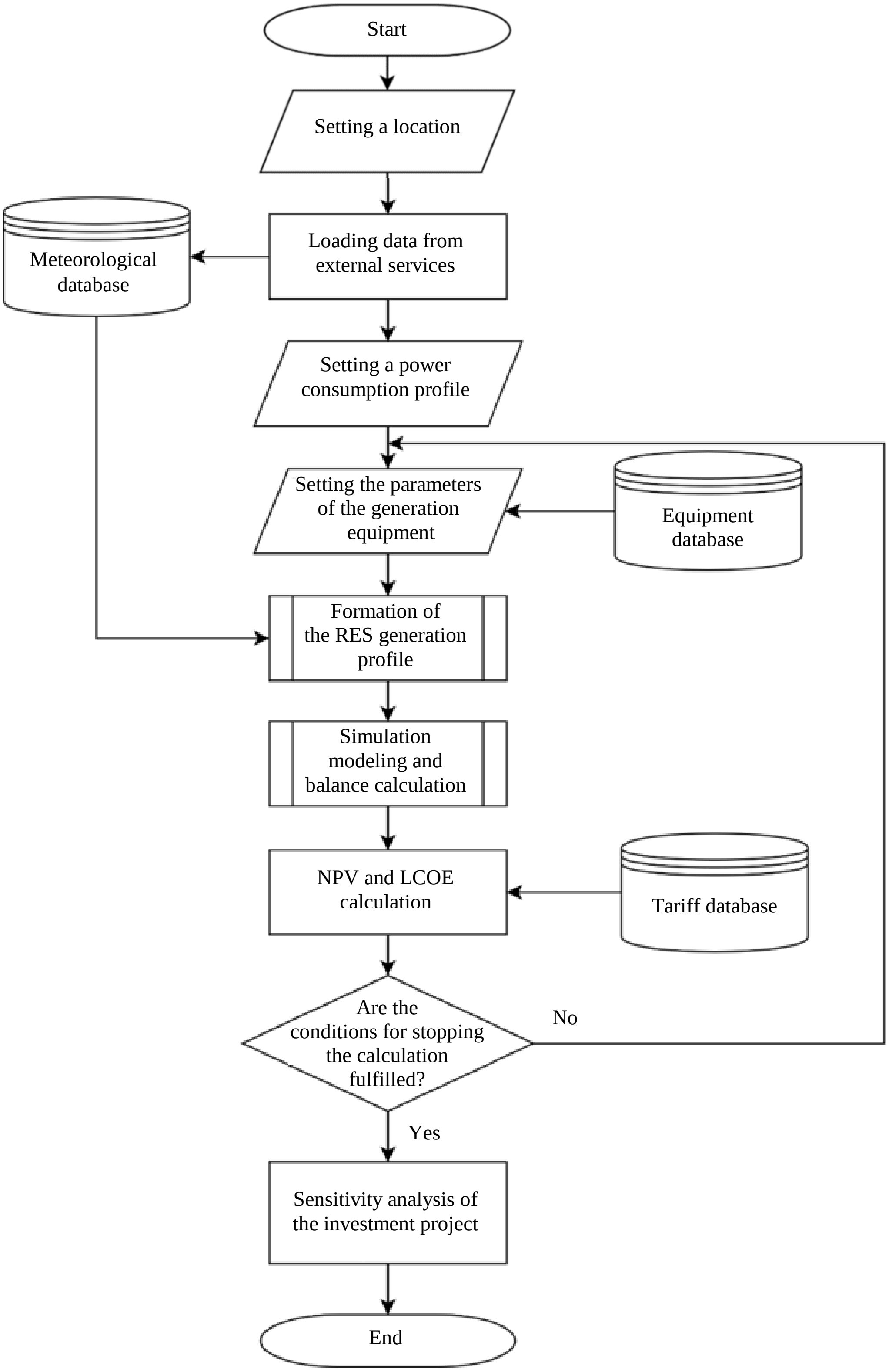


Fig.2. Algorithm for feasibility study of the RES integration at the mining enterprise

$$\mathrm{LCOE} = \frac{\mathrm{EUAC}}{E_{\mathrm{gen}}}, \qquad (2)$$

where EUAC – equivalent uniform annual cost taking into account discount rate, mln rub./year; $E_{\mathrm{gen}}$ – power generation per year, GW·h.

Equivalent uniform annual cost taking into account discounting, is determined by the formula

$$\mathrm{EUAC} = \mathrm{NPC}\frac{i(1+i)^N}{(1+i)^N - 1}, \tag{3}$$

where NPC – net present cost, mln rub.,

$$\mathrm{NPC} = \sum_{t=0}^{N} \frac{\mathrm{OPEX}_n}{(1+i)^n} + \mathrm{CAPEX}, \tag{4}$$

$\mathrm{OPEX}_n$ – operational expenditures in *n*-th year, mln rub.

The reduction in indirect carbon footprint for the year is calculated by the formula (3):

$$\mathrm{CO}_{2\,\mathrm{reduct}} = 1000 EF_{\mathrm{CO_2,\,year}} E_{\mathrm{gen}}, \tag{5}$$

where $EF_{\mathrm{CO_2,\,year}}$ – carbon dioxide emission factor $CO_2$, tonn/MW·h, accepted according to the site of JSC "ATS"[5].

As a condition for stopping the calculation, the condition for maximizing NPV is taken:

$$\max \mathrm{NPV}(P_{\mathrm{PVP}}, P_{\mathrm{WPP}}, P_{\mathrm{EESS}}) \text{ while} \begin{cases} 0 \le P_{\mathrm{PVP}} \le P_{\mathrm{PVPmax}}; \\ 0 \le P_{\mathrm{WPP}} \le P_{\mathrm{WPPmax}}; \\ 0 \le P_{\mathrm{EESS}} \le P_{\mathrm{EESSmax}}, \end{cases} \tag{6}$$

where $P_{\mathrm{PVP}}$, $P_{\mathrm{WPP}}$, $P_{\mathrm{EESS}}$ – installed capacities of the PVP, WPP, and EESS, MW; $P_{\mathrm{PVPmax}}$, $P_{\mathrm{WPPmax}}$, $P_{\mathrm{EESSmax}}$ – maximum values of the installed capacity of the PVP, WPP, and EESS which limit the search area for the optimal solution, MW.

In addition to economic effects, social effects were also calculated. According to the article [35], the potential of PVP to create new jobs is $0.27549 \cdot 10^{-7}$ kW·h/year.

• The sensitivity of the investment project was analyzed by determining the payback period sensitivity to changes in the unit cost of the installed capacity of PVP, WPP, and EESS, the discount rate, and the cost of electric energy and capacity. The developed computer program can be used to select the optimal RES generation configuration at other industrial enterprises.

**Results and discussion.** The research focuses on the power supply system of a coal mine. A time series of hourly power consumption measurements for the year 2020, obtained from a coal mine in the Kemerovo region, was utilized to model electricity consumption. This dataset spans a one-year time period and includes 8,784 measurements. The analysis proceeds under the assumption that such a time series accurately characterizes the profiles of electricity consumption of coal mining enterprises in Russia and undergoes minor changes when evaluating the economic effectiveness of the proposed solutions. The considered mine operates round-the-clock, with an average annual consumption of 8.51 MW. The annual and daily load profiles are shown in Fig.3. According to Fig.3, *a*, it can be observed that the consumption peaks of the coal mine mostly occur in the period after noon, around 20:00 local time. Hourly consumption values during this period can range from 2.6 to 17 MW. There is noticeable cyclicality in the technological process of the coal mine. The most demanding hours are 3-4 am, 12 pm, and 5 pm. The identified intervals of maximum load partially coincide with the peak load hours for wholesale and retail markets, as well as the peak load hour in the respective region of the Russian Federation. According to Fig.3, *b* the mine load has the lowest value during the summer months and the highest consumption during the autumn and spring periods. Seasonal

[5] Carbon dioxide emission factor for the first pricing zone of the UES of Russia (from JSC "ATS" website). URL: https://www.atsenergo.ru/results/CO2 (accessed 05.08.2022). For calculations, the actual value of the $CO_2$ emission factor for 2022 was used, which is 0.348 tonn/MW·h.

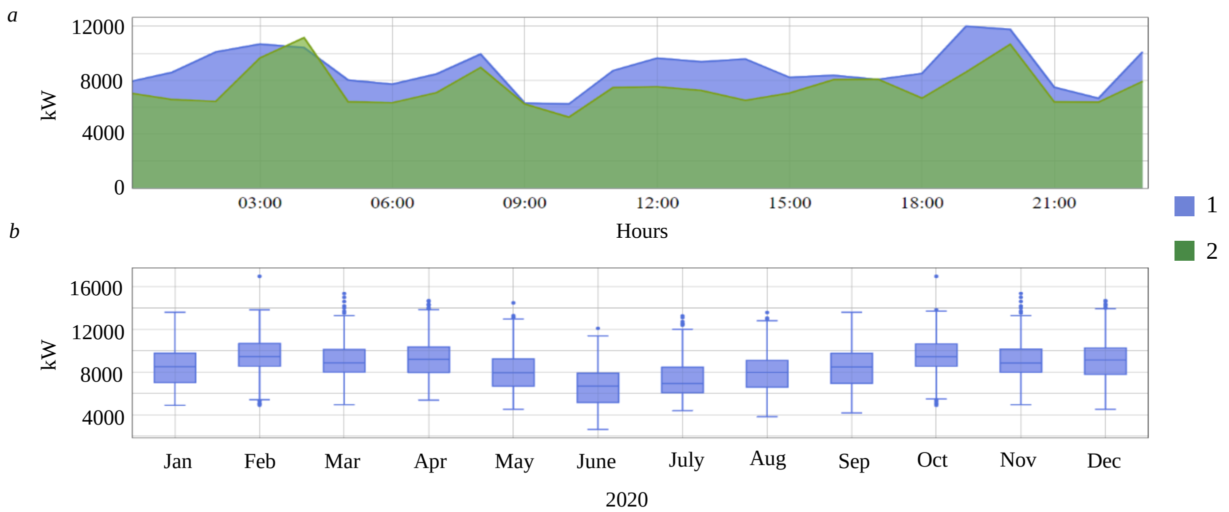


Fig.3. Load patterns of the considered coal mine: *a* – daily profile; *b* – annual profile
1 – winter; 2 – summer

variations in the coal mine consumption amount to approximately 25 %. Further examination of the effectiveness of renewable energy integration is carried out for the main coal mining regions in the Russian Federation.

The annual average values of parameters characterizing the renewable energy potential in coal mining regions are presented in Table 1. The data in Table 1 indicate that the Rostov region has the highest solar energy potential, with the total solar insolation being approximately 25-30 % higher than in the other considered regions. It is worth noting that the highest solar activity is recorded in June, while the lowest is in December. The insolation clearness index varies across the regions, ranging from 0.55 p.u. during the winter months to 0.72 p.u. in the spring period.

*Table 1*

**Average annual values of parameters by region**

| Parameters | Rostov region | Republic Sakha | Kemerovo region | Sakhalin region | Zabaikalsky krai | Primorsky krai | Krasnoyarsk krai | Komi Republic | Republic of Khakassia |
|---|---|---|---|---|---|---|---|---|---|
| Daily global horizontal irradiance (GHI), kW·h/m$^2$ | 3.85 | 2.98 | 3.01 | 3.09 | 3.36 | 3.62 | 2.66 | 2.29 | 3.31 |
| Insolation clearness index, p.u. | 0.66 | 0.66 | 0.66 | 0.69 | 0.72 | 0.7 | 0.66 | 0.61 | 0.68 |
| Wind speed, m/s | 6.80 | 3.66 | 5.57 | 5.26 | 4.89 | 4.54 | 5.52 | 4.76 | 5.25 |

Wind speed values were obtained from the NASA[6] database for a surface height of 50 m. In the considered territories the value of average wind speed during the year varies from 3 to 9 m/s. The highest wind energy potential is in Rostov region with an average annual wind speed of 6.8 m/s, while the lowest is in Sakha Republic with a value of 3.66 m/s, which is 54 % lower. The highest wind speed is observed in winter and spring months.

The most attractive region for the introduction of WPP and PV power plants is Rostov region, which has the greatest potential for wind and solar energy. Further, the installation of RES-based generation only in Rostov region as the most attractive region in terms of RES potential is considered.

Simulation modeling and calculation of balances are carried out. Structural schemes are presented in Fig.4. Specific values of capital and operating costs adopted for simulation modeling were determined as a result of the analysis of the Order of the Ministry of Energy of Russia[7] and are presented in Table 2.

[6] NASA Prediction of Worldwide Energy Resources. URL: https://power.larc.nasa.gov/data-access-viewer/ (accessed 01.03.2023).

[7] The Order of the Ministry of Energy of Russia N 146 dated 28.02.2022 "On approval of the scheme and program for the development of the unified energy system of Russia for 2022-2028".

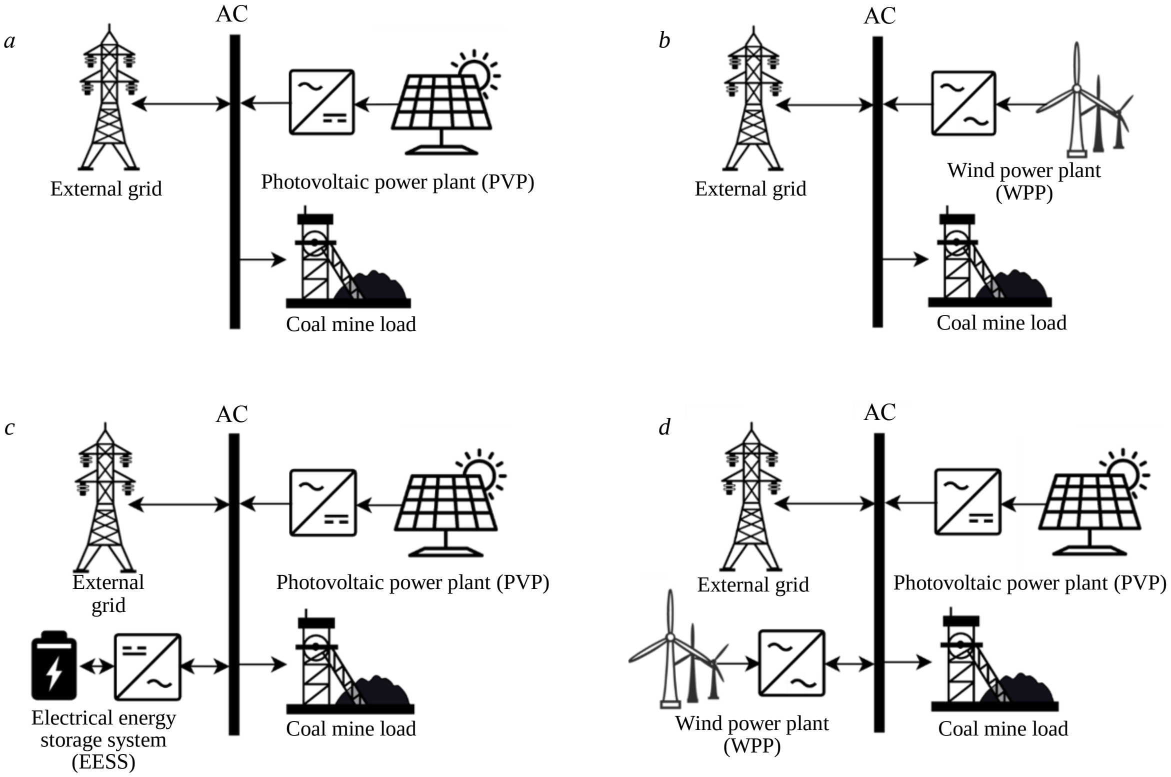


Fig.4. Considered variants of the hybrid energy system: *a* – solar generation; *b* – wind generation; *c* – solar generation and EESS; *d* – solar generation and wind generation

*Table 2*

**Specific values of capital and operating costs**

| Component of hybrid energy system | PVP | WPP | EESS |
|---|---|---|---|
| CAPEX[8] | 800 $/kW/ 61850 rub./kW | 2000 $/kW/ 154650 rub./kW | 800 $/kW·h/ 61850 rub./kW |
| OPEX for the year | 23 $/kW/ 1778 rub./kW | 100 $/kW/ 7732 rub./kW | 12 $/kW/ 928 rub./kW |

To select the installed capacity of solar panels, we used the method of coordinate descent [36] – a gradual decrease in the installed capacity of PVP, starting from a value equal to the peak consumption of the coal mine under consideration. At the same time, the library pvlib was used to select the required number of solar panels and inverters. The criterion for optimization was the net discounted income for 10 years (6). In the process of searching for the optimal configuration, it was found that the optimal installed capacity of PVP plant for the Rostov region is 8 MW (51040 polycrystalline solar panels ET-P660255WWAC from ET Solar Industry with a capacity of 255 W and a size of 1640×992 mm) with an area of 15 hectares. Figure 5 shows the energy balance graph of the coal mine during the period of maximum solar generation. The selection of the installed capacity of WPP was performed in the same way. The optimal option was the installation of one E-53/800 wind turbine with a total installed capacity of 0.8 MW. In the case of EESS and PVP plant implementation, the value of installed capacity of PVP plant determined in the first scenario was taken as the initial capacity for PVP plant. In this case, the accumulator was used for price arbitrage and absorption of excess solar generation during peak hours of solar activity with the purpose of further discharge during peak load hours. Figure 6 shows a graph of the EESS operation. The data in the figure shows that he storage device is charged during the solar maximum hours, the discharge takes in the hour with

[8] The exchange rate used in the calculations is 77.32 rub./dol.

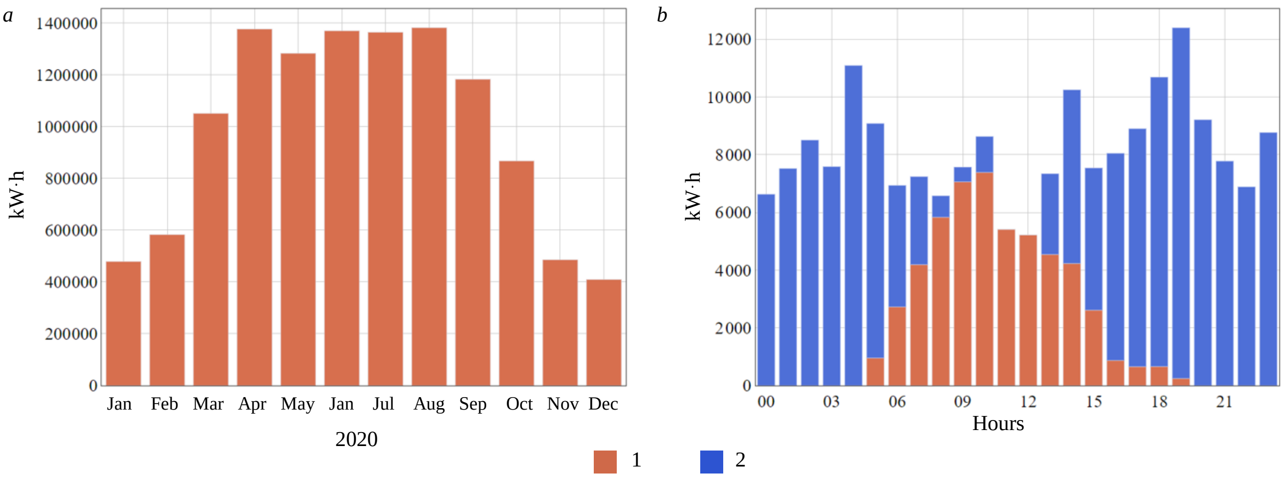


Fig.5. Seasonal (*a*) and daily (*b*) profile of solar generation with an installed capacity of 8 MW in the Rostov region
1 – solar generation; 2 – consumption from the external network

the sign of peak hour to get additional effect. Table 3 shows the comparison of the considered options. The LCOE value ranges from 0.07 to 0.1 $/ kW·h (from 5.41 to 7.73 rub./kW·h), which is higher than the world level, which is 0.048 $/kW·h according to IRENA[9] in 2021. The analyzed alternatives do not yield a return on investment within the 20-year study period, primarily due to the low cost of electricity and nominal penalties for $CO_2$ emissions (16 rub. per 1 ton of $CO_2$).

The sensitivity analysis of the investment project is given for the considered case for the implementation of EESS and PVP in the Rostov region. Since the greatest impact on the NPC has the unit cost of PVP and EESS, and the income values depend on the cost of $CO_2$ emission quotas and electricity tariffs, the parameters and values presented in Table 4 were taken for calculations.

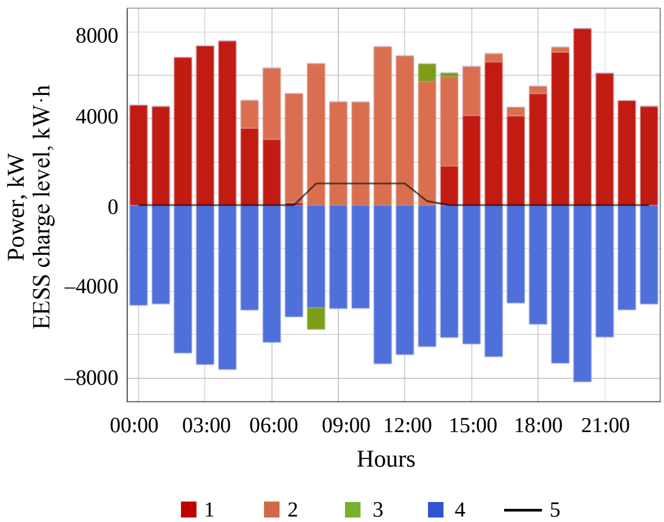


Fig.6. Daily operation profile of a hybrid PSS with WPP of an installed capacity of 9 MW and an EESS with a nominal energy capacity of 1 MW·h
1 – consumption from the external grid;
2 – solar generation; 3 – EESS; 4 – load; 5 – EESS charge level

*Table 3*

**Comparison of RES implementation options for Rostov region**

| Parameter | PVP 8 MW | WPP 0.8 MW | PVP 9 MW + + EESS 1 MW·h | PVP 8 MW + + WPP 0.8 MW |
|---|---|---|---|---|
| Electrical energy production, GW·h | 11.82 | 2.42 | 13.32 | 14.18 |
| Share of RES, % | 18.84 | 3.35 | 21.71 | 23.47 |
| NPC, million rub. | 639.56 | 187.48 | 790.52 | 827.04 |
| NPV for 20 years, million rub. | –14.35 | –61.21 | –85.69 | –78.8 |
| LCOE, rub./kW·h/$/kW·h | 5.11/0.066 | 7.32/0.093 | 5.60/0.071 | 5.51/0.07 |
| $CO_2$ emissions, kt | 22.97 | 26.41 | 22.46 | 22.11 |
| $CO_2$ emissions reduction, kt | 4.33 | 0.89 | 4.88 | 5.19 |
| Employment creation (for the project lifespan) | 9.77 | 2.00 | 11.01 | 11.72 |

[9] Renewable Power Generation Costs in 2021. URL: https://www.irena.org/publications/2022/Jul/Renewable-Power-Generation-Costs-in-2021 (accessed 01.04.2023).

*Table 4*

**Researched parameters in the sensitivity analysis of the investment project**

| Parameter | Value | Researched effect |
|---|---|---|
| PVP unit cost ratio, p.u. | 0.3-1.3 | NPC, LCOE |
| EESS unit cost ratio, p.u. | 0.3-1.3 | NPC, LCOE |
| Electrical power and energy tariffs, p.u. | 1-5 | NPV, DPP |
| $CO_2$ emissions quotas, $/t/rub./t | 0-100/0-7732 | NPV, DPP |

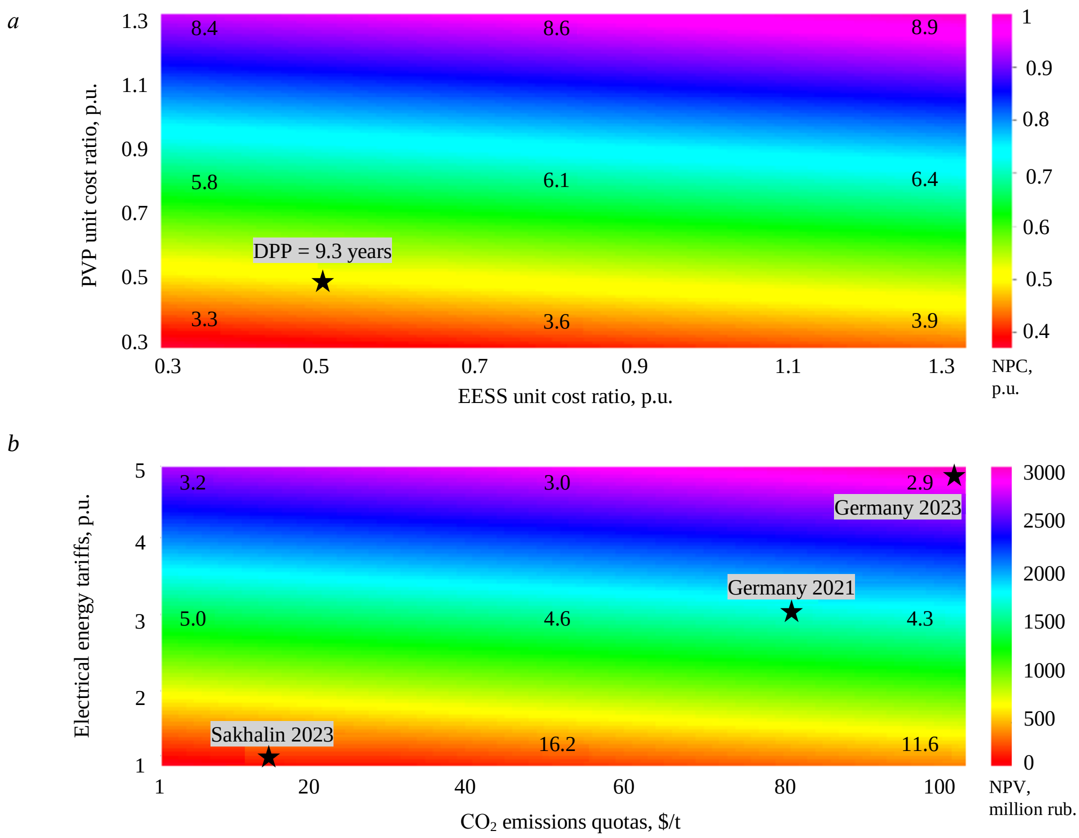


Fig.7. Sensitivity analysis of investment project results: *a* – PVP and EESS unit cost ratio impact on NPC and LCOE (LCOE values is shown on top of the figure); *b* – $CO_2$ emissions quotas (NPC – const) and electrical power and energy tariffs impact on NPV and DPP (DPP values is shown on top of the figure)

According to calculations, the unit cost of RES and EESS has decreased significantly over the past 10 years. Figure 7, *a* shows the effect of changing capital costs and LCOE in relation to current conditions.

The data in Fig.7, *a* show that the LCOE and NPC values can be reduced by up to 50 % if the unit costs of PVP and EESS are reduced by 70 %. It should be noted that in the Russian Federation the unit cost of renewable energy generation is 2-4 times higher than the world average, which creates significant barriers to the implementation of such projects. However, even a two-fold reduction in prices will reduce the payback period only to 9 years.

The cost of electricity and the cost of quotas impact on emissions is shown in Fig.7, *b*.

According to Fig.7, *b*, with an increase in the cost of emission quotas to the European level (80-100 $/t $CO_2$/6186-7732 rub./t $CO_2$), the level of investment attractiveness of the project (DPP) remains insufficient (≈11 years). In the case of setting the cost of quotas for $CO_2$ emissions equal to the values in the Sakhalin experiment (1000 rub. ≈ 12.8 $/t $CO_2$) of limiting greenhouse gas emissions[10], the payback period is reduced to only 18 years, which also remains unacceptable. It should be noted that tariffs for electric energy and power have the greatest impact on the payback period of such projects. Project does not pay off with the current tariff values. With electricity tariffs at the level of prices for industrial consumers in Germany in 2021[11] (0.21 \$/kW·h/16.24 rub./kW·h), the payback period is reduced to 4.5 years. With the current electricity price level (0.4 \$/kW·h/ 30.93 rub./kW·h in 2023), conditions are becoming even more favorable in Germany, which is helping to accelerate the development of renewable energy. In Russia, such conditions have not been created at the moment, and a renewable energy sources capacity delivery agreements is not designed to support industrial consumers. Thus, even in the context of the creation of a market for $CO_2$ emissions quotas and pricing at the level of the Sakhalin experiment, renewable energy at enterprises of the mineral resource complex in Russia remains unattractive and requires additional support.

**Conclusions.** Global goals to achieve carbon neutrality create new challenges for Russian enterprises of mineral resource complex. At the same time, additional problems arise that increase social tension, in particular, the reduction of jobs employed at coal mining enterprises, and, as a result, active depopulation and a decrease in the standard of living of single-industry towns. One of the options for solving the above problems is the introduction of RES. To evaluate the feasibility of this approach, the authors analyzed the RES potential of nine coal-mining regions of Russia and selected the Rostov region for further investigation. To assess the prospects for the introduction of renewable energy sources, the author's computer program was used, which allows modeling electric power balances when implementing RES generation. In further studies, it is planned to perform a feasibility study on the creation of a hydrogen cluster based on the infrastructure of a coal mine.

The presented study is important from the perspective of the climate agenda and achieving carbon neutrality in the Russian Federation by 2060. It shows that in the conditions of the Russian electricity and capacity market, even if a market for $CO_2$ emissions is created, additional funding will be required for projects to introduce RES at enterprises of MRC to ensure their payback. Thus, according to the authors' opinion, it is advisable to develop measures of state support for the decarbonization of enterprises of mineral resource complex to stimulate projects for their "greening".

The effectiveness of RES implementation also depends on the daily electrical load profile. In cases where power consumption and generation peaks do not align (and grid output restrictions exist), EESS are necessary to correct the RES generation profile and prevent the limitation of generated power. This requirement increases investments in the hybrid energy complex and extends its payback period. However, in the considered case of the implementation of a hybrid energy complex at a 24/7 operation enterprise, the entire potential of solar generation is utilized as there is no reduction in power consumption during peak solar activity hours.

**REFERENCES**

1. Faterina A.A. Ways to Ensure Economic and Energy Security During Decarbonization of Russian Economy. *Public Administration*. *E-journal.* 2022. Iss. 95, p. 41-52 (in Russian). DOI: 10.24412/2070-1381-2022-95-41-52

2. Plakitkina L.S., Plakitkin Yu.A., Dyachenko K.I. Decarbonization of economy as a factor of influence on the development of coal industry of the world and Russia. *Chernaya metallurgiya. Ferrous metallurgy. Bulletin of scientific, technical and economic information.* 2021. Vol. 77. N 8, p. 902-912 (in Russian). DOI: 10.32339/0135-5910-2021-8-902-912

3. Zonova O.V., Sheveleva O.B., Slesarenko E.V. Trends in the development of the coal industry in the face of external shocks. *Ugol*. 2023. N 2, p. 26-30 (in Russian). DOI: 10.18796/0041-5790-2023-2-26-30

[10] Federal Law N 34-FZ dated 06.03.2022 "On Conducting an Experiment to Limit Greenhouse Gas Emissions in Certain Federal Subjects of the Russian Federation".

[11] Industrial electricity prices including tax Germany 1998-2022. URL: https://www.statista.com/statistics/1050448/industrial-electricity-prices-including-tax-germany/ (accessed 02.04.2023).

4. Nepsha F., Belyaevsky R., Efremenko V., Varnavskiy K. Modern Problems of Increasing Coal Mines Power Supply Efficiency. E3S Web of Conferences. 2019. Vol. 105. N 03026. DOI: 10.1051/e3sconf/201910503026

5. Varnavskiy K.A., Nepsha F.S., Kostomarov R.V., Qingguang Chen. Business Diversification of Coal Mining Enterprises Based on the Development of Coal Mine Methane Utilization Infrastructure. IEEE International Multi-Conference on Engineering, Computer and Information Sciences (SIBIRCON), 11-13 November 2022, Ekaterinburg, Russian Federation. IEEE, 2022, p. 2060-2063. DOI: 10.1109/SIBIRCON56155.2022.10016919

6. Smirnova A., Varnavskiy K., Nepsha F. et al. The Development of Coal Mine Methane Utilization Infrastructure within the Framework of the Concept "Coal-Energy-Information". *Energies*. 2022. Vol. 15. Iss. 23. N 8948. DOI: 10.3390/en15238948

7. Abramovich B.N., Sychev Yu.A., Ustinov D.A. et al. Efficiency of distributed energy in the conditions of the mineral resource complex. *Promyshlennaya energetika*. 2019. N 5, p. 8-16 (in Russian).

8. Igogo T., Awuah-Offei K., Newman A. et al. Integrating renewable energy into mining operations: Opportunities, challenges, and enabling approaches. *Applied Energy*. 2021. Vol. 300. N 117375. DOI: 10.1016/j.apenergy.2021.117375

9. Ampah J.D., Chao Jin, Agyekum E.B. et al. Performance analysis and socio-enviro-economic feasibility study of a new hybrid energy system-based decarbonization approach for coal mine sites. *Science of the Total Environment*. 2023. Vol. 854. N 158820. DOI: 10.1016/j.scitotenv.2022.158820

10. Nepsha F.S., Voronin V.A., Liven A.S., Korneev A.S. Feasibility study of using cogeneration plants at Kuzbass coal mines. *Journal of Mining Institute.* 2023. Vol. 259, p. 141-150. DOI: 10.31897/PMI.2023.2

11. Schulz J., Scharmer V.M., Zaeh M.F. Energy self-sufficient manufacturing systems – integration of renewable and decentralized energy generation systems. *Procedia Manufacturing*. 2020. Vol. 43, p. 40-47. DOI: 10.1016/j.promfg.2020.02.105

12. Beier J., Thiede S., Herrmann C. Energy flexibility of manufacturing systems for variable renewable energy supply integration: Real-time control method and simulation. *Journal of Cleaner Production*. 2017. Vol. 141, p. 648-661. DOI: 10.1016/j.jclepro.2016.09.040

13. Lebedeva M.A., Idiyatullina E.F., Chuhlatyj M.S., Nabokov A.V. The feasibility of using renewable energy in industrial enterprises. *Engineering journal of Don.* 2019. N 9, p. 1-9 (in Russian).

14. Islam M.M., Zeyi Sun. Onsite generation system sizing for manufacturing plant considering renewable sources towards sustainability. *Sustainable Energy Technologies and Assessments*. 2019. Vol. 32, p. 1-18. DOI: 10.1016/j.seta.2019.01.004

15. Jinze Li, Pei Liu, Zheng Li. Optimal design of a hybrid renewable energy system with grid connection and comparison of techno-economic performances with an off-grid system: A case study of West China. *Computers & Chemical Engineering*. 2022. Vol. 159. N 107657. DOI: 10.1016/j.compchemeng.2022.107657

16. Abramovich B.N., Belskii A.A. Selecting parameters of wind and diesel power plant for power supply of mining intallations. *Journal of Mining Institute.* 2012. Vol. 195, p. 227-230 (in Russian).

17. Bogdanov I.A., Veprikov A.A., Kasyanova A.N., Morenov V.A. Increase of energy efficiency of electrotechnical complexes of cogeneration plants for power supply of objects of oil and gas enterprises. *International Research Journal.* 2017. N 12-5 (66), p. 59-63 (in Russian). DOI: 10.23670/IRJ.2017.66.144

18. Renbo Gao, Fei Wu, Quanle Zou, Jie Chen. Optimal dispatching of wind-PV-mine pumped storage power station: A case study in Lingxin Coal Mine in Ningxia Province, China. *Energy*. 2022. Vol. 243. N 123061. DOI: 10.1016/j.energy.2021.123061

19. Menéndez J., Loredo J., Galdo M., Fernández-Oro J.M. Energy storage in underground coal mines in NW Spain: Assessment of an underground lower water reservoir and preliminary energy balance. *Renewable Energy*. 2019. Vol. 134, p. 1381-1391. DOI: 10.1016/j.renene.2018.09.042

20. Menéndez J., Ordónez A., Fernández-Oro J.M. et al. Feasibility analysis of using mine water from abandoned coal mines in Spain for heating and cooling of buildings. *Renewable Energy*. 2020. Vol. 146, p. 1166-1176. DOI: 10.1016/j.renene.2019.07.054

21. Yao Tao, Xu Luo, Jianli Zhou et al. Site selection for underground pumped storage plant using abandoned coal mine through a hybrid multi-criteria decision-making framework under the fuzzy environment: A case in China. *Journal of Energy Storage*. 2022. Vol. 56. Part A. N 105957. DOI: 10.1016/j.est.2022.105957

22. Pujades E., Jurado A., Orban P., Dassargues A. Parametric assessment of hydrochemical changes associated to underground pumped hydropower storage. *Science of the Total Environment*. 2019. Vol. 659, p. 599-611. DOI: 10.1016/j.scitotenv.2018.12.103

23. Strazzabosco A., Gruenhagen J.H., Cox S. A review of renewable energy practices in the Australian mining industry. *Renewable Energy*. 2022. Vol. 187, p. 135-143. DOI: 10.1016/j.renene.2022.01.021

24. Maregedze L., Chingosho H., Madiye L. Use and cost optimization for underground mines electrical energy: A case of a mine in Zvishavane. *Energy*. 2022. Vol. 247. N 123374. DOI: 10.1016/j.energy.2022.123374

25. Hejuan Hu, Xiaoyan Sun, Bo Zeng et al. Enhanced evolutionary multi-objective optimization-based dispatch of coal mine integrated energy system with flexible load. *Applied Energy*. 2022. Vol. 307. N 118130. DOI: 10.1016/j.apenergy.2021.118130

26. Hongxu Huang, Rui Liang, Chaoxian Lv et al. Two-stage robust stochastic scheduling for energy recovery in coal mine integrated energy system. *Applied Energy*. 2021. Vol. 290. N 116759. DOI: 10.1016/j.apenergy.2021.116759

27. Qin C., Loth E. Isothermal compressed wind energy storage using abandoned oil/gas wells or coal mines. *Applied Energy*. 2021. Vol. 292. N 116867. DOI: 10.1016/j.apenergy.2021.116867

28. Limanskiy A.V., Vasilyeva M.A. Using of low-grade heat mine water as a renewable source of energy in coal-mining regions. *Ecological Engineering*. 2016. Vol. 91, p. 41-43. DOI: 10.1016/j.ecoleng.2016.02.008

29. Menéndez J., Ordóñez A., Álvarez R., Loredo J. Energy from closed mines: Underground energy storage and geothermal applications. *Renewable and Sustainable Energy Reviews*. 2019. Vol. 108, p. 498-512. DOI: 10.1016/j.rser.2019.04.007

30. Ting Bao, Meldrum J., Green C. et al. Geothermal energy recovery from deep flooded copper mines for heating. *Energy Conversion and Management*. 2019. Vol. 183, p. 604-616. DOI: 10.1016/j.enconman.2019.01.007

31. Burnside N.M., Banks D., Boyce A.J., Athresh A. Hydrochemistry and stable isotopes as tools for understanding the sustainability of minewater geothermal energy production from a 'standing column' heat pump system: Markham Colliery, Bolsover, Derbyshire, UK. *International Journal of Coal Geology*. 2016. Vol. 165, p. 223-230. DOI: 10.1016/j.coal.2016.08.021

32. Shklyarskiy Ya.E., Batueva D.E. Operation mode selection algorithm development of a wind-diesel power plant supply complex. *Journal of Mining Institute.* 2022. Vol. 253, p. 115-126. DOI: 10.31897/PMI.2022.7

33. Sinha S., Chandel S.S. Review of software tools for hybrid renewable energy systems. *Renewable and Sustainable Energy Reviews*. 2014. Vol. 32, p. 192-205. DOI: 10.1016/j.rser.2014.01.035

34. Thirunavukkarasu M., Sawle Y. An Examination of the Techno-Economic Viability of Hybrid Grid-Integrated and Stand-Alone Generation Systems for an Indian Tea Plant. *Frontiers in Energy Research*. 2022. Vol. 10. N 806870. DOI: 10.3389/fenrg.2022.806870

35. Chauhan A., Saini R.P. Techno-economic feasibility study on Integrated Renewable Energy System for an isolated community of India. *Renewable and Sustainable Energy Reviews*. 2016. Vol. 59, p. 388-405. DOI: 10.1016/j.rser.2015.12.290

36. Bagherian M.A., Mehranzamir K., Pour A.B. et al. Classification and Analysis of Optimization Techniques for Integrated Energy Systems Utilizing Renewable Energy Sources: A Review for CHP and CCHP Systems. *Processes*. 2021. Vol. 9. Iss. 2. N 339. DOI: 10.3390/pr9020339

***Authors*: Fedor S. Nepsha,** *Candidate of Engineering Sciences, Senior Researcher, Associate Professor, nepshafs@kuzstu.ru, https://orcid.org/0000-0002-7468-2548* (*T.F.Gorbachev Kuzbass State Technical University, Kemerovo, Russia*; *National University of Oil and Gas* "*Gubkin University*", *Moscow, Russia*), **Kirill A. Varnavskiy,** *Doctor of Philosophy, Head of Laboratory, https://orcid.org/0000-0001-7116-8765* (*T.F.Gorbachev Kuzbass State Technical University, Kemerovo, Russia*), **Vyacheslav A. Voronin,** *Candidate of Engineering Sciences, Senior Researcher, https://orcid.org/0000-0002-7242-9100* (*T.F.Gorbachev Kuzbass State Technical University, Kemerovo, Russia*), **Ilya S. Zaslavskiy,** *Technician, https://orcid.org/0000-0001-9226-6022* (*T.F.Gorbachev Kuzbass State Technical University, Kemerovo, Russia*), **Andrey S. Liven,** *Technician, https://orcid.org/0000-0001-9138-6858* (*T.F.Gorbachev Kuzbass State Technical University, Kemerovo, Russia*).

*The authors declare no conflict of interests.*

ISSN 2411-3336; e-ISSN 2541-9404

JOURNAL OF MINING INSTITUTE

Zapiski Gornogo instituta

Journal homepage: pmi.spmi.ru

Research article

# Increasing the energy efficiency of an autonomous power supply system of a drilling rig in case of voltage dips

**Sergey S. CHERVONCHENKO✉, Vladimir Ya. FROLOV**

*Peter the Great St. Petersburg Polytechnic University, Saint Petersburg, Russia*

***How to cite this article*:** Chervonchenko S.S., Frolov V.Ya. Increasing the energy efficiency of an autonomous power supply system of a drilling rig in case of voltage dips. Journal of Mining Institute. 2023. Vol. 261, p. 470-478. EDN MGAPVA

***Abstract*.** The article discusses the emergency modes of operation of an autonomous electrical complex of a drilling rig. The concept of voltage failure and its influence on the technological process of industrial enterprises is revealed. A description of the methods used in the power supply of industrial enterprises to overcome voltage dips and load surges in autonomous power systems is presented, from which it is possible to single out the accelerated lifting of critical equipment to prevent emergency conditions, as well as the use of backup storage, usually batteries. An algorithm has been developed for the interaction of the battery and the diesel generator set as backup power sources during various modes of operation of the electric motor, taking into account load surges, which allows successfully overcoming voltage dips in the system both in transient and in steady state. It is proposed to use a combined method to eliminate the voltage dip, a feature of which is the use of a combined structure of backup power sources as part of a diesel generator set and a battery, acting on the base of the proposed interaction algorithm in autonomous electrical complexes. The method makes it possible to overcome sudden load surges and voltage dips caused by a shortage of reserve power in the electrical system. The use of a rechargeable battery as a transitional element makes it possible to switch between the main and backup power sources without stopping the technological one and to expand the overload threshold of an autonomous electrical complex up to 60 %. The use of the combined method increases the energy efficiency of the autonomous complex due to a reduction in the number of emergency shutdowns of equipment, process interruptions and additional power consumption.

***Keywords*:** energy efficiency; voltage dip; generator; drilling rig; backup power

***Acknowledgment.*** The results of the study were obtained with the financial support of the Ministry of Science and Higher Education of the Russian Federation under the project FSEG-2023-0012.

***Received: 12.03.2023*** ***Accepted: 20.06.2023*** ***Online: 19.07.2023*** ***Published: 19.07.2023***

**Introduction.** Autonomous power supply systems of high power, remote from high-voltage electrical networks, are powered mainly from autonomous power plants with two diesel generator sets, one of which is the main one, and the other is a backup source [1-3]. The use of autonomous electrical complexes is widespread in the regions of the Far East and the Far North, where, for economic and technical reasons, it is difficult to carry out a centralized power supply. Remote isolated energy regions account for 60 % of the territory of the Russian Federation with extensive mineral reserves: 70 % of oil, 90 % of natural gas, 90 % of precious metals and stones. In isolated areas, the total number of generation sources is about 5,000 with a total capacity of about 2,500 MW.

Autonomous electrical complexes are divided according to the following features [4].

• Purpose and nature of consumers: for use in the power supply of the main technological consumers (industrial production, etc.); to provide power supply for the auxiliary needs of industrial facilities (industrial and domestic needs).

• According to the mode of operation: the main ones are power complexes with an operating time per year of more than 3000 hours, with a number of starts per year of less than 20, a continuous operation time of more than 350 hours, a start-up and acceptance time of 100 % load up to 30 minutes; reserve – power complexes with an operating time per year from 200 to 3000 hours, the number of starts from 20 to 50 and the time of starting and receiving 100 % of the load is not more than 5 minutes; emergency ones are power complexes with an operating time per year up to 200 hours, the number of starts per year over 50 and the time of starting and receiving 100 % of the load from 5 to 30 seconds. Emergency power complexes are used for emergency power supply to consumers of the first category and the first category of a special group, for which a break in power supply is allowed only for the duration of the ATS, when the main or backup power source is turned off.

• By type of prime movers: diesel; gas piston; gas turbine; microturbine; combined with renewable energy sources.

In systems with low load power, the backup power source is usually the battery [5]. In such isolated systems, special attention should paid to the indicators of the quality of electricity, on which the operability, reliability and efficiency of the equipment depend [6].

Voltage dip according to GOST 32144-2013 is a decrease in voltage in the electrical network below the threshold value of 0.9 to a minimum of 0.1 of the nominal voltage value. It is characterized by such parameters as the depth of the dip and its duration [7, 8]. After a voltage dip after a time interval of 10 ms, the voltage should be restored to a value of 90 % or more of the nominal value. A voltage dip below 0.1 of the nominal voltage for a certain period of time is a short-term power interruption. However, failures are the most critical emergency violations that lead to shutdowns, overload and failure of the electrical equipment of generators and consumers of electricity.

Due to short electrical connections, the lack of power maneuverability, as well as a small power reserve, autonomous power supply systems are sensitive to voltage dips. In addition, the performance of energy complexes is greatly affected by a high level of insulation pollution in industries with the stage of crushing/grinding ore, unauthorized contact with live parts with objects, errors in operational maintenance of personnel, natural factors, for example, lightning strikes. Starting high-power asynchronous electric motors with a squirrel-cage rotor leads to a decrease in frequency and, accordingly, voltage dips in isolated electrical networks, which has a direct impact on the operation of other consumers [9]. When the voltage in the electrical network decreases below the level allowed by GOST, it is possible to turn off the protection for the minimum voltage of the contactors of electric motors [10]. At the same time, which is relevant for the mining industry, voltage dips can occur due to various emergencies due to the peculiarities of the operation of electrical complexes, such as equipment jamming during drilling, etc. [11]. A voltage dip can also be caused by the onset and end of a short circuit or a sharp increase in the value of the flowing current in the electrical system or electrical installation connected to the mains, as well as disconnection of power supplies [12, 13].

For autonomous electrical complexes, there are three main causes of voltage dips: emergency shutdown of power supplies; a sharp increase in load caused by external technological circumstances; short circuits in the system.

Drill tool sticking is quite common during well drilling. One of the reasons leading to stuck drill strings is a voltage dip and inability to overcome the stick, and the subsequent power outage. To overcome these emergency modes, which account for a significant percentage of the total number of emergencies, a significant amount of time (at least 4 hours) and free reserve capacities in an isolated electrical network are required. To compensate for the negative impact of voltage dips on the continuous technological processes of industrial enterprises in the mining industry and to improve the reliability and stability of isolated power supply networks, it is necessary to develop integrated protection methods that take into account various disturbances in the power systems of electric drives of drilling rigs [14, 15].

The main difficulties in solving the problems of power supply for remote autonomous power supply systems of industrial enterprises are the remote location of mineral deposits from centralized power systems, the distributed location of production facilities within one mining and processing plant (up to 10 km), and a continuous technological process, the violation of which leads to significant economic costs for the enterprise [16].

An analysis of the literature and practical experience of various industrial plants in eliminating voltage dips allows us to identify the main and most common methods and devices: energy storage devices (uninterruptible power supplies, batteries), active filter, static compensator (STATCOM), boost converter and flywheel [17-19].

In electric drive systems of drilling rigs, in case of voltage dips, the speed of rotation of the drill string decreases, and due to the great depth of earth rocks and a relatively small moment of inertia, an instantaneous (up to 2-3 s) “sticking” of mechanisms. Accordingly, in the conditions of limited receipt of additional power from the external network, the search for ways to overcome voltage dips in isolated systems by using the reserves of existing equipment in a short period is relevant to minimize losses and increase the reliability of power supply to plants [20, 21]. The elimination of each "sticking" requires a restart of the technological process, which takes up to 4 hours and requires a significant consumption of electricity and financial resources [22].

The combined method [23, 24] is applied on the example of a drilling rig installed at a gold deposit in the Magadan region. According to statistics, in 2022 recorded an average of 19 emergency shutdowns at this field for each of the eight drilling rigs. The time of repeated restoration of the technological mode is 4 hours. Taking into account the fact that the capacity of the drilling rig is 500 kW, and the approximate cost of 1 kWh of electricity generated by a diesel generator set (DGS) is 25 rubles, the total annual additional costs for electricity are 7.6 million rubles. Thus, it is obvious that the task of improving the energy efficiency of an autonomous power supply system of a drilling rig in case of voltage dips is of great practical and scientific importance [25].

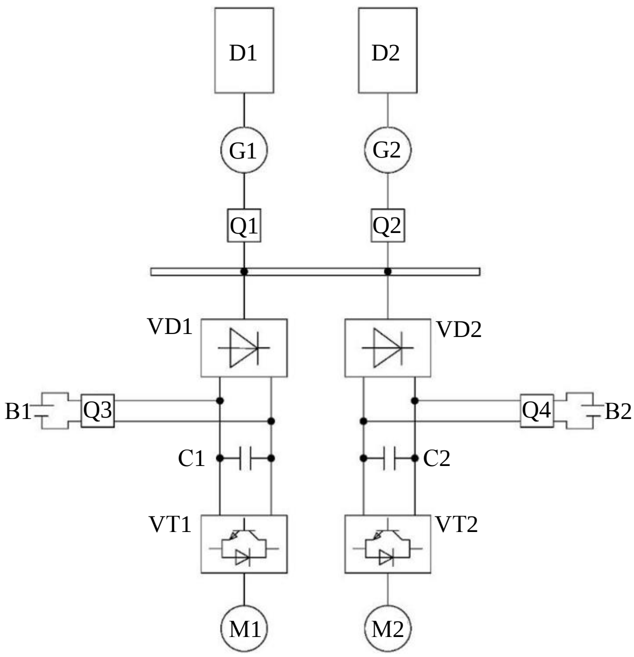


Fig.1. Schematic diagram of autonomous electrical complex (compiled by the authors)

**Methods.** Figure 1 shows a schematic diagram of an autonomous electrical complex, consisting of diesel generators, switches, a frequency converter and asynchronous load motors [26-28]. The diagram (Fig.1) uses the following designations: D1-G1, D2-G2 – diesel generators; Q1, Q2, Q3, Q4 – switching devices; VD1, VD2 – rectifiers as part of the frequency converter; B1, B2 – rechargeable batteries; C1, C2 – capacitors (filters) as part of the frequency converter; VT1, VT2 – controlled igbt-transistors as part of the frequency converter; M1, M2 – load motors.

The drilling rig located at a considerable distance from the main power complex (about 3 km), so the power comes from its own diesel generator set, located in close proximity to the consumer [29]. Uncontrolled rectifiers uses as the DC link of the frequency converter [30, 31].

*Journal of Mining Institute*. 2023. Vol. 261. P. 470-478


In this electrical complex, two-pole asynchronous electric motors with a squirrel-cage rotor 5AMN315M2 with a power of 250 kW are used, the main parameters of which are given below [32]: total electric motor power 284.5 kVA; nominal slip 0.0083 %; rated current of the stator winding 431 A; preliminary active resistance of the stator 0.017 Ohm; rotor active resistance 0.0043 Ohm; critical slip 0.044 %; stator active resistance 0.012 Ohm; stator leakage inductance 0.102 Ohm; inductive resistance of the magnetization circuit 1.968 Ohm; magnetizing circuit inductance 0.0063 H.

The calculated parameters uses for modeling electric motorsin the Simulink software package [33]. The Asynchronous Machine building block is used.

As an additional backup power source in the electrical complex, there are a stationary low-maintenance lead-acid battery (OPzS). The use of this type of battery is due to extensive operating experience, high reliability and low cost compared to other types of batteries, for example, lithium-ion [34].

The battery capacity calculate by the formula

$$C_{\text{B}} \geq \frac{I_{\text{B}} t_{\text{B}}}{K_g K_P}, \quad (1)$$

where $I_{\text{B}}$ is the amount of current consumed by the battery during load, A; $t_{\text{B}}$ is the period of operation of the battery during the load, $t_{\text{B}}$ = 0.5 h, taking into account the features of work and the categorization of consumers; $K_g$ – coefficient of available capacity, $K_g$ = 0.9-1 p.u.; $K_p$ – coefficient of the depth of discharge of the battery, $K_p$ = 0.5-0.7 p.u.

The amount of current drawn from the battery during load

$$I_{\text{B}} = \frac{P_{\text{load}}}{\eta_i U_{\text{B}}}, \quad (2)$$

where $P_{\text{load}}$ is the average value of the load power, W; $\eta_i$ – efficiency of converting direct current into alternating current using an inverter, $\eta_i$ = 0.9-0.95; $U_{\text{B}}$ – nominal voltage of the storage battery, V;

$$I_{\text{B}} = \frac{500000}{0.93 \cdot 380} = 1414.8 \text{ A},$$

$$C_{\text{B}} \geq \frac{1414.8 \cdot 0.5}{0.95 \cdot 0.6} = 1241 \text{ Ah}.$$

The operating time of the battery and, accordingly, the calculated capacity are taken based on the required time to ensure the reliability of power supply, according to the criterion of the probable maximum duration of the voltage dip, taking into account the necessary reserve to eliminate significant load surges.

Based on the calculations (1), (2), for further research of the voltage dip, the nearest value of the battery capacity is selected according to the factory catalogs – 1500 Ah (type 12 OPzS 1500) with the following parameters: voltage of one cell – 2 V; internal resistance – 0.21 mOhm; type – lead-acid; the type of positive electrode is a tubular plate.

The calculation of the required power of diesel generators was carried out in accordance with GOST R 53987-2010, according to which the continuous power of autonomous AC diesel generators is selected with a reserve of 30 % of the installed load power. Installed capacity the installed load power of the autonomous electrical complex is 500 kW from two 5AMN315M2 electric motors with a power of 250 kW. According to GOST R 53987-2010, the calculated power of a diesel generator set must be at least 500·1.3 = 650 kW.

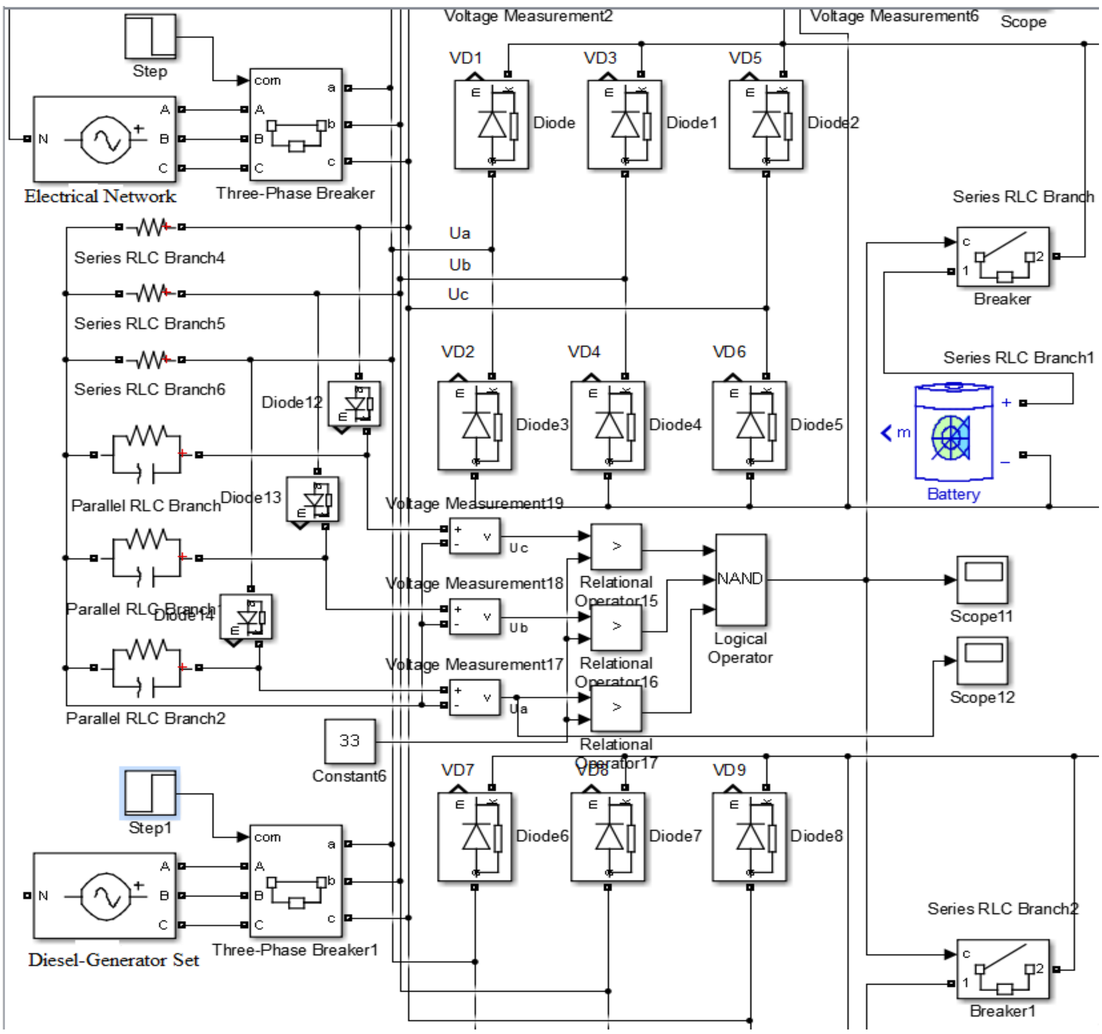


Fig.2. Computer model of the combined composition of backup power sources

Figure 2 shows a computer model of the combined composition of backup power sources (diesel generator set and battery) as part of an autonomous electrical complex of a drilling rig in the Simulink software package.

To ensure reliable power supply and continuity of technological processes, it is proposed to consider the combined operation of various backup power sources by introducing an appropriate algorithm (Fig.3) [35, 36].

The algorithm for the combined method of eliminating voltage dips is as follows: in the steady state operation of electric motors, when powered by one main diesel generator set, there is a sharp increase (surge) in the load on the shaft. For example, for drill strings – stuck in solid underground rocks. Accordingly, when the load is applied, the automatic control system sends two parallel control signals: the first to start the backup diesel generator, which will be ready to receive the load after reaching the nominal speed (approximately 3 s), the second to rapidly connect an additional backup power source – the battery. The task of this battery is to ensure short-term load acceptance together with the main diesel generator by issuing peak power – a seamless transition while maintaining the required level of voltage in the network until acceleration, reaching nominal speed and receiving the load of the backup diesel generator [37]. Then the battery is disconnected, the load distribute between two (main and standby) DGS.

**Journal of Mining Institute.** 2023. Vol. 261. P. 470-478


Computer simulation of the voltage dip process and its elimination is performed using the above-described algorithm for the interaction of a diesel generator set and a battery in the MatLab Simulink software package.

In the process of simulation, the acceleration of electric motors lasts 3 s until the moment of reaching the nominal speed of rotation of time, then there is a sharp increase in the load. According to the algorithm (Fig.3), at the time $t$ = 3 s, the battery connects to network. At the same time, a backup diesel generator set starts from the control action. Further, at the time $t$ = 5 s, power is transferred to the started backup diesel generator set and the operation mode continues until $t$ = 8 s.

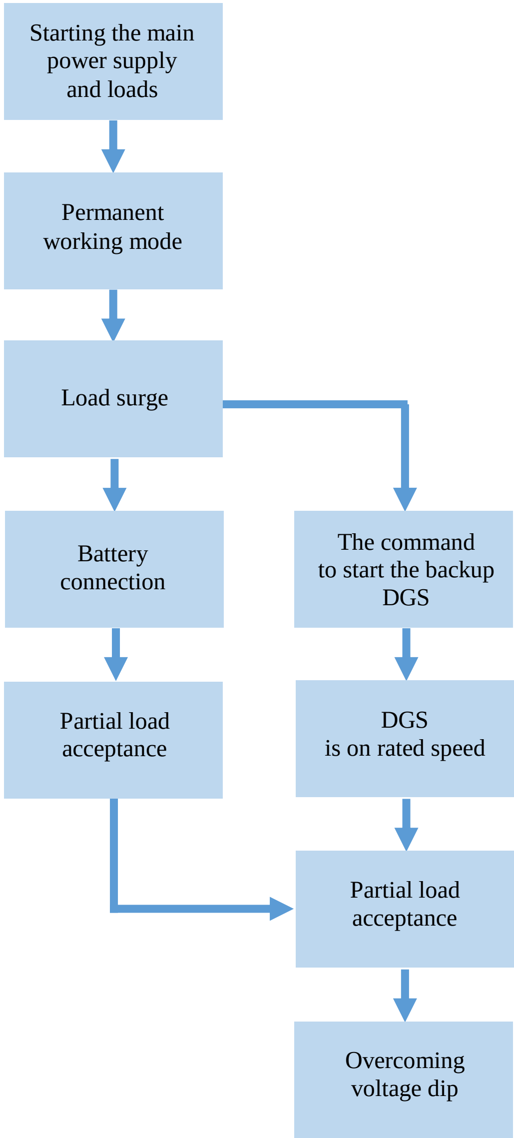


Fig.3. Algorithm for connecting sources of backup power (compiled by the authors)

**The discussion of the results.** Modeling of modes with different values of load surge was carried out. Figure 4 shows graphs for a load surge of 1600 Nm.

During the acceleration of the electric motor, the largest load value is 1000 Nm, accordingly, this value is taken as the rated power of the electric motor.

According to the calculations, with a load surge of 30 %, the operating mode of the electrical system is maintained with a minimum deviation of the voltage value (within the permissible limits according to GOST), while the rotation speed of the electric motor does not decrease. With this load value, the stator current is approximately 1750 A.

The data in Fig.4 show that the combined operation of the proposed composition of backup power sources, namely, the diesel generator set and the storage battery, based on the proposed control algorithm makes it possible to overcome the load surge of 60 % of the rated power of the main diesel generator without interruption of technological processes. Figure 4, *b* shows that when the battery is turned on, the rotation speed of the electric motor is maintained in the allowable range and the required time interval (3 s) for starting, accelerating, and connecting a backup diesel generator set.

Further calculations are performed to study the operating mode at a load surge of 65 and 70 % of the rated power of the system. In this mode, the estimated capacity of the battery is not able to ensure a smooth transfer of the load to the backup diesel generator set, since the battery is discharged in 2 s. In this case, the stator current reaches maximum (starting) values, which indicates an overload of the autonomous electrical complex. In addition, the rotation of the electric motors slows down almost instantly. In this case, according to the standard method, it is necessary to apply an emergency lifting of drilling mechanisms to save equipment and minimize financial costs.

Similar studies have been carried out on the operating modes of an autonomous electrical complex with load surges of various sizes with an increased capacity of a lead-acid battery up to a value of 2500 Ah.

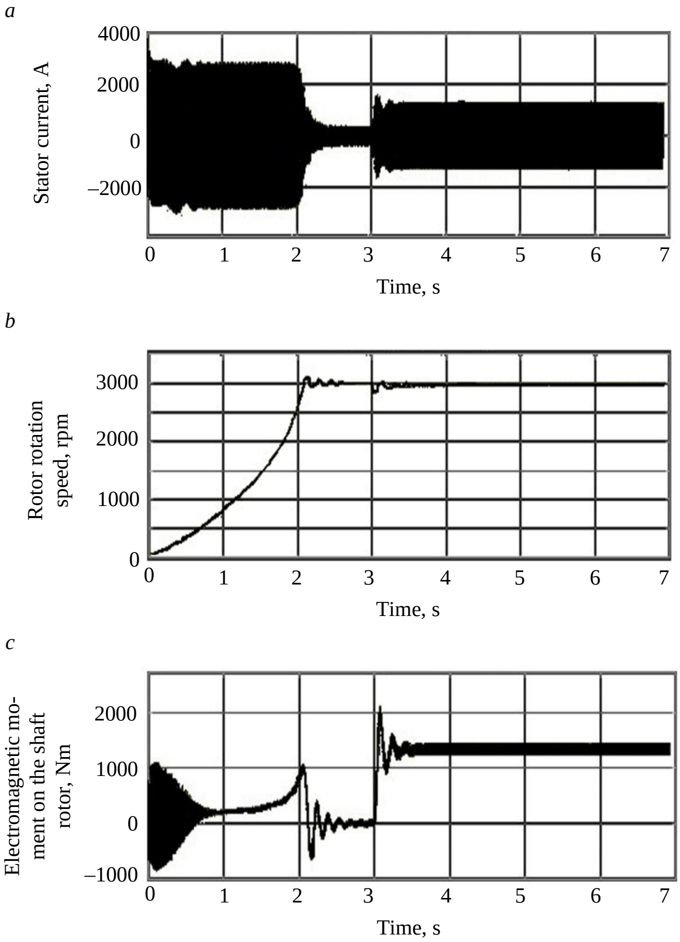


Fig.4. Graphs with a load surge of 1600 Nm:
*a* – stator current, A; *b* – rotor rotation speed, rpm;
*c* – electromagnetic torque on the rotor shaft, Nm

The power system, including the battery, copes with the load surge $T_m$ = = 1650 Nm. The rotation speed of the motors is slightly slowed down, but without affecting the continuous process. Accordingly, with an increase in the capacity of the battery from 1500 to 2500 Ah (by 66 %), the threshold for overload and system performance expands by 3.1 % (from 1600 to 1650 Nm). Compared to the value in accordance with GOST, the overload capacity of the energy complex has increased to 65 %.

Additionally, a mode with a load surge of 70 % ($T_m$ = 1700 Nm) of the nominal value of the diesel generator power was developed. The results show that for a battery with an increased capacity, this load is critical, the electric motors go into a sharp deceleration (rotation speed is 0 rpm in 1.2 s after the load is applied) and the process is not supported.

The results obtained show that with an increase in the capacity of the battery in excess of the calculated value, a significant improvement in the characteristics of an autonomous electrical complex for the ability of the power system to overcome voltage dips is not provided. There is a clear incommensurability of the resources spent on the achieved technical results.

**Conclusion.** As a result of applying the combined structure of backup power sources, acting on the base of the proposed interaction algorithm to overcome the voltage dips that occur in autonomous electrical complexes of drilling rigs, it has been established that the use of a rechargeable battery makes it possible to increase the allowable value of the system overload capacity by 23 % while ensuring the continuity of the technological process and switching between the main and backup diesel generator set in case of voltage dips.

At the same time, an increase in the battery capacity by 66 % relative to the calculated value (from 1500 to 2500 Ah) makes it possible to increase the maximum load surge that the autonomous power supply system can handle in the event of a voltage dip by 3.1 % (from 1600 to 1650 Nm).

It is shown that when using the combined composition of backup power sources together with the interaction algorithm, the number of shutdowns, restarts and, accordingly, additional power consumption decreases. The combined results lead to a reduction in operating costs and an increase in the energy efficiency of the complex.

The study proved that with an increase in the capacity of the battery in excess of the calculated value, a significant improvement in the characteristics of an autonomous electrical complex for the ability of the power system to overcome voltage dips is not provided. This decision leads to increased capital costs without the proper technical and economic effect.

**REFERENCES**

1. Georgilakis P.S., Hatziargyriou N.D. A review of power distribution planning in the modern power systems era: Models, methods and future research. *Electric Power Systems Research*. 2015. Vol. 121, p. 89-100. DOI: 10.1016/j.epsr.2014.12.010

2. Tavares B., Soares F.J. An innovative approach for distribution network reinforcement planning: Using DER flexibility to minimize investment under uncertainty. *Electric Power Systems Research*. 2020. Vol. 183. N 106272. DOI: 10.1016/j.epsr.2020.106272

3. Gouin V., Alvarez-Hérault M.-C., Raison B. Innovative planning method for the construction of electrical distribution network master plans. *Sustainable Energy, Grids and Networks*. 2017. Vol. 10, p. 84-91. DOI: 10.1016/j.segan.2017.03.004

4. Yu Yang, Fan Jinfu, Wang Zhongjie et al. A dynamic ensemble method for residential short-term load forecasting. *Alexandria Engineering Journal*. 2023. Vol. 63, p. 75-88. DOI: 10.1016/j.aej.2022.07.050

5. Bo Yang, Junting Wang, Yixuan Chen et al. Optimal sizing and placement of energy storage system in power grids: A state-of-the-art one-stop handbook. *Journal of Energy Storage*. 2020. Vol. 32. N 101814. DOI: 10.1016/j.est.2020.101814

6. Saneev B.G., Ivanova I.Yu., Tuguzova T.F. Development of renewable energy sector in the Russian east over the first half of the 21st century amidst national trends. *Energy policy*. 2016. Iss. 3, p. 66-73 (in Russian).

7. Shpiganovich A.N., Shpiganovitch A.A., Bogomolov I.I. Voltage sags in power systems. *Izvestiya Tula State University*. 2018. Iss. 12, p. 7-12 (in Russian).

8. Ershov S.V., Pigalov M.S. Analysis of means and methods of limitation of influence voltage fails. *Izvestiya Tula State University*. 2017. Iss. 12-1, p. 95-104 (in Russian).

9. Zarenia O., Salehpour M.J., Ghaedi R., Shafie-Khah M. Markov-Based Reliability Assessment for Distribution Systems Considering Failure Rates. *IEEE Access*. 2023. Vol. 11, p. 10018-10031. DOI: 10.1109/ACCESS.2023.3240778

10. Postigo Marcos F., Domingo C.M., San Román T.G. Improving distribution network resilience through automation, distributed energy resources, and undergrounding. *International Journal of Electrical Power & Energy Systems*. 2022. Vol. 141. N 108116. DOI: 10.1016/j.ijepes.2022.108116

11. Prathapaneni D.R., Detroja K.P. An integrated framework for optimal planning and operation schedule of microgrid under uncertainty. *Sustainable Energy, Grids and Networks*. 2019. Vol. 19. N 100232. DOI: 10.1016/j.segan.2019.100232

12. Besselmann T.J., Cortinovis A., Van de Moortel S. et al. Increasing the Robustness of Large Electric Driven Compressor Systems During Voltage Dips. *IEEE Transactions on Industry Applications*. 2018. Vol. 54. Iss. 2, p. 1460-1468. DOI: 10.1109/TIA.2017.2781638

13. Bagheri A., Bollen M.H.J., Gu I.Y.H. Improved characterization of multi-stage voltage dips based on the space phasor model. *Electric Power Systems Research*. 2018. Vol. 154, p. 319-328. DOI: 10.1016/j.epsr.2017.09.004

14. Rastgou A., Moshtagh J., Bahramara S. Improved harmony search algorithm for electrical distribution network expansion planning in the presence of distributed generators. *Energy*. 2018. Vol. 151, p. 178-202. DOI: 10.1016/j.energy.2018.03.030

15. Kandasamy M., Thangavel R., Arumugam T. et al. Strategic incorporation of DSTATCOM and distributed generations in balanced and unbalanced radial power distribution networks considering time varying loads. *Energy Reports*. 2023. Vol. 9, p. 4345-4359. DOI: 10.1016/j.egyr.2023.03.076

16. Zhukovskiy Yu.L., Kovalchuk M.S., Batueva D.E., Senchilo N.D. Development of an Algorithm for Regulating the Load Schedule of Educational Institutions Based on the Forecast of Electric Consumption within the Framework of Application of the Demand Response. *Sustainability*. 2021. Vol. 13. Iss. 24. N 13801. DOI: 10.3390/su132413801

17. Chervonchenko S.S., Frolov V.Ya. Voltage dip analysis of a drilling rig connected to a local power grid. VII Mezhdunarodnaya nauchno-prakticheskaya konferentsiya "Innovatsii i perspektivy razvitiya gornogo mashinostroeniya i elektromekhaniki": IPDME-2020, 23-24 aprelya 2020, Sankt-Peterburg, Rossiya. St. Pttersburg: Sankt-Peterburgskii gornyi universitet, 2020, p. 630-634 (in Russian).

18. Gukovskiy Yu.L., Sychev Yu.A., Pelenev D.N. The Automatic Correction of Selective Action of Relay Protection System against Single Phase Earth Faults In Electrical Networks of Mining Enterprises. *International Journal of Applied Engineering Research*. 2017. Vol. 12. N 5, p. 833-838.

19. Belsky A.A., Glukhanich D.Y., Carrizosa M.J., Starshaia V.V. Analysis of specifications of solar photovoltaic panels. *Renewable and Sustainable Energy Reviews*. 2022. Vol. 159. N 112239. DOI: 10.1016/j.rser.2022.112239

20. Barelli L., Bidini G., Pelosi D. et al. Comparative analysis of AC and DC bus configurations for flywheel-battery HESS integration in residential micro-grids. *Energy*. 2020. Vol. 204. N 117939. DOI: 10.1016/j.energy.2020.117939

21. Shonin O.B., Novozhilov N.G., Kryltcov S.B. Enhancing the stability of a sensorless V/F controlled VFD under voltage sags. *Izvestiya Tula State University*. 2016. Iss. 11-2, p. 507-519 (in Russian).

22. Bardanov A.I., Solovev S.V., Alvarez R. et al. Upgrading the Power Capacity of a Three-Conductor MVAC Line by Converting to DC. *Energies*. 2022. Vol. 15. Iss. 3. N 1080. DOI: 10.3390/en15031080

23. Munoz-Guijosa J.M., Kryltcov S.B., Solovev S.V. Application of an active rectifier used to mitigate currents distortion in 6-10 kV distribution grids. *Journal of Mining Institute.* 2019. Vol. 236, p. 229-238. DOI: 10.31897/PMI.2019.2.229

24. Iakovleva E.V., Guerra D.D. Improving the efficiency of the use of photovoltaic stations in the republic of Cuba. *Journal of Physics: Conference Series*. 2021. Vol. 1753. N 012056. DOI: 10.1088/1742-6596/1753/1/012056

25. Vasilkov O.S., Batueva D.E., Homyakov K.A., Palyanicin P.S. Aligning the load schedule of enterprises through the use of hybrid energy storage. *Izvestiya MGTU "MAMI"*. 2020. N 1 (43), p. 27-34 (in Russian). DOI: 10.31992/2074-0530-2020-43-1-27-34

26. Abramovich B.N. Uninterruptible Power Supply System for Mining Industry Enterprises. *Journal of Mining Institute.* 2018. Vol. 229, p. 31-40. DOI:10.25515/PMI.2018.1.31

27. Abramovich B., Sychev Yu.A., Pelenev D.N. Invariant protection of high-voltage electric motors of technological complexes at industrial enterprises at partial single-phase ground faults. *IOP Conference Series: Materials Science and Engineering*. 2018. Vol. 327. Iss. 5. N 052027. DOI: 10.1088/1757-899X/327/5/052027

28. Vasilyev B.Yu., Shpenst V.A., Kalashnikov O.V., Ulyanov G.N. Providing Energy Decoupling of Electric Drive and Electric Grids for Industrial Electrical Installations. *Journal of Mining Institute.* 2018. Vol. 229, p. 41-49. DOI: 10.25515/PMI.2018.1.41

29. Forcan J., Forcan M. Optimal placement of remote-controlled switches in distribution networks considering load forecasting. *Sustainable Energy, Grids and Networks*. 2022. Vol. 30. N 100600. DOI: 10.1016/j.segan.2021.100600

30. Ngom I., Mboup A.B., Thiaw L. et al. An Improved Control for DC-Link Fluctuation during Voltage Dip based on DFIG. 9th International Renewable Energy Congress (IREC), 20-22 March 2018, Hammamet, Tunisia. IEEE, 2018, p. 1-6. DOI: 10.1109/IREC.2018.8362458

31. Pazouki E., Sozer Y., De Abreu-Garcia J.A. Fault Diagnosis and Fault-Tolerant Control Operation of Nonisolated DC-DC Converters. *IEEE Transactions on Industry Applications*. 2018. Vol. 54. Iss. 1. P. 310-320. DOI: 10.1109/TIA.2017.2751547

32. Zhukovskiy Y.L., Korolev N.A., Koteleva N.I. About increasing informativity of diagnostic system of asynchronous electric motor by extracting additional information from values of consumed current parameter. *Journal of Physics: Conference Series*. 2018. Vol. 1015. Iss. 3. N 032158. DOI: 10.1088/1742-6596/1015/3/032158

33. Malarev V.I., Kopteva A.V., Nogtev R.A. Electric Drive Simulation for Drilling Machine Spinner. *IOP Conference Series: Earth and Environmental Science*. 2018. Vol. 194. Iss. 5. N 052012. DOI: 10.1088/1755-1315/194/5/052012

34. Savard C., Iakovleva E., Ivanchenko D., Rassõlkin A. Accessible Battery Model with Aging Dependency. *Energies*. 2021. Vol. 14. Iss. 12. N 3493. DOI: 10.3390/en14123493

35. Shklyarskiy Ya.E., Batueva D.E. Operation mode selection algorithm development of a wind-diesel power plant supply complex. *Journal of Mining Institute.* 2022. Vol. 253, p. 115-126. DOI: 10.31897/PMI.2022.7

36. Zhukovskiy Yu.L., Batueva D.E., Buldysko A.D. et al. Fossil Energy in the Framework of Sustainable Development: Analysis of Prospects and Development of Forecast Scenarios. *Energies*. 2021. Vol. 14. Iss. 17. N 5268. DOI: 10.3390/en14175268

37. Akbari K., Rahmani E., Abbasi A., Askari M.-R. Optimal placement of distributed generation in radial networks considering reliability and cost indices. *Journal of Intelligent & Fuzzy Systems*. 2016. Vol. 30. Iss. 2, p. 1077-1086. DOI: 10.3233/IFS-151883

***Authors*: Sergey S. Chervonchenko,** *Postgraduate Student, sergeychervonchenko@gmail.com, https://orcid.org/0009-0003-2839-9068* (*Peter the Great St. Petersburg Polytechnic University, Saint Petersburg, Russia*), **Vladimir Ya. Frolov,** *Doctor of Engineering Sciences, Professor, https://orcid.org/0000-0002-1744-4375* (*Peter the Great St. Petersburg Polytechnic University, Saint Petersburg, Russia*).

*The authors declare no conflict of interests.*

ISSN 2411-3336; e-ISSN 2541-9404

JOURNAL OF MINING INSTITUTE

Zapiski Gornogo instituta

Journal homepage: pmi.spmi.ru

*Research article*

# Improving the efficiency of autonomous electrical complex with renewable energy sources by means of adaptive regulation of its operating modes

**Vadim A. SHPENST, Aleksey A. BELSKY, Evgeny A. OREL**✉
*Saint Petersburg Mining University, Saint Petersburg, Russia*

***How to cite this article*:** Shpenst V.A., Belsky A.A., Orel E.A. Improving the efficiency of autonomous electrical complex with renewable energy sources by means of adaptive regulation of its operating modes. Journal of Mining Institute. 2023. Vol. 261, p. 479-492. EDN SNUKNA

***Abstract*.** Renewable energy sources are gradually becoming useful in mining industry. They are actively used in remote, sparsely populated areas to power shift settlements, geological and meteorological stations, pipeline equipment, mobile cell towers, helicopter pads lighting, etc. In comparison with diesel generators, systems with renewable sources do not require fuel transportation, have short payback periods and flexible configuration for different categories of electrical loads. The main obstacles to their spread are instability of generation and high cost of produced electricity. One of the possible ways to solve these problems is to develop new technologies, increase power density of generators and energy storage systems. The other way represents energy saving and rational use of affordable resources. The new solutions for implementation of the second method are proposed in this work. The object of the study is autonomous DC electrical complex with photovoltaic and wind power sources. In such systems the generated power from renewable sources is transferred to consumers via intermediate DC bus, the voltage level of which affects the power losses in the process of power transmission. The vast majority of complexes have a problem that their DC bus voltage is constant, while the optimum voltage level with lowest losses varies depending on the generated and consumed power. Therefore, electrical complexes potentially lose a part of the transmitted energy. To avoid this, a special algorithm was added to automatically adjust DC bus voltage to optimum level according to changes in working conditions. An additional contribution to efficiency improvement can be made by dynamic change of operating frequency in power converters depending on their load. The evaluation based on results of computer simulation showed that in a complex with rated power 10 kW active power losses during its lifetime can be reduced by 2-5 %.

***Keywords*:** renewable energy; efficiency; wind turbines; solar panels; power electronics

***Received: 02.03.2023*** ***Accepted: 20.06.2023*** ***Online: 19.07.2023*** ***Published: 19.07.2023***

**Introduction.** The global electrical industry is rapidly changing. Because of development of technologies, changes are not only quantitative, but also qualitative, irreversibly changing the principles of modern electrical systems. The key principles of such systems are decentralization, digitalization, and intellectualization of the processes of generation, distribution, and consumption of electrical energy.

New trends also have an impact on mining industry. The tasks of optimizing technological chains and increasing labor productivity come to the fore [1-3]. Thus the problem of providing electricity to remote and sparsely populated areas rich in deposits of natural resources is quite acute. The high cost of electricity there slows down the speed of development, forcing consumers to look for new power sources, as well as to form their own, more efficient small local power grids (microgrids) [4, 5].

Russia has a sustainable centralized power supply system, thus the use of autonomous microgrids with their own generation sources is justified only in the northern and northeastern regions [6-8]. In the past their inclusion in centralized power supply system was considered inefficient and too expensive. As a result, power supply in these territories was carried out from diesel generators with low efficiency and high cost of electricity generation, which reaches 80-120 rub./kW·h [9].

The use of renewable energy sources (RES) with a lifetime of 20-25 years can reduce the cost to 25-35 rub./kW·h [10]. The cost depends not only on money expenses, but also on the efficiency of energy conversion and transmission to the consumer. The purpose of this study is to propose a new approach to increase energy efficiency of autonomous microgrids with renewable energy sources. The relevance of the work is connected with the importance of the topic of energy saving for mining industry consumers placed in remote northern territories, which receive support of the Russian government.

**Methods.** The lifetime of microgrids with RES is more than 20 years. Money expenses include capital costs at the start of the project, annual maintenance costs, and disposal costs at the end of the project. The cost of electricity (COE) is equal to the ratio of total monetary expenses to the total consumed electricity. At the same time, the consumed electricity $W_c$ is not equal to the generated $W_{gen}$ due to the losses in the power system:

$$W_c = \eta W_{gen}, \tag{1}$$

где $\eta$ – efficiency of electrical energy transfer. The higher $\eta$, the lower the COE, in modern microgrids $\eta$ = 0,8-0,85 [11].

For mining industry the use of renewable energy is most justified for powering small loads (1-10 kW) that are tens and hundreds of kilometers away from the main power transmission lines [12-14]. Such consumers are small shift settlements, geological and meteorological stations, mobile cell towers, pipeline equipment, engines of small pumps, corrosion protection systems, helicopter pads lighting systems, security or communication objects, leak detection equipment, etc.

Microgrids with RES may have variety of architectures and control principles. The system can be based on direct or alternating current [15], centralized or decentralized control principles [16], may work autonomously or exchange energy with another microgrids [17, 18]. The simplest autonomous microgrid with RES is shown in Fig.1, *a*. Coordination of RES and loads is carried out through intermediate DC bus with $U_{DC}$ voltage level. The battery (BAT) is directly connected to the bus. The battery charge is carried out with energy received from solar panels and wind turbines and converted by pulsed DC/DC and AC/DC converters. All converters work independently of each other.

However, when the battery is directly connected to DC bus, it leads to its faster obsolescence [19]. Pulse currents of random magnitude and shape from plenty of generators and power loads connected to DC bus shorten the battery life. Depending on the degree of battery obsolescence and its charge level, the bus voltage can vary greatly, which causes problems with stability of the system. Real practice shows that most of the failures of autonomous microgrids consist precisely in the failure of batteries [20]. At the same time, the cost of battery replacing can be up to 60 % of the cost of the entire system.

To extend the battery lifetime, it is connected to DC bus not directly, but through a bidirectional DC/DC converter that controls battery charge and discharge processes [21]. This converter maintains the stability of DC bus voltage level and controls the battery current. The use of centralized control (Fig.1, *b*) ensures coherent operation of all converters. The stable operation of the complex has a balance in generated $P_{gen}$ and consumed $P_{load}$ power, which, taking into account losses $P_{loss}$, can be written as:

$$P_{gen} - P_{load} - P_{loss} = 0. \tag{2}$$

**Journal of Mining Institute.** 2023. Vol. 261. P. 479-492


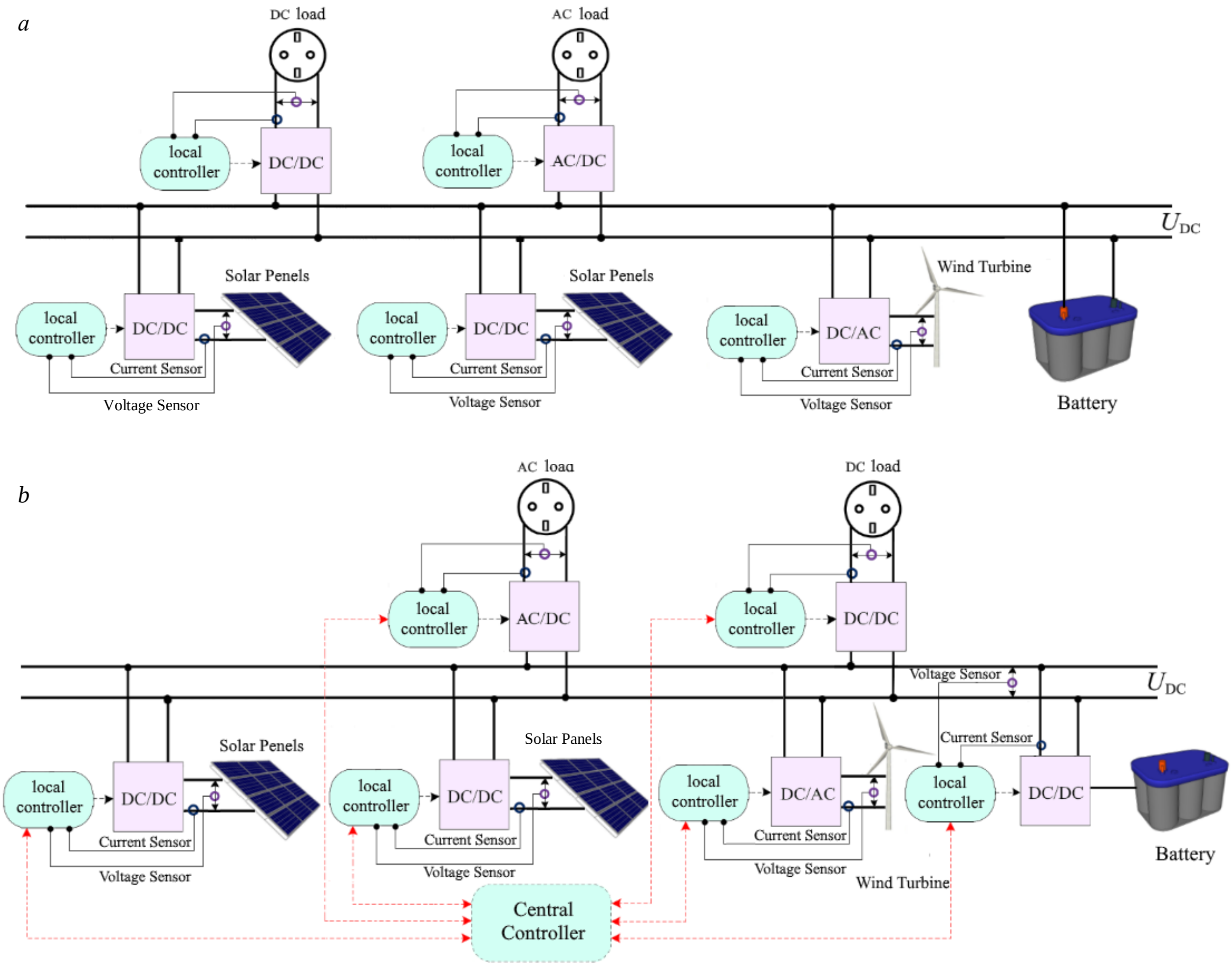


Fig.1. Microgrid with RES: battery is connected to DC bus directly (*a*), via bidirectional DC/DC converter (*b*)

All voltage converters connected with renewable energy sources operate in maximum power point tracking (MPPT) [22-24]. In this mode, their input resistance is regulated in such a way as to receive maximum power from RES [25, 26]. For example, operating point of a solar panel with a photovoltaic (PV) $P_{PV}$ output power (Fig.2, *a*) will be set to position A, and when the generated power changes, it will be automatically moved to position B (Fig.2, *b*).

Boost circuits are most often used as DC/DC converters with MPPT mode [27]. An increase of voltage is necessary since the output voltage of RES is usually small, especially during poor generation. The output voltage-ampere characteristic (VAC) of boost converter operating in MPPT mode is a hyperbola (Fig.2, *c*), the power at all points of which is the same (Fig.2, *d*). The maximum output current is limited at short-circuit current $I_{SC}$ of solar panel. The maximum output voltage is limited at level $U_{lim}$ by inner overvoltage protection circuit. The output current of MPPT converter depends on the voltage level of DC bus $U_{DC}$ and inversely proportional to it

$$I_{out} = \frac{P_{max}}{U_{DC}}. \qquad (3)$$

Considering by analogy the work of the other converters in microgrid, it is possible to identify general patterns. The principle of operation of bidirectional DC/DC battery charge-discharge converter is described in [28, 29], of inverter in [30, 31]. When microgrid operates, each converter has its own operating point. Since they are all connected to a common DC bus, the position of the points will be affected by the voltage level $U_{DC}$.

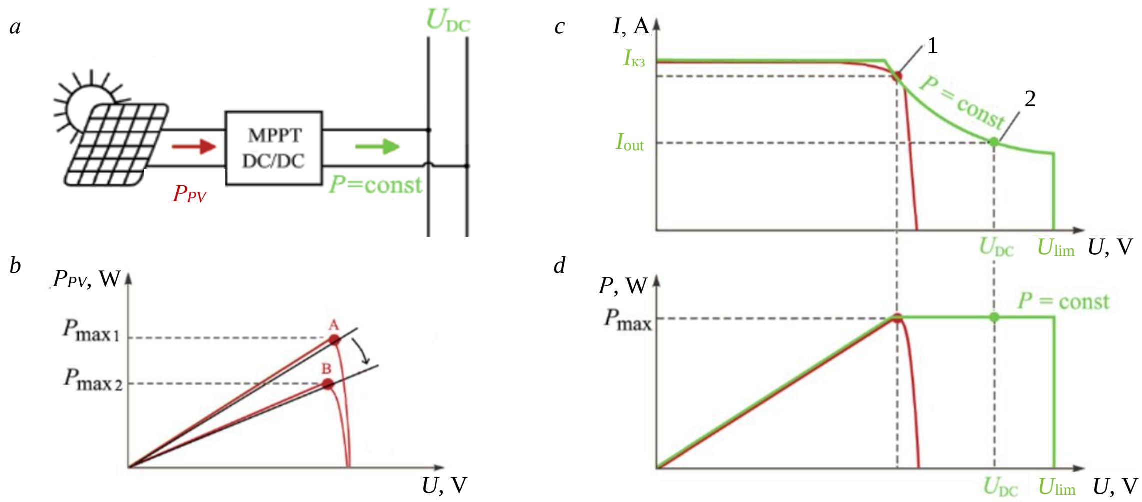


Fig.2. Operation of solar panel with boost DC/DC converter: *a* – scheme; *b* – MPPT mode; *c* – output VAC of the panel and converter; *d* – power characteristics of the panel and converter
1 – operating point of solar panel; 2 – of converter

The lower limit of permissible $U_{DC}$ values should be higher than the maximum output voltage generated by RES. The upper limit is limited by economic criterion – with an increase of $U_{DC}$ voltage, the electronic components of converters become more expensive. Works [32-34] are devoted to the choice of DC bus voltage. For household grids with rated power of up to 10 kW, the most common levels are 12, 24, and 48 V [35], for grids of greater power 380 and 400 V [36].

For the vast majority of microgrids DC bus voltage level is constant. When microgrid operates, voltage deviation is allowed within no more than ±10 % of the nominal value. At the same time, it was shown in [26, 37] that the optimum voltage, which will be characterized by the lowest losses during power transmission, varies depending on the volume of generation and consumption. As a result, microgrids with constant voltage level inevitably lose a part of the transmitted power.

The authors of [26, 37] have not shown how to implement automatic adjustment of DC bus voltage to the optimum, so this issue requires further exploration. As we already know, the efficiency of voltage converters in microgrid depends on the voltage level of DC bus $U_{DC}$. Having a mathematical model of power losses in each converter, this dependence can be calculated. The power loss model for boost DC/DC converters was obtained in [38], for buck converters in [39], for inverter in [40, 41], for bidirectional battery charge-discharge converter in [42, 43].

The active power losses in pulse converters, if all necessary parameters of the circuit are known and the operating frequency of conversion is determined, can be reduced to a function of three variables

$$P_{loss} = f(U_{in}, I_{out}, U_{out}), \quad (4)$$

where $U_{in}$, $U_{out}$ – input and output converter voltage; $I_{out}$ – output converter current. For DC-converters, these variables characterize direct current. For AC-converters, these variables are rms values of phase currents and voltages.

Since all converters in microgrid are connected to DC bus, one of these three variables represents $U_{DC}$ voltage. The flow of reactive power in microgrid, thanks to the use of DC bus and pulse voltage converters, is actually reduced to zero. Therefore, calculations of reactive power are not considered in this research. The efficiency of all converters will be related to active power losses $P_{loss}$ by formula

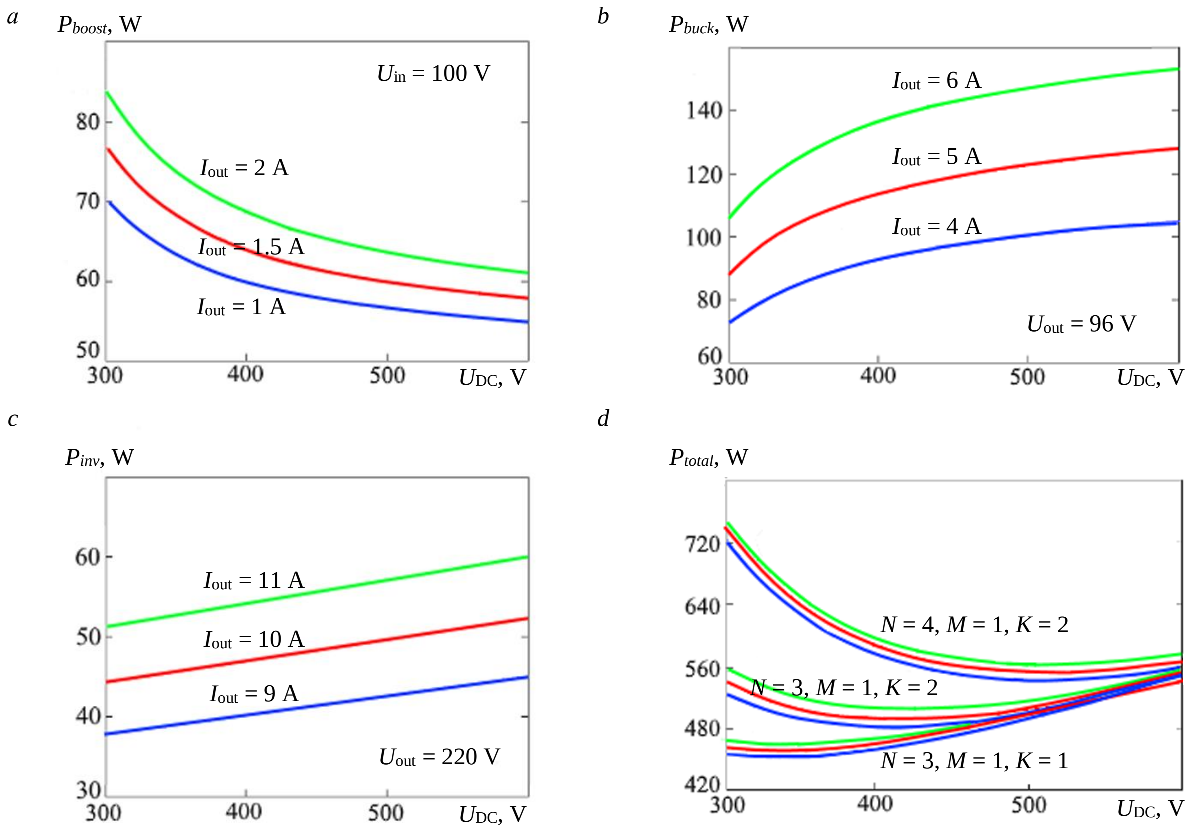


Fig.3. Graphs of the dependence of active power losses on DC bus voltage: *a* – for boost converter; *b* – for battery charge-discharge converter; *c* – for inverter; *d* – total losses in microgrid

$$\eta(U_{in}, I_{out}, U_{out}) = \frac{1}{1 + \frac{P_{loss}}{I_{out}U_{out}}}. \quad (5)$$

On the basis of mathematical models of losses according to the formula (4), the dependences of $P_{loss}$ on $U_{DC}$ bus voltage for boost converter, for battery charge-discharge converter, and for inverter were plotted (Fig.3, *a*-*c*). For plotting a microgrid with the total generated power of 4 kW was considered. The output voltage of RES was set to 100 V DC, the battery voltage was 96 V, the output voltage of inverter was 220 V, and the DC bus voltage range was 310-600 V. The graphs of losses were plotted with three different loads on every converter, i.e. by setting three different values of their output current $I_{out}$. Total power losses of the entire system will be equal to the sum of the losses of the converters:

$$P_{total}(U_{DC}) = NP_{boost}(U_{DC}) + MP_{buck}(U_{DC}) + KP_{inv}(U_{DC}), \quad (6)$$

where $N$ – number of operating boost converters; $M$ – number of battery charge-discharge converter; $K$ – number of inverters.

By summing up the loss graphs of all converters according to formula (6), the $P_{total}(U_{DC})$ loss dependence graph of the entire complex was determined. $P_{total}$ loss graphs ($U_{DC}$) were plotted with different values of $N$, $M$, and $K$ (Fig.3, *d*).

It can be seen from Fig.3, *d* that the point of minimum losses with different structure of microgrid and different converters load will be different. By adjusting the $U_{DC}$ voltage level of DC bus according to the minimum of losses during the microgrid operation, it is possible to increase the total energy efficiency.

In addition, power losses of the system can be reduced not only by varying the DC bus voltage, but also by changing the operating frequency of pulse converters depending on their load. Active power of the converter load

$$P = Ef_s, \quad (7)$$

where $E$ is the energy converted in one working cycle, J; $f_s$ is the operating frequency of the conversion, Hz.

The operating frequency affects the dynamic losses in switching semiconductor elements. The higher it is, the higher the losses. If load power changes, then at $E$ = const. according to the formula (7), the operating frequency can also be changed. Thus, if the load decreases, the efficiency of the converter can be improved by reducing its operating frequency.

The proposed algorithm for adaptive adjustment of operating modes of microgrid, which increases its energy efficiency, is based on the assessment of active power losses in converters using their mathematical models.

To carry out calculations, a computing unit (CU) has been added to the complex, in which power loss models of all converters are stored (Fig.4, *a*). In addition, the array of possible values of DC bus voltage $U_{DC}$ is stored in CU memory, from which the best value is determined as a result of calculations.

Communication channels are established between local controllers (LC) of voltage converters and CU. Local controllers, using current and voltage sensors, measure the variables which are necessary for calculating power losses according to formulas (4) and (6). According to the measured value of current, the load on the converter is estimated by local controller and, according to formula (7), the operating frequency of the conversion is adjusted.

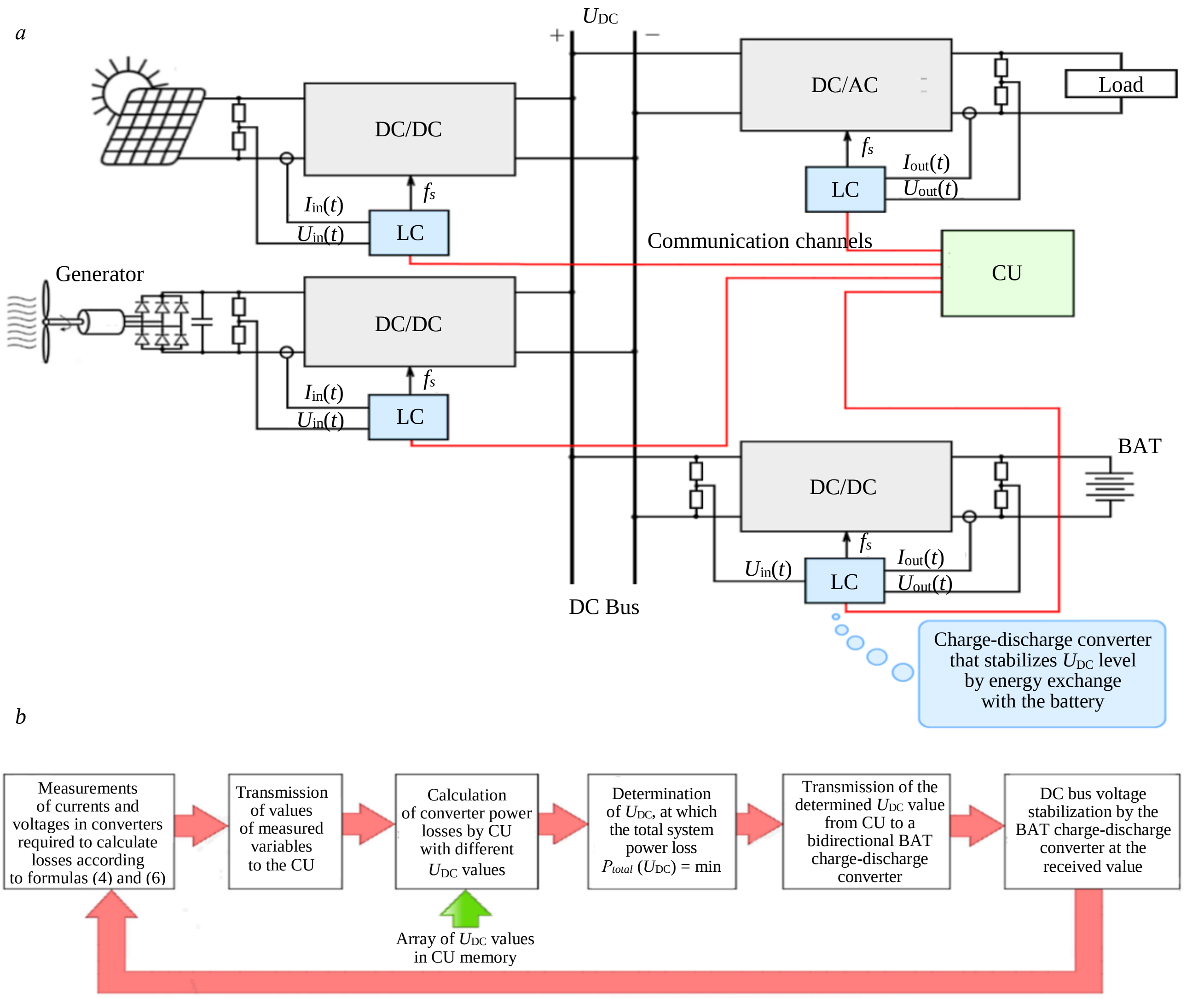


Fig.4. Microgrid with the search of the optimal mode of operation: *a* – scheme; *b* – algorithm for finding the optimal DC bus voltage level

Further, the measured values of variables are transmitted via communication channels to CU, which calculates converters power losses with different $U_{DC}$ bus voltage variants and selects the variant at which the total calculated losses $P_{total}(U_{DC})$ of the system would be minimal. The found value is transmitted from CU to the LC of the battery charge-discharge converter, which stabilizes the $U_{DC}$ bus voltage at the received value. The block diagram of the algorithm is shown in Fig.4, *b*. To test the proposed idea, a simulation computer model of an autonomous microgrid with rated power of 10 kW in MatLab Simulink software package was created.

Simulational models of solar panel and battery were taken from [44]. The model of the wind generator is based on [45], where the operation of wind turbine with diode rectifier was considered. The authors have shown that if a filter capacitance is connected after the rectifier, then the voltage at the output of the rectifier at the maximum generated power point is associated with this power by the expression

$$U_{WT} = \frac{3\sqrt{2}}{\pi}\left(\frac{1}{\sqrt{2}}K_V\sqrt[3]{\frac{P_{\max}}{\frac{1}{2}\rho\pi R^2 C_p(\lambda,\theta)\left(\frac{R}{\lambda}\right)^3}}\right) - U_{\text{d}}, \quad (8)$$

где $K_V$ – constructive coefficient of proportionality, $K_V = 0.69$ [45]; ρ – air density, $\rho = 1.225$ kg/m$^3$; $R$ – length of wind turbine blades; $C_p$ – wind turbine power coefficient, depending on tip speed ratio λ and pitch angle θ, lying in range 0-0.6; $U_{\text{d}}$ – voltage drop in diode rectifier.

At the same time, maximum power value taken from wind turbine depends on the wind speed *v*

$$P_{\max} = \frac{1}{2}\rho\pi R^2 v^3 C_p(\lambda,\theta). \quad (9)$$

The simulation computer model of the complex is shown in Fig.5. It comprises three arrays of solar panels and one wind turbine, which produces an already rectified DC voltage. Power loads are

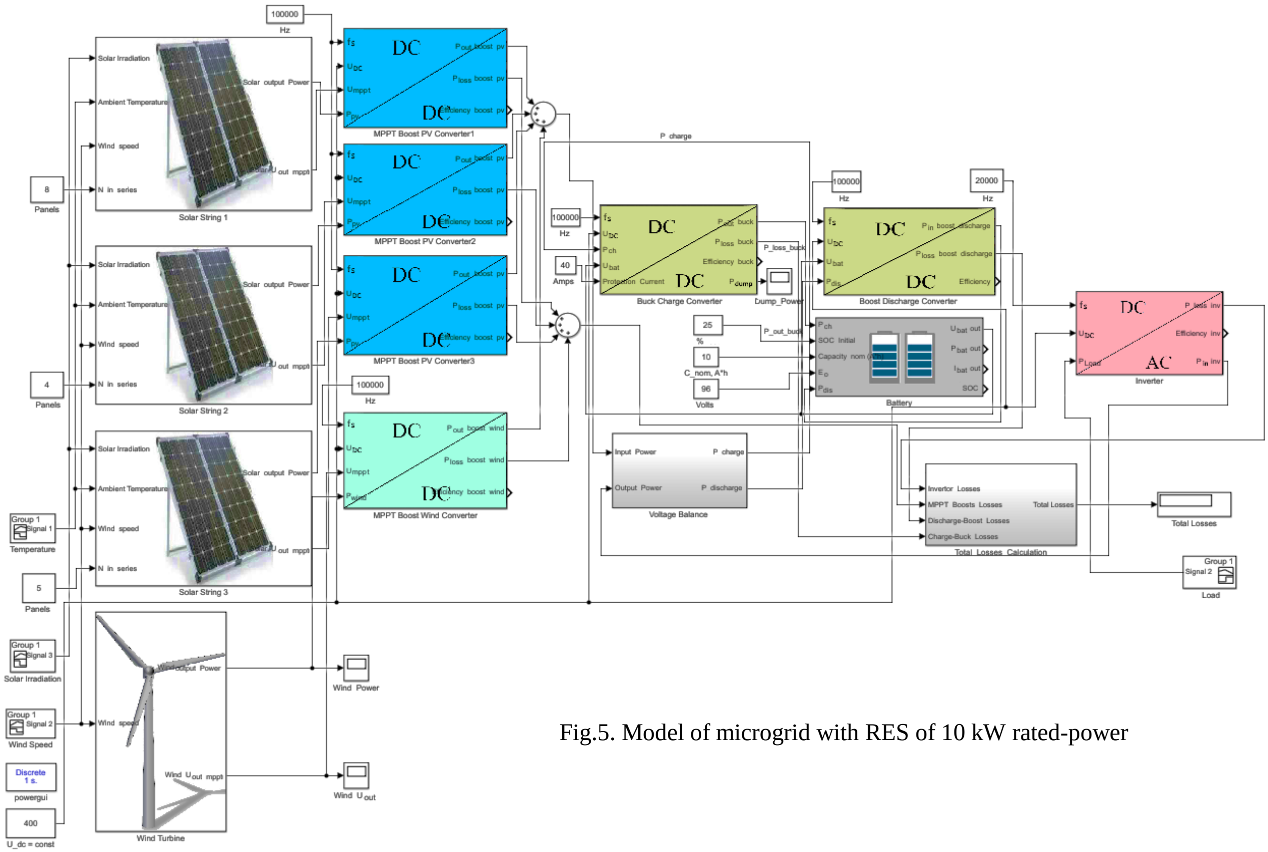


Fig.5. Model of microgrid with RES of 10 kW rated-power

simulated by *Load* unit powered by DC/AC voltage converter. The power taken from renewable sources is converted by pulsed DC/DC converters. The output power of these converters is summed up, as a result the total generated power is determined. After that, in *Voltage Balance* block, the power consumed by the loads is subtracted from the total generated power. If the difference turns out to be positive, it goes to the battery charge. If negative, it is replenished by discharging of battery. The bidirectional battery charge-discharge converter is represented by two DC/DC blocks: *Buck Charge Converter* – carrying out the charge, and *Boost Charge Converter* – carrying out the discharge. The parameters of RES and battery models are given in Table 1, the models of pulse voltage converters – in Table 2.

*Table 1*

**Parameters of RES and battery**

| Solar panel | Wind turbine | Battery |
|---|---|---|
| Nominal power 250 W | Nominal power 7500 W | Open circuit voltage 96 V |
| Open circuit voltage 37.98 V | Open circuit voltage 240 V | Capacity 10 A·h |
| Short current 9.04 A | Tip speed ratio λ = 7 | Input resistance 0.0048 Ohm |
| Voltage at maximum power point 30.63 V | Length of wind turbine 1.6 m | Permissible state of charge 20-100 % |
| Current at maximum power point 8.79 A | Permissible wind speed 3-14 m/s | Initial charge 25 % |

*Table 2*

**Parameters of pulsed converter models**

| Parameters | DC/DC of solar panel | DC/DC of wind turbine | DC/DC of charge-discharge battery | DC/AC |
|---|---|---|---|---|
| Operating mode | MPPT | MPPT | Stabilization of $U_{DC}$ | Stabilization of voltage for loads |
| Scheme | Boost converter [22] | Boost converter [43] | Buck-boost converter [28] | Full-bridge converter [30] |
| Transistors | | | | |
| Type | MOSFET | MOSFET | MOSFET | IGBT |
| Operating frequency | 100 kHz | 100 kHz | 100 kHz | 20 kHz |
| Open channel resistance/voltage drop in open state | 0.002 Ohm | 0.002 Ohm | 0.002 Ohm | 1.8 V |
| Average time of turn-on/turn-off | 30 ns | 30 ns | 30 ns | 42 ns |
| Output capacity | 100 pF | 100 pF | 100 pF | 200 pF |
| Gate threshold voltage | 12 V | 12 V | 12 V | 12 V |
| Diodes | | | | |
| Voltage drop | 0.3 V | 0.3 V | 0.3 V | 1 V |
| Dynamic resistance | 0.9 Ohm | 0.9 Ohm | 0.9 Ohm | 0.7 Ohm |
| Reverse recovery time | 45 ns | 45 ns | 45 ns | 60 ns |
| Inductor | | | | |
| Inductance | 70 uH | 50 uH | 50 uH | 30 uH |
| Resistive load | 0.3 Ohm | 0.2 Ohm | 0.15 Ohm | 0.8 Ohm |
| Electrolytic capacitors | | | | |
| ESR | 0.02 Ohm | 0.02 Ohm | 0.02 Ohm | 0.02 Ohm |

The input of the solar panel model receives the data about hourly intensity of solar radiation (Fig.6, *a*) and ambient temperature (Fig.6, *b*) throughout the year. The input of the wind turbine model receives the data about hourly wind speed (Fig.6, *c*). All of them are hourly average meanings taken from NASA meteorological database. Meteorological data from the north of Zabaikalskiy krai for 2022 were used for modeling.

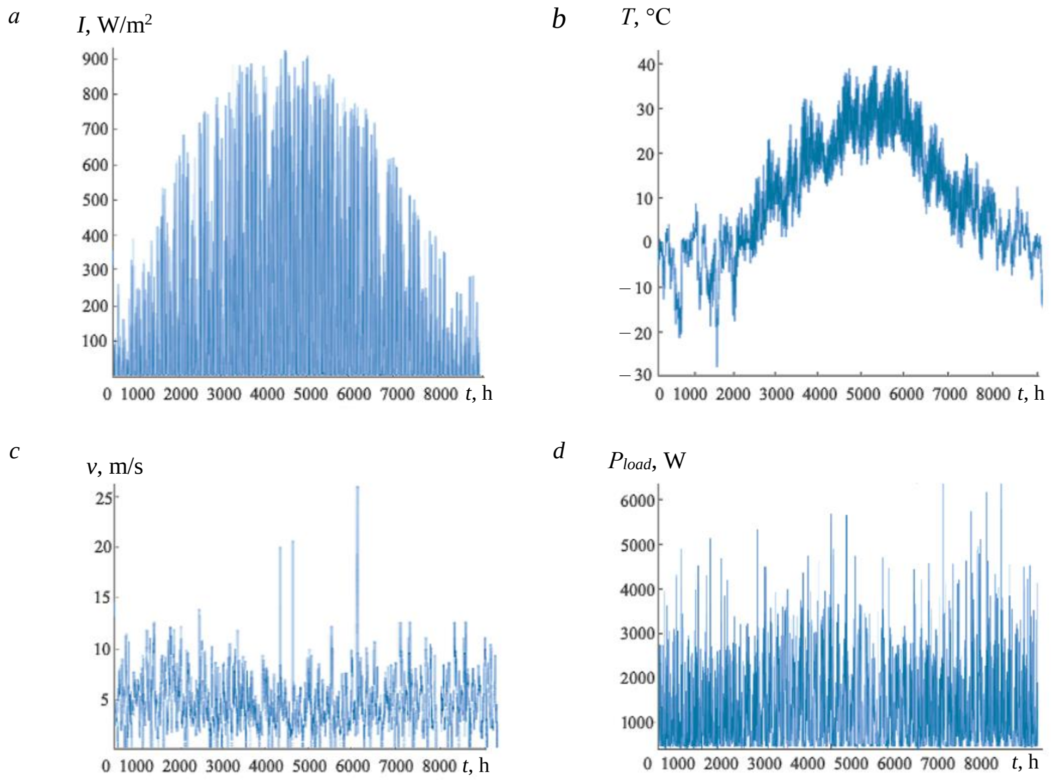


Fig.6. Data for modeling of microgrid: *a* – solar radiation intensity; *b* – ambient temperature; *c* – wind speed; *d* – hourly load consumption profile

Power taken from solar panels gets to DC/DC converters MPPT Boost PV Converter, which power losses model is based on formulas from [38]. The input data for the model represents operating frequency of conversion $f_s$, DC bus voltage $U_{DC}$, generated by solar panels voltage $U_{MPPT}$ and power $P_{PV}$. The output data represents calculated power losses $P_{loss\ boost\ PV}$, output power $P_{out\ boost\ PV}$ and efficiency of conversion *Efficiency boost PV*.

Power taken from wind turbine supplies DC/DC converter *MPPT Boost Wind Converter*, which power losses model is also based on [38]. The input data for this model represents generated by wind turbine power $P_{wind}$ and voltage $U_{MPPT}$, operating frequency $f_s$ and DC bus voltage $U_{DC}$. The output data represents losses $P_{loss\ boost\ wind}$, output power $P_{out\ boost\ wind}$, and efficiency of conversion *Efficiency boost wind*.

The DC/AC converter power losses model is based on [40, 41]. The input of the model receives the data about operating frequency of conversion $f_s$, hourly power consumption of the load $P_{load}$ (Fig.6, *d*), voltage level of DC bus $U_{DC}$. As a load a small shift settlement consisting of several residential structures was considered, where the main consumers are electrical appliances and lighting. The data about power consumption was taken from the LoadProfileGenerator* database. The output data for the DC/AC converter model represents power losses $P_{loss\ inv}$, efficiency of conversion *Efficiency* and consumed from the DC bus power $P_{in\ inv}$.

The DC bus model is represented by *Voltage Balance* block. This block compares total generated power *Input output* and total consumptive power *Output Power*. If their difference turns out to be greater than zero, then this excess power $P_{ch}$ is directed to the battery charge, if less, then the lack of this power $P_{dis}$ will be taken from the battery discharge.

Bidirectional DC/DC charge-discharge converter is represented by *Buck Charge Converter* and *Boost Discharge Converter* blocks. The model of converter in charge mode *Buck Charge Converter*

* LoadProfileGenerator – modeling tool for residential energy consumption. URL: https://www.loadprofilegenerator.de (accessed 02.03.2023).

is based on the works [39, 42]. This converter has a current protection circuit limiting the maximum charge current *Protection Current*. The input data for the model represents charge power $P_{ch}$, DC bus voltage $U_{DC}$, battery voltage $U_{bat}$, and operating frequency $f_s$. The output data represents power losses $P_{loss\ buck}$, output power $P_{out\ buck}$, efficiency of conversion *Efficiency buck*, and excess power dissipated on ballast resistors $P_{dump}$.

The model of converter losses in battery discharge mode *Boost Discharge Converter* is based on [43]. The input data represents operating frequency $f_s$, DC bus voltage $U_{DC}$, battery voltage $U_{bat}$, and power $P_{dis}$ injecting to DC bus. The output data represents power $P_{bat\ dis}$ taken from the battery, power losses $P_{loss\ boost\ dis}$, and efficiency of conversion *Efficiency*.

The calculation of total microgrid power losses is carried out in *Total Losses Calculation* block. The input of the unit receives information about power losses of all converters, then these losses are summed up.

**Results**. During the process of computer simulation our microgrid operation was reproduced throughout the year including 8760 hours. The simulation results are shown in Fig.7. In order to represent the waveforms on enlarged scale, the time interval only from 2000 to 2600 hours is shown. The RES output waveforms (Fig.7, *a*) is represented by two graphs: generated power of solar panels $P_{PV}$, generated power of wind turbine $P_{WT}$. $P_{load}$ is a waveform of load active power, state of charge (SOC) is a battery charging level.

The voltage $U_{PV}$ and current $I_{PV}$ waveforms generated by one array of solar panels are shown in Fig.7, *b*. The voltage $U_{WT}$ and current $I_{WT}$ waveforms of one wind turbine are shown in Fig.7, *c*. Battery voltage and charge-discharge current are shown in Fig.7, *d*. Efficiency of explored microgrid was assessed by measuring its total power losses $P_{total}$. Initially, these power losses were measured in case of constant DC bus voltage 400 V and constant operating frequency of converters: 100 kHz for DC/DC converters and 20 kHz for DC/AC converters. After that, power losses were adjusted to a minimum (for implementing $P_{total}$ = min) by means of regulation of operating frequency $f_s$ of the convertors (Fig.7, *e*) and DC bus voltage $U_{DC}$ (Fig.7, *f*). The values of 370-600 V were used as DC bus voltage range. Operating frequency of DC/DC converters varied between 20-100 kHz depending on their load.

The waveform of total microgrid power losses $P_{total}$ is shown in Fig.7, *g*. As a result of use of proposed technical solution, the microgrid losses were decreased. To quantify this decrease, $P_{total}$ power losses were summed up over 8760 hours, as a result of which the total losses for the year were determined. The increase of microgrid efficiency for one year was calculated as follows:

$$\Delta P_{total} = \left( \frac{P_{total2}}{P_{total1}} - 1 \right) \cdot 100\ \%, \tag{10}$$

where $P_{total1}$ represents total losses of active power for one year in case of constant DC bus voltage and operating frequency of all converters; $P_{total2}$ represents total losses of active power for one year in case of variable bus voltage and operating frequency of all converters.

The evaluation of $P_{total}$ showed that the use of proposed technical solution made it possible to decrease power losses for one year by 2 % with varying bus voltage and by 5 % with variation of both DC bus voltage and operating frequency of all converters. Since power losses throughout the entire life are equal to the sum of losses of separate years, the reduction of losses over the entire life of the microgrid thanks to the use of our proposed solution can be also estimated at 2-5 %.

**Discussion of the results**. The efficiency increase of autonomous microgrid with RES was achieved thanks to the adaptive regulation of its operating modes. The proposed method is based on the use of mathematical models of converters power losses, therefore, a large amount of calculations is required for its implementation. Specifically for this purpose, a separate CU was added to microgrid, storing all mathematical models in its memory. This unit is connected to the converters by communication channels and continuously receives from them the values of variables necessary for calculations. There are the following features of the system functioning:

*Journal of Mining Institute.* 2023. Vol. 261. P. 479-492



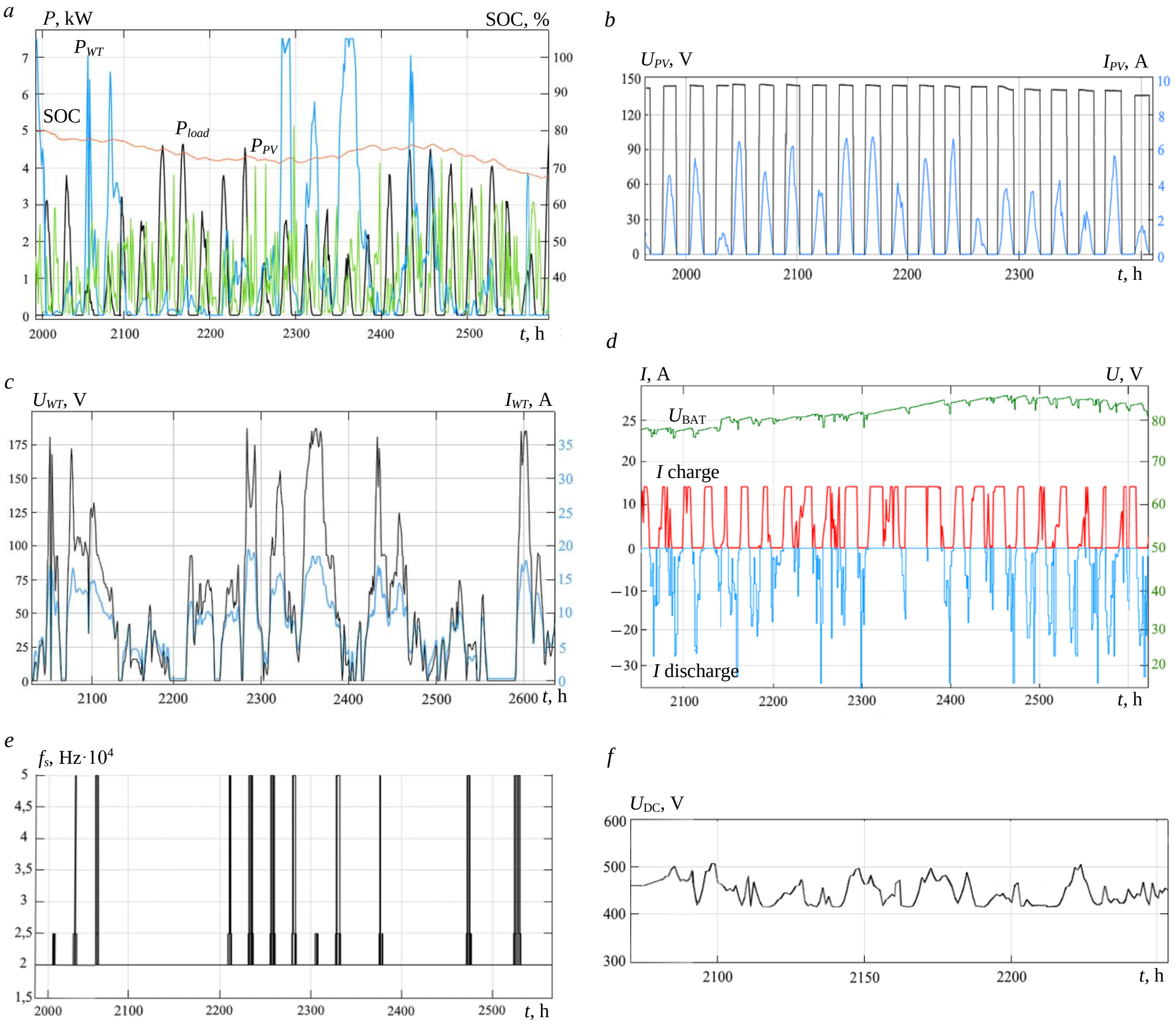


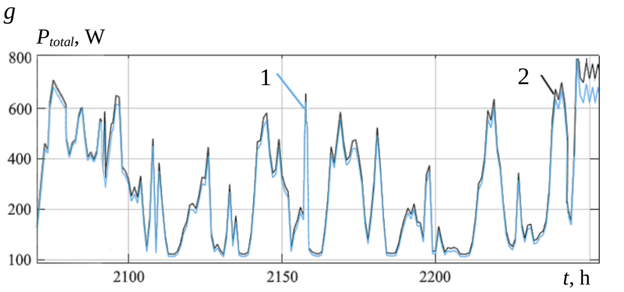


Fig.7. Microgrid modeling:
*a* – total generated and consumed power;
*b* – output voltage and current of one array of solar panels;
*c* – output voltage and current of wind turbine;
*d* – batery voltage and current;
*e* – regulation of DC/DC converters frequency;
*f* – DC bus voltage regulation;
*g* – total microgrid power losses
1 – adaptive regulation of DC bus voltage and converters operating frequency; 2 – constant DC bus voltage and frequency

• Digital control of converters is required using microcontrollers (MC) or Field-Programmable Gate Arrays (FPGA). With the help of current and voltage sensors, they measure the variables necessary to calculate power losses and transmit them to CU via communication channels. Based on the measured current, the operating frequency of the conversion is adjusted.

• Computing unit is a digital unit which represents a computer or a separate board with its own MC or FPGA, the memory of which stores mathematical models of power losses of all converters.

• Efficiency encrease depends on the accuracy of mathematical models. For this reason, calibration of models with real converters is desirable during the microgrid development. All electrical circuits and parameters of electronic components inside power converters should be known in advance. It is possible to replace the elements only with full functional analogues.

• The speed of data exchange between CU and LC of converters must be consistent with the speed of calculations, i.e. CU should have time to perform calculations before it receives new values of currents and voltages of the converters.

• Due to the above features, it will not be possible to use any converters available on the market. The system requires purposeful development of converters, which, however, is not very complicated process.

The developed method of intelligent microgrid control makes it possible to increase the efficiency of autonomous microgrids with RES. The disadvantages of the proposed method include the need to use digital controllers and the need to add some more communication channels for data exchange between converters and CU, which leads to increase of microgrid total cost. In addition, the system will be characterized by low flexibility, since any change in its structure or component elements will lead to a discrepancy between mathematical models embedded in CU and the actual microgrid operation. In this case, you will need to make edits to the models.

**Conclusion.** The new time dictates new requirements. That is why mining industry in modern world should be technological, efficient, reliable, safe, constantly improving sector of the economy. In our country most of the natural resources are located in remote, sparsely populated areas where there is no readily accessible electricity. The use of fuel generators is associated with low environmental friendliness and high cost of electricity generation, which hinders the development and forces mining companies to bear high money expenses. The use of renewable energy is a modern technological solution that can give a "second life" to many objects of mining industry and stimulate the development of new projects.

Despite the solution of logistical and environmental problems, the instability of electricity generation and the poor development of storage systems continue to be one of the main obstacles to the spread of autonomous microgrids with RES. One of the possible ways to solve these problems represents energy saving and rational use of affordable resources. A new solution was proposed to improve the efficiency of autonomous microgrid by adaptive regulation of its operating modes. The voltage level of intermediate DC bus and operating frequency of electric power converters in microgrid were considered as regulated parameters. In case of permanent changing of generated and consumed power typical for all power systems with RES, the optimum microgrid operating mode with least power losses also changes. In the course of the study, a new algorithm was developed for automatic regulation of microgrid operating modes, based on the use of mathematical models of converters power losses. The models make it possible, taking into account the volume of generated and consumed power, to calculate the optimal voltage level of the DC bus and the operating frequency of power converters for the current working conditions.

The results showed that in 10 kW microgrid the reduction of active power losses over the year was about 2 % with regulation of DC bus voltage only and about 5 % with regulation of bus voltage and operating frequency of power converters.

The direction of future research will be devoted to the efficiency estimation of hybrid microgrids with renewable energy sources and diesel generators.

## REFERENCES

1. Zhukovskiy Yu.L., Korolev N.A., Malkova Ya.M. Monitoring of grinding condition in drum mills based on resulting shaft torque. *Journal of Mining Institute.* 2022. Vol. 256, p. 686-700. DOI: 10.31897/PMI.2022.91

2. Pryakhin E.I., Troshina E.Yu. Study of technological and operational features of high-temperature-resistant composite films for laser marking of parts made of ferrous alloys. *Chernye metally.* 2023. N 4, p. 74-80 (in Russian). DOI: 10.17580/chm.2023.04.12

3. Sychev Yu.A., Kostin V.N., Serikov V.A., Aladin M.E. Nonsinusoidal modes in power-supply systems with nonlinear loads and capacitors in mining. *Mining Informational and Analytical Bulletin.* 2023. N 1, p. 159-179 (in Russian). DOI: 10.25018/0236_1493_2023_1_0_159

4. Gerasimova I.G., Oblova I.S., Golovina E.I. The Demographic Factor Impact on the Economics of the Arctic Region. *Resources*. 2021. Vol. 10. Iss. 11. N 117. DOI: 10.3390/resources10110117

5. Lavrik A., Zhukovskiy Yu., Tcvetkov P. Optimizing the Size of Autonomous Hybrid Microgrids with Regard to Load Shifting. *Energies*. 2022. Vol. 14. Iss. 16. N 5059. DOI: 10.3390/en14165059

6. Samylovskaya E., Makhovikov A., Lutonin A. et al. Digital Technologies in Arctic Oil and Gas Resources Extraction: Global Trends and Russian Experience. *Resources*. 2022. Vol. 11. Iss. 3. N 29. DOI: 10.3390/resources11030029

7. Khalturin A.A., Parfenchik K.D., Shpenst V.A. Features of Oil Spills Monitoring on the Water Surface by the Russian Federation in the Arctic Region. *Journal of Marine Science and Engineering*. 2023. Vol. 11. Iss. 1. N 111. DOI: 10.3390/jmse11010111

8. Kopteva A.V., Ushkova T.O. Development of methods for determining the relative weight of physical factors in pipeline paraffinization. E3S Web of Conferences. 2021. Vol. 266. N 04008. DOI: 10.1051/e3sconf/202126604008

9. Zmieva K.A. Problems of energy supply in the Arctic regions. *Russian Arctic*. 2020. N 8, p. 5-14 (in Russian). DOI: 10.2441/2658-4255-2020-10086

10. Lebedeva M.A. The state and prospects of renewable energy development in the regions of the Far North of Russia. *Problems of Territory's Development*. 2021. Vol. 25. N 4, p. 139-155 (in Russian). DOI: 10.15838/ptd.2021.4.114.8

11. Hongwei Wu, Sechilariu M., Locment F. Influence of Dynamic Efficiency in the DC Microgrid Power Balance. *Energies*. 2017. Vol. 10. Iss. 10. N 1563. DOI: 10.3390/en10101563

12. Martynov S.A., Masko O.N., Fedorov S.N. Innovative ore-thermal furnace control systems. *Tsvetnye metally*. 2022. N 4, p. 87-94 (in Russian). DOI: 10.17580/tsm.2022.04.11

13. Romasheva N., Dmitrieva D. Energy Resources Exploitation in the Russian Arctic: Challenges and Prospects for the Sustainable Development of the Ecosystem. *Energies*. 2021. Vol. 14. Iss. 24. N 8300. DOI: 10.3390/en14248300

14. Ilinova A., Solovyova V., Yudin S. Scenario-based forecasting of Russian Arctic energy shelf development. *Energy Reports*. 2020. Vol. 6. S. 9, p. 1349-1355. DOI: 10.1016/j.egyr.2020.11.022

15. Dastgeer F., Gelani H.E. A Comparative analysis of system efficiency for AC and DC residential power distribution paradigms. *Energy and Buildings*. 2017. Vol. 138, p. 648-654. DOI: 10.1016/j.enbuild.2016.12.077

16. Elistratov V.V. Renewable Energy Trends within the Concept of Low-Carbon Development. *Applied Solar Energy*. 2022. Vol. 58. Iss. 4, p. 594-599. DOI: 10.3103/S0003701X22040077

17. Rizzato Lede A.M., Molina M.G., Martinez M., Mercado P.E. Microgrid Architectures for Distributed Generation: A Brief Review. IEEE PES Innovative Smart Grid Technologies Conference – Latin America (ISGT Latin America), 20-22 September 2017, Quito, Ecuador. IEEE, 2017. DOI: 10.1109/ISGT-LA.2017.8126746

18. Abdallah W.J., Hashmi K., Faiz M.T. et al. A Novel Control Method for Active Power Sharing in Renewable-Energy-Based Micro Distribution Networks. *Sustainability*. 2023. Vol. 15. Iss. 2. N 1579. DOI: 10.3390/su15021579

19. Kumar D., Zare F., Ghosh A. DC Microgrid Technology: System Architectures, AC Grid Interfaces, Grounding Schemes, Power Quality, Communication Networks, Applications, and Standardizations Aspects. *IEEE Access*. 2017. Vol. 5, p. 12230-12256. DOI: 10.1109/ACCESS.2017.2705914

20. Aaron St. Leger. Demand response impacts on off-grid hybrid photovoltaic-diesel generator microgrids. *AIMS Energy*. 2015. Vol. 3. Iss. 3, p. 360-376. DOI: 10.3934/energy.2015.3.360

21. Jiechao Lv, Xiaoli Wang, Guishuo Wang, Yuhou Song. Research on Control Strategy of Isolated DC Microgrid Based on SOC of Energy Storage System. *Electronics*. 2021. Vol. 10. Iss. 7. N 834. DOI: 10.3390/electronics10070834

22. Ayop R., Chee Wei Tan. Design of boost converter based on maximum power point resistance for photovoltaic applications. *Solar Energy*. 2018. Vol. 160, p. 322-335. DOI: 10.1016/j.solener.2017.12.016

23. Seguel J.L., Seleme Jr S.I., Moráis L.M.F. Comparison of the performance of MPPT methods applied in converters Buck and Buck-Boost for autonomous photovoltaic systems. *Ingeniare. Revista chilena de ingeniería*. 2021. Vol. 29. N 2, p. 229-244. DOI: 10.4067/S0718-33052021000200229

24. Hanzaei S.H., Gorji S.A., Ektesabi M. A Scheme-Based Review of MPPT Techniques With Respect to Input Variables Including Solar Irradiance and PV Arrays' Temperature. *IEEE Access*. 2020. Vol. 8, p. 182229-182239. DOI: 10.1109/ACCESS.2020.3028580

25. Pande J., Nasikkar P., Kotecha K., Varadarajan V. A Review of Maximum Power Point Tracking Algorithms for Wind Energy Conversion Systems. *Journal of Marine Science and Engineering*. 2021. Vol. 9. Iss. 11. N 1187. DOI: 10.3390/jmse9111187

26. Belsky A., Dobush V., Ivanchenko D. Wind-PV-Diesel Hybrid System with flexible DC-bus voltage level. Electric Power Quality and Supply Reliability Conference (PQ), 11-13 June 2014, Rakvere, Estonia. IEEE, 2014, p. 181-184. DOI: 10.1109/PQ.2014.6866806

27. Honadia P.A.A., Barro F.I., Sané M. Performance Analysis of a Boost Converter with Components Losses. *Energy and Power Engineering*. 2018. Vol. 10. N 9, p. 399-413. DOI: 10.4236/epe.2018.109025

28. Yuan-Chih Chang, Hao-Chin Chang, Chien-Yu Huang. Design and Implementation of the Battery Energy Storage System in DC Micro-Grid Systems. *Energies*. 2018. Vol. 11. Iss. 6. N 1566. DOI: 10.3390/en11061566

29. Sayed Kh., Abo-Khalil A.G., Alghamdi A.S. Optimum Resilient Operation and Control DC Microgrid Based Electric Vehicles Charging Station Powered by Renewable Energy Sources. *Energies*. 2019. Vol. 12. Iss. 22. N 4240. DOI: 10.3390/en12224240

30. Ternifi T.Z., Atik L., Bachir G. et al. Quality improvement of the AC electrical energy produced by a modular inverter dedicated to photovoltaic applications. AIP Conference Proceedings. Technologies and Materials for Renewable Energy, Environment and Sustainability (TMREES), 15-18 April 2016, Beirut, Lebanon. AIP Publishing, 2016. Vol. 1758. Iss. 1. N 030048. DOI: 10.1063/1.4959444

31. Hannan S., Aslam S., Ghayur M. Design and real-time implementation of SPWM based inverter. International Conference on Engineering and Emerging Technologies (ICEET), 22-23 February 2018, Lahore, Pakistan. IEEE, 2018, p. 1-6. DOI: 10.1109/ICEET1.2018.8338637

32. Castillo-Calzadilla T., Cuesta M.A., Olivares-Rodriguez C. et al. Is it feasible a massive deployment of low voltage direct current microgrids renewable-based? A technical and social sight. *Renewable and Sustainable Energy Reviews*. 2022. Vol. 161. N 112198. DOI: 10.1016/j.rser.2022.112198

33. Habibi S., Rahimi R., Ferdowsi M., Shamsi P. DC Bus Voltage Selection for a Grid-Connected Low-Voltage DC Residential Nanogrid Using Real Data with Modified Load Profiles. *Energies*. 2021. Vol. 14. Iss. 21. N 7001. DOI: 10.3390/en14217001

34. Siraj K., Khan H.A. DC distribution for residential power networks – A framework to analyze the impact of voltage levels on energy efficiency. *Energy Reports*. 2020. Vol. 6, p. 944-951. DOI: 10.1016/j.egyr.2020.04.018

35. Lukutin B.V., Muravyev D.I. Prospects for decentralized DC systems with distributed solar generation. *Bulletin of the Tomsk Polytechnic University. Geo Assets Engineering*. 2020. Vol. 331. N 6, p. 184-196 (in Russian). DOI: 10.18799/24131830/2020/6/2688

36. Zhikang Shuai, Junbin Fang, Fenggen Ning, Z. John Shen. Hierarchical structure and bus voltage control of DC microgrid. *Renewable and Sustainable Energy Reviews*. 2018. Vol. 82. Part 3, p. 3670-3682. DOI: 10.1016/j.rser.2017.10.096

37. Elvira D.G., Blaví H.V., Pastor À.C., Salamero L.M. Efficiency Optimization of a Variable Bus Voltage DC Microgrid. *Energies*. 2018. Vol. 11. Iss. 11. N 3090. DOI: 10.3390/en11113090

38. Eichhorn T. Boost Converter Efficiency Through Accurate Calculations. *Power Electronics Technology*. 2008. Iss. 9, p. 30-35.

39. Das N., Kazimierczuk M.K. Power losses and efficiency of buck PWM DC-DC power converter. Proceedings Electrical Insulation Conference and Electrical Manufacturing Expo, 23-26 October 2005, Indianapolis, USA. IEEE, 2005, p. 417-423. DOI: 10.1109/EEIC.2005.1566330

40. Balıkcı A., Azizoğlu B.T., Durbaba E., Akpınar E. Efficiency Calculation of Inverter for PV Applications Using MATLAB and SPICE. International Conference on Optimization of Electrical and Electronic Equipment (OPTIM) & 2017 Intl Aegean Conference on Electrical Machines and Power Electronics (ACEMP), 25-27 May 2017, Brasov, Romania. IEEE, 2017, p. 593-598. DOI: 10.1109/OPTIM.2017.7975033

41. Geetha K., Sreenivasappa B.V. Power Loss Calculation for IGBT and SiC MOSFET. *Journal of Xi'an University of Architecture & Technology*. 2020. Vol. XII. Iss. VIII, p. 378-382. DOI: 10.37896/JXAT12.08/2637

42. Zheliazkov Y. Researching the efficiency of buck converter synchronous rectifier. *Technology Audit and Production Reserves*. 2020. Vol. 4. N 1(54), p. 44-50. DOI: 10.15587/2706-5448.2020.207893

43. Hinov N., Arnaudov D., Valchev V., Vuchev S. Comparative Loss Analysis of Boost and Synchronous Boost DC-DC Converters. XXVI International Scientific Conference Electronics (ET), 13-15 September 2017, Sozopol, Bulgaria. IEEE, 2017. DOI: 10.1109/ET.2017.8124347

44. Obukhov S.G., Plotnikov I.A. et al. Simulation model of operation of autonomous photovoltaic plant under actual operating conditions. *Bulletin of the Tomsk Polytechnic University. Geo Assets Engineering.* 2017. Vol. 328. N 6, p. 38-51 (in Russian).

45. Flores D.R.L., Gómez J.A.P., Herrera R.S., Alvarado M.S. Tracking Control of the Maximum Power Point (MPPT) in a Small Wind Turbine (SWT) for Isolated Residential Applications. *WSEAS Transactions on Circuits and Systems*. 2013. Vol. 12. Iss. 8, p. 253-261.

***Authors:*** **Vadim A. Shpenst,** *Doctor of Engineering Sciences*, *Dean*, *https://orcid.org/0000-0001-6091-6916* (*Saint Petersburg Mining University*, *Saint Petersburg*, *Russia*), **Aleksey A. Belsky,** *Candidate of Engineering Sciences*, *Associate Professor*, *https://orcid.org/0000-0002-2619-1496* (*Saint Petersburg Mining University*, *Saint Petersburg*, *Russia*), **Evgeny A. Orel,** *Postgraduate Student*, *orel.geny@yandex.ru*, *https://orcid.org/0000-0003-4965-0998* (*Saint Petersburg Mining University*, *Saint Petersburg*, *Russia*).

*The authors declare no conflict of interests.*